AHAPS

Adaptable High Altitude Platform System

Design Synthesis Exercise
Spring 2026 | Group 17

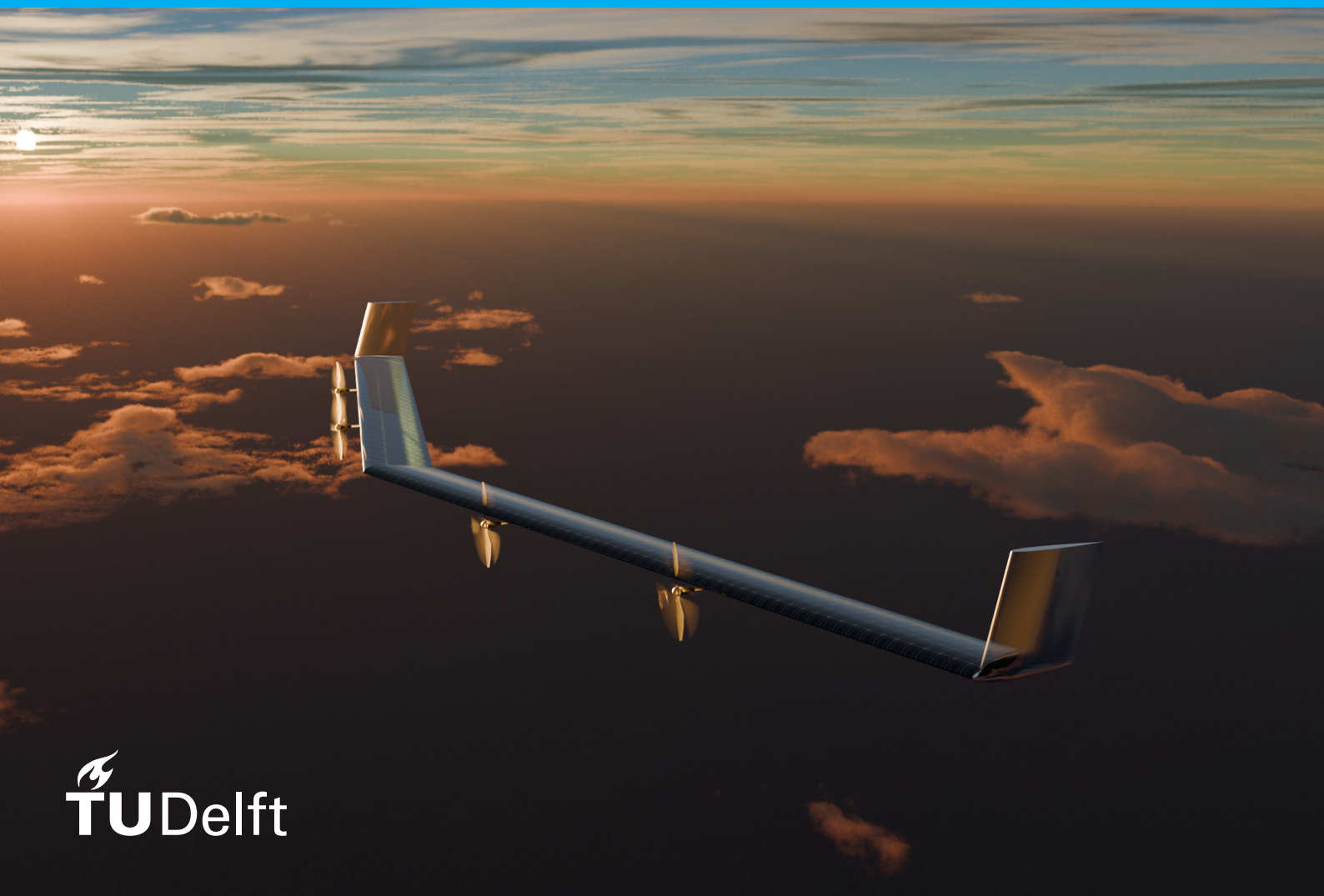

TU Delft

[*This page is intentionally left blank.*]

AHAPS

Adaptable High Altitude Platform System

by

DSE Group 17

Initials	Student Name	Student Number
SA	Stefan Amarfii	6020224
LB	Luuk van Breugel	6006183
IG	Ian Ghys	5904633
LH	Lennart Hubbers	5972272
JK	Jelmer van de Kamp	5774810
FL	Federico Laureri	5983630
JR	Jasper van Ruiten	6025668
BS	Bas van Strien	6038115
LT	Lowie Thierens	5919754
MV	Martijn van der Voort	5928796

Date: June 23, 2026
Course: AE3200 Design Synthesis Exercise
Faculty: Faculty of Aerospace Engineering, TU Delft
Tutor: Dr.ir. M.M. van Paassen
Coaches: J. Groot, A. Kumar
Cover: 3D Render of AHAPS
Version: Final

TU Delft

Executive Summary

High Altitude Platform Stations are an emerging alternative in sensor platform markets, blending the capabilities of semi-fixed stations such as satellites with the adaptability and cost-effectiveness of conventional aerial systems. Growth is particularly centred around developing countries, governmental, non-profit, and scientific use, which requires a cost-effective yet capable system. Existing solutions often fall short in one area, which leaves an opening in the market for a simultaneously affordable, manoeuvrable, and reusable system.

The Adaptable High Altitude Platform System (AHAPS) project aims to create a detailed conceptual design for a platform system offering a cost-effective, reliable, and modular alternative to a satellite in low Earth orbit. By cruising at 60,000 ft for a minimum of 28 days, it will provide capabilities such as ground observation and communications to areas with limited accessibility by making it rapidly deployable and efficiently transportable through the use of a 20 foot International Organisation for standardisation (ISO) container. Furthermore, the relatively low production costs compared to similar devices will ensure the AHAPS is accessible to a larger market share.

The market analysis, combined with a sustainability analysis and contractor requirements, led to a set of requirements that drive the design. The AHAPS aircraft shall be designed to cruise at a minimum altitude of 60,000 ft for at least 28 days, with year-round operation possible between latitudes 30°N and 30°S. It shall be able to carry a modular payload with a mass of up to 20 kg, providing 100 W of continuous power, 250 W of peak power to the payload, and 150 W of payload heat dissipation. Lastly, the AHAPS aircraft shall be certified by the European Union Aviation Safety Agency (EASA) under Operations Type 1, and have a manufacturing cost of no more than €900,000.

The first stage of development was to generate design options for the principal components of the AHAPS configuration. Based on feasibility and development risk, the design option trees were pruned down to four strawman concepts, varying only in the airframe and energy storage method used. These configurations consist of a tube-and-wing and flying wing, and batteries and fuel cells, as shown in Table 1.

Table 1: AHAPS preliminary design options, consisting of identical subsystems except with varying wing and power storage configurations.

Design Option	**Configuration**	**Energy Storage**	**Power generation**	**Launch System**	**Propulsion System**	**Landing System**
1	Tube-and-Wing	Batteries	Solar panels	Self-propelled	Open propeller	Landing gear
2	Tube-and-Wing	Fuel cells	Solar panels	Self-propelled	Open propeller	Landing gear
3	Flying wing	Batteries	Solar panels	Self-propelled	Open propeller	Landing gear
4	Flying wing	Fuel cells	Solar panels	Self-propelled	Open propeller	Landing gear

Following the selection of these preliminary design options, their characteristics were analysed in preparation for a trade-off. Starting with empirical mass fractions and an initial maximum take-off weight (MTOW) guess, the power system was sized. Afterwards, the wing area was determined through iteration, as shown in Figure 1, and subsequently the MTOW was calculated. Using the updated MTOW, wing and power sizing was reiterated until a stable MTOW was met.

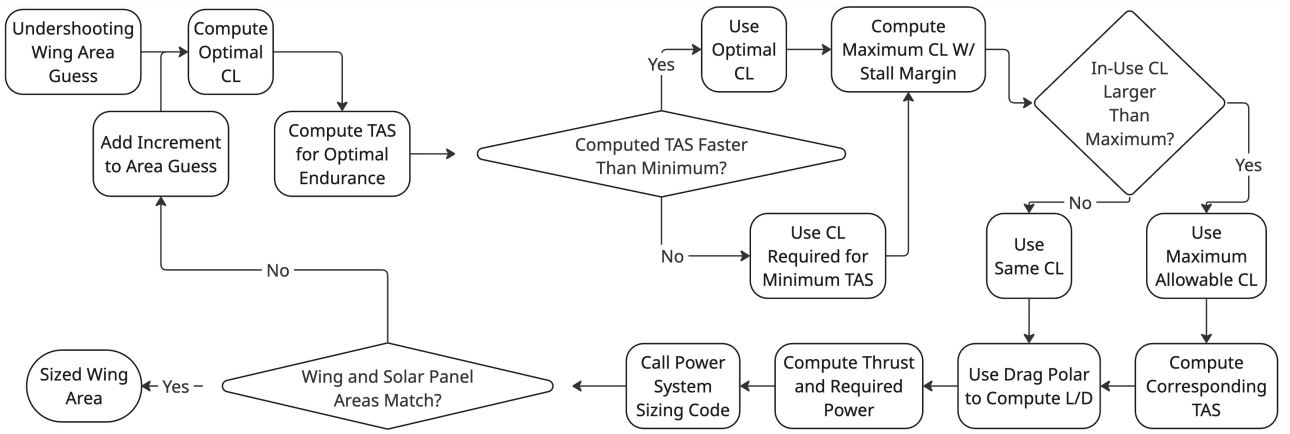

Figure 1: Inner iteration loop of the concept generation process. An initial wing area is guessed, whereby C_L is computed. With this, a drag polar is computed, allowing the required thrust and power to be found with the TAS. If wing and solar panel sizing results corroborate, a final sized wing area is obtained.

To choose the final preliminary concept, a trade-off is performed. The four chosen preliminary concepts are evaluated by assigning a score to five weighted criteria, which are given on a scale of zero to three. Additionally, the criteria are chosen based on the five main domains of the system requirements. The defined criteria are flight performance, development risk, costs, logistics, and sustainability. The flight performance criteria consist of endurance, deployability, stability, and controllability. Development risk consists of the Technology Readiness Levels (TRL) and the error margin of the concept characteristics. The costs consist of both non-recurring and recurring costs. The logistics consist of the sub-assembly mass and volume, and the assembly time. Finally, sustainability comprises manufacturing impact and degradation rate. The flying wing with batteries was ultimately selected for its excellent cost, logistics, and sustainability, as well as good flight performance and development risk. The reasoning for the selection and grading for this concept with respect to technical performance metrics is shown in Table 2. A sensitivity analysis on the trade-off method is subsequently performed, which demonstrates that the trade-off result is only impacted by the largest changes in the sensitivity analysis, such as removing the logistics criterion. As it is unfeasible to remove these criteria, it confirms that the flying wing configuration with batteries is the best option.

The detailed conceptual design follows a similar overall process to the preliminary conceptual design. Another nested optimiser is used, which is shown in Figure 2. This contains an inner loop determining the weight and geometries of the changing subsystems, which are summed to find the total aircraft geometry. Moreover, an outer loop takes initial MTOW and mass fraction guesses, which are fed to the inner loop, resulting in a new MTOW. This process is iterated until the MTOW converges to a set value, and consequently, a set design. This general sizing method includes all individual subsystem sizing tools, which are used to find the individual subsystem geometries within the inner loop. After obtaining a converged design, the compliance phase may start. This consists of using the design parameters, logistical performance, and deflection analyses. In the case that any of the requirements in this phase are not met, this sizing process is repeated to resolve this shortfall. With this, the iterative process is repeated until compliance is passed, whereby the final aircraft design and its associated parameters are frozen.

Table 2: Trade-off summary table for the airframe and power system configuration selection of the AHAPS. The highest overall score of 2.6 is obtained for the flying wing with batteries, indicating this should be selected for the final design.

CRITERION / OPTION / WEIGHTED SUM	**Flight Performance** 20%	**Development Risk** 20%	**Costs** 15%	**Logistics** 30%	**Sustainability** 15%
Tube-and-Wing; Batteries - 2.35	Excellent: Good deployability, good longitudinal stability and good endurance	Good: High scoring TRL, but medium sensitivity	Excellent: Lowest manufacturing and recurring costs	Good: Longer assembly time, easy to handle, relative big volume	Good: More CO_2 emissions, less degradation
Tube-and-Wing; Fuel cell - 2.2	Excellent: Good deployability, good longitudinal stability and good endurance	Good: Medium scoring TRL, with medium sensitivity	Good: Higher manufacturing and recurring costs	Good: Longer assembly time, easy to handle, relative big volume	Good: Less CO_2 emissions, more degradation
Flying wing; Batteries - 2.6	Good: Medium deployability, medium longitudinal stability and good endurance	Good: Medium scoring TRL, but high sensitivity	Excellent: Lowest manufacturing and recurring costs	Excellent: Shortest assembly time, easy to handle, small volume	Excellent: Medium CO_2 emissions, less degradation
Flying wing; Fuel cell - 2.1	Good: Medium deployability, medium longitudinal stability and good endurance	Correctable deficiencies: Low scoring TRL, with low sensitivity	Good: Higher manufacturing and recurring costs	Excellent: Shortest assembly time, easy to handle, small volume	Good: Less CO_2 emissions, more degradation

Red - 0 - Unacceptable	**Yellow - 1 - Correctable deficiencies**	**Cyan - 2 - Good**	**Green - 3 - Excellent**

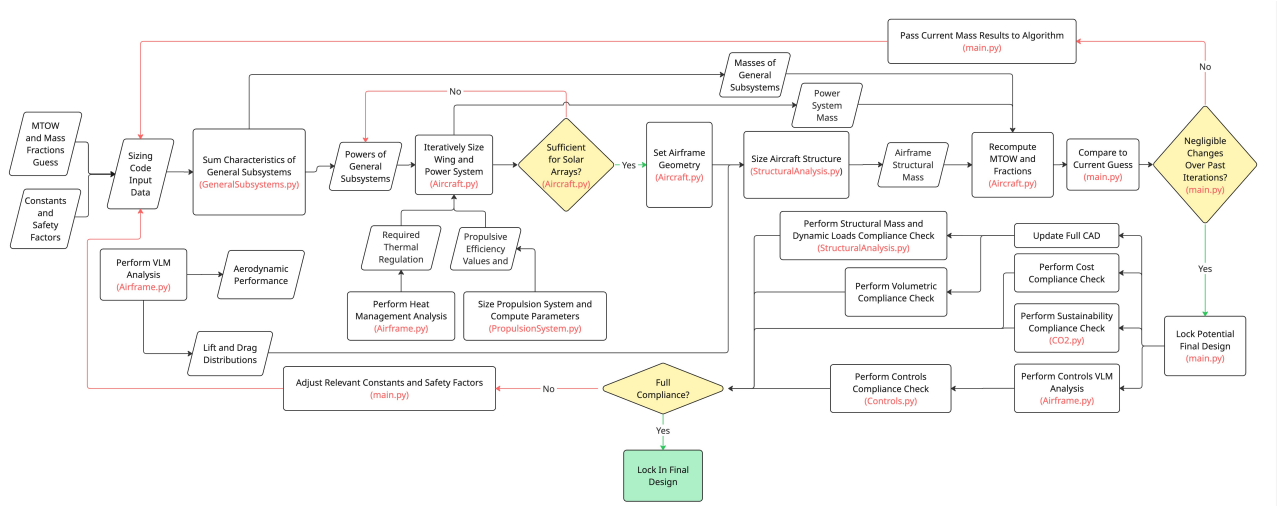

Figure 2: Detailed conceptual design iteration flow diagram.

Individual subsystems are sized according to their subsystem requirements. Firstly, the payload, flight condition, communication, and computer systems are unchanging with changing MTOW. Therefore, these can be sized independently and do not affect the results of other subsystems. The payload system consists of the supporting structure of the payload and the sensors necessary for its functioning. This is designed by simply creating a connection to attach the payload, along with sizing components necessary for communicating and monitoring the payload. Next, the flight condition system allows for the determination of the aircraft state, such as attitude, heading, altitude, and position. Therefore, this system was sized with sensors needed to establish these measurements. This is followed by the communication system, which was designed by sizing all components necessary for communication between other aircraft and ground stations. After this, the computer system was defined by finding all components necessary to allow the other aircraft subsystems to communicate with each other. Lastly, for the undercarriage system, the take-off system can be sized. This system is not part of the aircraft itself and is therefore taken as a simple structure comprised of lightweight tubes and bike wheels.

The remaining subsystem sizing is intertwined and interdependent, with changes in one subsystem impacting others. As a result, these systems are sized using tools in the inner loop of the aforementioned iteration process. Firstly, the airframe system is designed by analysing the aerodynamic forces on the wing and using an optimiser to create the lightest structure capable of sustaining and transferring these loads. Next, the power system is sized by observing the power required to fly for 28 days between the 30°N and 30°S latitudes. From this, solar modelling is used to size the necessary battery and solar panel sizes to accommodate this. Simultaneously, a propulsion system has to be designed to provide sufficient thrust. This system is optimised for the cruise altitude of 60,000 ft, although it still has to be designed to operate for the entire flight profile. Additionally, the control systems are also sized in parallel. These provide 3-axis controllability for the aircraft, all while maintaining stability. Following this, a temperature management system is also designed. This is because the temperature at cruise altitude can reach −60°C, thus, putting components in their operational temperature ranges requires systems of heaters and insulation. Lastly, the landing portion of the undercarriage system is designed. This is done by sizing an array of skids according to the landing loads and ground clearance, preventing critical subsystems from impacting the ground. Using the iterative process shown in Figure 2, converging to a design and showing compliance yields a final aircraft design. An overview of the final design system and subsystem characteristics is shown in Table 3.

Table 3: Final conceptual design characteristics summary of the AHAPS subsystems.

Characteristic	Symbol	Unit	Value	Characteristic	Symbol	Unit	Value
Payload				**Power**			
Payload Mass	m_{pl}	kg	20.0	Total Power System Mass	$m_{pow,total}$	kg	169.0
Total Payload System Mass	$m_{pl,total}$	kg	21.05	Battery Mass	$m_{power,bat}$	kg	135.5

Continued on next page

Characteristic	Symbol	Unit	Value	Characteristic	Symbol	Unit	Value
General				Battery Specific Energy	$E_{s,bat}$	Wh/kg	500
Total General System Mass	$m_{gen,total}$	kg	6.42	Solar Panel Mass	m_{sp}	kg	24.5
Total General System Power	$P_{gen,total}$	W	133	Solar Panel Area	S_{sp}	m^2	61.2
Airframe				Solar Panel Efficiency	η_{sp}	-	0.30
Total Airframe Mass	$m_{af,total}$	kg	85.98	**Propulsion**			
Spars Mass	m_{spar}	kg	16.74	Total Propulsion System Mass	$m_{prop,total}$	kg	16.5
Skin Mass	m_{skin}	kg	26.92	Blade Diameter	D_p	m	1.80
Clamps Mass	m_{clamps}	kg	7.60	Total Efficiency @ Cruise	η_{cruise}	-	0.76
Bolts Mass	m_{bolts}	kg	1.0	Total Efficiency @ Lift-off	η_{TO}	-	0.73
Ribs Mass	m_{ribs}	kg	3.82	Total Thrust @ Cruise	T_{req}	N	74.2
Outer Sleeve Mass	$m_{o/sleeve}$	kg	22.92	Total Thrust @ Lift-off	T_{TO}	N	283.8
Inner Sleeve Mass	$m_{i/sleeve}$	kg	2.18	Rotational Speed @ Cruise	n_{cruise}	rpm	1453
Winglets Mass	$m_{winglets}$	kg	4.8	Rotational Speed @ Lift-off	n_{TO}	rpm	649
Control				Power Available @ Cruise	$P_{a,cruise}$	W	2392
Total Control System Mass	$m_{control,total}$	kg	7.2	Power Available @ Lift-off	$P_{a,LO}$	W	3130
Hinge Line Chord Fraction	x_{hinge}	$\%_c$	0.75	**Temperature Management**			
Elevator Spanwise Fraction	$y_{elevator}$	$\%_{b/2}$	0.6 – 0.7	Total Temperature Management System Mass	$m_{TM,total}$	kg	4.5
Aileron Spanwise Fraction	$y_{aileron}$	$\%_{b/2}$	0.7 – 0.9	Total Heat Dissipation	P_{diss}	W	332.67
Rudder Winglet Fraction	z_{rudder}	$\%_{b/2}$	0 – 0.8	Power Budget Required	$P_{TM,req}$	W	256.55
Elevator Maximum Deflection	$\delta_{elevator}$	deg	±20	Aerogel Layer thickness	t_{TM}	cm	1.5
Aileron Maximum Deflection	$\delta_{aileron}$	deg	±20	**Undercarriage**			
Elevator Maximum Deflection	$\delta_{elevator}$	deg	±20	Total Take-off Gear Mass	$m_{TO_{gear}}$	kg	15.34
Rudder Maximum Deflection	δ_{rudder}	deg	±30	Total Skid Mass	m_{skid}	kg	9.15

Various iterative methods and design tools are used in the design synthesis, and they must therefore also be verified. This process is done in parallel with the design of the tools. Individual tools use calculation and code verification. Calculation verification is done by checking whether the sizing methods are correct by comparing formulae and methods to those used in literature, and using tests to measure the fidelity of these methods. Whereas code verification checks the implementation of the code, in the form of unit tests; testing individual code blocks, and system tests; testing the functionality of entire code functions and classes.

The detailed conceptual design leads to a final layout of the AHAPS system and subsystems. To transport the AHAPS, it is designed to fit within a 20 ft ISO container. As a consequence of this, the AHAPS has to be cut up into nine parts for transportation, as shown in Figure 3. This internal structure also has to accommodate all the subsystems. In Figure 4, a visualisation is given of the centre of gravity (C.G.) positions and internal layout of the AHAPS. In general, the payload, flight condition, communication, and computer system are located in the main wing section. The propellers, control surfaces, and batteries are placed based on their impacts on the stability and controllability of the aircraft. Moreover, the retractable skids are placed to prevent the aircraft from impacting the ground upon landing. Lastly, the wing spar and skin are distributed along the wing. Cross sections showing the specific positions of these components are shown in Figure 5. Further communication and interactions between subsystems are identified and mapped with hardware, software, and electrical diagrams.

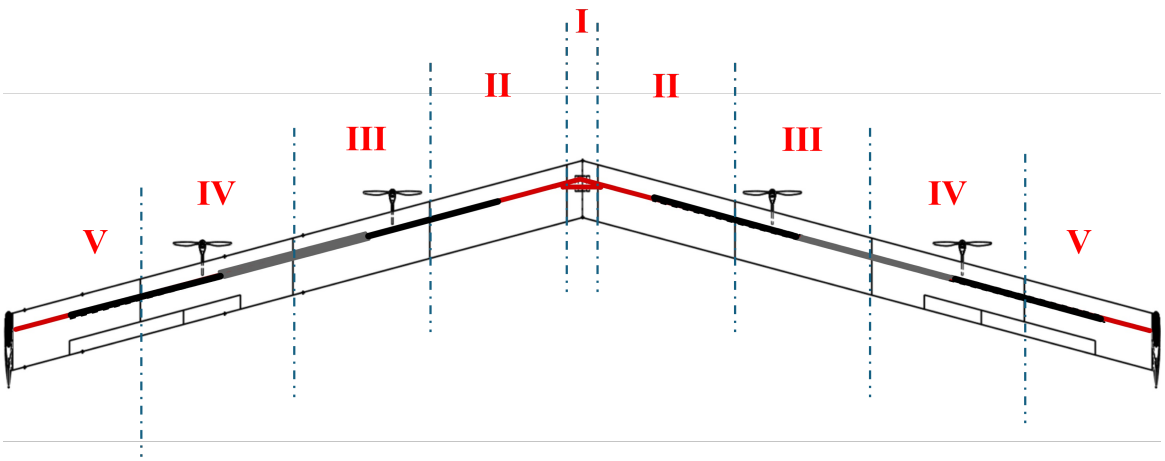

Figure 3: Wing Sections Definitions for the AHAPS; I - Main Wing Section, II - Middle Wing Section 1, III - Middle Wing Section 2, IV - Middle Wing Section 3, V - Wing Tip Section

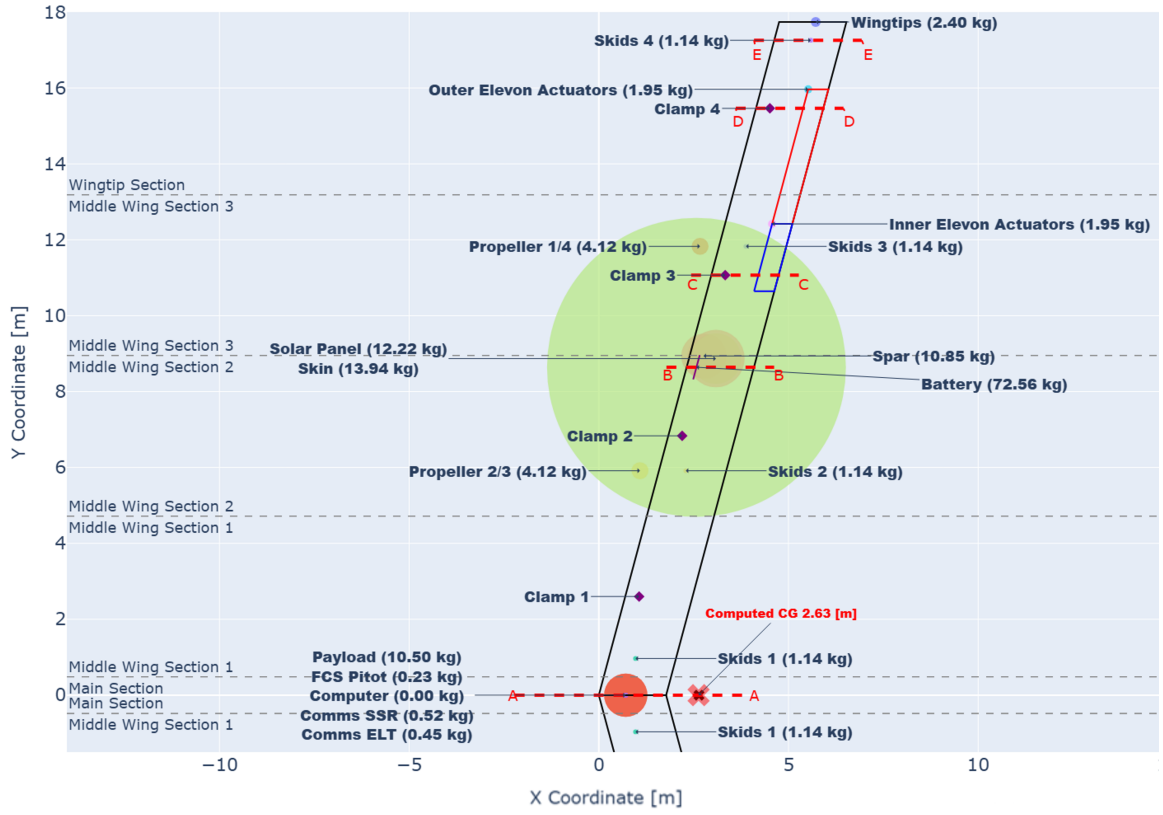

Figure 4: Centre of gravity plot with cross-sectional cuts corresponding to the cross sections A-E. Positioning and mass of the aircraft components are shown for the half-wing section. The size of opaque circles relates to the relative mass of said components.

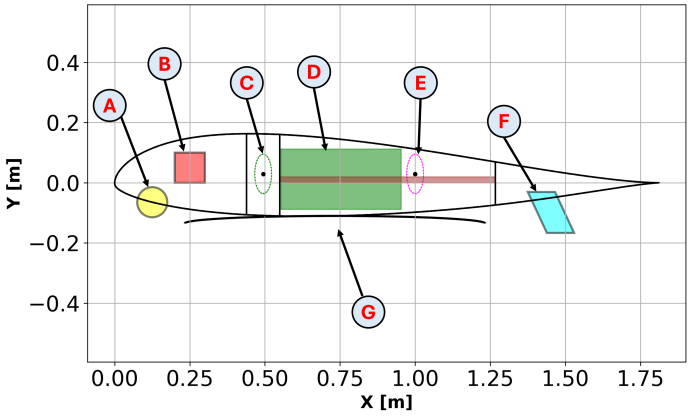

(a) Cut A; A - ADS-B ELT, B - computer, C - spar, D - payload bay, E - second spar, F - SSR, G - SAR.

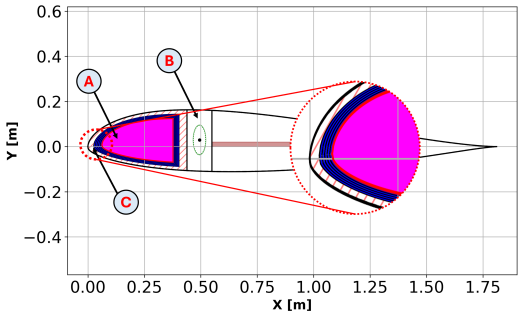

(b) Cut B; A - battery pack, B - spar, C - insulation.

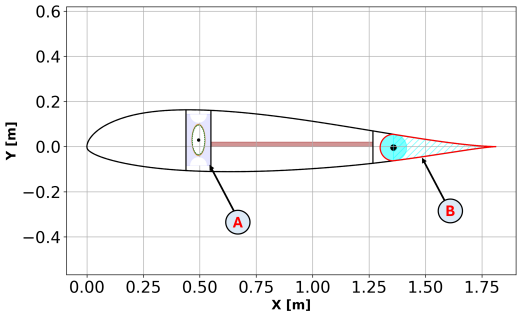

(c) Cut C; A - clamped spar, B - inner elevon.

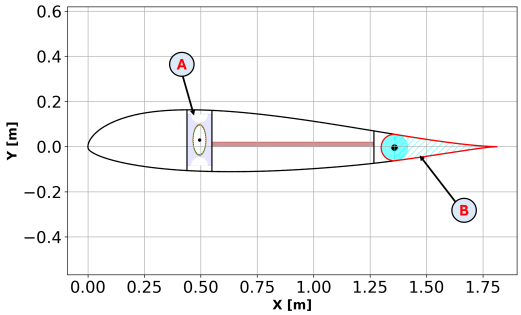

(d) Cut D; A - clamped spar, B - outer elevon.

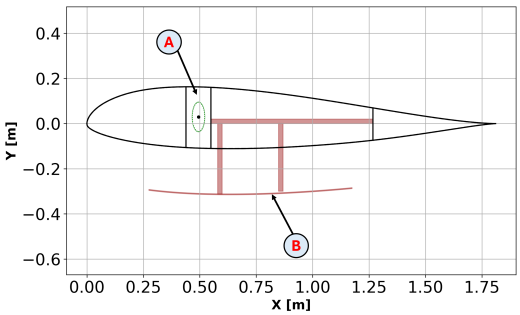

(e) Cut E; A - spar, B - skid.

Figure 5: Cross-section cuts of the final AHAPS design. Cross-sections A-E are shown and correspond to the cuts displayed in Figure 4.

A cost breakdown of the manufacturing, component, and material costs is performed for the sized design. This results in a total system cost of at least €819,000. Subsequently, a detailed sustainability analysis is performed. As a requirement, the aircraft is designed with components that are either inert or recyclable. It is also found that 89% of the aircraft by mass can be recycled, which is above the minimum imposed by the European Directive [1]. From the stakeholder requirements, solar panels and batteries must last a minimum of two years. After this time, the modularity of the system allows them to be replaced. Additionally, the materials have a longer lifespan than this, with the shortest, the CFRP, lasting at least 4 years before needing replacement. The last component of the lifecycle analysis is the emissions of production and operation. Since the aircraft is electrically powered, emissions arise purely from the production of the aircraft. The manufacturing process produces 18980 kg CO_2-eq, which is comparable to the production of two electric

cars[1].

In the design performance analysis, the design synthesised earlier is evaluated on its operational capabilities. The performance is analysed on the following: load-bearing capabilities, stability and control, deployability, and mission simulation. Regarding load-bearing capabilities, there is a variety of loads to be considered. Starting with manoeuvring loads, which are induced through the flight mechanics of the aircraft. The requirements for these are relatively flexible due to it being an unmanned aircraft, but follow from similar HAPS. The gust load approximations are based on CS-22, CS-23, and CS-25 regulations. As these static load approximations are almost certainly higher than the actual gust loads, this makes the gust load capabilities conservative. These two load types together make for the maximum load factors the structure needs to withstand, which are +2.5 g and −1 g.

With these load factors defined, structural analyses are performed. In addition to this, a deflection analysis is performed due to the very light structure and high aspect ratio wings. Using Aerosandbox the aerodynamic forces and moments are calculated [3]. From this, the wingtip vertical and twist deflections of 1.8 m and −2.1° are found for the cruise loads.

Regarding the stability and control of the aircraft, a static analysis was performed first. This resulted in stability for $\alpha_{cruise} = 10.3°$ and $C_{m_\alpha} = -1.17\ rad^{-1}$ for a $C.G.$ = 2.64 m aft of the nose. After this, a dynamic analysis is performed starting with the longitudinal performance. With the earlier named values, this results in a stable, highly-damped short-period mode, but a slightly unstable phugoid mode. For the latter, a fly-by-wire system with a speed controller will be introduced to keep it stable. Then, the elevators are sized to reach the pitch requirement of 3 $°/s$, resulting in elevators between 60% and 70% of the half span, with a hinge line at 75% of the chord.

Lateral performance also plays an important role in the design due to the absence of fuselage damping, large sweep, and potential control coupling. Polar analysis shows that both Dutch roll and spiral modes are stable. To meet the roll rate requirement of reversing a 45° turn in under 11.8 s, the aileron span was set from 70% to 90% of the half-span. Consequently, the rudders were sized to still reach the $5°/s$ requirement with the one engine inoperable (OEI) requirement. With the longitudinal and lateral performance analysed, the properties of the eigenmotions have been calculated, showing again that only the phugoid is slightly unstable. After analysing the control and stability of the aircraft, the aerodynamic properties were calculated. These determine the in-flight efficiency values of the aircraft and are a result of vortex lattice and quasi-linear lifting line methods. These values have been verified by an analysis using XFLR5. After selecting the airfoils, the XFLR5-solver can use the data obtained from doing a batch analysis at the expected Reynolds numbers and angles of attack.

A deployability plot is made that numerically computes the times throughout the year that the aircraft can be launched, such that it will reach cruising altitude with enough battery power to fly for at least 28 days. This is shown in Figure 6.

To lay out what the mission of the AHAPS will look like, an example of a mission simulation has been performed. This includes a climb profile which shows the AHAPS will take around 14 hours to reach cruise altitude, and will cover up to 1078 km of horizontal distance during its climb. Once the AHAPS is in its area of interest, it will fly parallel legs and turn whenever it reaches its area boundary.

Logistics plays a key role in the design of the AHAPS, since it needs to be adaptable. For this, a logistics flow chart has been made describing the steps needed to deploy and recover the aircraft. The aircraft is, as described, transported in a 20 ft ISO container. For this, a packing structure has been designed such that it fits, including 20% cushioning per component. Additionally, a plan is created for the ground station setup, which is used to store transmitted data from the AHAPS. To comply with the European labour law and still be able to perform assembly by three people, no part weighs more than 46 kg. An assembly plan of 21 steps accurately describes how the aircraft can be assembled from start to flight-ready. Additionally, a tool list is made to ensure the inventory is complete. For a proper take-off, limits have been set for the runway conditions. The AHAPS can take off from runways labelled at least "Hard Desert Sand", "Hard Grass", or "Small Tarmac Runway, Poor Foundation". The users are expected to prepare the runway sufficiently for the AHAPS

[1] https://www.zemo.org.uk

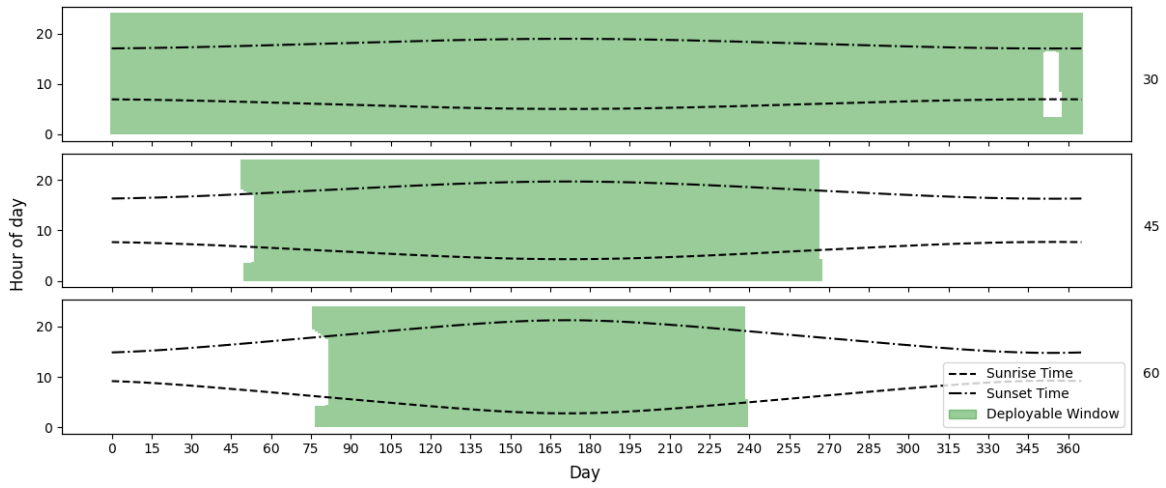

Figure 6: The 28-day deployability of the AHAPS concept throughout the year, at latitudes of 30°, 45° and 60° respectively. The green region indicates times within which the AHAPS can be launched and subsequently fly at cruising altitude for at least 28 consecutive days.

to take off. To ensure smooth flight operations and compliance with other air traffic, a communication flow diagram has been set up, showing the relation between the AHAPS, the ground station, air traffic control, and other aircraft.

To determine the design robustness, the design needs to be verified and validated. Firstly, the design and its performance are checked against all key and driving requirements, tabulating the results in a compliance matrix. This analysis showed that all set key and driving requirements were met, or not able to be evaluated. This demonstrates that a viable solution was found within the constrained design space.

Next, a verification and validation plan is created, which would be used to analyse a completed design. Here, the AHAPS system is hierarchically tested. This is done by first performing a verification and validation (V&V) analysis on the subsystems and then on the system as a whole. Since many of the subsystem requirements are repetitive, overarching verification methods can be used to test these, while unique requirements have independent verification methods. These verification methods are split into four main categories: analysis, testing, inspection, and demonstration. System requirements can be verified similarly. However, as these are higher-order requirements, general verification methods are no longer defined, as the system requirements are unique. As verification can be expensive, a cost analysis of the necessary facilities is performed, finding facility costs ranging from €5,000 to €25,000.

With verification performed, mission validation on a completed design is done by validating the stakeholder requirements. Here, validation methods are described that determine whether each stakeholder requirement is met. The methods used can be split up into two main campaigns: a pre-flight test inspection and a flight test. In the former, aircraft characteristics can be validated, while the latter allows for the validation of flight performance.

Following this, a technical risk assessment is executed. Firstly, contingencies for the design of each subsystem across the various design phases are established. Design risks are then identified and tabulated. This is followed by a risk assessment determining the likelihood level of the risk and the consequence level. These are then mitigated, obtaining new likelihood and consequence levels. The pre- and post-mitigation risk maps are consequently generated, determining the impact of mitigation on design risks.

Subsequently, a RAMS (reliability, availability, maintainability, and safety) assessment is implemented. This assessment ensures the aircraft is suitable for long-term operations. First, the reliability is computed, which takes into account the relationship between subsystems and uses the mean time between failures computed in the technical risk assessment. This results in pre-and post-mitigation reliabilities of 0.86 and 0.95, respectively. Then, maintenance is considered, where the types and frequencies of the necessary maintenance checks are laid out. Following this, the availability can be computed, which is the amount of time the aircraft is available for operations. Lastly, a brief safety analysis is done to ensure the aircraft is safe to use.

The last part of the design robustness is the sensitivity analysis. Here, the design iterator is tested with 2.5% changes in key design parameters. From this, it is found that the aircraft is most sensitive to changes in the MTOW, the power consumption, the energy density of the batteries, and the profile drag. These are all generally related to the power budget of the aircraft, as changes in these parameters require either higher power generation or power storage, which therefore need larger wing surface areas to increase solar panel coverage, or to account for extra weight needed for more batteries.

After checking the robustness of the design, the synthesis of the conceptual design is complete. Hereafter, a manufacturing, assembly, and integration plan is created. Manufacturing considers the processes necessary to manufacture the individual subsystem parts. After this, the assembly of the parts is detailed. Previously, assembly instructions were detailed, describing the in-field assembly; conversely, this manufacturing plan describes the assembly of components and structures into the nine distinct aircraft sections and structures. These are the structures that are the assembled sections, which are packed into the container to be assembled in the field.

This is followed by a detailed flow diagram and Gantt chart describing the necessary post-DSE processes. This includes the detailed design steps needed, as well as steps for the manufacturing and product distribution. Subsequently, the flow of aircraft operation and maintenance is described. Lastly, aircraft EoL is considered, whereby the decommissioning steps are laid out.

Ultimately, an investigation is undertaken on the commercial potential of the AHAPS. This is commenced with a final sales price determination, considering the costs of finalising the design, validating, and certifying it. This results in a remaining non-recurring cost of €15,642,500. For a sales-price contribution, this is then taken as being distributed over 1000 units. This is then summed with the materials and manufacturing cost of €900,000, and a 20% profit margin is applied, resulting in an ultimate minimal unit sale price of €1.1M. This sales price is less than that of other competitors serving the same market.

The return on investment of the AHAPS is then qualitatively analysed. This is done by analysing its performance in a variety of possible missions and comparing results to other commercially available designs. Here, characteristics such as coverage, time resolution, and flexibility are investigated. The main conclusion from this investigation is that the AHAPS is able to provide similar or higher quality services compared to the market standard, all the while having much lower operational and acquisition costs.

Although the design has been investigated and detailed in depth, due to a stakeholder requirement imposing 7 weeks to complete the conceptual design in a team of 10, some design aspects have not been thoroughly analysed. Firstly, an analysis of the impacts of radiation on the system was omitted. Flying at an altitude of 60,000 ft, this could have impacts on the reliability of electronic components. Additionally, dynamic loads were only considered in the control response of the aircraft. Further dynamic analyses such as dynamic gust loads, eigenfrequencies, fatigue, creep, aeroelasticity, and finite element modelling could be included, improving the validity and performance of the aircraft. Lastly, higher fidelity CFD (computational fluid dynamics) analyses could be used to optimise both the control surfaces and the propeller designs.

To conclude, the goal of the AHAPS is to fill the market gap between Low Earth Orbit satellites and commercially high-altitude platform systems. This is done by providing an adaptable high-altitude platform system that comes at a significantly lower cost than the competition, which is both modular and can be easily transported. A solar-powered flying wing was ultimately chosen based on stakeholder logistics, sustainability, and cost requirements. Ultimately, this conceptual design proves the feasibility of a sustainable, adaptable, and modular HAPS. This system is able to operate all year between the 30°N and 30°S latitudes, and can fly continuously for 28 days. Lastly, it carries a payload of up to 20 kg, flying at an altitude of 60,000 ft, with a total unit cost of €1.1M.

Acknowledgements

Design Synthesis Exercise
Spring 2026 | Group 17
Delft, June 2026

The authors would like to thank dr.ir. M.M. van Paassen, D.J. Groot, and A. Kumar for their support, expertise, and time given whilst providing feedback and guidance. In addition, the authors would like to thank ir. J.A. Melkert and the rest of the OSCC for the organisation of the Design Synthesis Exercise. Our thanks also go to H. Niemczyk, for her feedback on the design reports.

Executive Summary i

Acknowledgements xi

Nomenclature xiii

1 Introduction 1

2 Project Description 2
2.1 AHAPS Mission . . . 2
2.2 Stakeholder Needs . . . 2
2.3 AHAPS Requirement Lists . . . 2

3 Pre-Design Analyses 8
3.1 Subsystem Definition . . . 8
3.2 Functional Analysis . . . 10
3.2.1 Functional Breakdown Structure . . . 10
3.2.2 Functional Flow Diagram . . . 11
3.3 Engineering Budgets . . . 11
3.3.1 Volume . . . 11
3.3.2 Mass . . . 11
3.3.3 Costs . . . 12
3.4 Business Case . . . 12
3.5 Sustainable Development Strategy . . . 14
3.5.1 Sustainable Design Philosophy . . . 14
3.5.2 Design Considerations . . . 14

4 Design Synthesis 16
4.1 General Method . . . 16
4.1.1 General Assumptions . . . 16
4.1.2 Preliminary Conceptual Design Phase Summary . . . 17
4.1.3 Design Iterations Flow Diagram . . . 24
4.1.4 Performance Evaluation Approach . . . 26
4.1.5 Tool Verification . . . 27
4.2 Payload System . . . 28
4.2.1 Payload System Assumptions . . . 28
4.2.2 Payload System Design . . . 28
4.2.3 Payload System Tool Verification . . . 28
4.2.4 Payload System Characteristics Overview . . . 28
4.3 General Subsystems . . . 29
4.3.1 General Subsystems Assumptions . . . 29
4.3.2 General Subsystems Design Results . . . 29
4.3.3 General Subsystems Tool Verification . . . 31
4.3.4 General Subsystems Characteristics Overview . . . 31
4.4 Airframe System . . . 32
4.4.1 Airframe System Assumptions . . . 32
4.4.2 Airframe System Design . . . 33
4.4.3 Airframe System Tool Verification . . . 38
4.4.4 Airframe System Characteristics Overview . . . 38
4.5 Power System . . . 39
4.5.1 Power System Assumptions . . . 39
4.5.2 Power System Design . . . 40
4.5.3 Power System Tool Verification . . . 42
4.5.4 Power System Characteristics Overview . . . 43
4.6 Propulsion System . . . 44
4.6.1 Propulsion System Assumptions . . . 44
4.6.2 Propulsion System Design . . . 45
4.6.3 Propulsion System Tool Verification . . . 50
4.6.4 Propulsion System Characteristics Overview . . . 51
4.7 Control System . . . 53
4.7.1 Control System Assumptions . . . 54
4.7.2 Control System Design . . . 54
4.7.3 Control System Tool Verification . . . 58
4.7.4 Control System Characteristics Overview . . . 58
4.8 Temperature Management . . . 59
4.8.1 Temperature Management Assumptions . . . 59
4.8.2 Temperature Management System Design . . . 59
4.8.3 Temperature Management Tool Verification . . . 60
4.8.4 Temperature Management Characteristics Overview . . . 61
4.9 Undercarriage System . . . 61
4.9.1 Undercarriage System Assumptions . . . 61
4.9.2 Undercarriage System Design . . . 62
4.9.3 Undercarriage System Tool Verification . . . 63
4.9.4 Undercarriage System Characteristics Overview . . . 64

5 Design Overview 66
5.1 Detailed Design Visualisation . . . 66
5.1.1 AHAPS Drawing . . . 66
5.1.2 AHAPS Assembly Parts . . . 66
5.2 Design Overview Table . . . 67
5.3 System Architecture . . . 67
5.3.1 Subsystem Integration . . . 68
5.3.2 Hardware Diagram . . . 69
5.3.3 Electrical Diagram . . . 70
5.3.4 Data Handling Diagram . . . 70
5.3.5 Software Diagram . . . 70
5.4 Cost Breakdown . . . 70
5.5 Sustainability Aspects . . . 73
5.5.1 End-of-Life Recyclability . . . 74
5.5.2 Component Lifecycle . . . 75
5.5.3 Lifecycle Emissions . . . 75

6 Design Performance 77
6.1 Performance Analysis . . . 77
6.1.1 Load-bearing Capabilities . . . 77
6.1.2 Stability and Control . . . 80
6.1.3 Aerodynamic Performance . . . 83
6.1.4 Deployability . . . 85
6.1.5 Mission Simulation . . . 86
6.2 Operations and Logistics . . . 87
6.2.1 Transportation and Container Packing . . . 88
6.2.2 Ground Station Set-Up . . . 89
6.2.3 Assembly Instructions . . . 89
6.2.4 Runway Preparations . . . 92
6.2.5 Communication Flow Diagram . . . 93

7 Design Robustness 94
7.1 Sensitivity Analysis . . . 94
7.1.1 Potential Design Changes . . . 94
7.1.2 Expected Impact . . . 94
7.1.3 Observed Impact . . . 95
7.2 Technical Risk Assessment . . . 96
7.2.1 Contingency Management . . . 96
7.2.2 Design Risks . . . 96
7.2.3 Risk Mitigation . . . 98
7.2.4 Mean Time Between Failure . . . 100
7.3 Reliability, Availability, Maintainability, and Safety Assessment . . . 101
7.3.1 Reliability . . . 101
7.3.2 Maintainability . . . 103
7.3.3 Availability . . . 104
7.3.4 Safety . . . 105
7.4 Verification and Validation . . . 105
7.4.1 Compliance Matrix . . . 105
7.4.2 Second Order V&V . . . 108

8 Post Design Synthesis Recommendations 114
8.1 Design Recommendations . . . 114
8.1.1 Radiation . . . 114
8.1.2 Dynamic Analysis . . . 114
8.1.3 Control Surface Optimisation . . . 116
8.1.4 Propeller Optimisation . . . 116
8.1.5 Frequency Autonomy . . . 116
8.2 Project Design and Development Logic . . . 116
8.3 Manufacturing, Assembly and Integration Plan . . . 116
8.3.1 Sub-Assembly Manufacturing . . . 117
8.3.2 Sub-Assembly and Integration . . . 118
8.4 Commercial Potential . . . 118
8.4.1 Sales Price Determination . . . 119
8.4.2 Return On Investment . . . 120

9 Discussion and Conclusion 122

A Appendix 126
A.1 Functional Breakdown Structure . . . 126
A.2 Functional Flow Diagram . . . 128
A.3 Design Option Trees . . . 129
A.4 Post-DSE Work Flow Diagram . . . 130
A.5 Post-DSE Gantt Chart . . . 132
A.6 Technical Drawing AHAPS . . . 133

Nomenclature

Abbreviations

Abbrev.	Definition	Abbrev.	Definition
ADS-B	Automatic Dependent Surveillance-Broadcast	IMT	International Mobile Telecommunications
AHAPS	Adaptable High Altitude Platform System	IMU	Inertial Measurement Unit
AoA	Angle of Attack	IPA	Isopropyl Alcohol
ATC	Air Traffic Control	ISA	International Standard Atmosphere
AWG	American Wire Gauge	ISO	International Organisation for Standardisation
BEMT	Blade Element Momentum Theory	ITU-R	International Telecommunication Union – Radiocommunication Sector
BLDC	Brushless Direct Current	LCO	Limit Cycle Oscillations
BOM	Bill of Materials	LEO	Low Earth Orbit
CAD	Computer-Aided Design	LLT	Lifting Line Theory
CAGR	Cumulative Average Growth Rate	LTA	Lighter Than Air
CFD	Computational Fluid Dynamics	MEA	Middle East and Africa
CFRP	Carbon Fibre Reinforced Polymer	MTBF	Mean Time Between Failures
CNC	Computer Numerical Control	MTOW	Maximum Take-off Weight
CS	Certification Specification	NASA	National Aeronautics and Space Administration
COTS	Commercial Of The Shelf	NOAA	National Oceanic and Atmospheric Administration
DCIR	Direct Current Internal Resistance	OEI	One Engine Inoperative
DOD	Depth of Discharge	PAT	Pointing, Acquisition and Tracking
DOT	Design Option Tree	PET	Polyethylene Terephthalate
DSE	Design Synthesis Exercise	PVF	Polyvinylidene Fluoride
EASA	European Union Aviation Safety Agency	RAMS	Reliability, Availability, Maintainability, and Safety
EES	Electrical Energy Storage	RANS	Reynolds Averaged Navier-Stokes
ELT	Emergency Locator Transmitter	ROC	Rate of Climb
EOL	End Of Life	ROD	Rate of Descent
EOM	Equation(s) of Motion	ROI	Return on Investment
EPA	Environmental Protection Agency	SAR	Synthetic Aperture Radar
EPP	Expanded Polypropylene	SSR	Secondary Surveillance Radar
ESC	Electronic Speed Controller	SWOT	Strengths, Weaknesses, Opportunities, Threats
FBS	Functional Breakdown Structure	TAS	True Airspeed
FCS	Flight Condition System	TRL	Technology Readiness Level
FEM	Finite Element Method	UAV	Unmanned Aerial Vehicle
FFD	Functional Flow Diagram	UTP	Unshielded Twisted Pair
FL	Flight Level	V&V	Verification and Validation
GNSS	Global Navigation Satellite System	VHF	Very High Frequency
GPS	Global Positioning System	VLM	Vortex Lattice Method
HAPS	High Altitude Platform System	WFD	Work Flow Diagram
HTA	Heavier Than Air		

Symbols

Symbol	Definition	Symbol	Definition
	Latin Symbols		
A	Availability	N	Oktas cloud cover
A_{solar}	Solar panel area	N_b	Number of blades
a	Acceleration	N_{days}	Number of days from the winter solstice
a_x	Axial induction factor	n	Rotational speed
AM	Air mass	n_{cruise}	Rotational speed at cruise
b	Span	n_{TO}	Rotational speed at take-off
C_{atm}	System state: Atmospheric conditions	P_a	Power available
C_D	Wing drag coefficient	P_{cr}	Euler's buckling load
C_{D_0}	Wing zero lift drag coefficient	P_{ir}	Power to overcome DC internal resistance
C_d	Airfoil drag coefficient	P_r	Power required
C_L	Wing lift coefficient	p	Roll rate
$C_{L_{climb}}$	Wing lift coefficient during climb	p_{aoi}	Angle of incidence subsystem state

$C_{L_{cruise}}$	Wing lift coefficient during cruise
$C_{L_{max}}$	Wing maximum lift coefficient
$C_{L_{opt}}$	Optimal wing lift coefficient
$C_{L_{TO}}$	Wing lift coefficient at take-off
C_l	Airfoil lift coefficient
C_m	Airfoil moment coefficient
C_{m_α}	Change in moment coefficient due to AoA
C_{ne}	Yawing moment due to asymmetric thrust
C_P	Power coefficient
C_T	Thrust coefficient
C_{Xu}	Longitudinal stability derivative
$C_{X\delta_e}$	Control derivative
$C_{Y\delta_r}$	Control derivative
$C_{Z\alpha}$	Longitudinal stability derivative
C_{lp}	Lateral-directional stability derivative
C_{nr}	Lateral-directional stability derivative
c	Chord length
D	Drag
D_b	Lateral differential operator
D_c	Longitudinal differential operator
D_p	Propeller diameter
D_{ref}	Reference diameter
$Downtime$	Reliability metric: Downtime
E	Young's modulus
$E_{s,bat}$	Battery specific energy
e	Oswald's efficiency factor
F	Prandtl tip loss factor
F_{fric}	Friction force
h	Height
I	Current
I_s	Sun incidence angle
$\bar{I}_s$	Average daytime incidence angle
$I_{s,max}$	Maximum sun incidence angle
i_{in}	Input current
i_{out}	Output current
K	Column effective length factor
K_X	Radius of gyration (roll)
K_{XZ}	Product radius of gyration
K_Y	Radius of gyration (pitch)
K_Z	Radius of gyration (yaw)
k	Thermal conductivity
k_1	Drag polar linear coefficient
k_2	Drag polar quadratic coefficient
L	Lift
$\mathscr{L}$	Likelihood of failure
l	Length
l_{TM}	Aerogel layer thickness
M	Mach number
M_{pay}	Mission payload state
m_{TO}	Take-off mass
q	Pitch rate
q_∞	Freestream dynamic pressure
Q	Torque
R	Radius
$\mathscr{R}$	Reliability
r	Yaw rate
$\hat{r}$	Radial position
Re	Reynolds number
S	Surface area
T	Thrust force
T_{ref}	Computed reference thrust force
T_{req}	Thrust force required
T_s	Daylight time
T_{TO}	Total thrust force at take-off
t	Thickness
$t_{mission}$	Mission time
t_{rise}	Sunrise time
t_{TM}	Temperature management time budget
$Uptime$	Reliability metric: Uptime
V	Velocity
V_{climb}	Climb velocity
V_{EAS}	Equivalent air speed
V_{TAS}	True air speed
V_∞	Freestream velocity
W	Weight
w	Width

Greek Symbols

α	Angle of attack
$\alpha_{damping}$	Damping factor
β	Blade pitch angle
χ_{att}	Attitude system state
δ	Sun declination angle
δ_a	Aileron deflection
δ_e	Elevator deflection
δ_r	Rudder deflection
ΔT	Temperature difference
η	Efficiency
λ	Advance ratio
Λ	Wing sweep angle
μ	Rolling friction coefficient
μ_b	Lateral relative density parameter
μ_c	Longitudinal relative density parameter
θ	Pitch angle
φ	Geometric inflow angle
φ_0	Uninduced geometric inflow angle
ϕ	Latitude / roll angle
ρ	Density
ρ_E	Energy mass density
σ	Axial stress
σ_y	Axial yield stress
σ_{ult}	Ultimate axial stress
τ	Shear stress
τ_{ult}	Ultimate shear stress

1. Introduction

The world is more dependent on satellites than ever, providing global interconnectivity through essential services ranging from cellular communication to weather monitoring. However, satellites are limited by their high cost of development and launch. In addition, their payloads are fixed, with little possibility of changing the missions and capabilities of a satellite once it has been launched. High-altitude platform systems offer an alternative, with the capability of providing the same services as satellites but at a local scale. For this reason, a preliminary design for an adaptable high-altitude platform system (AHAPS) is developed.

For the design of the AHAPS, a preliminary design was performed, which led to the choice of a flying wing with a battery configuration. In this report, this design will be worked out during the detailed design phase, developing and sizing its core subsystems, leading to a final design at the end of this report, and with that, concluding the project.

Project Objective

This project aims to create a detailed conceptual design for an adaptable high-altitude platform system, in short, AHAPS. The system aims to offer a cost-effective but reliable and modular alternative to a satellite in low Earth orbit. By cruising at 60,000 ft for a minimum of 28 days, it will provide capabilities such as ground observation and communications to areas with limited accessibility, where needed, rapidly deployable and efficiently transportable through the use of a 20 ft ISO container. Furthermore, the relatively low production costs compared to similar devices will ensure the AHAPS is accessible and can be used to its full potential.

Report Structure

The report will go through the design synthesis of the final design in a structured way, starting from a project description and ending with a discussion and recommendations for the future. In Chapter 2, a description of the project and the requirements is given. This is followed by necessary pre-design analyses in Chapter 3, which cover aspects such as the functional analysis, the engineering budgets, and sustainability. Then, the actual design synthesis is performed in Chapter 4, in which the design process for all subsystems is documented. Having completed this major part of the report, Chapter 5 provides an overview of the entire design coming together, giving a bigger picture. After this design is established, its performance is evaluated in Chapter 6. Following this, the robustness of the design is evaluated in Chapter 7 through verification and validation, risk assessment, and a reliability, availability, maintainability, and safety (RAMS) analysis. To ensure a bright future for the design, recommendations are given together with a Gantt chart covering the AHAPS lifetime, a manufacturing plan, and a commercial potential assessment, in Chapter 8. Ending with a conclusion and discussion in Chapter 9, the final design is once more discussed, and the final parameters are given.

2. Project Description

This chapter provides context on the design that has been carried out. It starts with some background information on the mission need and project objective in Section 2.1. This is followed by a description of the stakeholder needs in Section 2.2. Lastly, the requirement lists are presented in Section 2.3.

2.1. AHAPS Mission

To make the services provided by low Earth orbit (LEO) satellites accessible on a local scale and for a lower price, the AHAPS is designed to address the market of developing countries that do not have access to conventional satellites and that do not have good ground infrastructure. It accommodates various payloads with possible functions such as crop monitoring, forest fire detection, and high-bandwidth communications in remote regions, all of which are sustained for extended periods of time [4]. Following the established requirements, the Mission Need Statement is '*Design a cost-effective and adaptable platform to provide consistent communication and sensing to regions where satellite or ground infrastructure is impractical or limited*'.

2.2. Stakeholder Needs

Many different stakeholders are affected by this system, including operators, citizens, regulators, and the environment. The list of stakeholder needs is as follows:

1. The system shall support a modular payload configuration to enable flexible mission adaptation.
2. The system shall operate with minimal ground monitoring requirements during flight.
3. The system shall achieve long endurance flight to maximise operational coverage.
4. The system shall enable easy assembly and disassembly to reduce ground handling time.
5. The system shall be capable of autonomous operation without continuous human intervention.
6. The system shall be easily transportable to enable deployment from varied locations.
7. The system shall operate at high altitude to provide wide-area coverage.
8. The system shall utilise recyclable materials and components to minimise environmental impact.
9. The system shall be designed for a long service life to reduce lifecycle costs.
10. The system shall hold appropriate certifications for operation in relevant airspace.
11. The system shall support telecommunication payloads and services.

To summarize the stakeholder needs and make them more explicit, the Project Objective Statement is *Design a modular, low-cost, adaptable high altitude platform system, capable of operating at* 60,000 *ft for at least* 28 *days, carrying a variety of equipment.*

2.3. AHAPS Requirement Lists

Based on the mission description and the stakeholder needs, lists of requirements have been formulated. The stakeholder requirements are presented in Table 2.1.

Table 2.1: Complete list of AHAPS stakeholder requirements.

ID	Category	Requirement Description
REQ-STK-1.1	Performance	The AHAPS shall maintain a minimum cruise altitude of 60,000 ft.
REQ-STK-1.2	Performance	The AHAPS shall sustain continuous flight operations for a minimum endurance of 28 days under all-season conditions.
REQ-STK-1.3	Performance	The AHAPS loitering operations shall be autonomous.
REQ-STK-1.4	Performance	The AHAPS shall be deployable between latitudes 30°S and 30°N.

Continued on next page

ID	Category	Requirement Description
REQ-STK-1.5	Performance	The AHAPS shall be capable of taking off and landing from unpaved but prepared flat surfaces.
REQ-STK-1.6	Performance	The AHAPS shall provide a horizontal communication range of at least 400 km between the platform and ground systems.
REQ-STK-1.7	Performance	The AHAPS shall have a Secondary Surveillance Radar (SSR) transponder.
REQ-STK-1.8	Performance	The AHAPS shall have an ADS-B transmitter.
REQ-STK-1.9	Performance	The AHAPS onboard power system shall have a service life of at least two years, assuming 50% utilisation equivalent to approximately 180 days of operational use per year.
REQ-STK-1.10	Performance	The AHAPS shall have a minimum payload data stream of 1 Mbit/s.
REQ-STK-2.1	Safety	The AHAPS shall require no intermittent human monitoring more than once per day by ground operators during operations.
REQ-STK-2.2	Safety	The AHAPS shall have a health monitoring system that provides data to support operational decision-making.
REQ-STK-2.3	Safety	The AHAPS shall have an Emergency Locator Transmitter (ELT) beacon.
REQ-STK-2.4	Safety	The AHAPS shall comply with EASA Civil Drones certification requirements, with operations conducted under type #1.
REQ-STK-3.1	Sustainability	The AHAPS shall be constructed from materials that are either recyclable or inert upon disposal.
REQ-STK-3.2	Sustainability	The AHAPS shall be designed for full retrieval without abandoned system components or debris in the environment.
REQ-STK-3.3	Sustainability	The AHAPS shall utilize a modular architecture that allows for the independent replacement, repair, or upgrade of high-impact components without requiring the disposal of materials.
REQ-STK-4.1	Engineering Budgets	The AHAPS shall provide a payload mass budget of at least 20 kg.
REQ-STK-4.2	Engineering Budgets	The AHAPS shall accommodate payload energy demands consisting of intermittent peak loads of up to 250 W within 5 minute windows.
REQ-STK-4.3	Engineering Budgets	The AHAPS shall have a sustained average payload power draw of 100 W.
REQ-STK-4.4	Engineering Budgets	The AHAPS shall be capable of managing payload heat dissipation of up to 150 W.
REQ-STK-4.5	Engineering Budgets	The AHAPS shall provide the structural and interface provisions necessary to mount a synthetic aperture radar (SAR) antenna with a footprint of 1×1 m.
REQ-STK-4.6	Engineering Budgets	The AHAPS shall provide a communications link to the payload supporting control.
REQ-STK-4.7	Engineering Budgets	The AHAPS shall provide a communications link to the system monitoring telemetry.
REQ-STK-5.1	Schedule	The AHAPS concept engineering phase shall be completed within 7 weeks by a design team of 10 persons.
REQ-STK-6.1	Cost	The AHAPS materials and manufacturing cost per unit shall not exceed 900,000 Euro.
REQ-STK-7.1	Transport	The AHAPS shall be transportable within a standard 20 ft ISO shipping container.
REQ-STK-8.1	Logistics	The AHAPS shall support final field assembly using limited tooling, without requiring specialist workshop infrastructure.
REQ-STK-8.2	Logistics	The AHAPS shall be fully self-contained where all components necessary for assembly, flight and monitoring shall be included.
REQ-STK-8.3	Logistics	The AHAPS shall not require any externally supplied consumables (e.g. fuel) for operation.

The driving and key subsystem requirements are presented in Table 2.2. These requirements have a large impact on the design process. Note that every TBD in the table is justified for in Section 7.4.1.

Table 2.2: AHAPS subsystem requirements.

ID	Subsystem	Description	Stakeholder ID	Type
REQ-SSY-1.02	Airframe	The airframe system shall provide heat management capabilities (dissipation, redirection, and generation) to sustain the operating temperatures of the payload, power, and computer systems.	REQ-STK1.1-MIS1.2-SYS1.4	
REQ-SSY-1.04	Airframe	The airframe system shall nominally generate sufficient lift during cruise to incur a load factor of 1.	REQ-STK1.1-MIS1.1-SYS1.01	Driving

Continued on next page

ID	Subsystem	Description	Stakeholder ID	Type
REQ-SSY-1.05	Airframe	The airframe system shall withstand a maximum lift equivalent to 2.5 times the nominal MTOW during cruise.	REQ-STK1.1-MIS1.1-SYS1.01	Driving
REQ-SSY-1.06	Airframe	The airframe system shall prevent a deflection of the wing greater than 5 m during nominal cruise conditions.	REQ-STK1.1-MIS1.2-SYS1.05-1.09	
REQ-SSY-1.07	Airframe	The airframe system shall withstand a maximum drag equivalent to 2.5 times the nominal drag during cruise.	REQ-STK1.1-MIS1.1-SYS1.01	Driving
REQ-SSY-1.08	Airframe	The airframe system shall structurally resist load factors of up to 2.5 g.	REQ-STK1.1-MIS1.2-SYS1.05-1.09	
REQ-SSY-1.15	Airframe	The airframe system shall facilitate take-off and landing from a prepared sand-covered runway.	REQ-STK1.5-MIS1.22-SYS-1.31	
REQ-SSY-1.16	Airframe	The airframe system shall facilitate take-off and landing from a prepared gravel runway.	REQ-STK1.5-MIS1.22-SYS-1.29	
REQ-SSY-1.17	Airframe	The airframe system shall facilitate take-off and landing from a prepared grass runway.	REQ-STK1.5-MIS1.22-SYS-1.30	
REQ-SSY-1.18	Airframe	The airframe system shall ensure appropriate operational radiation shielding for its inner content for a radiation level up to TBD rad/s.	REQ-STK1.1-MIS1.6-SYS1.12	
REQ-SSY-1.20	Airframe	The airframe system shall support a payload mass budget of at least 20 kg.	REQ-STK4.1-MIS4.1-SYS1.39	Driving
REQ-SSY-1.21	Airframe	The airframe system shall be capable of managing payload heat dissipation of up to 150 W.	REQ-STK4.4-MIS4.4-SYS1.43	Key
REQ-SSY-1.22	Airframe	The total cost of the airframe system shall not exceed €270,000.	REQ-STK6.1-MIS6.1-SYS6.2	Driving
REQ-SSY-1.23	Airframe	The materials and components cost of the airframe system shall not exceed 25% of the total system cost.	REQ-STK6.1-MIS6.1-SYS6.3	Driving
REQ-SSY-1.25	Airframe	The airframe system shall adhere to all of the general subsystem requirements.	All stakeholder IDs of REQ-SSY-9.X	
REQ-SSY-2.01	Communication	The communication system shall contain an ADS-B transmitter.	REQ-STK1.8-MIS1.25-SYS-1.34	
REQ-SSY-2.02	Communication	The communication system shall contain an Emergency Locator Transmitter (ELT) beacon.	REQ-STK1.8-MIS1.25-SYS-1.37	
REQ-SSY-2.03	Communication	The communication system shall provide a horizontal communication range of at least 400 km between the platform and ground systems.	REQ-STK1.6-MIS1.23-SYS1.32	Key
REQ-SSY-2.04	Communication	The communication system shall contain a Secondary Surveillance Radar (SSR) transponder.	REQ-STK1.7-MIS1.24-SYS1.33	
REQ-SSY-2.05	Communication	The communication system shall be capable of providing a minimum payload data stream of 1 Mbit/s.	REQ-STK1.10-MIS1.27-SYS1.36	Key
REQ-SSY-2.06	Communication	The communication system shall provide a communications link to the payload supporting control.	REQ-STK4.6-MIS4.6-SYS1.46	
REQ-SSY-2.07	Communication	The communication system shall provide a communications link to the system monitoring telemetry.	REQ-STK4.7-MIS4.7-SYS1.47	
REQ-SSY-2.08	Communication	The total cost of the communication system shall not exceed €67,500.	REQ-STK6.1-MIS6.1-SYS6.2	Driving
REQ-SSY-2.11	Communication	The AHAPS user shall not be required to allocate more than three individuals for external communications.	REQ-STK2.1-MIS2.2-SYS1.49	
REQ-SSY-2.12	Communication	The communication system shall adhere to all of the general subsystem requirements.	All stakeholder IDs of REQ-SSY-9.X	
REQ-SSY-3.2	Computer	The manufacturing cost of the computer system shall not exceed €2,000.	REQ-STK6.1-MIS6.1-SYS6.2	Driving
REQ-SSY-3.5	Computer	The computer system shall adhere to all of the general subsystem requirements.	All stakeholder IDs of REQ-SSY-9.X	

Continued on next page

ID	Subsystem	Description	Stakeholder ID	Type
REQ-SSY-3.7	Computer	The computer system shall be radiation-hardened for TBD rad/s.	REQ-STK1.1-MIS1.6-SYS1.12	
REQ-SSY-4.01	Control	The computer system shall be able to provide the control commands at a frequency of TBD Hz.	REQ-STK1.3-MIS1.9-SYS1.16	
REQ-SSY-4.03	Control	The control system shall be able to tolerate a radiation over time of TBD rad/s.	REQ-STK1.1-MIS1.6-SYS1.12	
REQ-SSY-4.04	Control	The manufacturing cost of the control system shall not exceed €70,000.	REQ-STK6.1-MIS6.1-SYS6.2	Driving
REQ-SSY-4.07	Control	The control system shall adhere to all of the general subsystem requirements.	All stakeholder IDs of REQ-SSY-9.X	
REQ-SSY-4.08	Control	The control system shall be able to loiter the product within an area of 400×400 km^2.	REQ-STK1.3-MIS1.9-SYS1.15	Key
REQ-SSY-4.09	Control	The control system shall provide a yawing effectiveness of at least 5 deg/s at sea level.	REQ-STK1.3-MIS1.9-SYS1.17	Key
REQ-SSY-4.10	Control	The control system shall provide a pitching effectiveness of at least ± 3 deg/s at sea level.	REQ-STK1.3-MIS1.9-SYS1.18	Key
REQ-SSY-4.11	Control	The control system shall be able to reverse a 45 deg turn in less than wingspan/3 sec.	REQ-STK1.3-MIS1.9-SYS1.19	Key
REQ-SSY-4.15	Control	The control system shall provide sufficient control authority to land the AHAPS in a One Engine Inoperative situation.	REQ-STK1.3-MIS1.10-SYS1.17-SYS1.18-SYS1.19	
REQ-SSY-5.1	Flight Condition	The manufacturing cost of the flight condition system shall not exceed €63,000.	REQ-STK6.1-MIS6.1-SYS6.2	Driving
REQ-SSY-5.2	Flight Condition	The materials cost of the flight condition system shall not exceed 25% of the total subsystem cost.	REQ-STK6.1-MIS6.1-SYS6.3	Driving
REQ-SSY-5.4	Flight Condition	The flight condition system shall adhere to all of the general subsystem requirements.	All stakeholder IDs of REQ-SSY-9.X	
REQ-SSY-5.6	Flight condition	The flight condition system shall be able to tolerate a radiation over time of TBD rad/s.	REQ-STK1.1-MIS1.6-SYS1.12	
REQ-SSY-5.7	Flight Condition	The flight condition system shall provide its location with error 0.1 NM.	REQ-STK1.3-MIS1.9-SYS1.15	Key
REQ-SSY-6.2	Payload	The payload system shall be capable of providing a minimum payload data stream of 1 Mbit/s to the communication system.	REQ-STK2.4-MIS2.5-SYS1.36	Key
REQ-SSY-6.3	Payload	The manufacturing cost of the payload system shall not exceed €22,500.	REQ-STK6.1-MIS6.1-SYS6.2	Driving
REQ-SSY-6.6	Payload	The payload system shall adhere to all of the general subsystem requirements.	All stakeholder IDs of REQ-SSY-9.X	
REQ-SSY-6.7	Payload	The payload system shall provide a modular payload bay of dimensions equal to at least $0.2 \times 0.4 \times 0.2$ m^3.	REQ-STK4.1-MIS4.1-SYS1.40	
REQ-SSY-6.8	Payload	The payload system shall provide the structural and interface provisions necessary to mount a synthetic aperture radar (SAR) antenna with a footprint of 1×1 m.	REQ-STK4.5-MIS4.5-SYS1.44	
REQ-SSY-7.01	Power	The power system shall have a service life of at least two years, assuming 50% usage (i.e., 180 days operative per year).	REQ-STK1.9-MIS1.26-SYS1.35	
REQ-SSY-7.02	Power	The power system shall maintain its temperature between 283 K and 318 K.	REQ-STK1.1-MIS1.2-SYS1.04-SYS1.21	
REQ-SSY-7.03	Power	The power system shall provide sufficient energy to sustain operations in cruise with full payload utilisation at all times for a minimum of 28 days.	REQ-STK1.2-MIS1.7-SYS1.13	Driving
REQ-SSY-7.04	Power	The power system shall store enough energy to maintain altitude and payload operations continuously, during nighttime at 60,000 ft during the winter solstice, without power generation.	REQ-STK1.2-MIS1.8-SYS1.14	

Continued on next page

ID	Subsystem	Description	Stakeholder ID	Type
REQ-SSY-7.05	Power	The power system shall provide the payload system with intermittent peak power of up to 250 W within 5 minute windows.	REQ-STK4.2-MIS4.2-SYS1.41	Driving
REQ-SSY-7.06	Power	The power system shall provide an average payload power of 100 W.	REQ-STK4.3-MIS4.3-SYS1.42	Driving
REQ-SSY-7.08	Power	The manufacturing cost of the power system shall not exceed €270,000.	REQ-STK6.1-MIS6.1-SYS6.2	Driving
REQ-SSY-7.11	Power	The power system shall adhere to all of the general subsystem requirements.	All stakeholder IDs of REQ-SSY-9.X	
REQ-SSY-7.12	Power	The power system shall provide enough energy to sustain climbing operations without depleting night reserves.	REQ-STK1.1-MIS1.1-SYS1.2	
REQ-SSY-7.13	Power	The power system shall generate sufficient power to complete the cruise phase at latitudes between 30°S and 30°N.	REQ-STK1.4-MIS1.11-SYS1.20	Driving
REQ-SSY-8.01	Propulsion	The propulsion system shall provide sufficient thrust to maintain a cruise speed of no less than 25.0 m/s.	REQ-STK1.1-MIS1.5-SYS1.10	
REQ-SSY-8.04	Propulsion	The propulsion system shall generate sufficient thrust for take-off and landing from a prepared sand-covered runway.	REQ-STK1.5-MIS1.22-SYS-1.31	
REQ-SSY-8.05	Propulsion	The manufacturing cost of the propulsion system shall not exceed €135,000.	REQ-STK6.1-MIS6.1-SYS6.2	Driving
REQ-SSY-8.08	Propulsion	The propulsion system shall adhere to all of the general subsystem requirements.	All stakeholder IDs of REQ-SSY-9.X	
REQ-SSY-8.09	Propulsion	The propulsion system shall generate sufficient thrust for take-off and landing from a prepared gravel runway.	REQ-STK1.5-MIS1.22-SYS-1.29	
REQ-SSY-8.10	Propulsion	The propulsion system shall generate sufficient thrust for take-off and landing from a prepared grass runway.	REQ-STK1.5-MIS1.22-SYS-1.30	
REQ-SSY-8.11	Propulsion	The propulsion system shall be able to tolerate a radiation over time of TBD rad/s.	REQ-STK1.1-MIS1.6-SYS1.12	
REQ-SSY-8.12	Propulsion	The propulsion system shall provide enough thrust to achieve a sea-level climb angle of 3 deg.	REQ-STK1.1-MIS1.1-SYS1.2	
REQ-SSY-9.01	General	The AHAPS product shall be chemically stable and non-toxic, with no hazardous byproducts upon disposal, as validated by environmental safety testing EPA compliance.	REQ-STK3.1-MIS3.1-SYS5.2	Key
REQ-SSY-9.02	General	The AHAPS product shall utilize a modular architecture that allows for the independent replacement, repair, or upgrade of high-impact components without requiring the disposal of materials.	REQ-STK3.3-MIS3.4-SYS4.3	
REQ-SSY-9.03	General	The AHAPS product shall include a maintenance report to ensure components are inspected, repaired, or replaced as needed to achieve 12 mission cycles.	REQ-STK3.2-MIS3.3-SYS4.1	
REQ-SSY-9.04	General	The AHAPS product shall be designed for final field assembly using only standard, handheld tools (e.g., wrenches, screwdrivers, pliers, torque wrenches) commonly available.	REQ-STK8.1-MIS8.1-SYS3.09	
REQ-SSY-9.05	General	All operational resources shall be included in the standard 20 ft ISO shipping container (e.g., tooling, consumables, and assembly components, etc.).	REQ-STK7.1-MIS7.2-SYS3.08	
REQ-SSY-9.06	General	The AHAPS product shall include a redundant and reusable recovery system.	REQ-STK3.2-MIS3.2-SYS3.01	
REQ-SSY-9.07	General	The AHAPS shall be designed to use standard, commercially available fasteners, connectors, and interfaces.	REQ-STK8.1-MIS8.1-SYS3.10	

Continued on next page

ID	Subsystem	Description	Stakeholder ID	Type
REQ-SSY-9.08	General	The AHAPS product shall have a health monitoring system that provides data to support operational decision-making.	REQ-STK2.2-MIS2.3-SYS3.11	
REQ-SSY-9.09	General	The AHAPS products shall be designed to not require any externally supplied consumables (e.g., fuel) for operation.	REQ-STK-8.3-MIS8.3-SYS3.12	
REQ-SSY-9.10	General	The AHAPS components necessary for assembly shall be designed to occupy no more than 95% of the 20 ft container volume.	REQ-STK8.2-MIS8.2-SYS3.13	
REQ-SSY-9.13	General	The AHAPS product shall include redundant trackable components using GPS to locate and retrieve the product.	REQ-STK3.2-MIS3.2-SYS3.02	
REQ-SSY-9.14	General	The AHAPS product shall be designed with materials and components able to withstand loads to fulfill at least 12 mission cycles before being decommissioned.	REQ-STK3.2-MIS3.3-SYS3.03	
REQ-SSY-9.15	General	The AHAPS product shall maintain all flight-critical functions for at least 12 mission cycles before being overhauled.	REQ-STK3.2-MIS3.3-SYS3.04	
REQ-SSY-9.16	General	The AHAPS concept engineering phase shall be completed within seven weeks by a design team of 10 persons.	REQ-STK-5.1-MIS5.1-SYS3.05	
REQ-SSY-9.17	General	The AHAPS product shall be designed to be collapsible or modular in no more than 40 parts to facilitate assembly, disassembly, and secure storage in the 20 ft ISO container.	REQ-STK7.1-MIS7.1-SYS3.07	
REQ-SSY-9.18	General	The AHAPS user shall not be required to allocate more than three individuals for transporting the AHAPS product to its designated launch site.	REQ-STK2.1-MIS2.2-SYS1.50	
REQ-SSY-9.19	General	The AHAPS user shall not be required to monitor the communication system more than once every 24-hour interval, starting from take-off.	REQ-STK2.1-MIS2.1-SYS1.48	Key
REQ-SSY-9.20	General	The AHAPS product shall be loaded and unloaded from the 20 ft ISO shipping container by three people.	REQ-STK7.1-MIS7.1-SYS1.51	
REQ-SSY-9.21	General	The AHAPS product shall be loaded and unloaded from the 20 ft ISO shipping container without external (not included in the container) machines.	REQ-STK7.1-MIS7.1-SYS1.52	Driving
REQ-SSY-9.22	General	The AHAPS product shall comply with EASA Civil Drones certification requirements, with operations conducted under type 1.	REQ-STK2.4-MIS2.5-SYS1.38	Driving

3. Pre-Design Analyses

This chapter covers the analyses conducted and the choices made during the pre-design phase, which will subsequently guide the team during the design process. Section 3.1 defines the subsystems of the AHAPS, Section 3.2 gives an overview of all the functions the aircraft must be able to perform, and Section 3.3 illustrates the estimations for volume, mass, and cost. Finally, Section 3.4 and Section 3.5 give an overview of the HAPS market and the sustainable development strategy the design team pursues.

3.1. Subsystem Definition

Subsystems of the AHAPS are defined based on a general aerial system. Together, they form the complete operational system. The definitions guide the design process. The subsystems are listed in Table 3.1. The temperature management system and the undercarriage are part of the airframe, yet are separately mentioned to address their respective designs. The subsystems interface with each other following the N2-chart shown in Figure 3.1. The adjacent table, Table 3.2, shows the symbol explanations for all subsystems.

Table 3.1: List of subsystem definitions.

Subsystem	**Abbreviation**	**Definition**
Payload	PAY	Systems necessary for securing and maintaining the payload.
Flight Condition	FCS	Systems for the determination of flight characteristics, such as velocity and altitude, but also for attitude and position.
Computer	COMP	All components necessary for the main flight computer, including data cables to all other subsystems.
Communication	COMMS	All systems necessary for communication.
Airframe	AIR	All structural parts of the AHAPS, including control surfaces.
- Temperature Management	TEMP	The systems that manage the temperature of the payload and other structures.
- Undercarriage	UCAR	The structures necessary to facilitate take-off and landing of the AHAPS.
Power	POW	The components that provide power to the AHAPS, including power cables to all other subsystems.
Propulsion	PROP	All systems included in the propulsion domain of the AHAPS.
Control	CTRL	Parts and systems for control of the AHAPS, excluding control surfaces.

Table 3.2: N2 chart symbol description.

Description	**Symbol**	**Unit**	**Description**	**Symbol**	**Unit**
Forces			***External Conditions***		
Propulsion System Weight	W_{prop}	N	Atmospheric Conditions Vector	$\mathbf{C}_{\text{atm}}$	various
Control System Weight	W_{ctrl}	N	Flight Motion Vector	$\mathbf{x}_{\text{mot}}$	various
Power System Weight	W_{pow}	N	Flight Attitude Vector	$\boldsymbol{\chi}_{\text{att}}$	rad
Computer System Weight	W_{comp}	N	***Powers***		
Communication System Weight	W_{comm}	N	Propulsion Power	P_{prop}	W
Payload System Weight	W_{pay}	N	Control System Power	P_{ctrl}	W
Flight Condition System Weight	W_{fcs}	N	Computer Power	P_{comp}	W
Thrust	F_{T}	N	Communication Power	P_{comm}	W
Aerodynamic Force Vector	$\mathbf{F}_{\text{aero}}$	N	Payload Power	P_{pay}	W
Vibrations			Flight Condition System Power	P_{fcs}	W
Propulsion System Vibration	$\mathbf{u}_{\text{prop}}$	m, Hz	Propulsion Power Required	$P_{\text{r,prop}}$	W
Control System Vibration	$\mathbf{u}_{\text{ctrl}}$	m, Hz	Control System Power Required	$P_{\text{r,ctrl}}$	W
Power System Vibration	$\mathbf{u}_{\text{pow}}$	m, Hz	Computer Power Required	$P_{\text{r,comp}}$	W

Continued on next page

(continued)

Description	Symbol	Unit	Description	Symbol	Unit
Computer System Vibration	$\mathbf{u}_{\text{comp}}$	m, Hz	Communication Power Required	$P_{\text{r,comm}}$	W
Communication System Vibration	$\mathbf{u}_{\text{comm}}$	m, Hz	Payload Power Required	$P_{\text{r,pay}}$	W
Payload System Vibration	$\mathbf{u}_{\text{pay}}$	m, Hz	FCS Power Required	$P_{\text{r,fcs}}$	W
Airframe Vibration	$\mathbf{u}_{\text{air}}$	m, Hz	***Signal Informations***		
Flight Condition System Vibration	$\mathbf{u}_{\text{fcs}}$	m, Hz	Outward Information (Transmission)	$\mathbf{i}_{\text{out}}$	bits
Internal Conditions			Inward Information (Reception)	$\mathbf{i}_{\text{in}}$	bits
Propulsion System Internal Temp	T_{prop}	K	Payload Measurement Vector	$\mathbf{M}_{\text{pay}}$	various
Control System Internal Temp	T_{ctrl}	K	***Settings***		
Power System Internal Temp	T_{pow}	K	Propulsion System Settings	$\mathbf{s}_{\text{prop}}$	–
Communication System Internal Temp	T_{comm}	K	Control System Settings	$\mathbf{s}_{\text{ctrl}}$	–
Payload Internal Temp	T_{pay}	K	Power System Settings	$\mathbf{s}_{\text{pow}}$	–
Airframe Internal Temp	T_{airf}	K	Communication System Settings	$\mathbf{s}_{\text{comm}}$	–
FCS Internal Temp	T_{fcs}	K	Payload System Settings	$\mathbf{s}_{\text{pay}}$	–
Propulsion System Heat Inflow	$\dot{Q}_{\text{in,prop}}$	W	Airframe Settings	$\mathbf{s}_{\text{airf}}$	–
Propulsion System Heat Outflow	$\dot{Q}_{\text{out,prop}}$	W	FCS Settings	$\mathbf{s}_{\text{fcs}}$	–
Control System Heat Inflow	$\dot{Q}_{\text{in,ctrl}}$	W	***Directions***		
Control System Heat Outflow	$\dot{Q}_{\text{out,ctrl}}$	W	Current Position Coordinates	$\mathbf{p}_{\text{cur}}$	∘, ∘, m
Power System Heat Inflow	$\dot{Q}_{\text{in,pow}}$	W	Area of Interest Coordinates	$\mathbf{p}_{\text{aoi}}$	∘, ∘, m
Power System Heat Outflow	$\dot{Q}_{\text{out,pow}}$	W	***Angles***		
Computer System Heat Inflow	$\dot{Q}_{\text{in,comp}}$	W	Roll Control Deflection	$\boldsymbol{\delta}_{\theta}$	rad
Computer System Heat Outflow	$\dot{Q}_{\text{out,comp}}$	W	Pitch Control Deflection	$\boldsymbol{\delta}_{\phi}$	rad
Communication System Heat Inflow	$\dot{Q}_{\text{in,comm}}$	W	Yaw Control Deflection	$\boldsymbol{\delta}_{\psi}$	rad
Communication System Heat Outflow	$\dot{Q}_{\text{out,comm}}$	W	Thrust Angle Vector	$\boldsymbol{\alpha}_{\text{T}}$	rad, rad, rad
Payload System Heat Inflow	$\dot{Q}_{\text{in,pay}}$	W			
Payload System Heat Outflow	$\dot{Q}_{\text{out,pay}}$	W			
FCS Heat Inflow	$\dot{Q}_{\text{in,fcs}}$	W			
FCS Heat Outflow	$\dot{Q}_{\text{out,fcs}}$	W			

Propulsion									T	$\mathbf{u}$	P_r							W	$\mathbf{u}$	$\dot{Q}$			
																		F_T	$\boldsymbol{\alpha}_T$				
			Control						T	$\mathbf{u}$	P_r							W	$\mathbf{u}$	$\dot{Q}$			
									$\boldsymbol{\delta}_\theta$	$\boldsymbol{\delta}_\phi$	$\boldsymbol{\delta}_\psi$							$\boldsymbol{\delta}_\theta$	$\boldsymbol{\delta}_\phi$	$\boldsymbol{\delta}_\psi$			
P			P			**Power**			T	P	$\mathbf{u}$	P			P			W	$\mathbf{u}$	$\dot{Q}$	P		
$\mathbf{s}$			$\mathbf{s}$			$\mathbf{s}$			**Computer**			$\mathbf{i}_{\text{out}}$	$\mathbf{s}$		$\mathbf{i}_{\text{in}}$	$\mathbf{s}$		W	$\mathbf{u}$	$\dot{Q}$	$\mathbf{s}$		
																		$\mathbf{s}$					
									T	$\mathbf{i}_{\text{in}}$	$\mathbf{u}$	**Comms**						W	$\mathbf{u}$	$\dot{Q}$			
									$\mathbf{p}_{\text{aoi}}$	P_r													
									T	$\mathbf{u}$	$\mathbf{M}$				**Payload**			W	$\mathbf{u}$	$\dot{Q}$			
									P_r														
$\mathbf{u}$	$\dot{Q}$		$\mathbf{u}$	$\dot{Q}$		$\mathbf{u}$	$\dot{Q}$		$\mathbf{u}$	$\dot{Q}$	T	$\mathbf{u}$	$\dot{Q}$		$\mathbf{u}$	$\dot{Q}$		**Airframe**			$\mathbf{u}$	$\dot{Q}$	$\mathbf{x}_{\text{mot}}$
																					$\boldsymbol{\chi}_{\text{att}}$		
									T	$\mathbf{C}_{\text{atm}}$	$\mathbf{x}_{\text{mot}}$							W	$\mathbf{u}$	$\dot{Q}$	**Flight Condition**		
									$\boldsymbol{\chi}_{\text{att}}$	$\mathbf{u}$	$\mathbf{p}_{\text{cur}}$							$\mathbf{F}_{\text{aero}}$					
									P_r														

Figure 3.1: N2 Interface Matrix with dropped subscripts for brevity.

3.2. Functional Analysis

A functional analysis is performed to find all the functions that the AHAPS product has to perform. Top-level functions are defined per mission stage, which are broken up into lower levels. The functional breakdown structure and functional flow diagram that are the result of this analysis are shown in Section 3.2.1 and Section 3.2.2.

3.2.1. Functional Breakdown Structure

The Functional Breakdown Structure (FBS), displayed in Section A.1, provides a non-temporal overview of all functions to be performed throughout the mission. The FBS is organised into five levels. The first level consists of the product initiation, the product introduction, and the product life. The product initiation includes the design, manufacturing, and making the documentation needed for the future life of the product. Product introduction is followed by the product life cycle. The product life consists of all the functions that the product will have to perform during its operational life-cycle, from transport to the launch site, to the decommissioning of the product. Level two includes the mission functions, and level three includes the system functions. Levels four and five go into the subsystem functions that have been derived from the stakeholder needs and requirements.

All functions have an identifier, and the lowest-level functions per branch have a designated colour. The

colours link the lowest-level functions to the designated subsystems. The subsystems have been defined as the propulsion system, control system, power system, computer system, communication system, payload system, airframe system, and the flight condition system. The temperature management system and the undercarriage system are part of the airframe system. Functions that are assigned to these two subsystems therefore have been given the colour for the airframe system.

3.2.2. Functional Flow Diagram

The Functional Flow Diagram (FFD), displayed in Section A.2, provides the temporal dependency structure of the functions defined in the FBS. Levels two and three are allocated to one of the seven mission systems. The mission systems include the design team, manufacturing team, maintenance team, decommissioning team, user (the operator), the product itself, and functions that are a combination of both the user and the product. These mission functions are then subdivided into system and subsystem functions. The lowest-level functions per branch have been allocated to a subsystem, as described in the FBS. The abbreviation 'REF' is used to reference a function 'F' and to expand it for a more organised structure.

3.3. Engineering Budgets

This section will outline the different initial engineering budgets set up before the design of the AHAPS. This includes the volumetric budget for the 20 ft ISO container in Section 3.3.1, the mass budget of the maximum take-off weight in Section 3.3.2, and finally the cost division of each subsystem in Section 3.3.3.

3.3.1. Volume

The volumetric budget for the AHAPS mission is largely restricted by the size of a 20 ft ISO container, in which the full product must fit, as stated by **REQ-STK-7.1**. This includes all product components and tooling to be used during in-field assembly. The 20 ft ISO container has internal dimensions of 5.898 m x 2.350 m x 2.390 m with a total internal volume of 33.13 m^3[1].

The container allocated volume for the different components that need to be transported is given by Table 3.3. Most of the tooling is contained in a toolbox, of which the size is up to 0.6 m^3[2]. Additional tooling, such as assembly jacks and a pallet truck, is estimated to take up no more than 1.0 m^3 extra space[3]. Overall, a 5% volume fraction is assumed for tooling. The monitoring equipment for the ground station is estimated to take up at most 10% of the ISO container volume[4].

The product is allocated 85% of the container volume, which leads to a volume of 28.16 m^3. Of that 85%, the 20 ft ISO container space utilization of a modular AHAPS aircraft is around 71.4% [5]. This leads to a utilization volume for the product of approximately 20.1 m^3. The exact layout of the container packing when the final design is chosen is explained in Section 6.2.1.

Table 3.3: Volume fraction estimations of the 20 ft ISO Container.

Component	**Volume Fraction (%)**	**Volume (m^3)**
Product	85	28.16
Tooling	5	1.66
Monitoring Equipment	10	3.31

3.3.2. Mass

The mass fraction allocates what percentage of the MTOW is allocated to each of the eight aircraft subsystems in Table 3.1. The mass fraction allocation given in Table 3.4 is a general estimation for the class of HTA HAPS aircraft [6]. The data used to estimate the mass fractions originates from HAPS with a significantly higher MTOW than planned for the AHAPS, meaning that the obtained fractions are limited in accuracy for this size class. For this reason, these mass fractions are mainly used to verify that the mass fractions obtained from the final sizing are in line with similar systems.

[1] https://freightfinders.com/container-transport/20-feet-iso-container/ [cited 11 June 2026]
[2] https://supplyapp.com/facility-maintenance-tool-set-tool-cart-p14vy75.html [cited 22 June 2026]
[3] https://amzn.eu/d/0jkMyx9I [cited 22 June 2026]
[4] https://www.albaorbital.com/alba-connect-station [cited 22 June 2026]

Table 3.4: Mass budget division as a percentage of the maximum take-off weight (MTOW) for a general heavier-than-air (HTA) high altitude platform system.

Subsystem	**HTA Mass Fraction (%)**
Propulsion	7.7
Control	1.0
Power	45.0
Computer	0.1
Communication	0.4
Airframe	37.0
Payload	8.7
Flight Condition	0.1

3.3.3. Costs

With **REQ-STK-6.1** being formed, this gives an upper limit for the material and manufacturing costs of the AHAPS product. To ensure that all subsystems have a properly assigned division of this budget, an initial division has been made, which can be seen in Table 3.5. These are the total expected costs for each subsystem, which gives an initial aim for the budgets. Next to the costs, the types of components that belong to each subsystem are listed together with the corresponding subsystems.

Table 3.5: Cost budget division, prices in the year 2026.

Subsystem	**Assigned Cost (€) (FY26)**
Airframe - Wing structure, control surfaces, internal structure, connections	€270,000
Power - Solar panels, batteries, power cables, thermal management	€315,000
Propulsion - Motors, motor mounting,propellers	€135,000
Communication - Transmitter/receiver, antenna	€25,000
Computer - Flight computer, data storage, cables connected to computer	€800
Control - Actuators	€90,000
Flight Condition - Sensors	€20,000
Payload - Payload mounting	€300

3.4. Business Case

High Altitude Platform Systems (HAPS) represent a growing market, with platforms capable of performing their mission in the stratosphere, typically at altitudes between 18 and 22 km[1]. The use cases for HAPS are vast and are thus an attractive alternative to already existing infrastructure and systems. Entering this emerging market requires knowledge about where potential customers are based, what platform customers may use, and how they would use it.

The size and growth of the HAPS market are difficult to estimate due to its nature as an emerging market. However, studies suggest the current market value sits between €100M and €1.5B[1][2][3][4]. The HAPS market, while still in its relative infancy, indicates a reasonably large growth rate with an expected Cumulative Average Growth Rate (CAGR) to be within $14\% - 20\%$ for the next six years. The relatively small market size, but large growth prospects, make it an ideal business opportunity.

The HAPS market itself can be split up into three main platform types: Heavier-than-Air (HTAs), balloons, and airships. HTAs benefit from technological maturity and great maneuverability, which help reduce regulatory barriers that exist for novel solutions. This results in HTAs being the most popular HAPS developed by competitors, with projections indicating they would account for 48% of the market between 2019 and

[1]https://www.grandviewresearch.com/industry-analysis/high-altitude-platforms-market-report [cited 29 April 2026]
[2]https://www.marketsandmarkets.com/Market-Reports/high-altitude-pseudo-satellite-haps-market-162217471.html [cited 29 April 2026]
[3]https://www.fortunebusinessinsights.com/high-altitude-pseudo-satellites-market-115062 [cited 29 April 2026]
[4]https://www.credenceresearch.com/report/high-altitude-platforms-haps-market [cited 29 April 2026]

2029[1]. These often share similar technical specifications, which include fixed-wing and solar panels, with rechargeable batteries. Balloon-type HAPS are well established for scientific and research purposes, but are limited in versatility and maneuverability [11]. Finally, airships provide a balance between manoeuvrability and low deployment cost, but this segment is expected to be the slowest to grow as a result of technical challenges.

The main applications for HAPS are surveillance, accounting for about 47% of the market[4]. Government operators will mostly dominate this application. Another market is communications, where HAPS can provide an alternative platform for deploying temporary connectivity-boosting systems in rural areas, which can compete with large and expensive satellite constellations.

The market can be segmented by geographical region. North America held, and is projected to continue to hold, the largest market share for HAPS. This is then followed by Europe and Latin America. Interestingly, the MEA and Asia markets hold the smallest shares, but have the highest expected CAGR [11]. The requirement to operate between 30°N and 30°S means that about 46% of the Earth's land mass can be covered by the AHAPS[1].

To illustrate the position of the proposed AHAPS concept in the market, a SWOT analysis is shown in Figure 3.2. This highlights the internal strengths and weaknesses, as well as the external opportunities and threats.

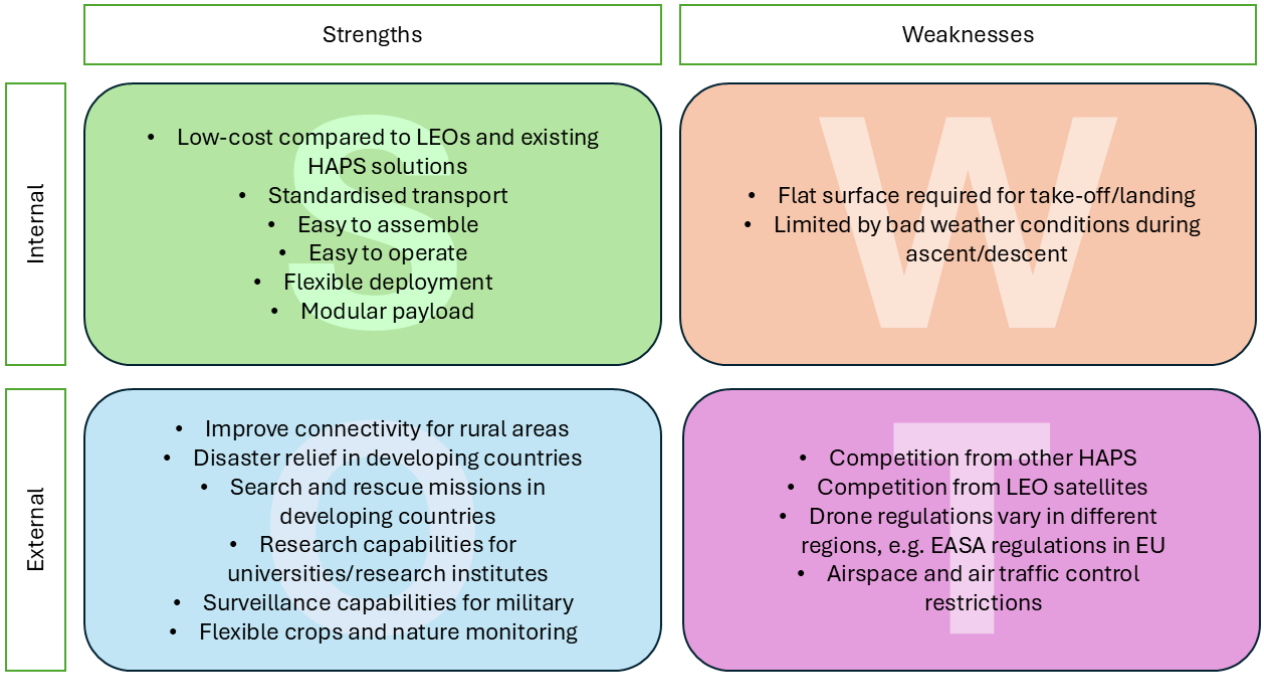

Figure 3.2: Market SWOT analysis of the proposed product compared to market competitors.

Different stakeholders have varying levels of interest and influence on the concept and the product design. This is qualitatively summarised in Figure 3.3. The main stakeholders with high levels of interest and influence include the principal contractor, the governments of developing countries, and research institutes. Regulatory bodies like EASA will have significant influence on the product as they ensure compliance with relevant laws and regulations. We also need to consider the general public, as they may be affected by the use of AHAPS systems.

[1]https://www.av8n.com/physics/land-water-latitude.htm [cited 23 June 2026]

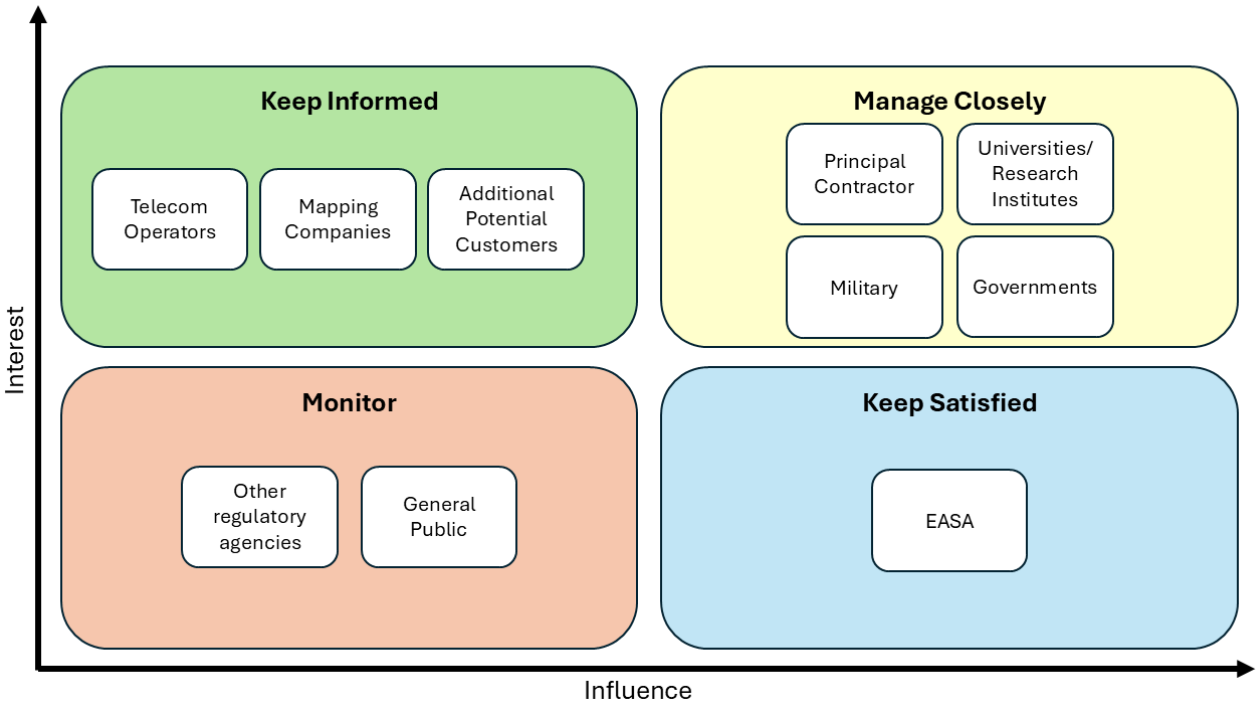

Figure 3.3: Stakeholder interest-influence map, this showcases all stakeholders and what design team aims to do.

3.5. Sustainable Development Strategy

A large part of the overall design process is sustainability. The AHAPS has to adhere to environmental legislation, such as the European Climate Law [**european_parliament_european_2021**]. To achieve this, sustainability has to be taken into account throughout the entire design process. The sustainable design philosophy is discussed in Section 3.5.1, and the effects of this philosophy on the subsystems are discussed in Section 3.5.2.

3.5.1. Sustainable Design Philosophy

The sustainable design philosophy of the design team is to push for a minimisation of emissions both during production and operations, while also contributing to a circular economy by prioritising reusability, repairability, modularity, and recyclability. This design philosophy guarantees compliance across four domains: the atmospheric and stratospheric domain, the circular and manufacturing domain, the energy and resource domain, and the social and regulatory domain.

3.5.2. Design Considerations

To comply with the sustainable design philosophy, considerations have to be taken into account throughout the design process. These are split into considerations to be taken for the operating life and the end of life of the AHAPS.

Operating Life

Compliance with the atmospheric and stratospheric domain and the regulatory domain is met through **REQ-STK-2.4**, which specifies the EASA Civil drones certification operations type #1[1]. The EASA regulations also take the acoustic footprint of take-off and landing into account, ensuring that sensitive ecological zones are not damaged. Furthermore, adhering to other stakeholders, such as the NOAA, which focuses on stratospheric integrity, ensures that no harm is done to the highly sensitive ozone layer[2].

This design philosophy is also reflected in **REQ-STK-3.1**, **REQ-STK-3.2**, and **REQ-STK-3.3**. The first requirement specifies that the AHAPS shall be constructed from materials that are either recyclable or inert upon disposal. This covers the manufacturing, energy, and resource domains of sustainability.

[1]https://www.easa.europa.eu/en/domains/drones-air-mobility/operating-drone/drone-rule-navigator [cited 29 April 2026]
[2]https://www.weather.gov/gjt/education_corner_balloon [cited 29 April 2026]

The second requirement covers the full retrieval of the system, ensuring that no debris or components are left in the environment. This requirement goes hand in hand with **REQ-STK-3.1**, as one cannot recycle a material that has not been recovered. The final sustainability requirement addresses the design's modularity. By standardising the airframe sections and other components, the design team ensures that parts are readily interchanged and repaired. All internal components are easily attachable or insertable into the airframe, making it easy to swap components in and out. Through modularity, the design team also takes the lifecycles of separate components into account. For example, it ensures that while the batteries might have a life cycle of two years, the airframe might serve for 10 years through multiple subsystem swaps. This limits the disposal of materials, ensuring a longer and more qualitative lifecycle.

End of Life

Until recently, end-of-life aircraft were abandoned in landfills around the globe [12]. In accordance with a European Directive on end-of-life vehicles, which states that 95% of an aircraft's weight must be recycled. The end-of-life process of the total aircraft is split up into decommissioning, disassembly, and smart dismantling [12]. Decommissioning consists of inspection, cleaning, and removal of any hazardous substances. Next, disassembly is defined as the systematic physical separation of the product into its constituent parts. This is also the point at which certain components can be deemed reusable or resellable. Finally, smart dismantling groups dismantle material types after which they are prepared for shredding and sorting, and sent to recovery channels [12].

4. Design Synthesis

This chapter covers the detailed design process of the AHAPS. Firstly, the all-encompassing design method is explained, including how subsystems are connected to iterate to a final design. In the subsequent sections, the sizing method of individual subsystems is outlined. Furthermore, the relevant assumptions made and tool verification conducted are described.

4.1. General Method

In this section, the general design, sizing, and iteration are described. First, in Section 4.1.1, the general systemwide assumptions are given. Subsequently, in Section 4.1.2, the steps taken to reach the prior preliminary design are briefly summarised. Following that, the iteration and sizing procedure of the entire aircraft is described in Section 4.1.3. Lastly, the procedure taken to evaluate the performance of the sized aircraft is outlined in Section 4.1.4.

4.1.1. General Assumptions

Several assumptions are made during the general design of the aircraft system. The system-wide assumptions used during the design process of the aircraft are given in Table 4.1.

Table 4.1: General assumptions list used during the whole design process.

Assumption ID	Category	Assumption	Justification (Quantitative)
ASP-SYS-1.1	Design	The salary of the design team is assumed negligible with respect to the product cost.	Design team is unpaid, so salary will be 0.
ASP-SYS-2.1	User	It is assumed that the user team shall not attempt launches of the AHAPS in hazardous weather conditions.	Weather conditions in departure and landing are non-negligible; weather accounts for 35% of aviation accidents[a]. Waiting out bad weather greatly improves chances of mission success.
ASP-SYS-3.1	Product	It is assumed that the cruise altitude of the AHAPS is situated between the upper troposphere and lower stratosphere, depending on latitude.	The troposphere ranges from Earth surface level to an altitude of max 54,000 to 60,000 ft, and the stratosphere extends until 150,000 ft, so the AHAPS with cruise altitude of 60,000 ft will be within those ranges[b].
ASP-SYS-3.2	Product	It is assumed that, at cruise altitude, the AHAPS shall be subject to no more than short, hours-long, low-frequency oscillations, light weather phenomena, which are thus avoidable.	In the stratosphere, temperature increases with altitude, which prevents convection. Therefore, clouds do not tend to reach into the stratosphere, and for similar reasons, weather effects are minimal[b].
ASP-SYS-3.3	Product	It is assumed that an ISA deviation of 10°C will occur at all times with respect to performance and thermal dissipation.	Atmosphere temperature at 60,000 ft varies approximately ±5°C, and ISA can vary approximately the same from true temperature [13].
ASP-SYS-3.4	Product	It is assumed that a minimum percentage of 20.9% of O_2 in the air is present at all times.	The fraction of oxygen does not vary to any meaningful degree at altitude, so the fraction is the same as the sea level fraction[c].
ASP-SYS-3.5	Product	It is assumed that a cloud cover of 4/8 or less will occur during take-off, climb, descent, and landing.	Aircraft should still perform with slight overcast conditions, with max assumed being 4/8 cloud cover where some solar power is lost [14].
ASP-SYS-3.6	Product	It is assumed that the payload will draw no power during take-off, climb, descent, and landing.	The payload is only operated during cruise; possible idle power when not operating is deemed negligible.

Continued on next page

Assumption ID	Category	Assumption	Justification (Quantitative)
ASP-SYS-3.7	Product	It is assumed that heat dissipation occurs uniformly through a bulk area.	For a Biot number < 0.1, a structure can thermodynamically be assumed as a lumped mass, which is typically true for metal and CFRPs.
ASP-SYS-3.8	Product	It is assumed that only the computer, payload, and power systems require specific operating temperatures of between −40 and 70°C, −20 and 50°C, and −20 and 80°C, respectively.	Industrial electronics can typically function until −40°C[d]. As the payload is unknown, a 20-degree margin is applied to reach a minimum of −20°C. Batteries can also operate safely until −20°C. Maximum temperature bounds are 70°C for the computer, 50°C for the battery, and payload[e], and 80° for the fuel cells [15].
ASP-SYS-3.9	Product	It is assumed that the airframe shall be equipped with damping systems sufficient to dampen oscillations to all vulnerable subsystems (e.g. payload bay).	A stable aircraft will damp out static and dynamic aerodynamic oscillations. Resonant frequencies of aircraft are generally spread over multiple peaks of lower magnitude [16]. Thus, resonance between subsystems and aircraft is unlikely and would be found during verification.
ASP-SYS-3.10	Product	It is assumed that navigator/indicator lights for low-light operations consume a power of 100 W.	Aircraft lights use non-negligible amounts of power, with light pulses using up to 35 J of energy[f]. This can add a noteworthy additional load to the power system.
ASP-SYS-3.11	Product	It is assumed that pressurisation is not required for internal subsystems.	Unmanned aircraft do not need pressurisation for their subsystems [**edge_pressurized_nodate**]. Although fuel tanks may be pressurised, this is caused by internal pressure from storing the fuel.
ASP-SYS-3.12	Product	It is assumed that there will be 0/8 cloud cover during the cruise.	Due to the absence of convection, clouds do not form in the lower stratosphere where the AHAPS mostly reside; therefore, cloud cover is assumed to be 0/8[b].

[a] https://flightsafety.org/asw-article/weather-concerns-for-general-aviation/ [cited 7 May 2026]

[b] https://www.noaa.gov/jetstream/atmosphere/layers-of-atmosphere [cited 7 May 2026]

[c] https://www.bmj.com/content/317/7165/1063 [cited 7 May 2026]

[d] https://www.electronics-cooling.com/2004/02/the-temperature-ratings-of-electronic-parts/ [cited 7 May 2026]

[e] https://www.mdpi.com/2313-0105/10/12/421 [cited 7 May 2026]

[f] https://prd-sc102-cdn.rtx.com/collinsaerospace/-/media/ca/product-assets/files/military-and-defense/lighting/pdfs/anti-collision-lights/06_0010-led-anti-collision-lighting-system-a320.pdf [cited 7 May 2026]

4.1.2. Preliminary Conceptual Design Phase Summary

Using the assumptions as guidelines, the preliminary sizing is started. The first step to creating a conceptual design of the AHAPS is to create a preliminary configuration of the system. With the aircraft subsystems described in Section 3.1, individual configurations can be found for each subsystem. With a fleshed-out configuration, further design synthesis is performed in this chapter for each subsystem. Firstly, various concepts can be generated; these can be described in a concept generation tree, where different viable options for each subsystem are explored. With this, feasible combinations are selected, which are the final concepts. Next, a trade-off method for the provided requirements and constraints is designed. The final concepts are evaluated to determine the best performer. To validate this choice, a sensitivity analysis is performed, where the trade-off method is varied, determining the impact on the trade-off result.

Design Option Creation

Following the requirement definition, one may start the process of generating and pruning the Design Option Tree (DOT). The number of DOTs that must be defined has been chosen based on the number of subsystems that have been deemed design-driving, such as the 28 day endurance requirement **REQ-STK-1.2**,

the deployability requirement **REQ-STK-1.4**, and the transport requirement **REQ-STK-7.1**. As such, the airframe, power, and propulsion systems have been considered for analysis, with the addition of a launch option question. The control, computer, communication, payload, and flight condition systems have thus been considered imposed, unlikely to change based on trade-offs, or tied to specific configurations. The remaining design option trees can be seen in Section A.3.

To isolate viable options, several labels have been defined and subsequently used in the filtering process. First and foremost, Non-Concepts were identified, which relate to entries that have been included purely for the sake of completeness or for which no past implementations can be found. Following this, Non-Feasibles are eliminated on the basis that they either violate the laws of nature or several practical limitations. From the ones that are left, Immediate Development Risks are tagged based on the technological maturity, complexity, or time constraints. The remaining DOT branches are then summarised with representatives called Strawman Concepts.

At the end of the DOT pruning process, the chosen strawman concepts consist of three airframe configurations, one general power system type, one propulsion option, and one launch configuration. The airframes in question are: airship, traditional fixed-wing, and flying wing. The traditional wing planform strawman further encapsulates the cruciform and T-tail options regarding the empennage. The power system tree has converged to the solar and electrochemical block. It, too, may be subdivided into hydrogen fuel cells and batteries, both of which have been deemed viable. Finally, the aircraft shall use open propellers for propulsion and launch without vehicle assistance. The DOTs can also be seen in Section A.3, where final and pruned options are shown. With the aforementioned sub-divisions, four combinations are possible in terms of trade-off. These are outlined in Table 4.2.

Table 4.2: The four remaining preliminary design options, consisting of identical subsystems except with varying wing and power storage configurations.

Design Option	**Configuration**	**Energy Storage**	**Power Generation**	**Launch System**	**Propulsion System**	**Landing System**
1	Tube-and-Wing	Batteries	Solar panels	Self-propelled	Open propeller	Landing gear
2	Tube-and-Wing	Fuel cells	Solar panels	Self-propelled	Open propeller	Landing gear
3	Flying wing	Batteries	Solar panels	Self-propelled	Open propeller	Landing gear
4	Flying wing	Fuel cells	Solar panels	Self-propelled	Open propeller	Landing gear

Concept Generation

With these four design options, each can be worked out into functional concepts. To generate the concepts for the system, the following five-step process is used. This process is shown below:

1. Obtain prerequisites
2. Select main wing characteristics based on literature.
3. Execute power sizing by selecting the power system mass fraction.
4. Find total wing geometry.
5. Finalise concept aspects with importance to the trade-off.

Firstly, obtaining prerequisites consists of getting any preliminary design tools or parameters required for any preliminary calculations. These are simply methods or values necessary for the further steps in the concept generation process.

Selecting wing characteristics is considered with two different planforms, which are a tube-and-wing, and a flying wing configuration. The E387 and E344 airfoils are selected for the tube-and-wing and the flying wing,

respectively, due to their moment coefficients and their low Reynolds-number performance[12]. Secondly, aspect ratios for the configurations are selected. For high-altitude slow cruising flight, high aspect ratios are typically necessary. However, higher aspect ratio wings have a downside of higher structural mass. Therefore, the aspect ratio is taken as 25 for both aircraft, as this fits within the range of typical HAPS aircraft [17]. Subsequently, the sweep angle is chosen. For the tube-and-wing configuration, no sweep is chosen, as this is not necessary for low speeds, and it betters modularity. Alternatively, for stability, flying wings typically have sweep, and as such, a sweep of 15° is chosen [18]. For modularity, both main wing planforms are chosen to be untapered, as this allows for identical modular sections. Moreover, dihedral is also taken as 0°, as wing deflection will tend to produce an induced dihedral. Lastly, for the tube-and-wing configuration, the empennage and fuselage can also be sized. A horizontal tail surface ratio of 0.15 was chosen, as it is deemed sufficient for any centre of gravity (C.G.) positioning [19].

Sizing the power system requires the power requirements from all subsystems. Power sizing for the propulsion system is the most critical, as this is the most power-intensive system of the AHAPS. An empirical sizing method was used for the power sizing, which calculates the propulsive efficiency based on advance ratio λ, thrust, and dynamic pressure q, through historically observed ratios [20]. A power sizing method using aircraft parameters and efficiencies results in propulsion system power consumption as a function of altitude and velocity [20]. Hereby, the most critical condition and the cruise condition are used. Solar panels are sized to take up the maximum possible space on the aircraft surface area, with a thin film, as this allows you to follow the form of the wing and save weight. Due to this, the wing area can be taken as $1.025 \cdot A_{solar}$. Besides this, two separate energy storage methods are considered: batteries and fuel cells. For each of these, specific energy density and volumetric energy density are used, with total energy needed determined by endurance requirements. Factors for efficiency and depth of discharge are added to account for any power losses.

To perform the sizing, an iterative process described in Figure 4.1 is followed. With payload and power system mass fractions of 0.2 and 0.45, respectively, and an MTOW guess [21]. The iterative procedure sizes the power system and wing, whereby MTOW is recalculated until a final concept is sized.

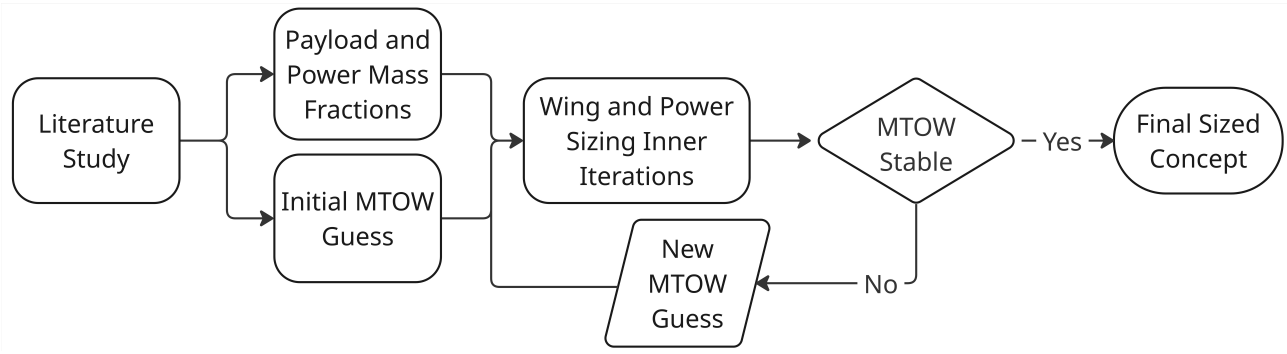

Figure 4.1: Outer iteration loop of the concept generation process. A literature study provides mass fractions and an initial MTOW [21]. These size the power system and wing, which causes an iteration until a final stable MTOW is produced, resulting in a sized concept.

The cruise lift coefficient was calculated using $C_{L_{cruise}} = 0.8 C_{L_{max}}$, which is different from the optimal C_L for endurance. This was done to account for a stall margin, as well as to mitigate any damage from gust loads. Similarly to the power system sizing, the wing surface sizing can be sized through an iterative process, as shown in Figure 4.2. This sizing is also contained within the power sizing, as an inner loop in the wing and power sizing block.

[1] http://airfoiltools.com/airfoil/details?airfoil=e334-il [cited 20 May 2026]
[2] http://airfoiltools.com/airfoil/details?airfoil=e387-il [cited 20 May 2026]

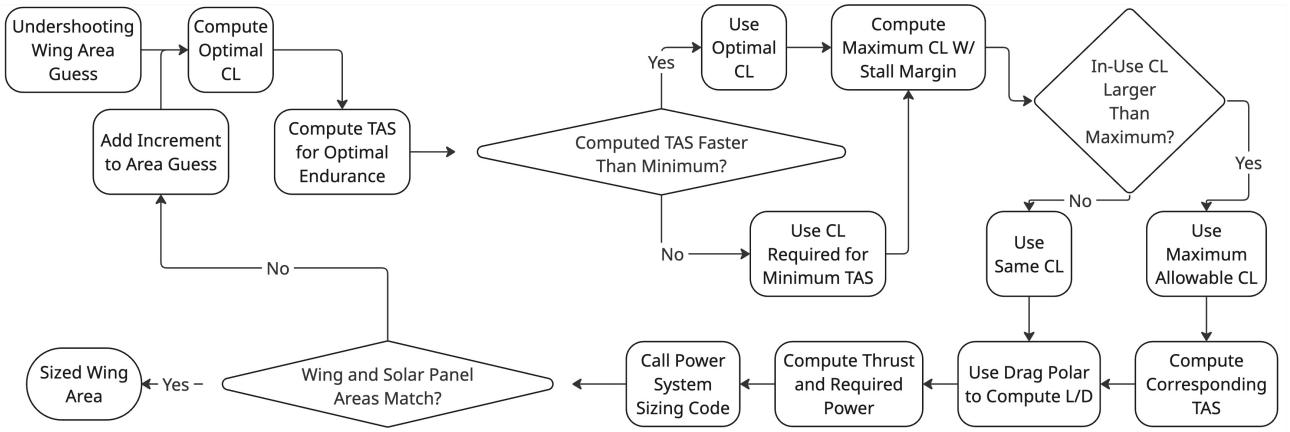

Figure 4.2: Inner iteration loop of the concept generation process. An initial wing area is guessed, whereby C_L is computed. With this, a drag polar is computed, allowing the required thrust and power to be found with the TAS. If wing and solar panel sizing results corroborate, a final sized wing area is obtained.

With this process, both the airframe and power systems are sized, which are then fed to the final concepts.

Final Concepts

Executing the concept generation process described in Table 4.1.2 results in the concept characteristics shown in Table 4.3. These concepts are all designed to meet the constraining power requirements **REQ-STK-1.4** and **REQ-STK-1.2**, imposing a 28 day endurance performance between the 30°N and 30°S latitudes throughout the entire year. Additionally, other constraining requirements that drove these concepts are the maximum cost of **REQ-STK-6.1** and the logistical requirements of fitting in a 20 ft ISO container from **REQ-STK-7.1**.

Table 4.3: The main characteristics and performance metrics of each of the four preliminary concepts.

Metric	**Tube-and-Wing with Batteries**	**Tube-and-Wing with Fuel Cells**	**Flying Wing with Batteries**	**Flying Wing with Fuel Cells**
Maximum Take-off Mass (kg)	207	165	176	150
Climb Time (hrs)	12.6	12.3	13.8	13.6
Cruise Speed TAS (m/s)	28.6	28.2	27.9	27.6
Technology Readiness Level	5.54	5.08	5.08	4.61
Total Manufacturing Cost (€) (FY26)	750,000	840,000	710,000	760,000
Recurring Costs (€/year) (FY26)	43,000	52,000	40,000	46,000
Number of Segments	11	11	7	7
Assembly Time (min)	152	152	112	112
CO_2 Emissions (full lifecycle) [kg]	7600	3900	6400	3500
Degradation Rate per Day (%)	0.016	0.028	0.016	0.028

Trade-off Method

The criteria considered have been determined according to the system requirements that have been imposed. The requirements have different importances, ranging from normal requirements to key requirements and, lastly, driving requirements. Relative weights for the trade-off criteria are determined by the importance of their associated requirements. Next, performance metrics are created to quantify the performance per trade-off criterion for each of the finalised concepts. A full breakdown of each of the chosen trade-off criteria, their weights, and associated performance metrics is shown in Table 4.4.

Table 4.4: Breakdown of the selected trade-off criteria, their weights, and associated performance metrics.

Trade-off Criterion	**Weight**	**Performance Metrics**
Flight Performance	20%	Endurance; Stability and manoeuvrability; Deployability
Development Risk	20%	Technology Readiness Level (TRL); Error margin of concept characteristics
Costs	15%	Manufacturing costs; Recurring costs
Logistics	30%	Sub-assembly mass; Sub-assembly volume; Assembly time
Sustainability	15%	Manufacturing impact; Degradation rate

Trade-off Execution

Based on the technical performance metrics and the strawman characteristics, a trade-off is conducted, favouring the flying wing with batteries, of which the results are given in Table 4.5. From the trade-off, it is evident that the best-performing design is the flying wing with batteries. This comes as a result of its "excellent" performance in the logistics, sustainability, and cost criteria. Additionally, it still scores a "good" in the remaining criteria of development risk and flight performance. The reasoning for each score is related to its performance in the technical performance metrics and is elaborated in each cell. The scoring for the flying wing with batteries produces a weighted score of 2.6, while the nearest competitor, the tube-and-wing with batteries, scores a 2.35. The trade-off, therefore, suggests that the flying wing with batteries is the best design with a perceptible margin.

Table 4.5: Trade-off Summary Table for the airframe and power system configuration selection of the AHAPS. The highest overall score of 2.6 is obtained for the flying wing with batteries, indicating this should be selected for the final design.

CRITERION / OPTION / WEIGHTED SUM	**Flight Performance** 20%	**Development Risk** 20%	**Costs** 15%	**Logistics** 30%	**Sustainability** 15%
Tube-and-Wing; Batteries - 2.35	Excellent: Good deployability, good longitudinal stability and good endurance	Good: High scoring TRL, but medium sensitivity	Excellent: Lowest manufacturing and recurring costs	Good: Longer assembly time, easy to handle, relative big volume	Good: More CO_2 emissions, less degradation
Tube-and-Wing; Fuel cell - 2.2	Excellent: Good deployability, good longitudinal stability and good endurance	Good: Medium scoring TRL, with medium sensitivity	Good: Higher manufacturing and recurring costs	Good: Longer assembly time, easy to handle, relative big volume	Good: Less CO_2 emissions, more degradation
Flying wing; Batteries - 2.6	Good: Medium deployability, medium longitudinal stability and good endurance	Good: Medium scoring TRL, but high sensitivity	Excellent: Lowest manufacturing and recurring costs	Excellent: Shortest assembly time, easy to handle, small volume	Excellent: Medium CO_2 emissions, less degradation
Flying wing; Fuel cell - 2.1	Good: Medium deployability, medium longitudinal stability and good endurance	Acceptable deficiencies: Low scoring TRL, with low sensitivity	Good: Higher manufacturing and recurring costs	Excellent: Shortest assembly time, easy to handle, small volume	Good: Less CO_2 emissions, more degradation

Red - 0 - Unacceptable	**Yellow - 1 - Correctable deficiencies**	**Cyan - 2 - Good**	**Green - 3 - Excellent**

Sensitivity Analysis

To validate the trade-off results, a sensitivity analysis on the trade-off method is performed, determining whether the method accurately chooses the best concept for the provided requirements and constraints. Moreover, good results in the sensitivity analysis increase confidence in the concept selection.

The sensitivity analysis is performed by varying the trade-off method in three distinct ways. Firstly, individual criterion weights are each changed by 5 percentage points. The results of this can be seen in Figure 4.3. Secondly, the assigned score for each criterion is varied by ± 1, which can be seen in Figure 4.4. Lastly, entire trade-off criteria are removed one at a time, with the score normalised to have other weights add up to 100%, which can also be seen in Figure 4.3. Executing this analysis over all concepts and all variations yields three distinct cases, whereby the flying wing with batteries is the best scorer. These are for the cases where: the logistics criterion is removed, the flying wing with batteries' logistics score is changed to 2, and when

the tube-and-wing with batteries' logistics score is changed to 3. In all of these cases, the flying wing with batteries is narrowly usurped by the tube-and-wing with batteries.

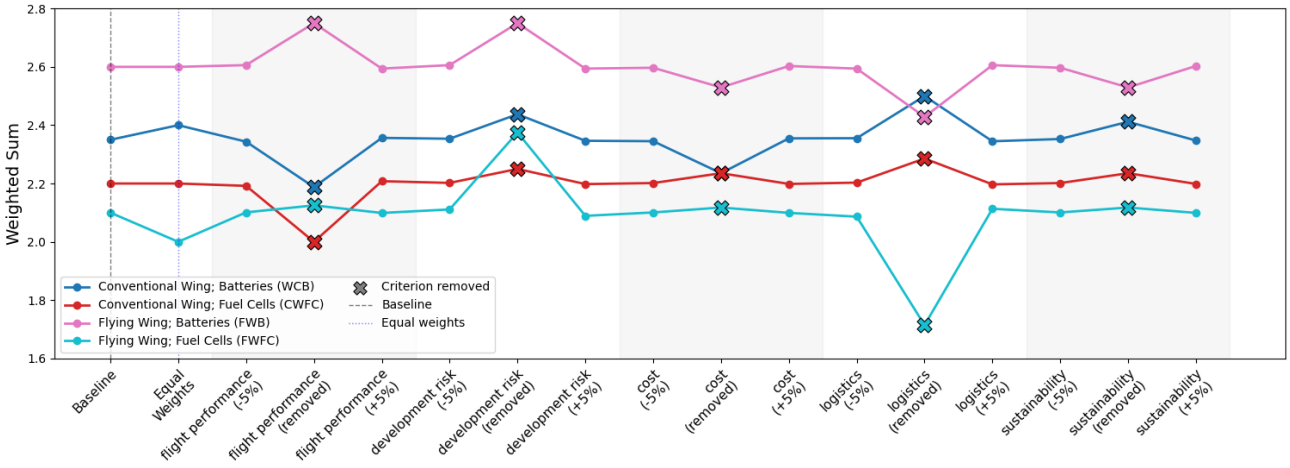

Figure 4.3: Sensitivity analysis weight deviations where criteria weights are reduced by their absolute weight.

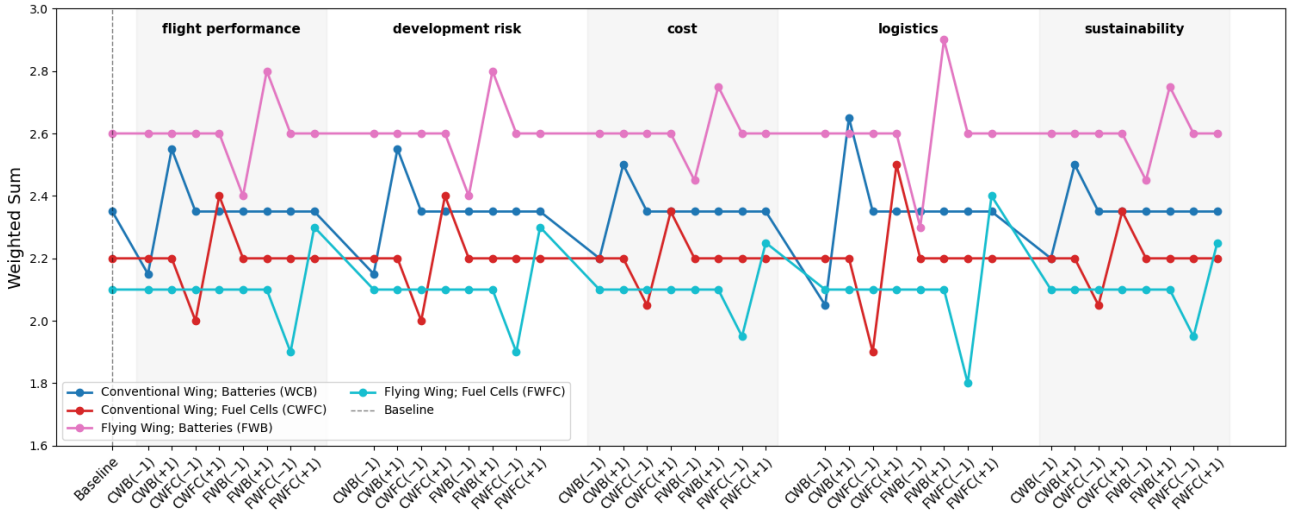

Figure 4.4: Sensitivity analysis score deviations where criteria weights remain the same, while individual scores are varied by positive and negative 1.

This shows that if this category is improperly graded, it could mean an incorrect final configuration is picked. To ensure the logistics grades are reasonable, a more in-depth analysis has been done on the Sub-assembly volume performance metric for logistics. Both the tube-and-wing and flying wing with batteries have been put in a simulated 20 ft ISO container based on **REQ-SSY-9.21**. The results of this test are presented in Figure 4.5a and Figure 4.5b. Here, it can be clearly seen that the fit for the flying wing significantly outperforms the tube-and-wing. Justifying the scores for both concepts in the logistics criterion. Moreover, the aforementioned requirement is significantly driving the final design; thus, removing this criterion entirely would be unrepresentative of a design choice.

Ultimately, this demonstrates that the trade-off result is only impacted by the largest changes in the sensitivity analysis. Removing the heaviest-weighted criterion alters results, but this would be infeasible. Alternatively, the scores within this criterion could be changed. Though, as demonstrated, this should not occur within the technical performance metrics. Consequently, it is justified with high confidence that the flying wing with batteries is the optimum concept.

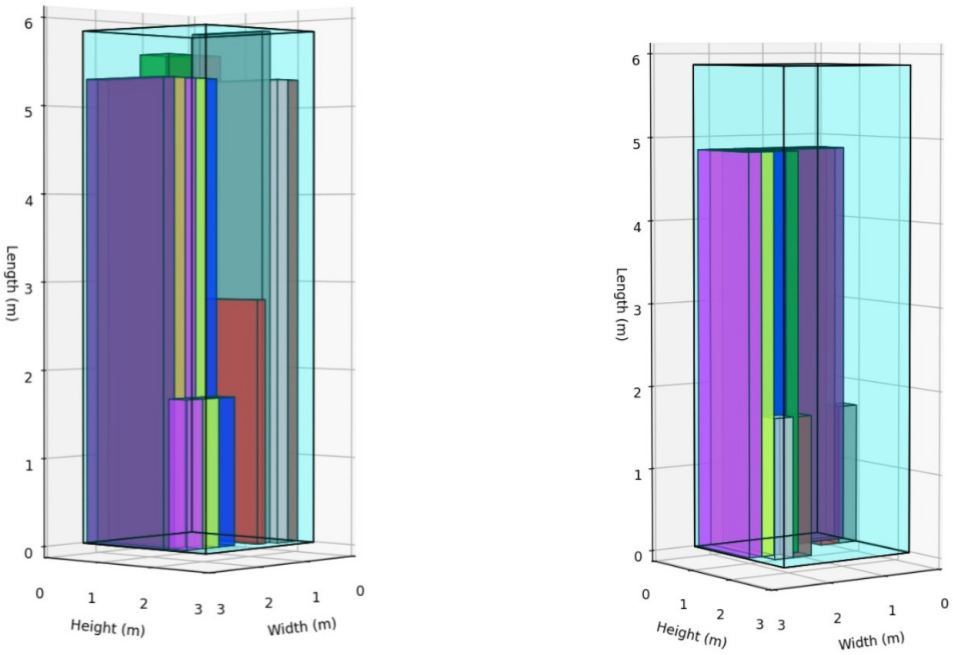

(a) Tube-and-wing with batteries stored in a 20 ft ISO container

(b) Flying wing with batteries stored in a 20 ft ISO container

Figure 4.5: Container packing configuration for two AHAPS configurations. Each box represents a discrete subsystem or section of a subsystem.

4.1.3. Design Iterations Flow Diagram

The detailed conceptual design sizing process follows an iterative structure generally similar to the one presented in Table 4.1.2. Two nested optimizers have been implemented: an outer MTOW estimation iterator and an inner geometry-determination loop. This structure may be visualised in a flow diagram, as per Figure 4.6.

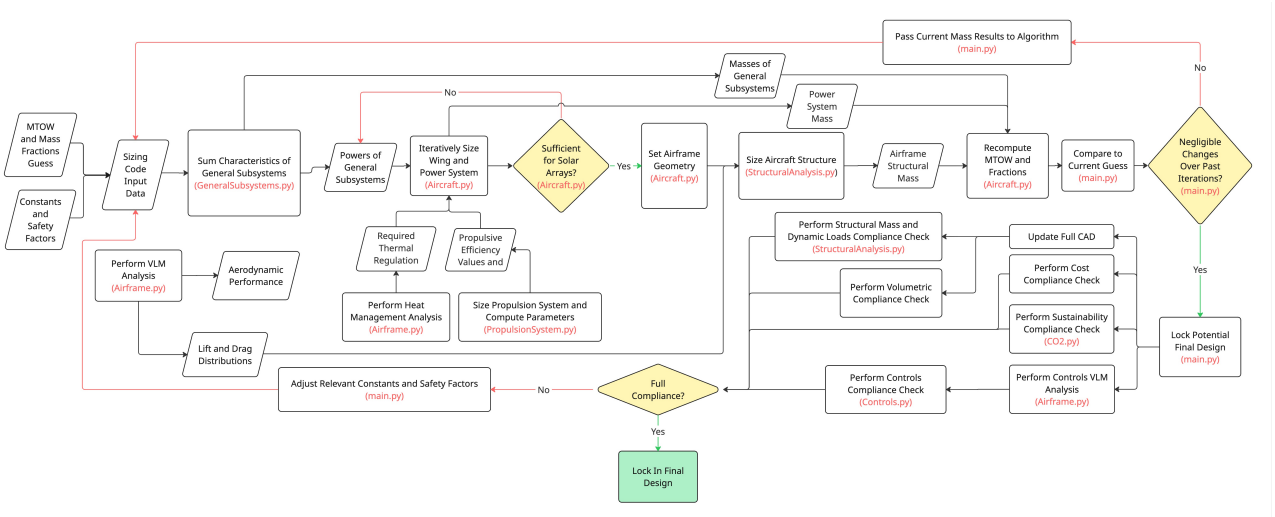

Figure 4.6: Detailed conceptual design iterator flow diagram.

Following the aforementioned workflow, the code's input data is comprised of initial MTOW and subsystem mass fraction guesses, as well as safety factors and constants. This total mass, as per Class II weight estimation methods, is to be used in subsystem sizing calculations. The mass fractions are only utilised for monitoring purposes alongside the MTOW in order to determine when an acceptable measure of convergence has been reached. Weight and geometric calculations are then performed for each subsystem, leading to a new MTOW value and mass fraction breakdown. If changes are above tolerances, the same pro-

cess is once again called. This outer loop is, in essence, a fixed-point iteration problem, which continues until increments to the input data are acceptably low.

As previously described, every iteration loop involves sizing calculations for all relevant subsystems. The first set of computations relates to the payload, as well as to the general subsystems category. These possess parameters that are either already known or have been established not to be subject to change so long as the design remains within the size class of the reference aircraft considered. With their associated mass and power values, the inner iteration process can begin.

The inner optimizer aims to obtain a wing surface area large enough to accommodate the aircraft's power generation requirements, while still flying as close to the endurance-optimal regime as possible and maintaining the minimum TAS required to satisfy **REQ-STK-1.6**. To this end, an iterative framework is employed. Starting from literature-dictated geometric parameters and a purposefully undershooting wing surface area guess, an aerodynamic analysis is performed as dictated in Section 4.4 to obtain a lift curve and drag polar. Afterwards, cruise conditions are determined based on three possible regimes: optimal endurance C_L, minimum V_{TAS}, or maximum allowable C_L. This simple decision tree is possible, since the increased aspect ratio of the AHAPS pushes the theoretical optimal lift coefficient to higher values, which have throughout this project been observed to often exceed conservative estimations for maximum lift coefficients. The margin for the maximum allowable coefficient has been empirically chosen to be 80% of the simulated maximum, which does in practice align with similar high-altitude aircraft, such as the U-2, which was known to operate at lift coefficients in the order of 0.6 to 0.7 at cruise [22].

After determining the flight regime, the corresponding cruise V_{TAS} is logged, and the simulated drag polar is used to output a lift-over-drag ratio. These quantities, coupled with the MTOW guess, are sufficient to calculate the required thrust and propulsive power, which can be used to size the propulsion system according to Section 4.6.2. The propulsive power output is then summed with the general subsystems and miscellaneous powers, resulting in the total power requirement at cruise. This value is then fed into the power system sizing tool, as described in Section 4.5.2. Its outputs are weight breakdowns of the battery and solar array systems, as well as the required solar panel area, which can now be compared with the current wing area guess.

It is known that it is not possible to cover the entire wing with solar arrays, as space must be left for control surface hinges, sensors, and other such fixtures. Therefore, a ratio of 1.025 has been chosen between the wing and solar panel areas, similar to the design of the SPACOM [23]. So long as the wing area guess does not meet the minimum of 1.025 times the computed solar array size S_{solar_i}, one can compute the next iteration's value $S_{wingi+1}$ as a function of the current S_{wing_i}

$$S_{wing_{i+1}} = S_{wing_i} + \min[\alpha_{damping}(1.025 \cdot S_{solar_i} - S_{wing_i}), 0.01] \tag{4.1}$$

This update formula includes a damping factor $\alpha_{damping}$, as is common in iterative methods, to avoid overshooting the optimal point. It is also the reason why the initial guess should undershoot feasible designs, since the algorithm functions akin to a positive ratchet. The minimum function is implemented simply to avoid asymptotic growth. Regardless, the number of inner iterations has often been observed to exceed 15. As such, it is time-wise unfeasible to compute a drag polar for every single one. To mitigate this, a boolean variable is introduced mandating a new simulation once either the wing area guess has been altered by more than 30%, or compliance with the power generation requirement has been detected.

With the AHAPS geometry defined, one can compute the approximate weight of the airframe and landing skids, as outlined in Section 4.4 and Section 4.9, respectively, thus completing the Class II weight estimation. The full mass breakdown of the design enables the MTOW and mass fractions to be recalculated. To determine if a design has converged, the sizing algorithms monitor the increments over the past five iterations. If the cumulative relative errors are acceptably small (below the significant figures taken into account), it stops and outputs all relevant design parameters. Otherwise, the new MTOW value is used for another iteration.

In the event of convergence, the compliance stage may begin. Taking into account the design parameters that have been obtained, a control system, deflection, and logistical analysis are performed. In case the air-

craft fails to meet requirements in any of these categories (insufficient stability margin, insufficient control authority, excessive deflections, inability to satisfy the 20 ft ISO container requirement, exceeds cost, etc.), the aforementioned safety factors and constants are updated to compensate for these deficiencies. For example, increasing the load factor and deflection thresholds in case aileron reversal is detected during the compliance phase.

Should the compliance phase pass without any such warning flags after a converged iterative process, the detailed conceptual design may be considered adequate and thus have its values frozen. With all relevant design parameters, its performance metrics can be quantified next, thus ensuring compliance with the imposed product requirements.

4.1.4. Performance Evaluation Approach

This section will illustrate on what criteria the design performance of the AHAPS will be evaluated and how it will be done. This section talks about the load-bearing capability, the stability and control, XFLR5, and the deployability and mission simulation.

Loadbearing Capability

A significant challenge in designing an aircraft with a slender wing is the load-bearing capabilities. It is of crucial importance that the AHAPS is able to sustain both static manoeuvring loads and dynamic gust loads. The bending deflection, the torsional stiffness of the skin, and the twist deflection are all considered to ensure compliance to the certification requirements chosen.

The bending deflections are calculated using the `aerosandbox` lifting line computation tool [3]. Furthermore, the derivative of deflection can be calculated using Euler-Bernoulli beam theory [24]. Integrating this results in full deflections as a function of the wingspan. The torsional loading is simply calculated using the thin-walled torsion equation [25]. Finally, the twist deflection is determined by the Bredt-Batho theory [24].

The recommendations for how to evaluate the performance even further, such as evaluating a dynamic analysis through FEM, aeroelasticity, fatigue, and eigenfrequencies, are explained in more detail in Section 8.1.

Stability and Control

The stability and control performance of the AHAPS is evaluated by looking at the lateral and longitudinal directions. Longitudinal performance is evaluated by looking at C_{m_α}, obtained from VLM and the phugoid and short-period motions, which are obtained through the symmetric EOM for a control surface deflection. Lateral performance is evaluated by comparing the obtained rudder and elevon deflections to the requirements set out in Section 4.7. Furthermore, the Dutch roll and the spiral motion are also evaluated based on the asymmetric EOM.

The recommendations for how to evaluate the performance even further are explained in more detail in Section 8.1.

XFLR5

The aerodynamic performance of the AHAPS is crucial in the context of fulfilling its endurance requirement. As such, it is important to verify that the simulations performed during the sizing process yield realistic results. To this end, an XFLR5 analysis of the final design is performed.

Lift, drag, and moment coefficients are first computed for the chosen airfoil, after which the wing geometry is defined, and an analysis is run for the correct atmospheric conditions and TAS, resulting in a set of polars. Afterwards, it is possible to verify that neither the profile nor induced drag has been significantly underestimated, as well as that the aircraft is stable, preferably as close to the cruise angle of attack as possible. The lift gradient, too, should be sufficient for the chosen angle, and the maximum lift coefficient should not be lower than the one computed by XFLR5.

Finally, lift-over-drag and endurance curves shall be examined. Values are noted and compared to those used during sizing, and angles of attack corresponding to maximum endurance are determined, as they should not be lower than the chosen cruise angle.

Deployability and Mission Simulation
One of the key performance characteristics of the AHAPS aircraft is its deployability. As specified by **REQ-STK-1.2** and **REQ-STK-1.4**, the AHAPS must be deployable year-round between latitudes of 30°N and 30°S. This means that the AHAPS must be able to sustain its altitude throughout the night on any day of the year, including the longest nights, such as during the winter solstice.

To validate the deployability of the AHAPS aircraft, the climb and cruise phases of flight are numerically simulated. First, the climb phase is assessed. For computations, the climb C_L is given by Equation 4.2,

$$C_{L_{climb}} = \min\left(0.8C_{L_{max}}, C_{L_{opt}} = \frac{k_1 + \sqrt{k_1^2 + 12C_{D_0}k_2}}{2k_2}\right), \tag{4.2}$$

where $C_{L_{opt}}$ is an approximation for the optimal C_L for best endurance of a propeller aircraft, and 0.8 is a safety factor taken to ensure that the aircraft is not too close to the stall point during flight[1].

With that, the rate of climb can be computed with Equation 4.3,

$$\text{ROC} = \frac{P_a - P_r}{W} V_{TAS}, \tag{4.3}$$

where P_a is power available from the motor(s), P_r is the power required to sustain level flight, W is the weight of the aircraft and V_{TAS} is the velocity of the aircraft.

For a given launch time, a numerical simulation of the altitude and battery levels of the aircraft throughout the climb is run. The aircraft begins the climb with a 100% battery level. The simulation runs until the cruising aircraft encounters its first sunset. If the battery is at least 90% charged by the time the first sunset during cruise is encountered, the aircraft has fully recovered from the increased power usage during climb and is able to start the cruise as designed. In this case, the aircraft passes the climb assessment.

For the cruise assessment, the battery level during the first two days of the cruise is computed. If the battery level does not fall below 10% during the first two days of cruise, the aircraft passes the cruise assessment. If the aircraft passes both the climb and the cruise assessment, it is deemed deployable at that particular launch time.

The deployability depends both on the time of day and the day of the year of launch, as well as other values that affect endurance, such as latitude, weather, and power used during climb. The effect of latitude and weather on solar panel effectiveness is explained in Section 4.5.2. The available power for climb is assumed to be 80% of take-off power, explained in Section 4.6.2.

4.1.5. Tool Verification

In order to ensure there are no errors in the calculations done to reach the design, proper tool verification must be carried out. Since much code is used for these tools, there are two types of verification to distinguish. There is code verification to ensure the code does not contain any fundamental errors, and there is calculation verification to ensure that the calculations used are logical and correct. Throughout this chapter, every subsystem that uses tools states the tools used, including the verification technique. For the code verification, pytest has been utilised extensively. Calculation testing is done to check whether the system displays the desired behaviour. Stability and behaviour are observed by making minor adjustments and analysing the reaction of the calculations. There are several types of calculation verification, which are listed below:

- CAD comparison - A comparison with the provided volume, mass, and C.G. estimation by the used CAD model and the calculated volume, mass, and C.G. budgets.

[1] https://eaglepubs.erau.edu/introductiontoaerospaceflightvehicles/chapter/flight-range-endurance/ [cited 20 May 2026]

- Sensitivity testing - Plotting the response of one output variable over one changing input variable and checking whether the graph matches theoretically based expectations. For example, plotting the lift over the velocity and checking if the plot matches the form of $y = x^2$ (since $L = \frac{1}{2} C_l \rho V^2 S$).
- Convergence testing - Checking if the discretisation schemes and meshes converge.
- Integration testing - Checking whether the expected output of the previous tool matches the expected input of the next tool, so that in the end, the whole system flows as intended.
- Monotonicity testing - In some cases, checking whether a model behaves in a consistently directional way, so when an input increases, the output either always decreases or increases, never both.

4.2. Payload System

In this section, the design of the payload system is provided. It is required to note that the payload bay is meant by the payload system and that the desired payload is interchangeable for the AHAPS user. The payload system is to accommodate the stakeholder requirements: from **REQ-STK-4.1** until **REQ-STK-4.5**.

4.2.1. Payload System Assumptions

The payload is expected to be packed as efficiently as possible, thus in a similar manner to CubeSats. A CubeSat of 16 units (consisting of $10 \times 10 \times 10$ cm^3 volume units) was chosen as a template[1]. Afterwards, the margin was applied purely negatively in terms of density, as it cannot be assumed that an identical packing efficiency can be achieved by the AHAPS, and extra payload volume may be desirable in terms of modularity. This leads to a geometric payload budget of 0.17 ± 0.01 m^3. This assumption, together with additional ones, is given a label in Table 4.6.

Table 4.6: Assumptions list used for the payload system design.

Assumption ID	Category	Assumption	Justification (Quantitative)
ASP-SSY-1.1	Payload Bay	The payload volume is 0.17 ± 0.01 m^3 geometrically.	This follows CubeSat packing according to the satellite industry[1].
ASP-SSY-1.2	Payload	Heat generated from the insulated components is neglected in the thermal analysis.	Power usages of components are low compared to heat losses, and power use is non-constant during flight [26].
ASP-SSY-1.3	Payload Mounting	The mounting of the payload to the airframe is 5% of the payload mass. This includes the payload bay.	This is a conservative estimate as a CFRP structure will be significantly lighter than the payload.
ASP-SSY-1.4	Payload Bay	The heat generated by the payload is directly utilised to heat itself at cruise altitude, so no heat sink is required.	This is due to the cruise altitude temperature of minus 60°C.

4.2.2. Payload System Design

For the design following assumption **ASP-SSY-1.1**, the payload bay has been designed. As the temperature at the cruise altitude is extremely low, no heat sink is required to be implemented for the payload, as it will need to heat itself. Other temperature management will be mentioned in Section 4.8. The payload bay is made of 1610 $\times$ 10 $\times$ 10 cm^3 cubes ordered in a $2 \times 4 \times 2$ manner. Then, a casing is made to cover the aforementioned volume, which is the payload bay.

4.2.3. Payload System Tool Verification

For the payload system, no design tools were necessary to design the payload bay. The designed payload bay was only tested to determine whether or not it fit within the main wing section in all dimensions.

4.2.4. Payload System Characteristics Overview

In this subsection, the characteristics of the payload system are shown.

[1] https://nanoavionics.com/small-satellite-buses/16u-cubesat-nanosatellite-m16p/ [cited 1 May 2026]

Table 4.7: Overview of the off-the-shelf components in the payload system. For each component, the mass, power draw, and cost are shown.

Category	Component	Reference Model	Mass (kg)	Power (W)	Cost (€) (FY26)
Payload	Customer Payload	Custom	20.00	100 (avg), 250 (peak)	–
Payload	Payload Computer	Raspberry Pi 5[a]	0.05	3	160
Payload	Temperature Sensor (4)	RS PRO SHT3x-DIS[b]	0.01	1	30
Payload Bay	CFRP Casing	Custom	0.8	–	4,000[c]
Mounting	Titanium Bracket	Custom	0.20	–	520[de]
Total	–	–	21.05	–	4,790

[a] https://pip-assets.raspberrypi.com/categories/892-raspberry-pi-5/documents/RP-008348-DS-6-raspberry-pi-5-productbrief.pdf [cited 11 May 2026]

[b] https://nl.rs-online.com/web/p/temperature-humidity-sensor-ics/2465631 [cited 16 June 2026]

[c] https://www.supreemcarbon.com/cost-guide-custom-carbon-fiber-pricing-explained.html [cited 9 June 2026]

[d] https://www.pakshalsteel.com/titanium-metal-price.html [cited 17 June 2026]

[e] https://www.mecomeco.com/blog/how-much-does-it-cost-to-get-a-metal-part-made-the-complete-2026-pricing-guide/ [cited 17 June 2026]

4.3. General Subsystems

The general subsystems are those made entirely of off-the-shelf components, which do not change with design iterations. This consists of three distinct subsystems: the flight condition system, the communication system, and the computer system. The design of these systems is driven by the stakeholder, system, and subsystem requirements.

4.3.1. General Subsystems Assumptions

In the design and sizing process of the general subsystems, a couple of assumptions are made. These relate to both the heat management of the individual components. These are considered due to the fact that not all components can function at the atmospheric conditions of $-60°C$ without heating; thus, the assumptions simplify the component selection process.

Table 4.8: Assumptions list used for general subsystem sizing.

Assumption ID	Category	Assumption	Justification (Quantitative)
ASP-SSY-3.1	General	Thermal management of internal components not rated for cruise temperature is neglected.	Components will be selected for the cruise temperature. Where suitable temperature-resistant components cannot be found, others are used. Extra power or mass added for thermal management of these small and limited components is negligible [26].
ASP-SSY-3.2	Flight Control System (FCS)	Heating of externally placed FCS components is activated intermittently, when necessary for de-icing.	Partial vapour pressure of water is negligible at cruise, with ice-formation mostly occurring during climb and descent[a].

[a] https://flightsafety.org/asw-article/weather-concerns-for-general-aviation/ [cited 7 May 2026]

4.3.2. General Subsystems Design Results

The next step is to size the general subsystems. Firstly, the flight condition system will be sized, followed by the computer and communication systems.

Flight Condition System

The flight condition system consists of all sensors needed to determine flight characteristics, such as velocity, attitude, and position, are determined and chosen. Firstly, a pitot-static tube is used to measure indi-

cated airspeed. With this, a pitot-static tube had to be chosen that could perform at all altitudes from sea level to cruise altitude, as these would be encountered during climb and descent. Because of this, a heated pitot-static tube is needed for de-icing. Moreover, the pitot-static tube has to be able to operate at the cruise air temperatures. Because of this, the HPS-1 was chosen, as it fulfils all of these and is used commercially[1]. Next, for satellite navigation, simple off-the-shelf components are considered that can sustain low temperatures. Because of this, the Mosaic-X5 was chosen, as it fulfils these requirements at a relatively low cost, while being readily used by UAVs. After this, a system is needed for attitude and heading determination. To do so, an all-in-one flight controller was chosen that includes IMUs, a barometer, and magnetometers with redundancy[2]. For these tasks, the Pixhawk 6C was chosen due to its altitude performance and its low cost. Following this, an angle of attack vane is needed. Consequently, the RAOA-022 was chosen for its lightweight structure and its low cost. Lastly, a temperature probe is needed. For its commercial availability and large operating temperature range, the 0129G is used. As sensors within this subsystem are more prone to failure, and due to regulatory requirements , redundant components are used for all components in the flight condition system[3][4]. For external components, this has the added advantage of providing bilateral symmetry.

Computer System

For the AHAPS to communicate between its subsystems, a computer system is needed that acts as a centralised point where data is sent, received, and transferred. Although significant amounts of data are transferred between all subsystems, using requirement **REQ-STK-1.10** of the minimum data stream of 1 Mbit/s provides a lower bound for the data handling rate of the computer system. With this data mostly being transferred without much processing, a single-board computer can be used. Here, a Raspberry Pi 5 was chosen due to its low cost, small footprint, and sufficient clock speed for the use case at 2.4 GHz[5]. Additionally, the network cables connecting the computer system to the other subsystems are also sized. Most of the systems in need of a network connection are placed close to the computer system. This is except for the control systems, which are outboard on the wings and at the wingtips. Therefore, total network cable length must be greater than the wingspan of the aircraft, and as such, a conservative estimate of 50 metres was taken, approximately 1.5 wingspans. Here, the Prysmian Cat5e SF/UTP cable was used, again for its price and off-the-shelf availability. Together, these components allow for communication and connection of the subsystems while still maintaining low masses, volumes, and power draws.

Communication System

After the computer system, the communication system must be sized. Firstly, to fulfil the 1 Mbit/s requirement, the antenna used must be sized. The first step to do so is to determine the frequency band at which the HAPS will communicate. Typical communication at FL600 is done within the UHF band[6]. For the sizing of the necessary power, the highest frequency of this band was chosen, as this would be a conservative calculation, as data transfer at higher frequencies requires more power. To calculate the power, free space loss for the 400 km communication range described in **REQ-STK-1.6**, atmospheric attenuation, and noise are considered. Resulting from a link budget analysis, a reasonable transmitting power of 15 W was found for this antenna. The L3Harris C98-1 is consequently chosen, which is a typical aircraft UHF antenna[7]. Next, to broadcast the GPS position of the aircraft, an ADS-B (Automatic Dependent Surveillance-Broadcast) transmitter is needed; for the best price to performance capabilties the ping 20Si was chosen. After this, an ELT (Emergency Locator Transmitter) is required by **REQ-STK-2.3**, for similar reasons as the ADS-B; the Artex ELT 345 was chosen here. Lastly, an SSR (Secondary Surveillance Radar) is also required by **REQ-STK-1.7**. For this, the Garmin GTX 345 is selected, due to its also being commercially used in similar applications. Moreover, it has a favourable price and temperature performance.

[1] https://www.swiss-airdata.com/products/pitot-static-probes/hps-1 [cited 12 June 2026]

[2] https://www.reichelt.com/nl/nl/shop/product/pixhawk_6c_vliegregelaar_pm02_powermodule-340476 [cited 12 June 2026]

[3] https://www.southernwings.co.nz/aircraft-flight-instruments-explained/ [cited 16 June 2026]

[4] https://www.easa.europa.eu/en/document-library/easy-access-rules/easy-access-rules-unmanned-aircraft-systems-regulations-eu [cited 16 June 2026]

[5] https://pip-assets.raspberrypi.com/categories/892-raspberry-pi-5/documents/RP-008348-DS-6-raspberry-pi-5-productbrief.pdf [cited 11 May 2026]

[6] https://wiki.radioreference.com/index.php/Aircraft [cited 12 June 2026]

[7] https://www.l3harris.com/sites/default/files/2021-05/C7-C98-1-Series-Antenna-Spec-Sheet-SAS-60958-Web-1.pdf [cited 22 June 2026]

4.3.3. General Subsystems Tool Verification

In the sizing of the general subsystems, only one design tool is used. This is done for the antenna sizing of the communication system. A link budget tool was used to find the necessary transmitter power, which was used to select an appropriate antenna. This tool was verified with code tests using pytest. An overview of these tests can be seen below in Table 4.9. Moreover, the exact equations used were verified by comparing with sizing methods from literature.

Table 4.9: General subsystems tool code verification test descriptions and outcomes.

Test ID	Test Description	Test Pass Criteria	Result
CODE-VER-3.1	Link budget tool null value test	Returns null transmitter and receiver power.	Passed
CODE-VER-3.2	Link budget tool order-of-magnitude test	Returns transmitter power between 0 and 50 dBm; receiver power between −100 and 50 dBm[a].	Passed
CODE-VER-3.3	Link budget tool constant initialisation test	Returns Boltzmann constant and speed of light.	Passed
CODE-VER-3.4	Link budget tool class variable initialisation test	Returns inputted values for data rate, transmission frequency, modulation method, and link margin.	Passed
CODE-VER-3.5	Link budget tool output type test	Returns floats for both transmitter and receiver power usage.	Passed
CODE-VER-3.6	Link budget analytical test	For given inputs, it returns reasonable transmitter and receiver power usages[a].	Passed
CODE-VER-3.7	Link budget monotonicity test	Returns increased powers when increasing: link margin, transmission frequency, and data rate.	Passed

[a] https://www.tme.eu/en/news/library-articles/page/75352/decibels-in-electronics-db-dbm-dbv-a-guide-to-units/ [cited 16 June 2026]

4.3.4. General Subsystems Characteristics Overview

The flight condition, computer, and communication system all consist of off-the-shelf commercially available parts. Therefore, it is trivial to find the total cost of each of the systems, with their attributed masses and power usage. A full summary of these results is shown in Table 4.10. For redundancy, two of every component in the Flight Condition system are used. Additionally, 50 m of network cabling was considered, which is sufficient to stretch the entire wingspan of the aircraft, with a 50% margin.

Table 4.10: Overview of the off-the-shelf components in the general subsystems. This system is broken up into three subsystems: the flight condition system, the computer system, and the communication system. For each component in these systems, its mass, power draw, and cost are shown.

Category	Component	Reference Model	No.	Mass per unit (kg)	Power per unit (W)	Cost per unit (€) (FY26)
Flight Condition	Flight Computer	Pixhawk 6C[a]	2	0.06	8	410
Flight Condition	GNSS	Mosaic-X5[b]	2	0.01	1	480
Flight Condition	Heated Pitot Tube	HPS-1[cd]	2	0.09	60	17,900
Flight Condition	Angle of Attack Vane	RAOA-022[e]	2	0.05	2	500
Flight Condition	Temperature Probe	0129G[fg]	2	0.18	1	3,540
Communication	ADS-B	Ping 20Si[h]	1	0.02	20	3,380

Continued on next page

Category	Component	Reference Model	No.	Mass (kg)	Power (W)	Cost (€)
Communication	ELT	Artex ELT 345[i]	1	0.91	5	1,400
Communication	SSR	Garmin GTX 345[j]	1	1.04	18	6,600
Communication	Antenna	L3Harris C98-1[kl]	1	0.37	15	1,000
Computer System	Computer	Raspberry Pi 5[m]	2	0.05	3	160
Computer System	Network Cables	Prysmian Cat5e SF/UTP[n]	1	3.20	–	140
Total				**6.42**	**133**	**60,000**

[a] https://www.reichelt.com/nl/nl/shop/product/pixhawk_6c_vliegregelaar_pm02_powermodule-340476 [cited 12 June 2026]
[b] https://docs.sparkfun.com/SparkFun_GNSS_mosaic-X5/assets/component_documentation/Septentrio_mosaic-X5_LR.pdf [cited 20 May 2026]
[c] https://www.swiss-airdata.com/products/pitot-static-probes/hps-1 [cited 12 June 2026]
[d] https://www.seaerospace.com/sales/product/Aerosonic/PST305/PST305 [cited 16 June 2026]
[e] https://www.radiantinstruments.com/product-page/angle-of-attack [cited 16 June 2026]
[f] https://ww2.txtav.com/Parts/PartSearch/PartsDetail/0129G [cited 16 June 2026]
[g] https://aeroval.com/ref/531892/0129G/ [cited 16 June 2026]
[h] https://uavionix.com/wp-content/uploads/2025/06/Ping20Si-DataSheet_Rev20J.pdf [cited 11 May 2026]
[i] https://www.acrartex.com/wp-content/uploads/downloads/1783/ELT_345_-_Bifold_-_web.pdf [cited 11 May 2026]
[j] https://www.aero-hesbaye.be/dossiers/GTX335/GTX%20345%20335%20installation.pdf [cited 11 May 2026]
[k] https://www.l3harris.com/sites/default/files/2021-05/C7-C98-1-Series-Antenna-Spec-Sheet-SAS-60958-Web-1.pdf [cited 22 June 2026]
[l] https://www.seaerospace.com/sales/product/L3Harris/DMC7-3 [cited 22 June 2026]
[m] https://pip-assets.raspberrypi.com/categories/892-raspberry-pi-5/documents/RP-008348-DS-6-raspberry-pi-5-productbrief.pdf [cited 11 May 2026]
[n] https://dk.prysmian.com/sites/default/files/atoms/files/UC_Datakabler_Cat_5-6-7-8-web.pdf [cited 18 May 2026]

4.4. Airframe System

In this section, the design process of the airframe system is outlined. The airframe system consists of the general wing planform and associated ìnternal structural elements.

4.4.1. Airframe System Assumptions

Due to time constraints and limits imposed on the detailed conceptual design phase of the AHAPS project, several important assumptions were necessary during the design and sizing process of the airframe system. They have been summarised and presented in Table 4.11.

Table 4.11: List of assumptions and their justifications in the design and sizing of the aircraft's airframe.

Assumption ID	Category	Assumption	Justification (Quantitative / Qualitative)
ASP-SSY-4.1	Spar Structure	Internal bending and shear loads are only carried by the spar structure, excluding clamps and rubber linings.	These loads are predominantly carried by the spar [25]. Doing so is a conservative calculation, as these structures are assumed to carry higher structural loads, thus being slightly overdesigned.

Continued on next page

Assumption ID	Assumption	Justification (Quantitative / Qualitative)	
ASP-SSY-4.2	Spar Structure	Clamp is a hollow structure; thus, a 0.25 weight factor is applied to its weight.	The clamp is sizeable; assuming solid would grossly overestimate mass, especially as it is not designed to be load-bearing. Non-load-bearing aerospace structures are typically hollow to save weight [25].
ASP-SSY-4.3	Spar Structure	CFRP spar maximal directional strength is in the direction of the spar.	CFRP is anisotropic, so it will be designed so that the strength is maximised in the direction carrying most loads [25].
ASP-SSY-4.4	Spar Structure	The second spar is as heavy as one sleeve, as it has similar geometry and weight.	Root section has a smaller width than sleeve length; additionally, sleeve has a lower specific strength than the CFRP of the spar, so this assumption is conservative.
ASP-SSY-4.5	Spar Structure	The clamp leg width is three times the diameter of the selected bolts.	This allows for sufficient threading space and is conservative[a].
ASP-SSY-4.6	Spar Structure	The clamp length is five times the clamp leg width, thus 15 times the bolt diameter.	This is conservative and allows for sufficient pressing area over the sleeve.
ASP-SSY-4.7	Airframe Skin	Minimum wing skin thickness is 0.15 mm.	Using a skin much thinner than this reduces puncture resistance and structural integrity[b].
ASP-SSY-4.8	Spar Structure	Spar and its fasteners are manufactured untwisted, with only ribs and skin twisted.	Twisted ribs and skin are sufficient to provide the required wing twist. Untwisted spars simplify manufacturing and enable modularity.
ASP-SSY-4.9	Airframe Skin	Wing skin contributes to torsional stiffness for wing twist deformation.	The skin has a large cross-sectional area compared to the spar, compensating for lower stiffness; thus, its contribution to torsional rigidity is non-negligible.
ASP-SSY-4.10	Structure Loading	Only static loads are considered; dynamic loads are not included.	Dynamic load analysis is beyond the scope of conceptual design and will be addressed in later design stages.
ASP-SSY-4.11	Structure Loading	Maximum stress on spar is calculated by taking the position as half of the maximum thickness of the airframe.	As the spar sustains all loads, its centroid is the neutral point; thus, the maximal distance from this point will be half the max airframe thickness. Additionally, this overestimates loads and is therefore conservative.

[a] https://eurocodeapplied.com/design/en1993/bolt-design-properties [cited 16 June 2026]

[b] https://www.wescap.nl/polyester-film?

4.4.2. Airframe System Design

The airframe is composed of many systems, all of which have to be sized for the AHAPS. Both the aerodynamic design and the structural design are part of the airframe system. The aerodynamic design is conducted and outlined under the airfoil selection and aerodynamic analysis subheadings. Following that, the spar, skin, and rib geometry design and sizing methods are explained.

Airfoil Selection

Airfoil selection for a high-altitude, long-endurance aircraft requires consideration of multiple criteria. The airfoil must be optimised for high lift and low profile drag. Furthermore, the pitching moment of the wing must be as close to zero as possible to ensure stability and minimize drag at the maximum lift-to-drag ratio. Additionally, due to the absence of a large fuselage, the thickness-to-chord ratio must be sufficiently large to accommodate the internal components of the AHAPS. Finally, the stall angle of attack and the maximum C_l are compared between airfoils. Four different airfoils were selected to perform a trade-off for application in flying wing designs, shown below in Table 4.12 [27]. Based on the trade-off, the MH91 airfoil was selected.

Table 4.12: Airfoil trade-off

CRITERION / OPTION / WEIGHTED SUM	Max C_l/C_d 20%	t/c (%) 20%	Stall α 15%	C_m at max. C_l/C_d 30%	Max. C_l 15%
MH61	84.36 @ $\alpha = 5.25°$	10.26	11	-0.0074	1.0242
MH60	82.8 @ $\alpha = 6.25°$	10.08	12	-0.0101	1.2465
EPPLER 344	94.9 @ $\alpha = 10.5°$	14.7	14	-0.0355	1.5419
MH91	78.1 @ $\alpha = 9°$	14.98	14	0.0106	1.3519

Aerodynamic Analysis

As described in Section 4.1.3, the aerodynamic analysis of the airframe is crucial for its geometric sizing and subsequent structural analysis and weight estimation. To this end, the quasi-linear lifting line method, as implemented in the `aerosandbox` Python library, was initially considered [3, 28]. It approximates viscous effects and enables full parametric definitions of wing planforms, fuselages, and nacelles, being thus convenient to include in the inner iteration loop [3].

The outputs of this analysis include a lift curve, drag polar, and panel force distribution. It is worth noting, however, that the `aerosandbox` library had to be locally copied and modified in order for the aforementioned distribution to be accessed. The lift curve has been approximated as a linear function via a polynomial fit of the analysis results, as has been done for the drag polar, where a three-term polar has been assumed. To ensure accurate results for sizing purposes, the region used to obtain the polynomial fit of the drag polar has been restricted to values between 20% of the minimum lift coefficient and 95% of its maximum. The reason for this is that the AHAPS is known to operate at relatively high lift coefficients for most of its mission profile, with this especially being the case during cruise.

After repeated runs of the optimizer, however, it has been observed that a pure quasi-linear lifting line method analysis, as is implemented in `aerosandbox`, yields unrealistically low results for the AHAPS' wing planform. For an aircraft with an aspect ratio as high as the current design, one can reasonably expect a maximum lift-to-drag ratio above or around 40 and a span efficiency factor above 0.7 [17, 29]. For comparison, the code's actual outputs predicted a maximum lift-to-drag ratio of around 30 and a span efficiency in the order of 0.4. To mitigate this issue, it has been decided to instead combine the results of an inviscid vortex lattice method analysis with the profile drag computed by the aforementioned lifting line method,

yielding results similar to the polar obtained in Figure 4.7.

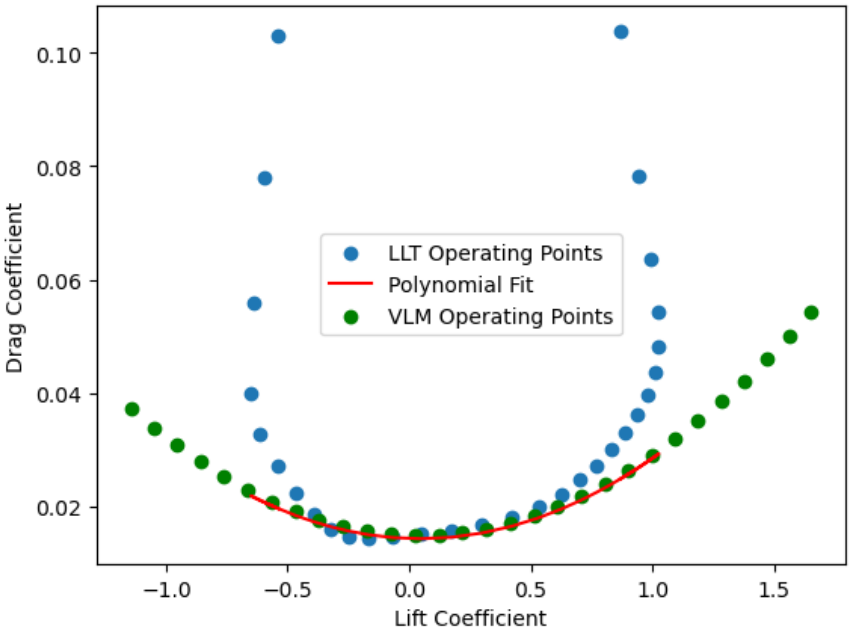

Figure 4.7: Drag polar of the wing obtained by combining the vortex lattice and lifting line methods.

As can be observed from the aforementioned graph, the vortex lattice analysis predicts noticeably lower induced drag, leading to lift-over-drag values between 40 and 42. To verify the validity of this method, a more detailed XFLR5-analysis shall be conducted during the compliance phase. Its results can be found in Section 6.1.3.

Spar Geometry Generation

The spar is the main load-carrying element of the airframe. According to **ASP-SSY-4.1** in Table 4.11, these are to carry all bending and shear loads. Therefore, the sizing and design of the spars will be based on the total loads incurred by the aircraft. Provided a wing planform, the resulting force and moment distributions are obtained via the aforementioned aerodynamic analysis. The most limiting load from this analysis is bending about the x-axis, which can be seen in Figure 4.8. Provided the loads, the spar can subsequently be sized. Based on reference HAPS and due to its excellent stiffness and strength, CFRP was chosen for the main spar structure[1]. Together with a load factor from static manoeuvring and gust loads calculated in Section 6.1.1, the maximum loads the spar must sustain are computed. This loading, combined with material yield stress and using the max airfoil thickness position, provides minimums for the area moments of inertia of the spar in the x and z directions. Since wing bending is typically the critical load case for aircraft, this is used to size the spar [25]. For the wing spar, an elliptical cross-section was chosen due to its greater performance in terms of stress concentration, and as it is simpler to manufacture tubular structures out of CFRP[2].

Since one continuous spar does not fit within the 20 ft ISO container, the spar needs to be broken up into sections and bonded together. This structure needs to sustain the same loads as the spar at its discontinuities. Therefore, the connector design needs to have a structure that both transfers the loads while also sustaining them. To do so, a connector consisting of two separate connector parts is considered. It consists of a sleeve that is slid over the top of the spar, along with clamps that hold these together, as shown in Figure 4.9. In this case, the sleeve takes over the loads of the spar at the discontinuity, while the connector allows for the transfer of the load and for the joining of the spar section. Since the spar is elliptical, an elliptical

[1]https://www.uncrewed-systems.com/explores-the-development-of-this-solar-powered-uav-engineered-to-deliver-a-variety-of-services-from-the-stratosphere/ [cited 29 April 2026]
[2]https://element6composites.com/carbon-fiber-manufacturing-methods/ [cited 10 June 2026]

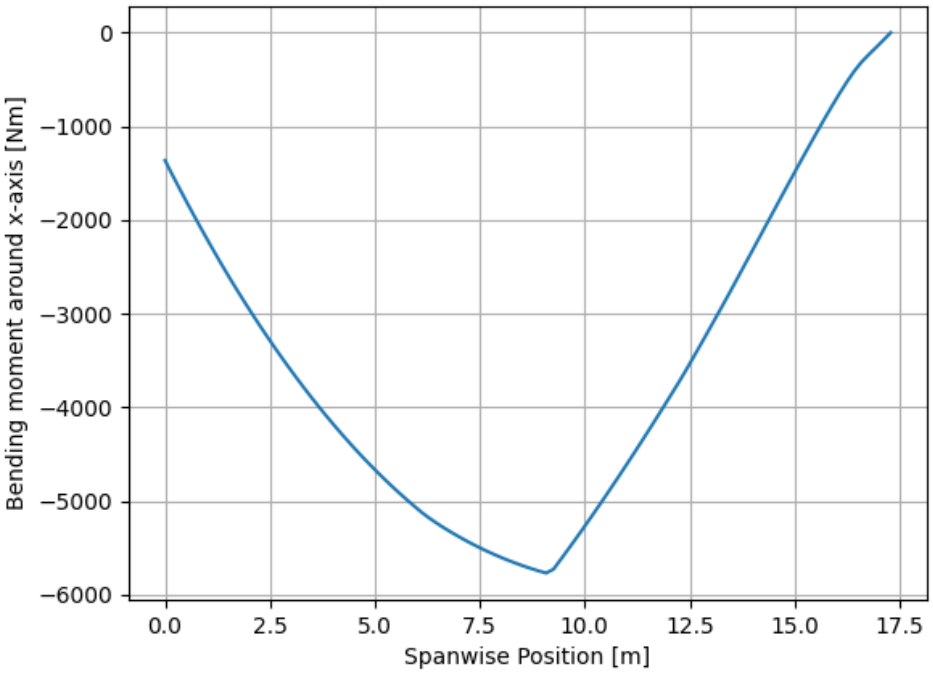

Figure 4.8: Bending around the x-axis over the span half-span of the aircraft. This analysis includes bending relief from component masses.

sleeve around it will not allow for any lateral relative motion between the sleeve and spar. Thus, clamping only needs to prevent spanwise slipping. To clamp the sleeve, three clamps are added to the sleeve, at each end and in the middle. These clamps need to be lightweight while still holding shape, so they are made of a lightweight nylon 6 structure. The overall structure is not filled, with it only being assumed to be 0.25% of the volume. As the sleeve is slightly deformed in clamping, it can no longer be made of CFRP, as this is not a ductile material. Therefore, titanium was chosen instead for its relatively high specific stiffness for a ductile material. Because of this, the sleeve was chosen to be made of titanium.

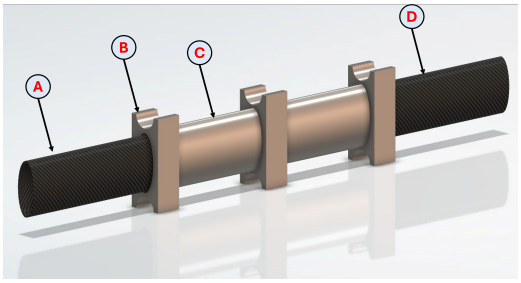

(a) This is the assembly of the clamp structure. Where: A - spar 1, B - clamp, C - sleeve, D - spar 2.

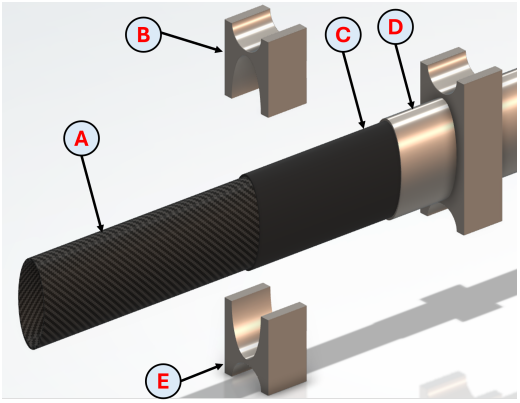

(b) This is an exploded view of the clamp structure. Where: A - spar, B - top clamp, C - rubber lining, D - sleeve and E - bottom clamp.

Figure 4.9: CAD model of the clamp structure.

With the provided area moments of inertia and the wing geometry for the aerodynamic analysis, the spar structure can be optimised. There are four variables to be optimised simultaneously: clamp width, eccentricity ratio, which is the ratio between the semi-major and semi-minor axes of the ellipse, spar thickness, and sleeve thickness. For this optimisation, an available width is given around the airfoil maximum thick-

ness location, selected to be 20% of the chord length. This allows sufficient cross-sectional area for the batteries to be in front of the spar structure, which constrains the clamp width. To simplify the analysis of stress concentrations, a maximum eccentricity factor of 5 is specified, while maintaining a minimum of 1.5 to preserve the advantages of an elliptical structure. The minimum spar thickness is given by the physical limit of CFRP, with a hard limit of 0.0005 m thickness[1]. The sleeve thickness is given by the limit of titanium. Whilst titanium has no limit within the order magnitude of the AHAPS design, a limit of 0.0005 m is chosen to avoid deterioration issues[2].

Skin Geometry Generation

Proceeding from this, the structure of the airframe skin can be sized. With a large surface area, it is prioritised to have the lightest possible structure. Moreover, with the assumption that the spar is able to sustain all bending and shear loads, the structure can be designed to be both lightweight and have low stiffness. With this, a trade-off was performed to determine the optimal material for the skin. Trade-off criteria have been determined, resulting in a trade-off for five different materials [30]. This trade-off is shown in Table 4.13. The trade-off criteria here determined that the most important factors are the weight of the material, which is followed by repairability, and lastly, the remaining categories of torsional stiffness, cost, and temperature range. From this, a clear winner of mylar was determined, with excellent performance in all but one category. The remaining category of "Torsional Stiffness" received good. This was deemed to be less important, as the spar was assumed to carry the twist load, and by compatibility with a higher shear stiffness of the spar, this would carry the majority of the load. The airframe skin thickness was set to the greater of two values, namely either the minimum thickness required to withstand all torsional loads, or a baseline thickness of 0.00015 m, which is comparable to a standard plastic bag[3].

Table 4.13: Skin material trade-off table.

CRITERION / OPTION	**Weight** 35%	**Torsion Stiffness** 15%	**Cost** 15%	**Temp Range** 15%	**Reparability** 20%
CFRP	Substantial weight for intended purpose	Great torsional stiffness	Expensive	Undesired, but manageable temperature range	Complex to repair
Mylar (PET film)	Extremely light compared to competitors	Moderate torsional stiffness	Very cheap	Excellent temperature range	In-field tape repairable
Kevlar	Substantial weight for intended purpose	Moderate torsional stiffness	Moderately cheap	Good temperature range	In-field patch repairable
EPP foam + film	Substantial weight for intended purpose	Great torsional stiffness	Very cheap	Good temperature range	In-field repairable, but hard to do so
Tedlar (PVF film)	Reasonably light	Poor torsional stiffness	Moderately cheap	Excellent temperature range	In-field tape repairable

[1] https://www.carboncenter.pl/en/tubes/ [cited 11 June 2026]

[2] https://knowledge.bsigroup.com/products/aerospace-series-sheets-cold-rolled-in-titanium-and-titanium-alloys-thickness-0-2-mm-a-6-mm-dimensions

[3] https://www.plasticbags.com.au/what-thickness-do-i-need/ [cited 11 June 2026]

Rib Geometry Generation
After having sized the spar section and the skin, the ribs can be designed. This is done according to a buckling analysis for the wing spar. With this, a minimum spacing across the span of the wing is determined. Spar spacing and sizing the webs and flanges is done according to Chiozzotto [31]. The material chosen for the ribs is CFRP, similar to the spar. This is because they are loaded in the same fashion and do not have to deform plastically.

4.4.3. Airframe System Tool Verification
In this section, the airframe sizing tools are verified. This justifies their usage for the AHAPS design.

Table 4.14: Airframe system tool code verification test descriptions and outcomes.

Test ID	Test Description	Test Pass Criteria	Result
CODE-VER-4.1	Aerodynamics order of magnitude test.	For large aspect ratio untapered wing, returns maximum C_L between 1 and 3; returns CD_0 between 0.0 and 0.1; returns maximum L/D above 40; returns e between 0.7 and 1 [17, 29].	Passed after correction
CODE-VER-4.2	Structural loading order of magnitude test.	Returns second area moment of inertia requirements between 10^{-10} and 10^{-5} m^4; Returns deflections between 0% and 50%.	Passed
CODE-VER-4.3	Structural sizing order of magnitude test.	Returns total structural mass between 10 and 1000 kg.	Passed
CODE-VER-4.4	Structural sizing optimizer constraints test.	Returns values with boundaries; optimizer did not over/undershoot set constraints.	Passed
CODE-VER-4.5	Structural sizing feasibility test.	Returns geometry that is feasible, all separate parts fit within each other.	Passed
CODE-VER-4.6	Structural sizing weight computation test.	Returns correct fractions of weight structure.	Passed
CODE-VER-4.7	Structural sizing constants initialisation test.	Returns correct material properties ρ, E, σ_y, σ_{ult}, and τ_{ult} for CFRP, titanium, aluminium, mylar and nylon.	Passed
CODE-VER-4.8	Structural sizing class initialisation test.	Returns inputs such as aircraft layout and structural loading.	Passed
CODE-VER-4.9	Aerodynamic class initialisation test.	Returns the inputted aircraft layout, including span, aspect ratio, chord length, sweep, taper, and twist.	Passed
CODE-VER-4.10	Aerodynamic output type test.	Returns floats for aerodynamic constants.	Passed
CODE-VER-4.11	Structural loading output type test.	Returns floats for second area moments of inertia and deflections.	Passed
CODE-VER-4.12	Structural sizing output type test.	Returns float for masses.	Passed
CODE-VER-4.13	Aerodynamic monotonicity test.	Returns positive quadratic lift-drag curve; returns higher e ratio with bigger aspect ratio, taper closer to 0.445 [32].	Passed
CODE-VER-4.14	Structural loading monotonicity test.	Returns higher deflections when input with higher loads; Returns higher second area moments of inertia when input with higher loads or lower stress tolerance.	Passed

4.4.4. Airframe System Characteristics Overview
The general characteristics of the sized airframe are provided in Table 4.15.

Table 4.15: Overview of the masses and costs of each component of the airframe system. Some components are off-the-shelf components that require no additional manufacturing, which are shown by both columns being combined. The cost of the sleeves is estimated by the price of off-the-shelf circular tubes of similar dimensions. The cost and mass of the winglet are estimated as proportional to the rest of the wing based on its span.

Component	**Material**	**Cross Sectional Dimensions**	**Quantity**	**Mass [kg]**	**Material Cost (€) (FY26)**	**Manufacturing Cost (€) (FY26)**
Spar	CFRP	$a \times b \times t = 82.70 \times 34.87 \times 1.2$ mm	l = 37.73 m	16.74	3,400[a]	44,000[b]
Skin	Mylar	t = 0.15 mm	S = 129.11 m^2	26.92	500[c]	
Clamps	Nylon 6	$l \times w \times h$ = 90 × 109 × 129 mm	30 units	7.60	100[d]	5,000
Bolts	Titanium	$l \times d$ = 129 mm, M6	48 units	1.00[e]	1,500[fg]	
Ribs	CFRP	MH91 airfoil (c = 1.77 m, t/c = 0.15)	23 units	3.82	1,000[a]	92,000[b]
Outer sleeve	Titanium	$a \times b$ = 86 × 36 mm	l = 9.0 m	22.92	1,000[h]	
Inner sleeve	Rubber	$a \times b$ = 83 × 35	l = 9.0 m	2.18	50[i]	
Winglet	CFRP spar and ribs, mylar skin	NACA0012 airfoil, $h \times c$ = 2.0 × 1.77 m, t/c = 0.12	2 units	4.80	3,000	
Total Airframe System				**85.98**	**152,000**	

[a] https://www.supreemcarbon.com/cost-lifecycle-aerospace-carbon-fiber.html [cited 15 June 2026]
[b] https://www.supreemcarbon.com/cost-guide-custom-carbon-fiber-pricing-explained.html [cited 9 June 2026]
[c] http://easycomposites.eu/mylar-release-film [cited 15 June 2026]
[d] https://businessanalytiq.com/procurementanalytics/index/pa6-price-index/ [cited 15 June 2026]
[e] https://www.engineeringtoolbox.com/metal-alloys-densities-d_50.html [cited 15 June 2026]
[f] https://www.ebay.com/itm/175792725655 [cited 15 June 2026]
[g] https://www.fastpreci.com/blog/titanium-vs-stainless-steel/ [cited 15 June 2026]
[h] https://performancetubeproducts.com/collections/titanium-tube-1-2mm-wall/products/titanium-tube-63-5mm-2-1-2-1-2mm-wt-1220mm-length
[i] https://themetalhouse.co.uk/product/1mm-thick-1-metre-wide-rubber-sheet/ [cited 15 June 2026]

4.5. Power System

The power system is a key component of the design, defining the endurance capabilities of the aircraft. This section outlines how the power system characteristics are chosen and how they are sized.

4.5.1. Power System Assumptions

Table 4.16: Assumptions list solar modelling.

Assumption ID	**Category**	**Assumption**	**Justification (Quantitative)**
ASP-SSY-5.1	Solar Modelling	The energy required during daytime is equal to the energy needed during nighttime.	This is a conservative estimation, but most of the systems used during the daytime can also be active during the night.
ASP-SSY-5.2	Solar Modelling	The solar constant is assumed to be the vacuum value of 1361 W/m^2.	The solar constant in a vacuum is similar to the solar constant experienced at 60,000 ft, during cruise [33].

Continued on next page

Assumption ID	Category	Assumption	Justification (Quantitative)
ASP-SSY-5.3	Solar Modelling	The Earth's axial tilt is fixed at 23.45°.	This value is standard for the average Earth axial tilt [34].
ASP-SSY-5.4	Solar Modelling	The Earth's declination angle is modelled as a sine wave over the year.	A sine is a close enough approximation for preliminary sizing [34].
ASP-SSY-5.5	Solar Modelling	The cloud top height is assumed to be up to cruise altitude at 60,000 ft.	This is a safety margin, as cloud top height changes day by day.
ASP-SSY-5.6	Solar Modelling	Solar noon occurs at 12:00, such that sunrise and sunset times are given relative to this time.	Local noon varies by region due to time zones, so instead computations are based on solar time, which can be shifted later depending on specific timezone conditions.
ASP-SSY-5.7	Solar Modelling	Solar conditions at 60000 ft are AM0	Valid due to the high degree of thinning of the atmosphere [33]
ASP-SSY-5.8	Solar Modelling	Solar conditions below 60000 ft are estimated with sea level empirical relations	Conservative as solar conditions improve at higher altitudes[a].
ASP-SSY-5.9	Battery	All properties of Amprius' 500 Wh/kg batteries are equal to their 450 Wh/kg batteries.	Amprius' high-density batteries have similar compositions, making it likely that their new batteries have similar or better properties than their older models[b].
ASP-SSY-5.10	Battery	Battery degradation is exponentially proportional to depth of discharge, of which the exponent is estimated based on similar battery performance.	This relation is proven and used commonly as a back-of-the-envelope calculation if no better data is available[c].
ASP-SSY-5.11	Solar Panel	The solar cells have an out-of-factory efficiency of 30%.	Silicon-based multijunction solar panels with an efficiency of 30% are deemed feasible for production in the near future at a low cost[d].
ASP-SSY-5.12	Solar Panel	The solar cells have a packing density of 94%.	Triple junction solar cells are proven to have a packing density of 94% [35].
ASP-SSY-5.13	Solar Panel	The solar cells have an annual degradation rate of 2%.	Conservative value based on statistics of previously used solar panels[e] [36].
ASP-SSY-5.14	Solar Panel	The solar cells are estimated to have an area-mass density of 400 g/m^2.	This is similar to area-mass densities found for triple-junction solar cells, with an added margin for other internal components [35].
ASP-SSY-5.15	Miscellaneous	Additional power system components such as electrical wiring, cabling, and power distribution unit mass have a total mass of 9 kg and an estimated cost of €4000	Estimated 40 m of 8 AWG copper power wiring, together with required power distribution unit, plus an added 100% safety margin[fgh].

[a] https://www.pveducation.org/pvcdrom/properties-of-sunlight/air-mass [cited 8 June 2026]

[b] https://amprius.com/solutions/sicore/ [cited 6 May 2026]

[c] https://solarmathlab.com/content/batteries/battery-lifespan-cycles-vs-DoD-estimator.html [cited 8 June 2026]

[d] https://www.k-online.com/en/Media_News/News/NREL,_Swiss_scientists_power_past_solar_efficiency_records [cited 10 June 2026]

[e] https://digitalcommons.usu.edu/smallsat/2023/all2023/212

[f] https://wiregaugecalculator.com/tools/wire-weight [cited 8 June 2026]

[g] https://www.ercmarket.com/UAVSYS-1200amp-power-distribution-board-pdb-for-industrial-uav/ [cited 8 June 2026]

[h] https://www.vicorpower.com/products?productType=cfg&productKey=V375B12C300BL [cited 8 June 2026]

4.5.2. Power System Design

This subsection goes into more depth into how the power storage and power generation are sized based on the endurance and deployability requirements. Multiple options are looked into based on cost and performance.

Solar Panel Design and Sizing

To design the solar panel, a solar model is used to compute the solar power that can be absorbed during the day. The daylight time in hours can be computed with Equation 4.4 [34, 38]. This equation underestimates the daylight time because it does not take into account refractive effects in the atmosphere, making the results conservative but a suitable approximation for the purposes of solar panel sizing [38].

$$T_s = \frac{2 \cdot 3600}{15} \cdot \frac{180}{\pi} \cdot \arccos(-\tan(\phi)\tan(\delta)), \tag{4.4}$$

where T_s is the daylight time in seconds, ϕ is the observer's latitude, and δ is the declination of the sun, both given in radians. The declination δ as a function of day of the year is approximately given by Equation 4.5,

$$\delta = 23.45 \sin\left(\frac{2\pi(274 + n_{days})}{365}\right), \tag{4.5}$$

where n_{days} is the number of days from the winter solstice, the day with the least daylight time in the northern hemisphere [34].

Subsequently, the angle of incidence of the sun on a horizontal surface I_s as a function of time in seconds t is given by Equation 4.6,

$$I_s(t) = \arccos\left(\cos(\phi)\cos\left(\frac{15}{180 \cdot 3600}\pi\left[\frac{T_s}{2} - (t - t_{rise})\right]\right)\cos(\delta) + \sin(\phi)\sin(\delta)\right), \tag{4.6}$$

where t_{rise} is the sunrise time in seconds after midnight, with $t = 0$ at midnight [34].

With these equations, a year-round solar model can be developed to analyse the power and endurance of any preliminary design. This enables the proper sizing of the solar panels.

The design team has, in coordination with the stakeholders, prioritised compliance with the all-season requirement **REQ-STK-1.2** and the cost requirement **REQ-STK-6.1**. This led to an all-year deployment latitude between 30°N/S. To comply with the cost requirement of €900,000, silicon-based multijunction solar cells are chosen instead of classic Gallium Arsenide panels, as the silicon-based cells are cheaper to produce[1][2]. These panels are still in active development, with efficiencies up to 36%, but for conservative calculations, an efficiency of 30% and a surface mass density of 0.400 kg/m^2 are assumed[1] [35]. Its properties are justified by assumptions in **ASP-SSY-5.9** to **ASP-SSY-5.12**.

The total area of the solar panels required is determined by calculating the power required during the day, divided by the power the solar panel can generate per m^2. The power output per unit area is limited to the predefined power limit or determined by the product of the solar panel efficiency, the solar constant, and the cosine of the average angle of incidence I_s. The total power requirement during daylight hours is computed to ensure sufficient energy is generated to cover both daytime and nighttime consumption. Finally, the surface area is derived by dividing the daylight power requirement by the power generated per square metre, and the mass is estimated by multiplying the area by the surface density of the panel. Given a constant power required P_r, a daylight time T_s, and a solar panel efficiency η, the solar panel size can be computed with Equation 4.7,

$$S = \frac{86400 P_r}{T_s} \frac{1}{\eta \cos(\bar{I}_s)}, \tag{4.7}$$

where the average daytime incidence angle $\bar{I}_s$ is computed with Equation 4.8,

[1] https://www.k-online.com/en/Media_News/News/NREL,_Swiss_scientists_power_past_solar_efficiency_records [cited 10 June 2026]

[2] https://sinovoltaics.com/learning-center/solar-cells/gaas-solar-cells/ [cited 6 May 2026]

$$\bar{I_s} = \frac{\pi}{2} - \frac{2}{\pi}\left(\frac{\pi}{2} - I_{s_{max}}\right), \tag{4.8}$$

assuming that the incidence angle follows a sinusoidal pattern during the day [39].

The solar radiation changes depending the path through the atmosphere that the radiation takes[1]. This is only prevalent at lower altitudes, with atmospheric effects being negligible at the cruising altitude of 60,000 ft, justified in **ASP-SSY-5.7**. During the climb phase, the solar intensity is approximated by sea-level relations justified in **ASP-SSY-5.8**, shown in Equation 4.9[1].

$$\eta_{atm} = 1.1 \cdot 0.7^{AM^{0.678}}, \tag{4.9}$$

where

$$AM = \frac{1}{\cos(I_s) + 0.50572(96.07995 - I_s \cdot \frac{180}{\pi})^{-1.6364}}. \tag{4.10}$$

Lastly, cloud cover needs to be addressed. Following **ASP-SYS-5.5**, a 4/8 Oktas cloud cover is assumed during non-cruise operations. The effectiveness of the solar panels is calculated using Equation 4.11, where N is the level of Oktas cloud cover [14].

$$\eta_{clouds} = 1 - 0.75(N/8)^{3.4} \tag{4.11}$$

Energy Storage System Design and Sizing
For the energy storage system, solid-state lithium-ion batteries are chosen for their reliability and simplicity, making them desirable for modular aircraft.

In particular, industry-leading Amprius lithium-ion batteries with an energy density of 500 Wh/kg are chosen, which are also used in the Zephyr aircraft[2]. Its remaining properties are assumed to be similar to Amprius' other high-density batteries, as explained in **ASP-SSY-5.9**[3]. Its lifetime is calculated based on depth of discharge and an exponent value computed from Amprius' 400 Wh/kg batteries, as explained in **ASP-SSY-5.10**[3].

The battery mass can be computed given a constant power required P_r, a daylight time T_s, and an energy mass density ρ_E, which is shown in Equation 4.12,

$$m = \frac{P_r(86400 - T_s)}{\rho_E}. \tag{4.12}$$

Notably, other manufacturers have also started mass-manufacturing 500 Wh/kg lithium-ion batteries intended for aerospace applications[4]. This indicates that the technology has matured and reached commercialisation, making it more viable.

4.5.3. Power System Tool Verification

Several tools are made to size the power system, including the solar model, the solar panel sizing tool, and the battery sizing tool. The tools have to be verified, both through code tests with pytest and through analytical tests based on theory.

[1] https://www.pveducation.org/pvcdrom/properties-of-sunlight/air-mass [cited 8 June 2026]
[2] https://amprius.com/the-all-new-amprius-500-wh-kg-battery-platform-is-here/ [cited 8 June 2026]
[3] https://web.archive.org/web/20240918163649/https://amprius.com/documents/Amprius_Product_Portfolio_0824_website.pdf [cited 19 May 2026]
[4] https://www.catl.com/en/news/6015.html [cited 9 June 2026]

Table 4.17: Power system tool code verification test descriptions and outcomes.

Test ID	Test Description	Test Pass Criteria	Result
CODE-VER-5.1	Battery sizing tool null value test.	Returns null battery mass and volume.	Passed
CODE-VER-5.2	Solar panel sizing tool null value test.	Returns null solar panel mass and area.	Passed
CODE-VER-5.3	Battery sizing tool order-of-magnitude test.	Returns battery mass between 1 and 1000 kg; volume between 0.01 and 1.0 m^3.	Passed
CODE-VER-5.4	Solar panel sizing tool order-of-magnitude test.	Returns solar panel area between 1 and 100 m^2; mass between 0.1 and 100 kg.	Passed
CODE-VER-5.5	Solar model order-of-magnitude test.	Returns daylight time of less than 24 hours.	Passed
CODE-VER-5.6	Battery sizing tool constant initialisation test.	Returns preset mass-energy density and volume-energy density.	Passed
CODE-VER-5.7	Solar panel sizing tool constant initialisation test.	Returns preset efficiency, power limit, and area-mass density.	Passed
CODE-VER-5.8	Solar model constant initialisation test.	Returns maximum solar incidence angle of 23.5° [38].	Passed
CODE-VER-5.9	Battery sizing tool class variable initialisation test.	Returns the input values for power required, DoD, latitude, and day.	Passed
CODE-VER-5.10	Solar panel sizing tool class variable initialisation test.	Returns the input values for power required, latitude, and day.	Passed
CODE-VER-5.11	Solar model class variable initialisation test.	Returns the input values for latitude and day.	Passed
CODE-VER-5.12	Battery sizing tool output type test.	Returns floats for mass and volume.	Passed
CODE-VER-5.13	Solar panel sizing tool output type test.	Returns floats for mass and area.	Passed
CODE-VER-5.14	Solar model output type test.	Returns float for daylight time.	Passed
CODE-VER-5.15	Solar model analytical test.	For given inputs, it returns the correct daylight time and solar incidence angle according to Equation 4.4 and Equation 4.6.	Passed
CODE-VER-5.16	Solar panel sizing tool analytical test.	For given inputs, it returns the correct solar panel area according to Equation 4.7.	Passed
CODE-VER-5.17	Battery sizing tool analytical test.	For given inputs, it returns the correct battery mass according to Equation 4.12.	Passed
CODE-VER-5.18	Solar model monotonicity test.	Returns shorter daylight times at higher latitudes during the winter solstice period.	Passed
CODE-VER-5.19	Solar panel sizing tool monotonicity test.	With longer daylight time or higher efficiency, returns lower solar panel surface area output.	Passed
CODE-VER-5.20	Battery sizing tool monotonicity test.	With longer daylight time or higher energy density, returns lower battery mass output.	Passed

4.5.4. Power System Characteristics Overview

The overview of power system characteristics for the AHAPS is given in Table 4.18 and Table 4.19.

Table 4.18: Final parameters of the chosen solid-state lithium-ion batteries.

Parameters	Value
Specific Energy (Wh/kg)	500[a]
Volumetric Energy Density (Wh/L)	1100[b]
Efficiency (%)	96[b]
Life Cycles (100% DOD)	150[b]
Life Cycles (80% DOD)	255[bc]
Life Cycles (68% DOD)	375[bc]
Operating Temperature (°C)	10-45[b]
Specific Cost (€/kWh)	600 [40]
Total Capacity (Wh)	**67,750**
Total Mass (kg)	**135.5**
Total Cost (FY26) (€)	**41,000**

Table 4.19: Final parameters of the chosen silicon-based multijunction solar panels.

Parameters	Value
Efficiency (%)	30[d]
Mass-Area Density (kg/m^2)	0.4 [35]
Yearly Degradation Rate (%)	2.0 [36, 37]
Packing Density (%)	94 [35]
Specific Cost (€/m^2)	2,560[d]
Total Area (m^2)	**61.5**
Total Mass (kg)	**24.6**
Total Cost (FY26) (€)	**160,000**

[a] https://amprius.com/the-all-new-amprius-500-wh-kg-battery-platform-is-here/ [cited 8 June 2026]

[b] https://web.archive.org/web/20240918163649/https://amprius.com/documents/Amprius_Product_Portfolio_0824_website.pdf [cited 19 May 2026]

[c] https://solarmathlab.com/content/batteries/battery-lifespan-cycles-vs-DoD-estimator.html [cited 8 June 2026]

[d] https://www.k-online.com/en/Media_News/News/NREL,_Swiss_scientists_power_past_solar_efficiency_records [cited 10 June 2026]

Additional power system components such as electrical wiring, cabling, and power distribution unit have an additional mass of 9 kg and a cost of €4000. This assumption is justified in **ASP-SSY-5.14**.

4.6. Propulsion System

In this section, the propulsion system design synthesis will be presented. The synthesis process is broken down into three different phases. First, a trade-off for the propeller orientation, distribution, configuration, and motor type is done. This is followed by the blades being sized to be optimised for cruise, for which a motor and electronic speed controller are chosen, after which the propulsion system's performance at take-off and climb is analysed to verify its performance.

4.6.1. Propulsion System Assumptions

The assumptions made during the detailed design of the propulsion system are listed in Table 4.20. They include assumptions related to, amongst others, the operating environment, as well as the cost and mass of components.

Table 4.20: Assumption list for the propulsion system.

Assumption ID	Category	Assumption	Justification (Quantitative)
ASP-SSY-5.1	Propulsion	The low temperature at cruising altitude allows for sufficient cooling.	Most electric motors are designed for low altitudes and require additional cooling at peak performance, which is not needed at cruising altitude.
ASP-SSY-5.2	Propulsion	All components of the propulsion system retain their sea-level properties at −60°C	This aspect is beyond the scope of the current project, requiring this assumption to be made.
ASP-SSY-5.3	Propulsion	The motor efficiency is equal to 90%.	This is the top of the range for brushless direct current motors, which is reasonable for this high-performance application [41].
ASP-SSY-5.4	Propulsion	The electronic speed controller efficiency is equal to 99%.	This value corroborates with results from past experiments [42].

Continued on next page

Assumption ID	Category	Assumption	Justification (Quantitative)
ASP-SSY-5.5	Propulsion	The value for $C_{L_{TO}}$ is 80% of the value for $C_{L_{max}}$.	This is conservative from Raymer [43].
ASP-SSY-5.6	Propulsion	The values for the Reynolds' number on the blade elements during take-off and cruise are 1,000,000 and 100,000, and it is linearly interpolated during climb for computational efficiency.	At cruise and take-off, these represent the Reynolds' numbers at the most effective blade section r = 0.75R following the methodology of Giljarhus et al. [44].
ASP-SSY-5.7	Propulsion	The value of the Reynolds' number is constant along the propeller blade.	The Reynolds' number is calculated for the centre of the blade, and this area is the most effective in creating thrust. The error was less than 5%, as verified by a simulation with varying Reynolds' number.
ASP-SSY-5.8	Propulsion	All assumptions that are made in *Performance Calculation and Design of Stratospheric Propeller* by Liu and He [45] are applicable.	This is valid as the context of the paper is a validated method for the design of a stratospheric propeller [45].
ASP-SSY-5.9	Propulsion	The propeller mass is 70% of a CFRP theoretical solid laminate equivalent mass calculated from the CAD model (30% weight reduction).	The use of a low-density core can achieve weight savings around 50% for an equivalent stiffness, which makes a 30% reduction a conservative estimate[e].
ASP-SSY-5.10	Propulsion	The rod connecting the nacelle to the wing is a cylinder of 0.500 m made of solid CFRP.	This ensures sufficient clearance between the propeller blade and the wing leading edge. The rod will be manufactured from CFRP. The mass estimate from a solid rod is conservative and ensures sufficient rigidity. In reality, the rod will be hollow to accommodate power and data cables.
ASP-SSY-5.11	Propulsion	The weight, material cost, and manufacturing cost of the motor mechanical assembly are 0.200 kg, €1500, and €1500, respectively.	The selection of these components is beyond the scope of the project, resulting in the assumption to be necessary.
ASP-SSY-5.12	Propulsion	The rolling friction coefficient during the take-off run is 0.08 [43].	From Raymer, typical μ values for ground rolling resistance are presented with the most conservative value μ_{runway} = 0.08 for wet grass surfaces [43].
ASP-SSY-5.13	Propulsion	The lift-to-weight ratio required for take-off is 1.2.	This is a conservative value from Raymer to ensure the AHAPS can climb after lifting off [43].
ASP-SSY-5.14	Propulsion	The AHAPS will be assisted during the take-off run by humans to achieve an initial velocity of 5 m/s.	This assumption is required for the model to work. The average human can run at this speed for a limited duration of time, but long enough for the take-off.

4.6.2. Propulsion System Design

For a couple of design decisions, it was necessary to perform trade-offs. These include propeller orientation, distribution, and configuration, and motor type, as shown in Table 4.21, Table 4.22, Table 4.23, and Table 4.24. Aerodynamic efficiency is the criterion with the largest weight. The endurance of the AHAPS is highly dependent on the aerodynamic efficiency, as higher efficiency means less power is required for the propulsion system. As such, it is given a weight of 30%. Following that, the thermal management of a subsystem operating in an ambient environment of −60°C and low air density is an important criterion, as no air molecules are available to carry heat away. This criterion is set at 25% to consider thermal management, but not designing in detail for it, as stated in **ASP-SSY-5.2**. Regarding structures and mass, 20% is chosen to take into account the physical weight limits the subsystem needs to obey, but also the weight distribution over the structure. Development and mechanical risk is allocated 15% to take into account system redundancy during a 28-day mission and punish complex, low-TRL options that come with high risks. Lastly, the cost and logistics are assigned the lowest weight of 10% not to overshoot the given budget and to comply with the logistics requirements.

Some design decisions were already made before the trade-off after consulting the other subsystem departments. The number of 2 blades per propeller was chosen to accommodate the landing. The two blades

allow the propeller to be stopped horizontally, reducing the required ground clearance, as shown by the Airbus Zephyr and the BAE Systems PHASA-35[12]. Additionally, the propulsion system's position is extended with a rod from the leading edge to provide enough clearance between the wing and the blades, as also shown by the Airbus Zephyr[1].

For the propeller orientation, shown in Table 4.21, the tractor propeller wins the trade-off with a combined score of 2.4, against 2.05 and 1.85 for the pusher and contra-rotating propellers, respectively.

Table 4.21: Propeller orientation trade-off.

CRITERION / OPTION	**Aerodynamic Efficiency** 30%	**Thermal Management** 25%	**Structure & Mass** 20%	**Development & Mechanical Risk** 15%	**Cost & Logistics** 10%
Tractor	Drag penalty for wing - 2	High airspeed for cooling - 3	Standard nacelle mass - 2	Standard for HAPS - 3	Standard - 2
Pusher	Undisturbed flow to wing - 3	Trailing wake - 1	Extended structure - 2	Thermal risk - 2	Standard - 2
Contra rotating	Recovers swirl - 3	Dual motor - 2	Concentrated mass - 1	Low TRL, coaxial gearboxes - 1	High costs, complex - 1

For the propeller distribution, the distributed set-up wins the trade-off with a combined score of 2.45, against 2.4 and 1.65 for the twin and single motor options, as shown in Table 4.22. The difference between the distributed and twin motor options is very small, with only 0.05. Operational risk was additionally considered to strengthen the motivation for the distributed propulsion. More motors mean that an OEI condition has a lower consequence level, as a smaller proportion of the thrust is lost. A four-motor distribution is preferred over a higher number to limit the efficiency drop that is associated with a smaller propeller diameter.

Table 4.22: Propeller distribution trade-off.

CRITERION / OPTION	**Aerodynamic Efficiency** 30%	**Thermal Management** 25%	**Structure & Mass** 20%	**Development & Mechanical Risk** 15%	**Cost & Logistics** 10%
Twin motor	Optimizes Reynolds number - 3	Localised heat zones - 2	Localised wing bending moments - 2	High TRL, OEI problem - 2	Minimal parts - 3
Distributed (4 – 6)	Suboptimal blade efficiency - 2	Distributed heat zones - 3	Spread mass, landing - 3	Moderate TRL, control mapping - 2	More components - 2
Single motor	Single-disk sweep efficiency - 2	Single high thermal signature - 2	Concentrated mass - 1	Zero redundancy - 1	One part, heavy - 2

[1]https://www.youtube.com/watch?v=BM805h7SUpc [cited 9 June 2026]
[2]https://www.youtube.com/watch?v=QSfhUOILHp0 [cited 9 June 2026]

For the propeller configuration, shown in Table 4.23, the fixed-pitch propeller wins the trade-off with a combined score of 2.7, against 2.45 and 1.45 for the variable-pitch and folding propellers, respectively. The fixed-pitch propeller scores excellent on all criteria, except for the aerodynamic efficiency, which is only optimal during cruise. In the AHAPS application, the vast majority of the mission will be conducted in the cruise regime. Therefore, the fixed-pitch propeller will operate at maximum efficiency most of the time, resulting in it being the undisputed best option.

Table 4.23: Propeller configuration trade-off.

CRITERION / OPTION	**Aerodynamic Efficiency** 30%	**Thermal Management** 25%	**Structure & Mass** 20%	**Development & Mechanical Risk** 15%	**Cost & Logistics** 10%
Fixed Pitch	Only optimal during cruise - 2	Convenient thermal properties - 3	Very simple and lightweight - 3	Well established, reliable technology - 3	Cheap, easy assembly - 3
Variable Pitch	Optimal for all flight phases - 3	Convenient thermal properties - 3	Variable load directions - 2	More moving parts - 2	High cost, complicated - 1
Folding Propeller	Only beneficial at landing - 1	Suboptimal thermal properties in folded configuration - 2	Variable load directions - 2	High complexity, not used in UAVs - 1	High cost, complicated - 1

Lastly, the trade-off for the motor type is performed with new criteria that are more suitable for electric motors and are shown in Table 4.24. The first criterion, with a weight of 30%, is chosen for the same reason as the aerodynamic efficiency for the other trade-offs. Then, thermal performance and reliability are important criteria, hence the weight of 25%, as the consistent operation of all motors is very important. The third criterion is cost, with a weight of 20%. This is for the same budget reason as before, but the weight is higher, as the motors can potentially be very expensive, and the different motor types have very diverse prices. Power density is the fourth criterion, weighted at 15%, to favour light-weighted motors. Lastly, the control criterion, with a weight of 10%, is added as the propellers have to be oriented horizontally during landing, for which a certain amount of control is required.

Table 4.24: Motor type trade-off.

CRITERION / OPTION	**Efficiency** 30%	**Thermal Performance & Reliability** 25%	**Cost** 20%	**Power Density** 15%	**Control** 10%
Brushless Direct Current	Up to 90% - 2	Reliably used in aerospace applications - 3	Mass-production reduces purchasing cost - 3	Moderate due to large surfaces - 2	Few degrees - 2
Permanent Magnet Synchronous	Up to 95% - 3	Concentrated heat, no proven applications - 1	High purchasing cost due to complexity - 1	Compact, lightweight - 3	Very precise - 3
Axial Flux Permanent Magnet	Up to 93% - 3	Not optimal, but manageable 2	Expensive due to complex geometry - 1	Compact, lightweight - 3	Few degrees - 2

The brushless direct current motor wins this last trade-off with a combined score of 2.45, against 2.1 and 2.25 for the permanent magnet synchronous motor and axial flux permanent magnet motor. All the propulsion system decisions following from the trade-off tables are presented in Table 4.25.

Table 4.25: Propulsion trade-off summary.

Trade-off	Design Decision
Propeller Orientation (Table 4.21)	Tractor
Propeller Distribution (Table 4.22)	Distributed (4)
Propeller Configuration (Table 4.23)	Fixed Pitch
Motor (Table 4.24)	Brushless Direct Current (DC)

Cruise Optimisation

The propellers are designed using a Blade Element Momentum Theory (BEMT) model to optimize the geometry for cruise conditions by analysing the propeller efficiency [45]. To achieve the highest propeller efficiency for the given cruise airspeed at low-density atmospheric conditions, the advance ratio needs to be determined. The advance ratio is how the AHAPS's forward speed is related to its propeller's rotational speed and size, as shown in Equation 4.13.

$$\lambda = \frac{V_\infty}{nD} \tag{4.13}$$

To set up the geometry of the propeller, an optimised blade twist and chord length distribution for a stratospheric propeller is taken as shown in Figure 4.10a, together with a set of possible airfoils [45]. These include the S1223 [45], NACA4412 [46], E387 [47], SD7037 [48], and FX63137 [49], which all show great performance at low Reynolds numbers and in applications of propellers for high-altitude platform systems. The lift-over-drag performance, taken from NeuralFoil, of the airfoils is shown in Figure 4.10b [3].

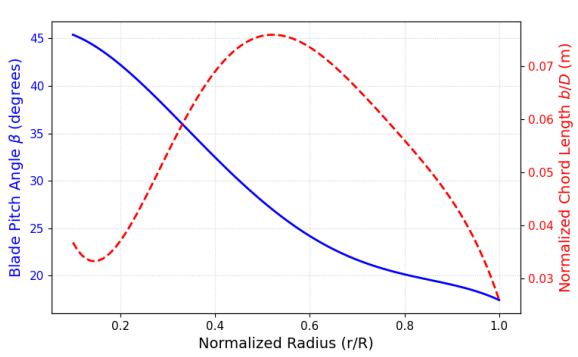

(a) Propeller blade twist angle (β) and normalised chord length (b/D_p) optimised for stratospheric use [45].

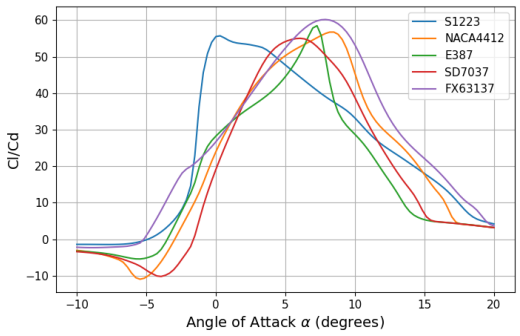

(b) Lift coefficient over drag coefficient (C_l/C_d) over angle of attack (α) for the S1223, NACA4412, E387, SD7037, and FX63137 airfoils at Re = 100,000 and M = 0.09.

Figure 4.10: Propeller geometry distribution and possible airfoils.

By setting the momentum equation equal to the blade element equation, as shown by Lui and He, Equation 4.14 forms [45]. This function is solved to find the true angle of attack α, with the first term representing the lift of the blade element and the second term decreasing with the angle of attack, resulting in a unique root. The uninduced geometric inflow angle φ_0 is a function of both the forward speed of the aircraft and the rotational speed of each specific blade section, as shown in Figure 4.11.

$$f(\alpha) = C_L(\alpha)\frac{N_B b}{2\pi n\hat{r}} - 4\sin(\beta-\alpha)\tan(\beta-\alpha-\varphi_0) = 0, \qquad \varphi_0 = \arctan\frac{V_\infty}{2\pi n\hat{r}} \tag{4.14}$$

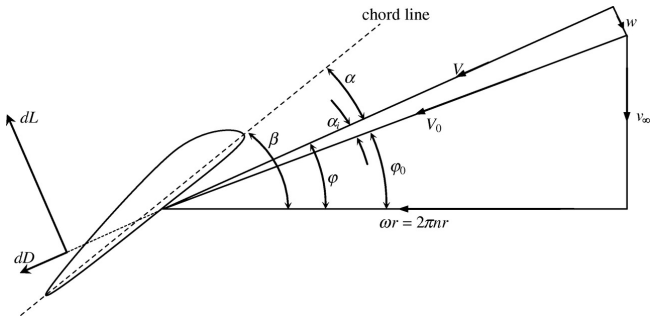

Figure 4.11: Propeller schematic of angles and flow [50].

The thrust and torque of the propeller can be established by integrating the forces along the blade radius. In Equation 4.15, the thrust and torque equations include an axial induction factor a_x and a Prandtl tip loss factor F to take into account the finite number of blades [45]. Other parameters include the number of blades N_B, the chord of the blade b, and the dynamic pressure $q_\infty = \frac{1}{2}\rho V_\infty^2$, which is defined by the cruise conditions.

$$T = q_\infty N_B \int_{\hat{r}_{hub}}^{R} b \frac{(1+a_x)^2}{\sin^2\varphi}(C_L\cos\varphi - C_D\sin\varphi)F\,d\hat{r}, \qquad Q = q_\infty N_B \int_{\hat{r}_{hub}}^{R} b \frac{(1+a_x)^2}{\sin^2\varphi}(C_L\sin\varphi + C_D\cos\varphi)\hat{r}F\,d\hat{r} \tag{4.15}$$

After having established the thrust and torque of the propeller, the thrust and power coefficients are calculated to compute the propeller efficiency as shown in Equation 4.16.

$$C_T = \frac{T}{\rho n^2 D_p^4} \qquad C_P = \frac{2\pi nQ}{\rho n^3 D_p^5} \qquad \eta_{prop} = \frac{C_T}{C_P}\lambda \tag{4.16}$$

These equations are used together with the optimised geometry from Lui and He, and the propeller performance across a span of advance ratios is analysed at a diameter of 2.0 m [45]. In Figure 4.12, it is shown that the best propeller efficiency of 85% is achieved around an advance ratio of 0.75 with the SD7037 airfoil, which is chosen for the design [48].

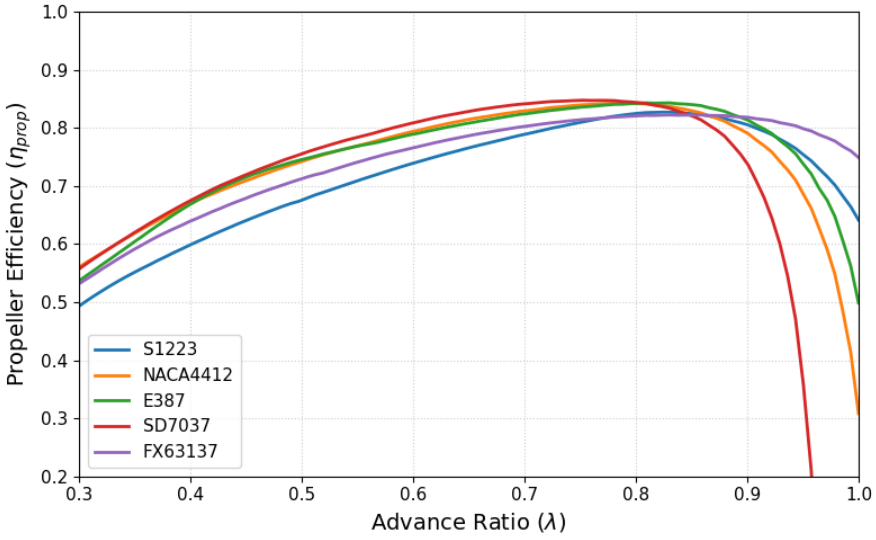

Figure 4.12: Propeller efficiency (η_{prop}) at cruise vs. advance ratio (λ) for the S1223, NACA4412, E387, SD7037, and FX63137 at a diameter of 2.0 m.

After having established the airfoil, the blade is sized using propeller similarity theory [45]. The theory states that if two propellers have the same shape and operate at the same advance ratio, they will have the same

thrust coefficient. Following from Equation 4.16 and Equation 4.13, and using the required thrust, T_{req}, and true airspeed at cruise, the diameter can be optimised for cruise by using the computed thrust, T_{ref}, for the reference diameter D_{ref} of 2.0 m as can be seen in Equation 4.17.

$$D_p = D_{ref}\sqrt{\frac{T_{req}}{T_{ref}}} \tag{4.17}$$

Motor and ESC

The motor and Electronic Speed Controller (ESC) components were selected from COTS components. The selection of the electric motor was done based on the required power, torque, and rotational speed at cruise. Care was taken to select a motor that exceeds the required specifications. The selected motor is the PrimoPal PBLR105FH-671118[1]. In order to drive the motors based on the commands from the computer system, an Electronic Speed Controller is required per motor. The Trampa VESC 75/300 was selected due to its established reliability in drones and UAVs[2]. Furthermore, it comes with built-in watchdog functionality. This feature automatically detects faults and reboots the controller and, with that, the motor. Faults that occur due to radiation, which is a valid concern at the cruising altitude, can therefore automatically be nullified, contributing to the radiation toleration requirement and the limited human monitoring requirement [51].

Take-off and Climb Performance

The highly-pitched propeller is now sized for an altitude of 60,000 ft and cruise airspeed performance. The aircraft still has to take off from the ground at sea level and climb.

During take-off, the motor requires more power than the electrical system can provide. The conservative rated power per motor (1162 W[1]) is taken to find the rotational speed and thrust generated by the propeller using the BEMT tool, which is explained in cruise optimisation. The take-off is then simulated using a time-step numerical integration. As stated in the assumptions, in order to make the BEMT model work, an initial ground-roll speed of 5 m/s is needed. From this initial speed until the required lift-off speed is simulated using lift, drag, and the rolling friction relation shown in Equation 4.18.

$$F_{fric} = \mu_{runway}\max(0, W - L) \qquad a = \frac{T_{total} - D - F_{fric}}{m_{TO}} \tag{4.18}$$

During the climb, a power setting of 80% of the power during take-off is used as power input into the motors. The AHAPS must fly faster as the air gets thinner, which results in varying propeller performance. With Section 4.1.4, the lift coefficient $C_{L_{climb}}$ and the flight velocity V_{climb} are determined at each altitude step. Similarly to take-off, the corresponding rotational speed and thrust are computed with a scaled local Reynolds number from 1,000,000 to 100,000.

4.6.3. Propulsion System Tool Verification

The propulsion sizing tool is used during the design process to optimize for cruise conditions and afterwards analyses take-off and climb performance. This tool has to be verified with both pytests and analytical tests as shown in Table 4.26.

Table 4.26: Propulsion system tool code verification test descriptions and outcomes.

Test ID	Test Description	Test Pass Criteria	Result
CODE-VER-6.1	Propulsion sizing null value test.	Input zero airspeed velocity V_∞, and returns advance ratio, thrust, torque, and propeller efficiency of zero.	Passed
Continued on next page			

[1]https://primopal.com/wp-content/uploads/2025/08/PBLR105FH.pdf [cited 4 June 2026]
[2]https://trampaboards.com/resources/manuals/256.pdf [cited 4 June 2026]

Test ID	Test Description	Test Pass Criteria	Result
CODE-VER-6.2	Propulsion sizing order-of-magnitude test.	Returns torque between $1-20$Nm, thrust between $1-400$N, total mechanical power between $500-9000$W, and a diameter between $0.2-4$m.	Passed
CODE-VER-6.3	Propulsion sizing constant and class initialisation test.	Returns correct cruise velocity, maximum take-off mass, required thrust, wing area, and $C_{L_{max}}$ from optimizer.	Passed
CODE-VER-6.4	Propulsion sizing output test.	Returns floats for total electrical power and mass of propulsion system.	Passed
CODE-VER-6.5	BEMT-tool validation.	Input parameters of Lui and He, D_p = 2.5m, N_B=3, V_∞ = 30 m/s, n = 960rpm, and the airfoil S1223 should represent similar results [45].	Passed after correction.
CODE-VER-6.6	Tip Mach number verification.	The local Mach number at the tip of the blade must be less than 0.8 [45].	Passed
CODE-VER-6.7	Thrust scaling verification.	Recalculating the thrust with the optimised diameter to assert the same output value.	Passed
CODE-VER-6.8	Motor and ESC compatibility verification.	Analyse the torque, rotational speed, and power not exceeding the maximum specified values[ab].	Passed

[a] https://primopal.com/wp-content/uploads/2025/08/PBLR105FH.pdf [cited 4 June 2026]

[b] https://trampaboards.com/resources/manuals/256.pdf [cited 4 June 2026]

4.6.4. Propulsion System Characteristics Overview

After having established the propulsion configuration and the verified BEMT tool optimised for climb, the subsystem characteristics are gained. This section will outline the propulsion system characteristics, starting with a system overview, followed by all the characteristics during the different phases of the mission.

The full sub-assembly of the propulsion system is presented in Figure 4.13. In this figure, an exploded view shows the propeller blade and hub assembled and connected to the motor with a shaft. This is followed by the ESC. The shaft, motor, its mechanical assembly, and ESC are all housed within the nacelle, which is sized to follow the shape of the propeller hub aerodynamically around the components. Finally, the rod connects the nacelle to the wing.

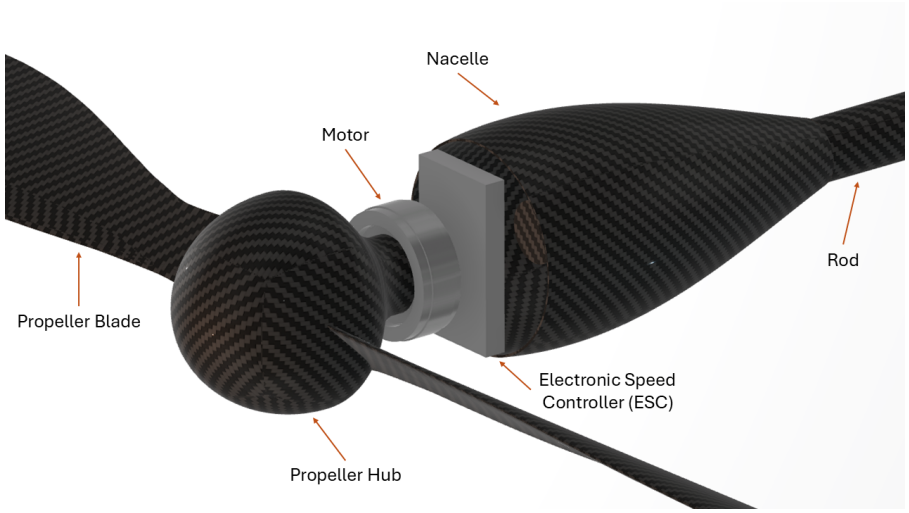

Figure 4.13: Propulsion system CAD model exploded view.

The specifications of the chosen motor, the PrimoPal PBLR105FH-671118, and ESC, the Trampa VESC 75/300, are listed in Table 4.27 and Table 4.28.

Table 4.27: Overview of the motor characteristics[a].

Motor	PrimoPal PBLR105FH-671118
Outer dimensions (mm)	D105 x 36
Rated speed (rpm)	1850
Rated torque (Nm)	6
Rated power (W)	1162
Efficiency (η_{motor}) (-)	0.90

[a]https://primopal.com/wp-content/uploads/2025/08/PBLR105FH.pdf [cited 4 June 2026]

Table 4.28: Overview of the ESC characteristics[a].

ESC	Trampa VESC 75/300
Outer dimensions (mm)	140 x 82 x 18
Peak voltage (V)	300
Peak current (A)	75
Efficiency (η_{esc}) (-)	0.99

[a]https://trampaboards.com/resources/manuals/256.pdf [cited 4 June 2026]

The optimised propeller characteristics for both cruise and take-off, at the point of lift-off, are shown in Table 4.29.

Table 4.29: Overview of the propeller characteristics.

Characteristics	Cruise	Take-off (Lift-off)
Diameter [m]	1.80	1.80
Advance ratio λ (-)	0.754	0.570
Propeller efficiency η_{prop} (-)	0.85	0.82
Rotational speed (rpm)	1453	649
Total thrust (N)	74.2 (T_{req})	283.8
Torque per motor (Nm)	4.64	14.02
Power available per propeller (W)	598.06	782.42

For climb, the performance characteristics are shown in Figure 4.14 with torque on each propeller and the corresponding rotational speeds at each altitude in Figure 4.14a, and the total amount of power available and thrust generated in Figure 4.14b.

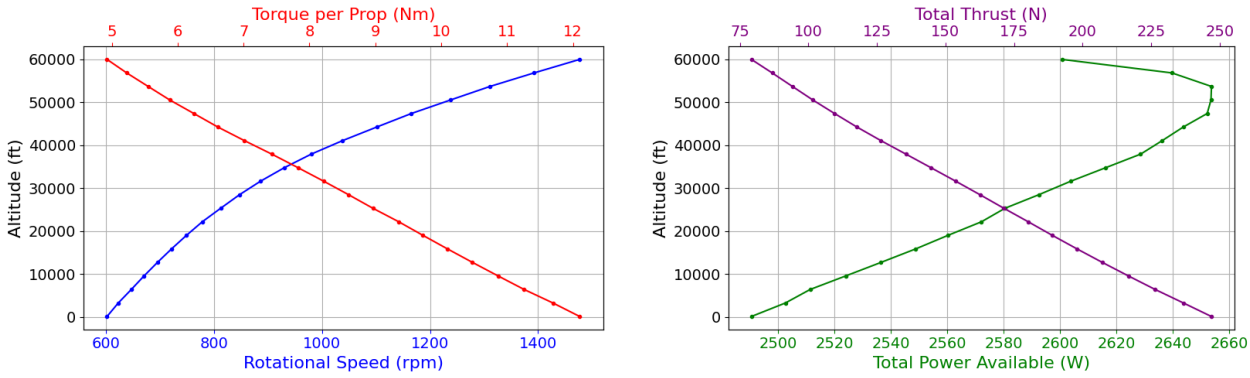

(a) Rotational speed in rotations per minute and torque per propeller during full climb profile.

(b) Total generated thrust during climb and power available during full climb profile.

Figure 4.14: Propulsion climb performance characteristics.

As mentioned in Table 4.20, the propeller blades are mainly made from CFRP, likewise the other custom components. The mass of each custom CFRP component is measured in CAD, with the assumed reduction in weight of the propellers by the use of a low-density core from Table 4.20. All custom carbon fibre parts'

costs are estimated using practical price ranges for a prepreg and autoclave method, including material and manufacturing costs[1]. With this method, the more complex the geometries are, such as the propeller blade as shown in Figure 4.15, the higher costs are assigned from the practical price ranges[1]. The motor and ESC retail prices are taken, and the motor mechanical assembly is conservatively assumed. An overview of all the masses and costs of the propulsion system is given in Table 4.30.

Table 4.30: Overview of the masses and costs per unit of each component of the propulsion system.

Component	**Model**	**Mass (kg)**	**Material/Component Cost (€) (FY26)**	**Manufacturing Cost (€) (FY26)**
Motor	PrimoPal PBLR105FH-671118[a]	0.80	190 [52]	N/A
Motor mechanical assembly	Cables, connectors, brackets, insulation	0.20	1,500	1,500
Connecting rod	CFRP cylinder	0.29	120	350
Electronic Speed Controller	Trampa VESC 75/300[b]	0.52	290[b]	N/A
Propeller	Custom design	1.70	680	19,000
Hub	Custom design	0.40	160	1,500
Nacelle	Custom design	0.20	80	1,500
Total per unit		**4.11**	**3,020**	**23,850**
Total propulsion system (4x)		**16.45**	**12,070**	**95,400**

[a] https://primopal.com/wp-content/uploads/2025/08/PBLR105FH.pdf [cited 4 June 2026]
[b] https://trampaboards.com/resources/manuals/256.pdf [cited 4 June 2026]

The final propulsion system, as presented in Figure 4.15, will cost €27,000 and weigh 4.1 kg per unit, which results in a total subsystem cost of €108,000 and a weight of 16.5 kg.

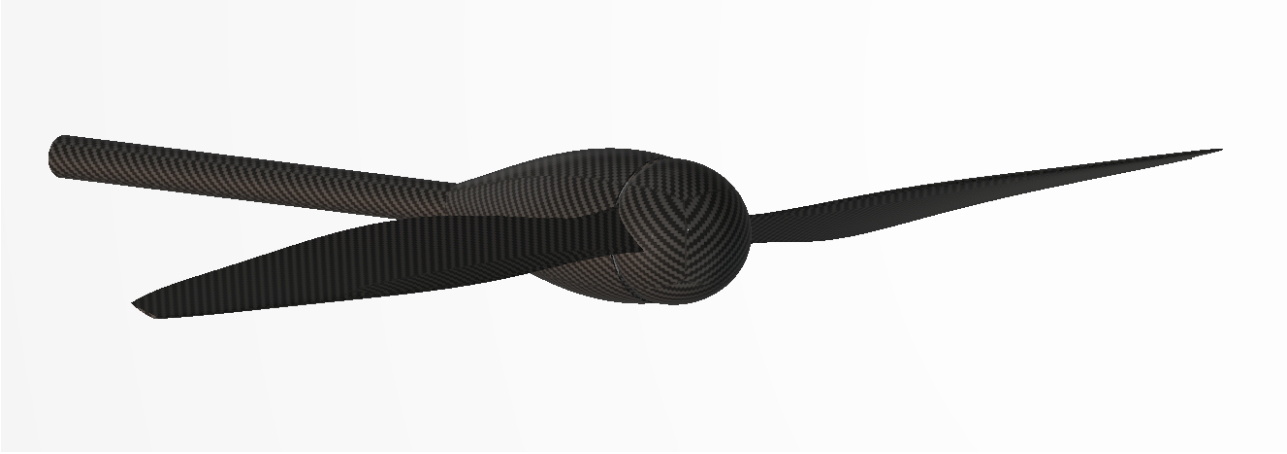

Figure 4.15: Propeller assembly showing the custom carbon fibre components.

4.7. Control System

In this section, the design process of the control system is outlined. The control system sizes the control surfaces and ensures that stability and controllability requirements are met. First, a control trade-off is performed to select the optimal control methods. Then, stability and control derivatives are investigated and the control system design is iterated to obtain stability and controllability.

[1] https://www.supreemcarbon.com/cost-guide-custom-carbon-fiber-pricing-explained.html [cited 9 June 2026]

4.7.1. Control System Assumptions

In order to properly design the control system of the AHAPS, a set of assumptions must be documented on which the design will be based. These assumptions largely follow from documentation, which is provided in the table. An overview of the assumptions can be found in Table 4.31.

Table 4.31: Assumption list for the propulsion system.

Assumption ID	Category	Assumption	Justification (Quantitative)
ASP-SSY-7.2	Control	The maximum deflection of the elevons is 20°.	As simulation is unreliable for deflection angles greater than around 20°, the aircraft will be designed for those angles (positive and negative). This is a reasonable value, and if deflection angles were to increase in the future, this could be easily implemented [19]. For rudders, the maximum deflection does not change.
ASP-SSY-7.3	Stability	The motors are vertically aligned with the centre of gravity of the aircraft.	Since the vertical deviation from the centre of gravity is negligibly small, the induced moment on the y-axis of the body reference frame is assumed to be zero.
ASP-SSY-7.4	Control	The inner elevon is for pitch, and the outer elevon is for roll.	For simplicity, it is assumed that the inner elevon only controls the pitch of the aircraft, while the outer elevon controls roll.
ASP-SSY-7.5	Stability	The location of the centre of gravity stays constant.	Due to the implementation of batteries, as well as a constant payload mass of 20 kg, the shift in centre of gravity is marginal. This has no noticeable effect on the stability and control, so it has been neglected.
ASP-SSY-7.6	Control	The aerodynamic influences of control surfaces on other control surfaces are neglected.	As the aircraft flies at low speed and the control surfaces are uncoupled, this effect is not noticeable for the AHAPS.
ASP-SSY-7.7	Stability	The value of the constant k in the yawing moment equation of OEI is assumed to be 2.	For propeller-driven aircraft, this value is typically between 1.5 and 2 [53]. To account for the worst-case scenario during design, this value has been set to 2.
ASP-SSY-7.8	Stability	For the longitudinal stability analysis, it has been assumed that the stick was fixed.	As a result of using a fly-by-wire control system, the control surface is held in place by actuators.
ASP-SSY-7.9	Stability	For C.G. computation, all components/subsystems below 1 kg were omitted for computation.	Their impact is negligible, since their mass is less than 1% of the total mass.

4.7.2. Control System Design

In order to properly design the control system of the AHAPS, a trade-off must be performed to determine the best combination of control systems. Afterwards, stability and control coefficients are obtained and used to determine the eigenmotion characteristics and control responses. The control surfaces can then be sized to meet the requirements.

Control Trade-off

Before a detailed analysis of the stability and controllability of the aircraft can be performed, the final layout of the control surfaces must be determined. For flying wings and for HAPS systems, the most commonly used options for control are inboard and outboard elevons, wingtip rudders, differential thrust, and split drag rudders. Four different configurations of these options are looked into to control the aircraft in pitch, roll, and yaw.

The five criteria used to trade-off the options are control authority, development risk, cost, logistics, and one engine inoperable (OEI) handling. Control authority looks into how effective the control surfaces are at the flight conditions of the aircraft, development risk looks at whether it has been used on previous AHAPS

designs and how complex it is to design, and the OEI handling looks into the potential loss of control in the case the most critical motor fails during operations.

Based on the trade-off given below in Table 4.32, the configuration consisting of outboard and inboard elevons together with wingtip rudders is deemed the best option. The main issue with drag rudders is that they make use of asymmetric drag for yawing, which is not ideal for a high-endurance aircraft, where the goal is to minimize drag. The problem with only using differential thrust is that, due to the low thrust per motor and the thin airfoil profile, insufficient moment can be created by the motors for pitch and roll. For yawing the aircraft, the use of differential thrust is sufficient, but in the case of OEI, this yawing capability declines, while the yawing authority for wingtip rudders is not changed for OEI.

Table 4.32: Control surface trade-off for the AHAPS flying wing.

CRITERION / OPTION / WEIGHTED SUM	**Authority** 20%	**Development Risk** 20%	**Costs** 15%	**Logistics** 30%	**OEI Handling** 15%
Elevons + Wingtip Rudders	Excellent: Simple, effective at both high and low speeds (inboard and outboard), high pitch and yaw authority.	Good: Coupling effects need to be kept in mind	Good: Some additional costs due to actuators.	Good: Longer assembly time, easy to handle.	Excellent: Maintaining yaw, pitch, and roll with one motor out.
Elevons + Differential thrust	Excellent: Simple, effective at both high and low speeds (inboard and outboard). Similar yaw moment with rudder.	Good: Medium scoring TRL, with medium sensitivity	Good: Some additional costs due to actuators.	Good: Longer assembly time, easy to handle	Correctable deficiencies: yaw moment decreases substantially with OEI.
Elevons + Split Drag Rudders	Good: good authority, but the asymmetric use of drag is not ideal for endurance.	Good: coupling effects need to be taken into account for both elevons and split drag	Good: Some additional costs due to actuators.	Good: Longer assembly time, easy to handle	Excellent: Maintaining yaw, pitch, and roll with one motor out.
Differential Thrust	Unacceptable: Not sufficient control for pitch and roll	good: low relative complexity when using a gearbox	Excellent: low cost due to no surfaces and actuators	Excellent: Short assembly time, easy to handle, no additional parts outside of the motor	Unacceptable Due to the already unacceptable authority

Equations of Motion Symmetrical Flight

The flight dynamics for symmetrical flight of an aircraft are characterised by the equations of motion seen

in Equation 4.19 [53]. These equations describe the full motions of the aircraft, which involve symmetry.

$$\begin{bmatrix} C_{X_u} - 2\mu_c D_c & C_{X_\alpha} & C_{Z_0} & 0 \\ C_{Z_u} & C_{Z_\alpha} + (C_{Z_{\dot{\alpha}}} - 2\mu_c) D_c & -C_{X_0} & C_{Z_q} + 2\mu_c \\ 0 & 0 & -D_c & 1 \\ C_{m_u} & C_{m_\alpha} + C_{m_{\dot{\alpha}}} D_c & 0 & C_{m_q} - 2\mu_c K_Y^2 D_c \end{bmatrix} \begin{bmatrix} \hat{u} \\ \alpha \\ \theta \\ \frac{q\bar{c}}{V} \end{bmatrix} = \begin{bmatrix} -C_{X_{\delta_e}} \\ -C_{Z_{\delta_e}} \\ 0 \\ -C_{m_{\delta_e}} \end{bmatrix} [\delta_e] \tag{4.19}$$

In this equation, the stability derivatives, along with additional terms, can be found in the matrix on the left. To start, D_c, is the dimensionless differential operator. The terms μ_c and K_Y are the moments and products of inertia, respectively. Furthermore, $\hat{u}$ is the velocity, α is the angle of attack, θ is the pitch angle, and $\frac{q\bar{c}}{V}$ is the non-dimensional pitch rate. Lastly, δ_e is defined as the elevator deflection in radians.

Equations of Motion Asymmetrical Flight

Similarly to the equations of motion for symmetric flight, Equation 4.20 describes the equations of motion involved in asymmetric flight and, with that, can be used to analyse the lateral stability of the aircraft [53].

$$\begin{bmatrix} C_{Y_\beta} + (C_{Y_{\dot{\beta}}} - 2\mu_b) D_b & C_L & C_{Y_p} & C_{Y_r} - 4\mu_b \\ 0 & -\frac{1}{2} D_b & 1 & 0 \\ C_{\ell_\beta} & 0 & C_{\ell_p} - 4\mu_b K_X^2 D_b & C_{\ell_r} + 4\mu_b K_{XZ} D_b \\ C_{n_\beta} + C_{n_{\dot{\beta}}} D_b & 0 & C_{n_p} + 4\mu_b K_{XZ} D_b & C_{n_r} - 4\mu_b K_Z^2 D_b \end{bmatrix} \begin{bmatrix} \beta \\ \phi \\ \frac{pb}{2V} \\ \frac{rb}{2V} \end{bmatrix} = \begin{bmatrix} -C_{Y_{\delta_a}} & -C_{Y_{\delta_r}} \\ 0 & 0 \\ -C_{\ell_{\delta_a}} & -C_{\ell_{\delta_r}} \\ -C_{n_{\delta_a}} & -C_{n_{\delta_r}} \end{bmatrix} \begin{bmatrix} \delta_a \\ \delta_r \end{bmatrix} \tag{4.20}$$

In this equation, all the stability derivatives can be found together with additional terms. The control derivatives are found on the right side multiplied by δ_a and δ_r, which are the aileron deflection and the rudder deflection, respectively. D_b here serves as the dimensionless differential operator. μ_b, K_X, K_{XZ}, and K_Z are defined to be the moments and products of inertia for asymmetric motion. Last, β is sideslip, ϕ the roll angle, $\frac{pb}{2V}$ the dimensionless roll rate, and $\frac{rb}{2V}$ the dimensionless yaw rate.

Stability Coefficients

With the equations of motion for both symmetrical and asymmetrical flight described above, the combination of coefficients describes the flight dynamics of the AHAPS. To examine the stability properties of the flying wing and size the control surfaces, these control & stability derivatives are required. These are acquired through the AeroBuildup method from the `aerosandbox` Python library, which assesses the stability characteristics of the aircraft and can include control surface deflections in its analysis. The analysis was run under the following conditions, as detailed in Table 4.33.

Table 4.33: AeroBuildup VLM Simulation Conditions for the AHAPS.

Parameter	**Value**
True Airspeed V_{TAS}	32.70 m/s
Angle of attack α	10.3 °
Density ρ	0.1153 kg/m^3
Reynolds number Re	400,000

To determine the moments and products of inertia, a preliminary tool has been made. The tool calculates the moment of inertia tensor based on the mass distribution of the main subsystems. These are then converted into their respective radii of gyration and non-dimensional radii of gyration.

Control Surface Sizing

Rather than depending on an empirical method to size the inner elevons, the outer elevons, and the wingtip rudders, the AeroBuildup method from the AeroSandBox Python Library was used as stated above. This

generated the stability coefficients based on a defined wing geometry. The sizing of the surfaces is iterated by comparing the response for each degree of freedom against the requirements at the critical case, until the surface geometry is optimised. As a result of the hinge line being set to 75% of the chord by the cross-section geometry, the sizing was performed by varying the surfaces' spanwise lengths.

Longitudinal Control and Stability

In order to assess the general longitudinal stability of the aircraft, parameters from the Python programme will be used. To ensure static stability, the following requirements must be satisfied:

$$C_{m_{trim}} = 0$$

$$C_{m_\alpha} < 0$$

To reach the first requirement, the centre of gravity must, at all times, remain in front of the neutral point of the flying wing. The location of the neutral point depends on the wing geometry and has been retrieved through the AeroBuildup code.

To meet the centre of gravity requirement, the subsystems and components are required to be placed carefully. In consultation with other departments, a list of requirements for subsystem positions was set up, shown in Table 4.34. This was done utilising the N2-chart shown in Figure 3.1, in Section 3.1. To converge to the target centre of gravity, the battery pack will be distributed within one wing section.

Table 4.34: Position Requirements

Subsystem/Component	**Positioning Requirement**
Payload System	Position on wing root, due to mass
Computer System	Position on wing root, due to heating concerns
Flight Condition System	Position on wing root, due to connection to computer
Communication system	Position on wing root, due to connection to computer
Propeller 2 (left) & 3 (right)	Position is 1/3 of the half span from the root on each wing
Propeller 1 (left) & 4 (right)	Position is 2/3 of the half span from the root on each wing
Battery Pack	The entire battery pack needs to fit into one wing section to accommodate efficient insulation and heating

After determining the centre of gravity range, this requirement could be satisfied. Regarding the second one, the trim authority should be enough to satisfy this requirement, while keeping enough longitudinal control authority at the same time. Subsequently, dynamic stability is examined through the stability of the phugoid and short-period modes.

Lateral Control and Stability

The lateral stability of the aircraft covers the aircraft's response to disturbances involving sideslip, roll, and yaw. The lateral stability is governed by some important stability derivatives such as the yaw stability C_{n_β}, the roll stability C_{l_β}, the yaw damping C_{n_r}, and the roll damping C_{l_p}.

Aside from these stability derivatives, there is also the OEI condition to consider. This introduces an additional yaw, which can be seen in Equation 4.21, that must be countered by the rudder deflection.

$$C_{n_e} = k\frac{Ty_{motor}}{0.5\rho V_{cr}^2 Sb} \tag{4.21}$$

In this equation, k is a factor that depends on the type of motor and is set to 2 in this case. y_{motor} is the distance from the centre of gravity to the motor that is out, together with the missing thrust that, when multiplied, calculates the moment.

Another major part of lateral control and stability is to consider the eigenmotions of the sized aircraft. To do this, the compliance with the Routh-Hurwitz criterion is evaluated [53]. This is to ensure that the aircraft is both spiral stable and has a converging Dutch roll. The criterion is given in Equation 4.22.

$$C_{l_\beta} C_{n_r} - C_{n_\beta} C_{l_r} > 0 \tag{4.22}$$

In the event the criterion is not met, C_{l_β} can be made more negative by increasing the dihedral or the sweep of the wing. Furthermore, C_{n_r} can be made more positive by increasing the winglet sizes, which offers an alternative way to meet the Routh-Hurwitz criterion.

4.7.3. Control System Tool Verification

The tools used to size the control surfaces need to be verified to ensure the code performs as intended without errors and to verify that the stability coefficients obtained are physically possible. To verify the tools used to size the control surfaces, various tests are performed as outlined below in Table 4.35.

Table 4.35: Control and stability tool code verification test descriptions and outcomes.

Test ID	Test Description	Test Pass Criteria	Result
CODE-VER-10.1	Static code inspection test.	Code structure, syntax, and implemented functions are logically correct with no identified errors.	Passed
CODE-VER-10.2	Order of magnitude test.	Calculated aerodynamic, stability, and dynamic response values remain within physically realistic ranges, according to Mulder [53].	Passed
CODE-VER-10.3	Value-limit and null-value test.	For extreme or zero-valued inputs, the tool produces expected limiting behaviour without numerical failures.	Passed
CODE-VER-10.4	Hand calculation verification test.	Computed results match independent analytical hand calculations within acceptable error margins.	Passed
CODE-VER-10.5	Assumed constants cross-verification test.	Aerodynamic, atmospheric, and physical constants correspond to accepted literature values.	Passed
CODE-VER-10.6	Function unit test.	Individual functions return outputs with correct values, data structures, and error handling.	Passed
CODE-VER-10.7	Class initialisation and integration test.	Class variables are correctly initialised, and class methods interact to produce expected outputs.	Passed

4.7.4. Control System Characteristics Overview

This subsection will give an overview of the entire control system. First, the dimensions of the control surfaces will be given after which the hardware overview is shown, together describing the full control system.

Control Surface Overview

Each half-wing will contain an elevator, an aileron, and a wingtip rudder. The characteristics of these surfaces are compiled in Table 4.36.

Table 4.36: Final sizing and positioning of the control surfaces.

Control Surface	Spanwise/Winglet fraction	Hinge line chord fraction	Maximum deflection (deg)
Elevator	0.6 - 0.7	0.75	±20
Aileron	0.7 - 0.9	0.75	±20
Rudder	0 - 0.8	0.75	±30

Control Hardware Overview

The six control surfaces require reliable actuator operation. The Volz DA 30-Duplex actuator is chosen for its integrated redundancy and proven operation at temperatures below what is expected at 60,000 ft[1]. In the event of hardware failure, the actuator will continue to function with degraded performance. This eliminates the need for two redundant actuators, reducing the overall weight of the control system. The actuator specifications are found below in Table 4.37.

Table 4.37: Basic characteristics of the chosen Volz DA 30-Duplex actuator.

Actuator Characteristics	**Value**
Weight per unit (kg)	1.20 kg
Cost per unit (€)	€8,910
Rated torque (Nm)	20 Nm
Operating temperature range (°C)	-70...+70
DC Supply voltage (V)	28
Rated current (A)	3.2
Rated speed (at rated torque) [°/s]	110
Total weight (kg)	**7.20**
Total cost (FY26) (€)	**54,000**

This leads to a total weight of 7.2 kg and a cost of €54,000 for the actuators.

4.8. Temperature Management

In this section, a temperature management system is sized to ensure that no systems get overheated due to the lack of sufficient heat dissipation, or that any systems get below their minimum operating temperature.

4.8.1. Temperature Management Assumptions

To make a preliminary heat budget, the assumptions listed in Table 4.38 were made.

Table 4.38: Assumption list for the temperature management.

Assumption ID	**Category**	**Assumption**	**Justification (Quantitative)**
ASP-TEM-8.1	Thermodynamics	It is assumed that there is no airflow within the airfoil during cruise. Thus, the inside is in the full-conduction regime.	Due to the low cruise Reynolds number and the high chord-to-thickness ratio with compact internal packaging, this assumption is valid according to Nusselt [26].
ASP-TEM-8.2	Packing	It is assumed that the used insulating aerogel can be formed in any desired three-dimensional shape, without any declination of its insulating characteristic purpose.	The manufacturer states the insulator is a "high-performance flexible aerogel and supports a longer service life"[a].
ASP-TEM-8.3	Internal Resistance	All resistance properties of Amprius' 500 Wh/kg batteries are equal to their 450 Wh/kg batteries.	Amprius' 450 Wh/kg batteries have better resistance properties than the 400 Wh/kg model, making it reasonable to assume the 500 Wh/kg batteries and the 450 Wh/kg batteries have atleast equal properties[b].

[a] http://aerohik.ch/products/aerogel-insulations/thermhik-ct

[b] https://amprius.com/solutions/sicore/ [cited 6 May 2026]

4.8.2. Temperature Management System Design

Because the operating temperature of the lithium-ion batteries is at least 10°C, a temperature management analysis is done. Since it is assumed that the AHAPS is in the full conduction regime, a calculation has

[1] https://www.volz-servos.com/actuators/detail/da-30-d/ [cited 19 June 2026]

been made for the heat flow through the insulation material to the outside to have an equilibrium using Equation 4.23 (ΔT = 70°C). For the insulation material, an inert aerogel currently available in the market has been chosen. Its parameters can be found below in Table 4.39.

Table 4.39: Parameters used for chosen insulation aerogel[a].

Parameter	**Thermal Conductivity (W/mk)**	**Operating Temperature** ($°C$)	**Density (kg/m^3)**	**Compressive strength (kPa)**	**Cost (€/kg) (FY26)**
Value	0.017	$-200 < T < +125$	170	35	600

[a] http://aerohik.ch/products/aerogel-insulations/thermhik-ct

The thermal conductivity is taken as 0.017 W/mk, which is the value at sea level[1]. This is the most conservative value, as the thermal conductivity improves for both a decrease in temperature and a decrease in pressure [54].

$$Q = \frac{kS_{ref}\Delta T}{t} \tag{4.23}$$

The reference surface area has been optimised to be as small as possible by packing the heaters all at the front of the chord before the spar in only two wing sections, which also minimises the amount of heaters needed. The thickness of the aerogel has been made as thick as possible whilst still being able to put all the batteries in the assigned sections. Both these volumes have been put in the full volume budget iteration loop to optimize for a sufficient centre of gravity, since the battery mass is a significant part of the MTOW. The combination of battery and aerogel placements led to a total heat dissipation of 332.67 W. This heat dissipation can be partly compensated for by the internal heat dissipation of the batteries themselves, which can be determined by calculating the power required to overcome the direct current internal resistance (DCIR) of 29 mΩ[2].

$$P_{ir} = I^2 \cdot DCIR \tag{4.24}$$

The heat dissipation for one battery of 0.159 W is multiplied by the number of batteries active based on the cruise power required and subtracted from the total heat dissipation to calculate the power budget needed for the heaters.

4.8.3. Temperature Management Tool Verification

To verify the temperature management tool, the tests described in Table 4.40 were applied.

Table 4.40: Temperature management tool code verification test descriptions and outcomes.

Test ID	**Test Description**	**Test Pass Criteria**	**Result**
CODE-VER-9.1	Temperature management tool null value test.	Returns null battery heat dissipation and power required.	Passed
CODE-VER-9.2	Temperature management tool order-of-magnitude test.	Returns battery heat dissipation between 0.01 and 10 W; power required between 1 and 1000 W.	Passed
CODE-VER-9.3	Temperature management tool constant initialisation test.	Returns preset heat dissipation and internal resistance.	Passed

Continued on next page

[1] https://linkinghub.elsevier.com/retrieve/pii/S0022309398001252 [cited 19 June 2026]

[2] https://web.archive.org/web/20240918163649/https://amprius.com/documents/Amprius_Product_Portfolio_0824_website.pdf [cited 19 May 2026]

Test ID	Test Description	Test Pass Criteria	Result
CODE-VER-9.4	Temperature management tool class variable initialisation test.	Returns inputted values for current, DCIR, and aerogel characteristics.	Passed
CODE-VER-9.5	Temperature management tool output type test.	Returns floats for heat dissipation and power required.	Passed
CODE-VER-9.6	Temperature management tool monotonicity test.	Returns less heat dissipation and less power required for less internal resistance and current.	Passed

4.8.4. Temperature Management Characteristics Overview

The final heat and aerogel insulation characteristics are presented in Table 4.41 and Table 4.42, respectively.

Table 4.41: Overview of the characteristics of the heaters.

Characteristic	Value
DCIR	29 Ω
Internal resistance per cell	0.159 W
Total heat dissipation	333 W
Power budget required	257 W
Heater max output (per unit)	150 W[a]
Heater cost (per unit) (FY26)	€95[a]

Table 4.42: Overview of the characteristics of the aerogel insulation[b].

Characteristic	Value
Thermal Conductivity	0.017 W/mk
Operating Temperature	−200°C, +125 °C
Layer Thickness	1.5 cm
Total weight	4.5 kg
Compressive strength	35 kPa
Total cost (FY26)	€2,700

[a] https://archeat.com/index.php?route=product/category&path=17_63 [cited 17 June 2026]

[b] http://aerohik.ch/products/aerogel-insulations/thermhik-ct

4.9. Undercarriage System

For the design of the undercarriage, the biggest constraint is the adaptability of the systems, for which it is required to fit in the 20 ft ISO container (**REQ-MIS-7.1**) and be assembled by only three people **(REQ-SYS-1.51)**. This leads to the design option for which minimal logistics is required and which shows feasibility.

4.9.1. Undercarriage System Assumptions

To make a preliminary sizing of the undercarriage systems, several assumptions were made. These assumptions are listed in Table 4.43.

Table 4.43: Assumptions list for the undercarriage.

Assumption ID	Category	Assumption	Justification (Quantitative)
ASP-SSY-9.1	Take-off	The added drag from the jettisonable take-off gear can be overcome by a human guide during take-off.	Feasibility of this has been proven by the take-off of the Phasa-35[a].
ASP-SSY-9.2	Take-off	The take-off gear strut will only experience compressive loads.	This limits the scope of the take-off gear design.
ASP-SSY-9.3	Take-off	A clearance of 300 mm for the propeller tip to the runway is sufficient.	This limits the scope of the take-off gear design.
ASP-SSY-9.4	Take-off	The maximum ground operations load factor is 3g.	This is a conservative assumption, overestimating the load on the strut.
ASP-SSY-9.5	Take-off	The connecting structure for the take-off gear has a mass of 1 kg and costs €1000 per unit.	This limits the scope of the take-off gear design.

Continued on next page

Assumption ID	Category	Assumption	Justification (Quantitative)
ASP-SSY-9.6	Take-off	The cost for the integration of the strut with the wheel and the connection point is 50 times the cost of the strut by itself.	These costs cannot be neglected, so this estimation is conservative.
ASP-SSY-9.7	Landing	For the landing manoeuvre, the propeller motors can be turned off such that the dual blades align with the horizon to give the landing gear sufficient clearance.	Feasibility of this has been proven by the landing of the Zephyr[b].
ASP-SSY-9.8	Landing	The skid struts endure only compressive and shear loads, with axial stress, shear stress, and column buckling modelled.	This is sufficient for modelling both friction loads during landing and static weight loading.
ASP-SSY-9.9	Landing	The skid pads endure only compressive loads, with axial stress and thin-sheet buckling modelled.	This is sufficient for modelling both friction loads during landing and static weight loading.
ASP-SSY-9.10	Landing	Friction coefficient assumed to be 1.0.	Conservative value used for sizing.
ASP-SSY-9.11	Landing	Skid mass not related to structure has a mass equal to twice the extended skid strut structure mass.	Conservative value, used to take into account potential masses of connections and the mechanism.

[a] https://www.youtube.com/watch?v=QSfhUOILHp0 [cited 9 June 2026]

[b] https://www.youtube.com/watch?v=BM805h7SUpc [cited 8 June 2026]

4.9.2. Undercarriage System Design

This subsection goes into the details of the design of the take-off wheels and the landing skids.

Take-off System

The take-off system is desired to prevent the high maintenance required for the airframe and take-off system itself, while minimising the total drag during cruise to optimize the AHAPS performance. Since the propeller motors are required to be turned on during take-off, the lowest point of the AHAPS to be protected by the take-off system will then be too low to be reasonably protected with a fixed take-off/landing system without raising the drag too significantly. Also, a retractable system will be too big and complex for the infield engineers to assemble and maintain. Thus, it has been decided that a jettisonable take-off gear will be used. The launch will be guided by human force to overcome the extra drag from the take-off gear[2].

During the take-off run, buckling of the strut is the critical failure mode. Euler's buckling load, Equation 4.25, is computed to size the strut, with a column effective length factor of 1 [55].

$$P_{cr} = \frac{\pi^2 EI}{(KL)^2} \tag{4.25}$$

The strut is made of a hollow CFRP tube, and the wheels are general lightweight mountain bike wheels. Taking the maximum allowable tire loading of 280 kPa into account, 8 struts with 1 wheel each are sufficient. The struts are placed at the same spanwise locations as the landing skids, which are elaborated upon in the next section.

Landing System

For the landing system, it is unreasonable to assume either a human team or a landing vehicle can safely catch the plane out of the sky. The plane must be able to land safely on its own without damaging itself in order to limit maintenance requirements. This means a built-in landing structure is necessary.

Initially, a wheel system was proposed. However, it was determined that this would add too much drag to the aircraft, due to the limited availability of aircraft tires for this class of aircraft [56, 57]. In addition,

a landing gear retraction mechanism was deemed too complicated for this aircraft. Therefore, a previous concept involving skids was reconsidered.

Skids were initially eliminated due to their required maintenance. However, as landing gear requires similar, if not more, maintenance, this makes skids again a viable alternative. Several other HAPS aircraft also skid on landing, such as the Zephyr, which simply skids on its wing, and the Phasa-35, which skids on its motor nacelles[1][2]. Overall, skidding is a proven technique to land HAPS-type aircraft.

For the AHAPS, the wing and other components must not be damaged on arrival. It is important to make sure that critical aerodynamic and payload components do not impact the ground directly upon landing. Therefore, it was decided to implement structural skids, scattered across the wing span, which can distribute and carry the landing load and ensure that critical components are not damaged by the surface.

A certain height clearance is needed to prevent components from impacting the ground. This involves not only the wings and motors, but also certain payload components such as a 1x1 m synthetic aperture antenna. However, it is assumed in **ASP-SSY-9.7** that the propeller can be switched off and set parallel to the surface before landing, such that no extra clearance requirements stem from the propellers. In addition, as the ground is prepared but unpaved, it is safe to assume that it is relatively flat. Therefore, only a limited height clearance margin is required. The height of the skid structure must also be low enough to prevent the aircraft from tipping over the skids upon touchdown. As a preliminary estimate, a 20 cm clearance between the lowest point of the aircraft body and the ground is used.

The forces the skids have to endure are relatively low, meaning that the skid struts can be composed of simple, lightweight tubular beam structures. The struts are assumed to experience axial forces due to weight and shear forces due to friction, with an assumed friction coefficient of 1.0 as a conservative estimate. Two 20 cm long aluminium tube struts with an outer diameter of 2 cm and a thickness of 4 mm can withstand an axial and shear load factor exceeding 2, including column buckling, which is deemed sufficient in accordance with **ASP-SSY-9.8**[3]. For preliminary sizing, the skid pads are composed of an aluminium sheet with a width of 4 cm and a thickness of 4 mm, combined with a length of 0.9 metres per skid. In this configuration, eight skids provide sufficient surface area to prevent sinking into even soft clays, which have among the lowest load-bearing capacity, even with the 3.0 load factor stated in **ASP-SSY-9.4**[4]. They can handle more than twice the regular axial stresses without thin sheet buckling, even when the most conservative buckling coefficient of 0.25 is used[5]. Aluminium is used instead of a lighter material like CFRP in order to mitigate the release of microplastics due to abrasion, which harm the environment [58].

For drag purposes, it is ideal to keep the landing skids retracted during flight. For landing skids, this mechanism is quite simple, with the skids being held inside the wing until it is released for landing. A simple telescoping mechanism can allow for this. The skids are locked in the retracted position during the take-off and cruise phase of the flight. For landing, the skids are unlocked, allowing them to extend to and lock into the landing position. Considering the low loads that need to be carried, there are not many structural concerns regarding such a mechanism. This mechanism is therefore not sized in more detail, with its mass included in the miscellaneous mass as stated in **ASP-SSY-9.10**.

This skid sizing is highly preliminary. Other options can be considered in later stages of the design process, such as removable pads made of higher-durability and more abrasion-resistant materials.

4.9.3. Undercarriage System Tool Verification

A tool is used to size the undercarriage system, particularly the landing skids. The tool computes the stresses the various components experience, comparing them with the yield stresses or buckling stresses. This ensures that the landing skids are able to sustain the most important forces. In this section, the code verification of this tool is outlined, shown in Table 4.44.

[1] https://www.youtube.com/watch?v=BM805h7SUpc [cited 8 June 2026]
[2] https://www.youtube.com/watch?v=QSfhUOILHp0 [cited 8 June 2026]
[3] https://www.engineeringtoolbox.com/euler-column-formula-d_1813.html [cited 8 June 2026]
[4] https://environment.uwe.ac.uk/geocal/foundations/founbear.htm#BEARINGCAPACITY [cited 8 June 2026]
[5] https://eng.libretexts.org/@go/page/95322?pdf [cited 8 June 2026]

Table 4.44: Undercarriage system tool code verification test descriptions and outcomes.

Test ID	Test Description	Test Pass Criteria	Result
CODE-VER-9.1	Null value test.	For null inputs, returns null structural mass.	Passed
CODE-VER-9.2	Order of magnitude test.	Returns total mass between 0.1 and 10 kg per skid.	Passed
CODE-VER-9.3	Constants initialisation test.	Returns correct material properties for ρ, E, σ_y, σ_{ult}, and τ_{ult}.	Passed
CODE-VER-9.4	Class variables initialisation test.	Returns correct inputted values for skid strut dimensions, skid pad dimensions, weight force, load factor, and number of skids.	Passed
CODE-VER-9.5	Output type test.	Returns float for mass.	Passed
CODE-VER-9.6	Column buckling analytical test.	For given inputs, it returns the correct buckling load[a].	Passed
CODE-VER-9.7	Thin sheet buckling analytical test.	For given inputs, it returns the correct buckling load[b].	Passed
CODE-VER-9.8	Axial stress analytical test.	For given inputs, it returns the axial stress.	Passed
CODE-VER-9.9	Shear stress analytical test.	For given inputs, it returns the shear stress.	Passed
CODE-VER-9.10	Axial stress monotonicity test.	Thicker structure reduces axial stress.	Passed
CODE-VER-9.11	Shear stress monotonicity test.	Thicker or larger area structure reduces shear stress.	Passed
CODE-VER-9.12	Buckling monotonicity test.	Larger thickness or greater radius structure increases buckling load[ab].	Passed

[a] https://www.engineeringtoolbox.com/euler-column-formula-d_1813.html [cited 8 June 2026]

[b] https://eng.libretexts.org/@go/page/95322?pdf [cited 8 June 2026]

4.9.4. Undercarriage System Characteristics Overview

An overview of the take-off gear characteristics is given in Table 4.45. After that, the high-level characteristics of the sized skid structure are given in Table 4.46.

Table 4.45: Overview of take-off gear characteristics per unit.

Component	Design	Mass (kg)	Cost (€) (FY26)
Strut	CFRP tube of length 800 mm, outer diameter of 20 mm and thickness of 1 mm[a]	0.06	1,190
Wheel	HUNT Proven Carbon Trail H-core MTB Mullet[b]	0.86	730
Connection	Custom design	1.00	1,000
Total per unit		**1.92**	**2,910**
Total for 8 units		**15.34**	**23,300**

[a] https://www.easycomposites.eu/22mm-woven-finish-carbon-fibre-tube [cited 11 June 2026]

[b] https://www.huntbikewheels.com/products/hunt-proven-carbon-trail-h_core-mtb-mullet-wheelset [cited 11 June 2026]

Table 4.46: Characteristics of the sized skid structure for the AHAPS aircraft.

Component	Design	Mass (kg)	Cost (€) (FY26)
Strut	Two Aluminium 6061-T6 tubes each of extended length 200 mm, outer diameter of 20 mm and thickness of 4 mm	0.24[a]	30[b]
Skid Pad	Aluminium 6061-T6 sheet of length 0.9 m, width 50 mm, and thickness 4 mm	0.48[a]	20[c]

Continued on next page

Component	Design	Mass (kg)	Cost (€) (FY26)
Miscellaneous	Connection pieces, mechanism, etc	0.42	500
Total per unit		**1.14**	**550**
Total for 8 units		**9.15**	**4,400**

[a] https://www.matweb.com/search/datasheet.aspx?MatGUID=b8d536e0b9b54bd7b69e4124d8f1d20a&ckck=1 [cited 8 June 2026]
[b] https://amzn.eu/d/0f4d21QT [cited 8 June 2026]
[c] https://www.dhm-online.com/en/aluminum/4525-237032-aluminium-sheet-cut-to-measure-industrial-material-plates.html [cited 8 June 2026]

5. Design Overview

In this chapter, the AHAPS design will be presented, which was the result of the design synthesis in Chapter 4. In Section 5.1, the detailed design will be visualised using a CAD model. In Section 5.2, the top-level characteristics are given for all subsystems together with the general system characteristics. In Section 5.3, the internal system architecture is shown together with the individual positions of all components. In Section 5.4, a top-level cost breakdown is provided of the AHAPS. In Section 5.5, all sustainable aspects of the AHAPS will be discussed.

5.1. Detailed Design Visualisation

This section presents the overall geometry of the AHAPS through a fully dimensioned technical drawing. Furthermore, the outline of all the assembly sections of the wing is illustrated.

5.1.1. AHAPS Drawing

A comprehensive technical drawing of the AHAPS, including all dimensions, is shown in Section A.6. This drawing only presents the external perspective of the AHAPS, including the wing, propulsion, and payload assembly. The locations of the cross sections of the wing A to E that are shown in Section 5.3 are also displayed in the drawing.

5.1.2. AHAPS Assembly Parts

In order to transport the AHAPS, it is designed to be entirely transportable within a standard 20 ft ISO shipping container. Due to the strict volumetric constraints imposed by this requirement, the main wing cannot be manufactured or transported as a single continuous structure. This results in the wing of the AHAPS being cut up into nine modular parts. The wing sections and their respective section numbers are shown in Figure 5.1.

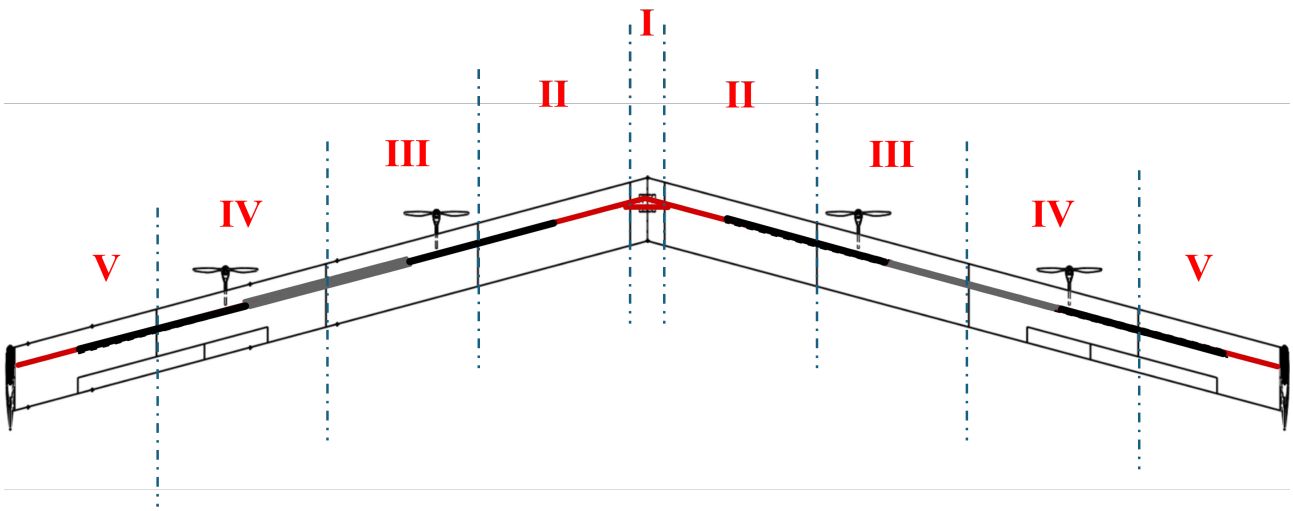

Figure 5.1: Wing Sections Definitions; I - Main Wing Section, II - Middle Wing Section 1, III - Middle Wing Section 2, IV - Middle Wing Section 3, V - Wing Tip Section. The red lines represent spars already integrated in the section, whilst black lines represent spars which will be assemble in-field.

5.2. Design Overview Table

In this section, an overview of both the final design main characteristics in Table 5.1 and the final design characteristics per subsystem in Table 5.2 are presented.

Table 5.1: Final main design characteristics of the AHAPS.

Characteristic AHAPS	Symbol	Unit	Value
Maximum Take-off Mass	m_{TO}	kg	320
True Airspeed @ Cruise	V_∞	m/s	32.7
Wing Surface Area	S	m^2	62.9
Wing Span	b	m	35.5
Wing Chord	c	m	1.77
Wing Sweep	Λ	deg	15
Lift over Drag @ Cruise	L/D	-	42.2
Power Consumption @ Cruise	P_{cruise}	W	3746

Table 5.2: Final design characteristics of each subsystem.

Characteristic	**Symbol**	**Unit**	**Value**	**Characteristic**	**Symbol**	**Unit**	**Value**
Payload				**Power**			
Characteristic	*Symbol*	*Unit*	*Value*	*Characteristic*	*Symbol*	*Unit*	*Value*
Payload Mass	m_{pl}	kg	20.0	Total Power System Mass	$m_{pow,total}$	kg	169.0
Total Payload System Mass	$m_{pl,total}$	kg	21.05	Battery Mass	$m_{power,bat}$	kg	135.5
General				Battery Specific Energy	$E_{s,bat}$	Wh/kg	500
Characteristic	*Symbol*	*Unit*	*Value*	Solar Panel Mass	m_{sp}	kg	24.5
Total General System Mass	$m_{gen,total}$	kg	6.42	Solar Panel Area	S_{sp}	m^2	61.2
Total General System Power	$P_{gen,total}$	W	133	Solar Panel Efficiency	η_{sp}	-	0.30
Airframe				**Propulsion**			
Characteristic	*Symbol*	*Unit*	*Value*	*Characteristic*	*Symbol*	*Unit*	*Value*
Total Airframe Mass	$m_{af,total}$	kg	85.98	Total Propulsion System Mass	$m_{prop,total}$	kg	16.5
Spars Mass	m_{spar}	kg	16.74	Blade Diameter	D_p	m	1.80
Skin Mass	m_{skin}	kg	26.92	Total Efficiency @ Cruise	η_{cruise}	-	0.76
Clamps Mass	m_{clamps}	kg	7.60	Total Efficiency @ Lift-off	η_{TO}	-	0.73
Bolts Mass	m_{bolts}	kg	1.0	Total Thrust @ Cruise	T_{req}	N	74.2
Ribs Mass	m_{ribs}	kg	3.82	Total Thrust @ Lift-off	T_{TO}	N	283.8
Outer Sleeve Mass	$m_{o/sleeve}$	kg	22.92	Rotational Speed @ Cruise	n_{cruise}	rpm	1453
Inner Sleeve Mass	$m_{i/sleeve}$	kg	2.18	Rotational Speed @ Lift-off	n_{TO}	rpm	649
Winglets Mass	$m_{winglets}$	kg	4.8	Power Available @ Cruise	$P_{a,cruise}$	W	2392
Control				Power Available @ Lift-off	$P_{a,LO}$	W	3130
Characteristic	*Symbol*	*Unit*	*Value*	**Temperature Management**			
Total Control System Mass	$m_{control,total}$	kg	7.2	*Characteristic*	*Symbol*	*Unit*	*Value*
Hinge Line Chord Fraction	x_{hinge}	$\%_c$	0.75	Total Temperature Management System Mass	$m_{TM,total}$	kg	4.5
Elevator Spanwise Fraction	$y_{elevator}$	$\%_{b/2}$	0.6 – 0.7	Total Heat Dissipation	P_{diss}	W	332.67
Aileron Spanwise Fraction	$y_{aileron}$	$\%_{b/2}$	0.7 – 0.9	Power Buget Required	$P_{TM,req}$	W	256.55
Rudder Winglet Fraction	z_{rudder}	$\%_{b/2}$	0 – 0.8	Aerogel Layer thickness	t_{TM}	cm	1.5
Elevator Maximum Deflection	$\delta_{elevator}$	deg	±20	**Undercarriage**			
Aileron Maximum Deflection	$\delta_{aileron}$	deg	±20	*Characteristic*	*Symbol*	*Unit*	*Value*
Rudder Maximum Deflection	δ_{rudder}	deg	±30	Total Take-off Gear Mass	$m_{TO_{gear}}$	kg	15.34
				Total Skid Mass	m_{skid}	kg	9.15

5.3. System Architecture

After the external structure is visualised in Section 5.1. In this section the AHAPS internal architecture will be shown. First, the internal locations of all subsystem will be addressed. Then, the hardware diagram further displays the subsystem integration into the airframe. After that, the electric diagram shows the

power system application. Then, the data handling diagram will present the internal data processing within the AHAPS. The external mission communication will be shown in Section 6.2. All software of computers and controllers will be shown in the software diagram.

5.3.1. Subsystem Integration

The C.G. plot with the respective positions of all components and subsystems is shown in Figure 5.2. Each component is positioned in accordance to Table 4.34. The determined target C.G. to acquire adequate control performance was 2.63 m from the nose. This was achieved by positioning the battery pack at the end of the middle wing section two. The battery pack is distributed over one metre of the span; this allows for sufficient insulation.

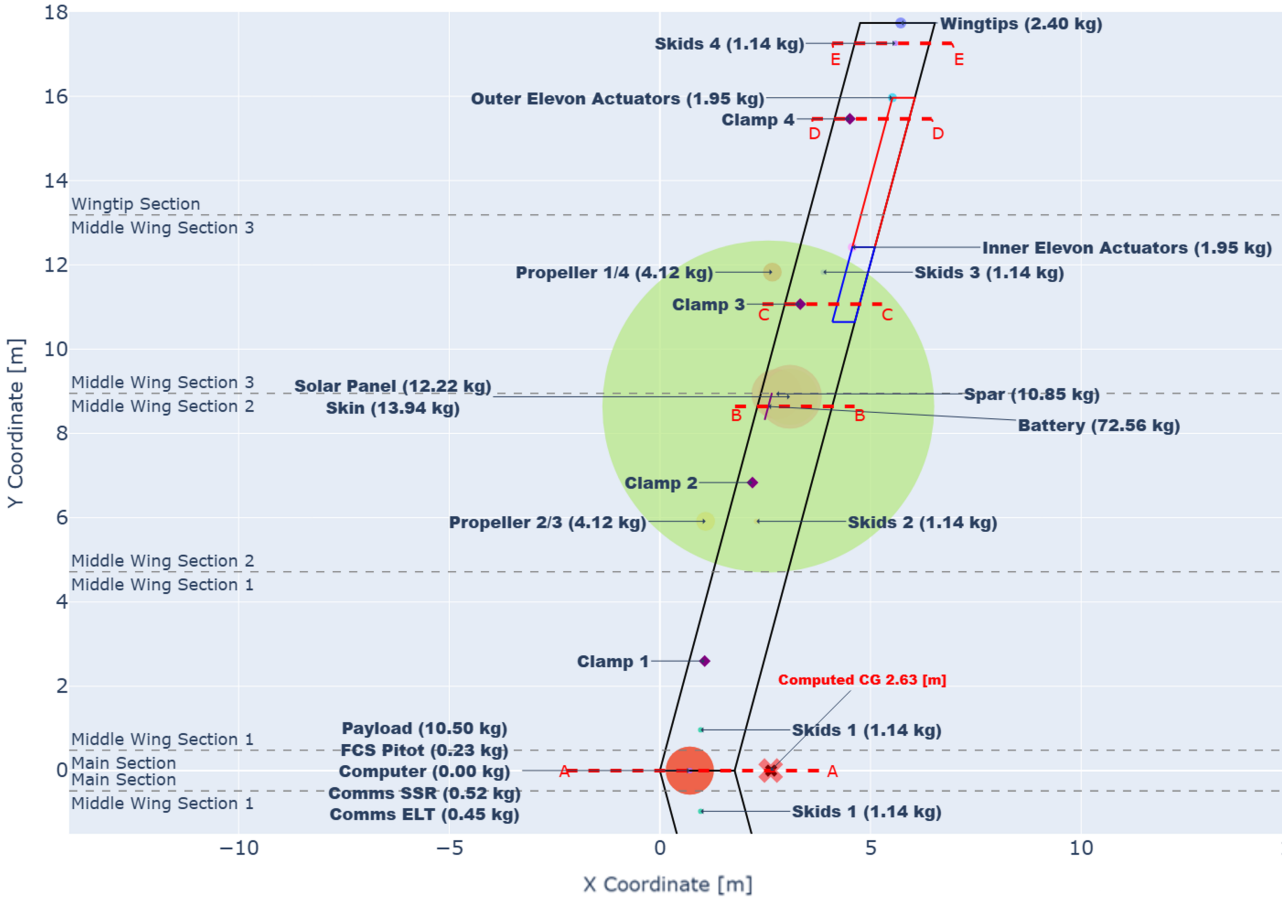

Figure 5.2: C.G. plot with cross-sectional cuts corresponding to the cross-sections A-E.

After all subsystem and component positions are shown in the C.G. plot, the cross sections are shown in Figure 5.3. In Figure 5.3a, the nose cross-section is shown. In this cross-section, the main communication components are placed together with the computer and payload. These are placed closely together as they communicate continuously, and their residual heat is then combined to minimise undercooling issues at cruising altitude. In Figure 5.3b, the battery pack is shown. The battery pack is distributed in front of the spar structure. The battery pack is insulated by five layers of aerogel and air, totalling 1.5 cm. This is shown in blue. In Figure 5.3c, the inner elevon is shown together with the cross-section of the clamp. In Figure 5.3d, the outer elevon is shown together with the cross-section of the clamp. In Figure 5.3e, the fourth, most outward, skid is shown. In the plot, the skid is fully extended to its landing configuration. In its cruising configuration, it acts as the skin of the airfoil. This is shown by the shape of the skid.

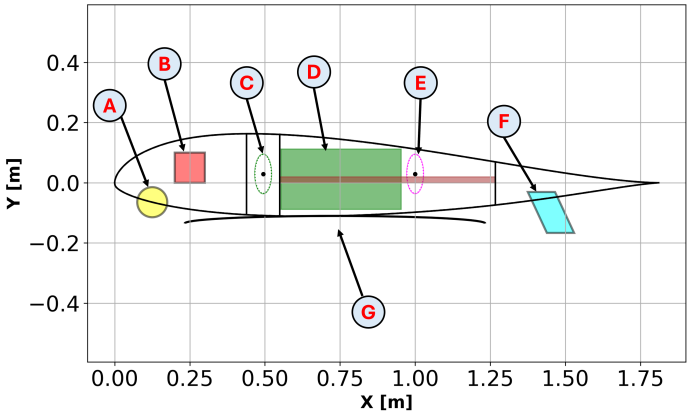

(a) Cut A; A - ADS-B & ELT, B - Computer, C - Spar, D - Payload Bay, E - Second Spar, F - Secondary Surveillance Radar, G - Synthetic Aperture Radar

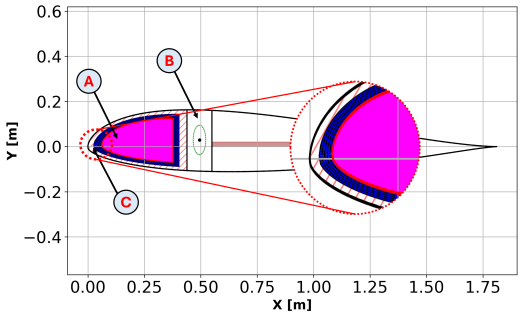

(b) Cut B; A - Battery Pack, B - Spar, C - Insulation

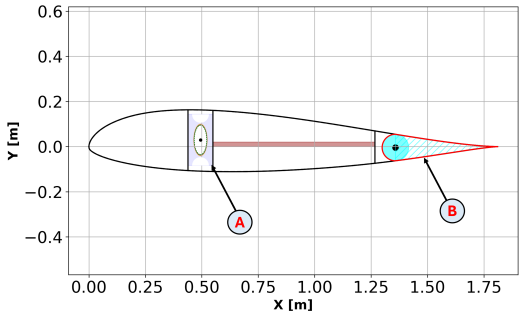

(c) Cut C; A - Clamped Spar, B - Inner Elevon

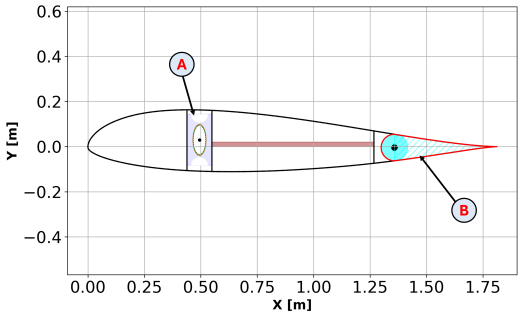

(d) Cut D; A - Clamped Spar, B - Outer Elevon

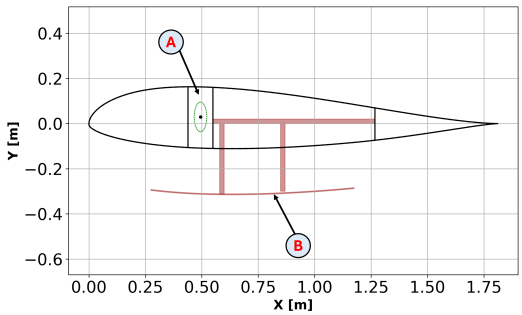

(e) Cut E; A - Spar, B - Skid

Figure 5.3: Cross-section cuts A–E.

5.3.2. Hardware Diagram

In this section, a hardware diagram is shown in Figure 5.4. It displays the right-hand side of the AHAPS as a top view. It shows the subsystems lying within a certain wing section in accordance with Figure 5.1. The arrows indicate mounting from and to a certain subsystem with the airframe.

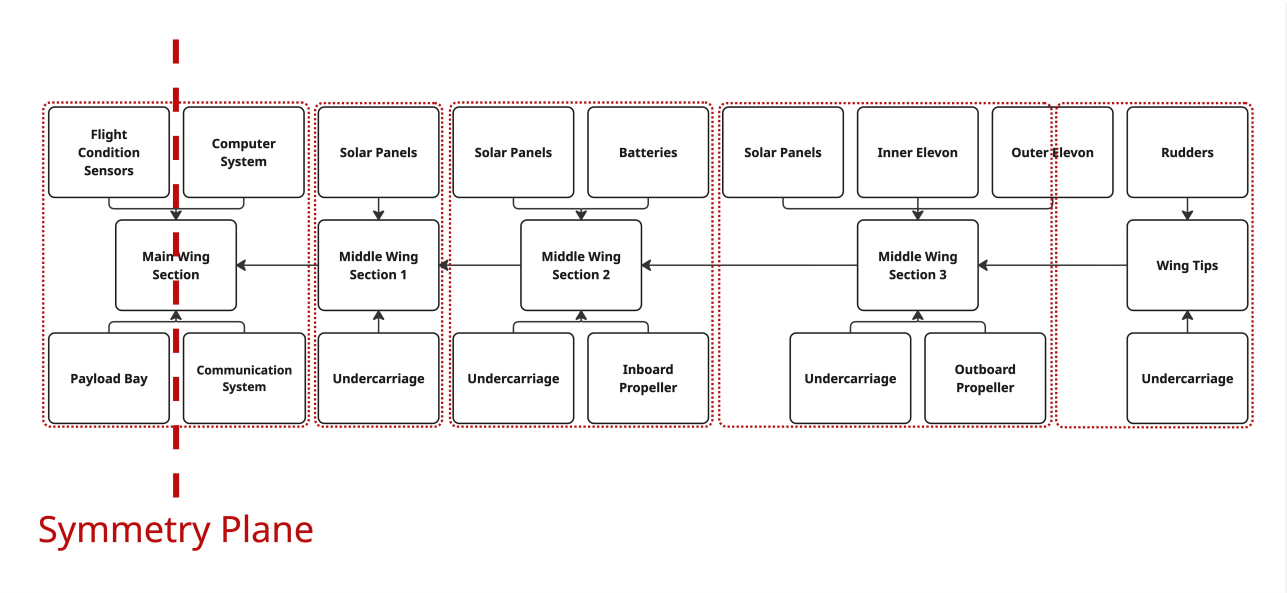

Figure 5.4: Hardware diagram of the right-hand side of the AHAPS. Each wing section is illustrated together with the corresponding hardware that is put into each section.

5.3.3. Electrical Diagram

In this section, the electrical diagram is shown to elaborate further on the workings of the power system. The power system has the battery as the central component. It charges with the solar panel and discharges current to all power-requiring subsystems. The battery pack average current is 4 A, together with the required powers, leads to the voltages needed per component as per Equation 5.1[1].

$$P = U \cdot I \tag{5.1}$$

The diagram is shown in Figure 5.5.

5.3.4. Data Handling Diagram

The data handling follows a specific structure, as shown in Figure 5.6. It can be seen that the main flight computer is the heart of this structure, making decisions to be executed by the subsystems. It sends instructions to all subsystems in a general way. These instructions are relatively generic, for example, to lower the flight altitude. The different controllers are responsible for translating the instructions to their respective actuators, which is explained in more detail in Section 5.3.5. Feedback loops are integrated throughout the entire AHAPS. These feedback signals are returned to the main flight computer, which then can adjust the instructions when necessary. All of these connections are in accordance with the previously shown N2-chart, shown in Figure 3.1.

5.3.5. Software Diagram

The purpose of the software diagram is to show the execution logic of the instructions obtained from the main flight computer by the individual subsystem controllers. The individual controllers are responsible for carrying out a specific task. For example, when the instruction by the main flight computer is to lower the altitude to 59,000 ft, the controllers are responsible for monitoring the current altitude and adjusting specific actuator commands to obey the instruction of the main flight computer. This structure is shown for the various subsystems in Figure 5.7.

5.4. Cost Breakdown

The main cost drivers of the AHAPS design are shown in the cost breakdown. During the detailed design of each subsystem, the materials and manufacturing costs of the components and services making up various

[1] https://web.archive.org/web/20240918163649/https://amprius.com/documents/Amprius_Product_Portfolio_0824_website.pdf [cited 19 May 2026]

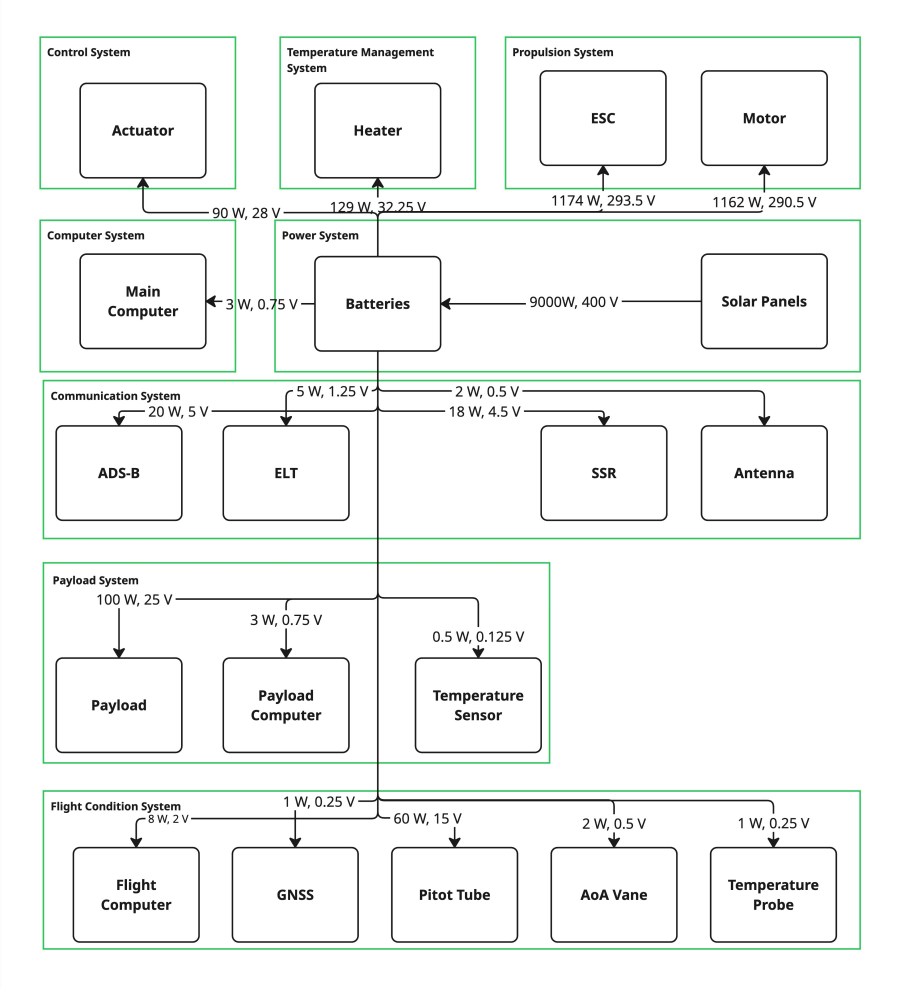

Figure 5.5: Electrical diagram showing the specific power and voltages for each component coming from the battery.

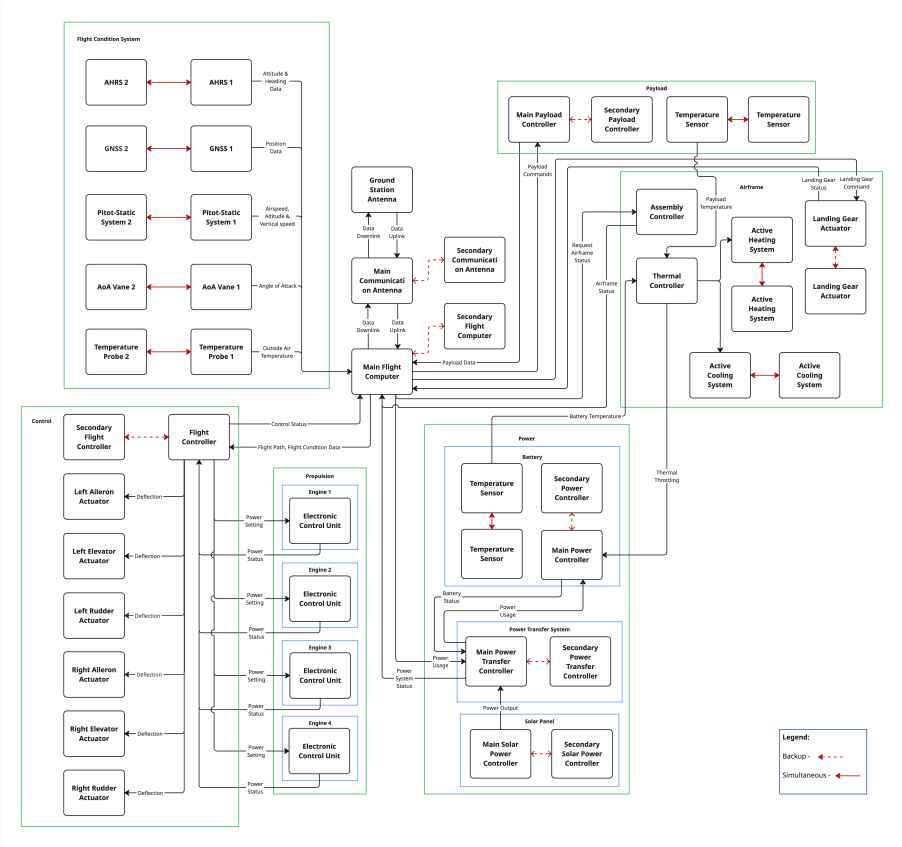

Figure 5.6: Data handling diagram showing the flow of data between different subsystems.

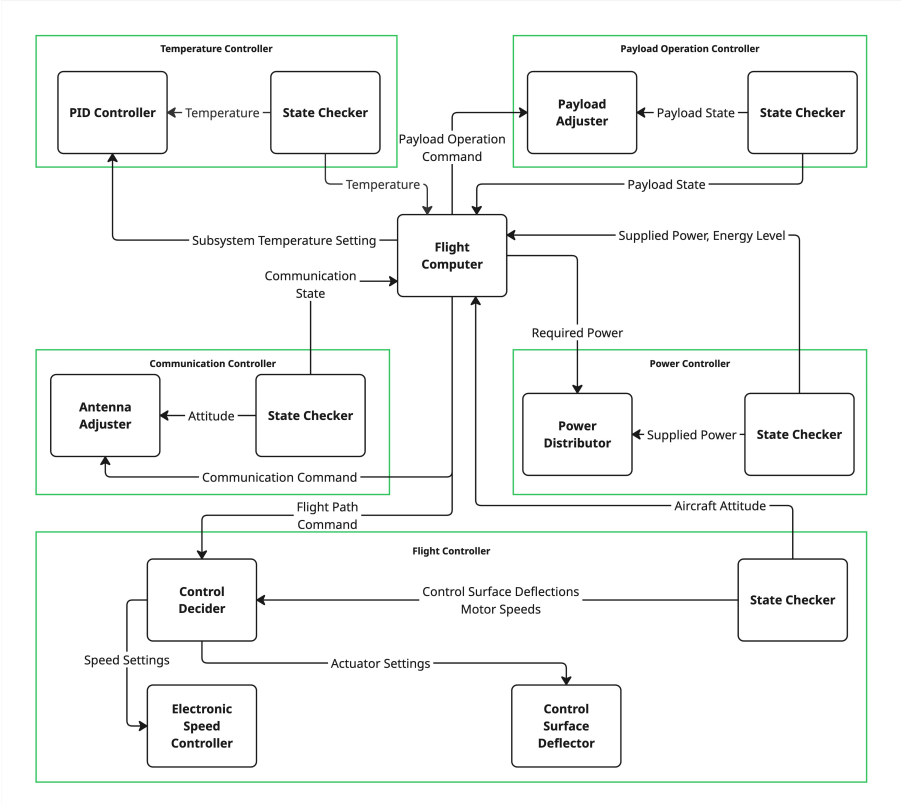

Figure 5.7: Software diagram showing the execution logic of the instructions obtained from the main flight computer.

subsystems have been estimated. The summary of the costs of the individual subsystems are shown in Table 5.3.

Table 5.3: Cost breakdown of materials and manufacturing cost of the complete AHAPS per subsystem, given in fiscal year 2026 euros. An extra margin of 20% is added on top of the individual subsystem costs in order to account for uncertainties in the cost values obtained.

Subsystem	**Cost (€) (FY26)**
Payload	€5,000
Flight Condition	€46,000
Computer	€1,000
Communication	€13,000
Airframe	€152,000
Power	€205,000
Propulsion	€108,000
Control	€54,000
Temperature Management	€3,000
Undercarriage	€28,000
Ground Station	€60,000[a]
Tooling	€7,000[bc]
Cost Margin	+20%
Total	**€**820,000

[a] https://www.albaorbital.com/alba-connect-station [cited 22 June 2026]

[b] https://supplyapp.com/facility-maintenance-tool-set-tool-cart-p14vy75.html [cited 22 June 2026]

[c] https://amzn.eu/d/0jkMyx9I [cited 22 June 2026]

The estimated costs are significantly lower compared to the budget allocated to them in Section 3.3.3. As many emerging technologies are employed in subsystems such as the power system and the airframe system, there is a significant uncertainty in the respective estimated materials, components, and manufacturing cost. Besides this, inflation might occur in the time period between this estimation and the actual production of the AHAPS, which is why the cost is computed for the reference year 2026. Furthermore, due to the current geopolitical situation, price fluctuations are very prevalent in the global markets. Due to all of these reasons, a margin of 20% is added to the overall cost of the aircraft to arrive at a conservative total material and manufacturing cost estimation of €820,000.

The cost of the payload system consists of the payload computer, a temperature sensor, the casing and brackets, and network cables, as outlined in Section 4.2. The flight condition system cost is built up from the cost of the COTS sensors that are included in the system. For the computer system, costs include the COTS computer and data cables. The communication system costs consist of the ADS-B, ELT, SSR, and the antenna. For these general subsystems, the cost breakdown is further detailed in Section 4.3.2. The airframe cost is estimated from the individual structural components, such as the spar, skin, clamps, bolts, ribs, sleeve, and winglet, shown in Section 4.4. Power system cost estimation takes the cost of the batteries and the solar panels into account, as explained in Section 4.5. Motor, electronic speed controller, and propeller cost, as well as other structural costs, are estimated for the propulsion system in Section 4.6. The actuators make up the cost for the control system, as detailed in Section 4.7. Heaters and insulation are the contributors towards the temperature management system cost in Section 4.8. Lastly, the cost for the undercarriage system is separated into costs for the take-off system and costs for the landing skids, as shown in Section 4.9.

5.5. Sustainability Aspects

To quantify the sustainability of the design, the subsystems assumed to contribute to the emissions are the airframe system, power system, and computer system. This is due to the fact that most of the lifecycle emis-

sions will originate from the material used for manufacturing and the degradation of both the structural materials and the batteries.

Table 5.4: Assumptions list sustainability tools.

Assumption ID	Category	Assumption	Justification (Quantitative)
ASP-DES-9.1	Sustainability	The structure of the AHAPS is constructed from carbon fibre reinforced polymers.	Scientifically backed-up information can be used for the manufacturing emission estimations by the tools.
ASP-DES-9.2	Sustainability	Emissions of CO_2 are considered dominant with respect to emissions of other molecules like N_2.	The tool focuses on CO_2-emissions, so neglecting the other emissions is required for proper functionality.
ASP-DES-9.3	Sustainability	Emissions related to the materials, solar and power systems, and the computer system are the only contributors to the total emissions.	This limits the scope of the tool, making it more efficient to use. The absolute error will not be negligible, but due to consistency, the relative estimations will still be correct.
ASP-DES-9.4	Sustainability	Degradation mainly affect the airframe and energy storage system.	This is a typical assumption for the degradation of aerospace systems.
ASP-DES-9.5	Sustainability	The degradation rate is constant over time.	This allows for the use of various sources that present degradation rates in different time windows. Consistently applying this assumption will ensure that the relative degradation rates will be correct.

5.5.1. End-of-Life Recyclability

EoL recyclability is driven by two main factors: **REQ-STK-3.1** and the European Directive target of recycling 95% of the total aircraft weight, with a minimum of 85% [1]. To verify compliance, a detailed overview of the percentage of recyclability or reusability per component is given in Table 5.5. As there are many different electrical components, a conservative general recyclability of 53.6% is used[1].

Table 5.5: Recyclable/reusable mass fraction per subsystem material.

Material/Component	Mass (kg)	Recyclable/Reusable (%)
Airframe		
Spar & ribs (CFRP)	21.5	90 [59]
Skin (Mylar)	28.5	85[a]
Sleeves (Titanium)	24.33	95 [60]
Clamps (Nylon 6)	7.6	90[b]
Power		
Solar panels (Si multijunction)	24.6	90 [61]
Li-ion batteries	135.5	90[c]
Additional Power Components (incl. cables)	9.0	97.2 [62]
Propulsion		
BLDC motors	3.2	53.6[d]
Propellers (CFRP)	6.8	90 [59]
ESCs	2.1	53.6[e]
Cables	0.8	97.2 [62]
Connecting rods (CFRP)	1.2	90 [59]
Nacelles/hubs (CFRP)	2.4	90 [59]
Computer		
Raspberry Pi 5	0.05	53.6[e]
Network/power cables	3.20	97.2 [62]
Communication		

Continued on next page

[1] https://www.epa.gov/sites/default/files/2014-05/documents/handout-10-circuitboards.pdf

Material/Component	Mass (kg)	Recyclable/Reusable (%)
ADS-B, ELT, SSR, antenna	2.34	53.6[e]
Flight Condition		
Flight computer, GNSS, pitot tube	0.78	53.6[e]
Control		
Actuators	7.2	53.6[e]
Take-off & Landing		
Struts (CFRP)	0.464	90 [59]
Wheels (CFRP)	6.88	90 [59]
Struts (Aluminium)	1.92	92 [63]
Skid pad (Aluminium)	3.84	92 [63]

[a] https://www.bopet-film-china.com/new_detail/Is-PET-Film-Recyclable.html [cited 13 June 2026]

[b] https://www.sciencenews.org/article/polymer-breakdown-reaction-offers-possible-way-recycle-nylon [cited 16 June 2026]

[c] https://www.kedglobal.com/batteries/newsView/ked202307310010 [cited 12 June 2026]

[e] https://www.epa.gov/sites/default/files/2014-05/documents/handout-10-circuitboards.pdf

All of the components that are not fully recyclable are ensured to be inert upon disposal so that no hazardous materials are expelled from the manufacturing process. This leads to a total of 89% of the 334.6 kg total weight (MTOW + take-off/landing structure) that can be recycled. This lies above the European Directive minimum of 85% [1].

5.5.2. Component Lifecycle

An overview of AHAPS degradation is estimated from the individual degradations of the airframe and power system, as these are the two most costly subsystems to replace during their lifecycle.

During the sizing of the solar panel area and the number of batteries, an operational lifetime of two years has been assumed, as discussed in Section 4.5.2. This already limits the lifetime of the whole power system to two years. After this, the whole 145.2 kg of Li-ion batteries and 24.5 kg of solar panels will need to be decommissioned. This comes down to a replacement cost of €205000 every two years. There is the option to extend the operational lifetime of the solar panels and batteries beyond two years, but this comes with decreased deployability performance, as per the needs of the operator.

For the airframe, the degradation rates of the main materials are given in Table 5.6. Based on a conservative service-time-to-90% retention and the assumption that these materials are constantly operated at cruise altitude, the Mylar film will have to be replaced after ≈ 16.5 years, the CFRP after ≈ 4 years [64]. Due to the small amounts of degradation of aluminium and titanium, these components are not taken into account.

Table 5.6: Degradation rate of Mylar and CFRP.

Material	Degradation Rate
Mylar	≈ 0.6% per year [65]
CFRP	≈ 2.5% per year [64]

Due to the relatively small degradation rates of the structural components, it is more likely that these will be replaced earlier. After each flight, the airframe and other components will be checked for potential cracks or failures and will be interchanged if necessary.

5.5.3. Lifecycle Emissions

Since the aircraft uses electric motors, it will not emit emissions during its operations. This leads to the lifecycle emissions of the AHAPS consisting only of the manufacturing emissions.

The manufacturing emissions of the different subsystems will be quantified based on their estimated net CO_2 emissions. These emissions will be calculated in 'kilograms CO_2-equivalent' (kg CO_2-eq), which accounts for the entire lifecycle from production until destruction with an assumed lifetime of a hundred

years. Since the hundred-year lifetime is standardised for the unit and the AHAPS' lifetime will be significantly shorter, this means that the CO_2 emission estimates will be conservative. The emissions per subsystem material are calculated per unit of required product. The emissions for the used materials are summarized in Table 5.7. The total emissions are calculated by summing all the products of the individual emission factors and their respective mass.

Table 5.7: Emission factors and total emissions per material.

Required Product	**Emission Factor (kg CO_2-eq)**	**Total Mass (kg)//Energy Consumption (kWh)**	**Total Emission (kg CO_2-eq)**
CFRP	67.79 /kg	78.4	5314
Mylar	3.0 /kg	26.9	80
Titanium	48.3 /kg[a]	24.6	1188
Aluminium	14.8 /kg [63]	24.8	367.0
Nylon 6	9.3 /kg[b]	5.6	52
Batteries (Li-ion)	60.0 /kg	145.2	8712
Heterojunction silicon (solar panels)	0.02 /kWh	163500	3270

[a] https://www.climatiq.io/data/emission-factor/91c20b20-5f6c-4cd7-bf17-0bd743af6534 [cited 16 June 2026]

[b] https://switch.unibloom.world/data/emissions-factor/nylon-6-europe [cited 16 June 2026]

Based on this, the total emissions from the manufacturing process are 18980 kg of CO_2. This emission is comparable to the manufacturing emission of two battery electric cars, which have a production emission of 8800 kg of CO_2 each[1]. Once the product enters scaled-up production, total emissions are expected to further decrease.

6. Design Performance

This chapter centres on the performance of the AHAPS and how it will operate. In Section 6.1, the performance metrics for the AHAPS are outlined to show the technical feasibility to prove that the AHAPS is capable of successfully executing its mission. Following the technical performance evaluation, Section 6.2 details the practical operations and logistics required to successfully deploy the system in the field.

6.1. Performance Analysis

In this section, multiple performance metrics of the AHAPS are shown. First, in Section 6.1.1, the structural performance is assessed by a static analysis. Additionally, a dynamic analysis option will be addressed. Second, in Section 6.1.2, a dynamic analysis is done on the AHAPS to address its eigenmotion performance. Third, in Section 6.1.3, using XFLR5 an aerodynamic analysis is performed to validate the earlier use of VLM and LLT. Fourth, in Section 6.1.4, the deployability of the AHAPS is addressed by showing the day-to-day deployability at 30' latitude. Finally, in Section 6.1.5, the mission is simulated to show its performance and route throughout the 28-day mission.

6.1.1. Load-bearing Capabilities

A significant challenge in the design of a large surface area, large aspect ratio aircraft is ensuring it has sufficient structural load-bearing capabilities. Aircraft are certified to withstand both dynamic and static loads [66]. The AHAPS structure needs to be able to sustain both static manoeuvring loads and dynamic gust loads.

Manoeuvring loads are usually defined as static loads, which have different certification standards depending on the type of aircraft [66, 67, 68]. For HAPS, the manoeuvring load requirements defined by certification requirements, such as CS-22 for sailplanes, or CS-23 and CS-25 for commercial aircraft, are too constraining [69]. Due to flexible certification requirements for unmanned aircraft, smaller static load factors can be considered[1]. Based on the load factor analysis of a similar HAPS aircraft, a maximum positive and negative manoeuvring load factor of 2.0 and -1.0 is determined for the AHAPS aircraft [69]. The negative manoeuvring load factor decreases to 0.0 at the maximum design speed, in line with CS-23 certification guidelines [68, 69].

Gust loading is often defined as dynamic loads, particularly for larger aircraft, such as in CS-25 [66]. Sailplanes and smaller commuter planes often focus on quasi-static gust loading certification [67, 68]. Despite this, for flying wing aircraft similar to the AHAPS, quasi-static gust loading is usually inaccurate compared to dynamic analysis [70]. However, due to time constraints, a dynamic load analysis is beyond the scope of this conceptual design. Therefore, the conceptual aircraft structure is sized with a static gust load approximation based on CS-22 and CS-25 regulations [66, 67]. CS-25 lists standard gust speeds between 0 and 60,000 ft, which are halved for HAPS aircraft and used in Pratt's formula to approximate gust loads between the aircraft's minimum cruise speed and maximum design speed, with the gust speeds again halved at the maximum design speed [66, 69]. However, if at a certain velocity, the load factor obtained from Pratt's formula is higher in magnitude than 1.25 times the stall load factor, then the latter load factor is used instead, in accordance with CS-22 sailplane guidelines [67].

In general, the use of quasi-static loads in the analysis of the AHAPS is a conservative estimation [70]. The static load factors obtained are almost certainly higher than the actual load factors that the aircraft can encounter, especially considering that the AHAPS is only to be deployed in sufficiently good weather conditions. Therefore, using these approximate load factors to size the AHAPS results in a structure that will most likely comply with the structural integrity requirements.

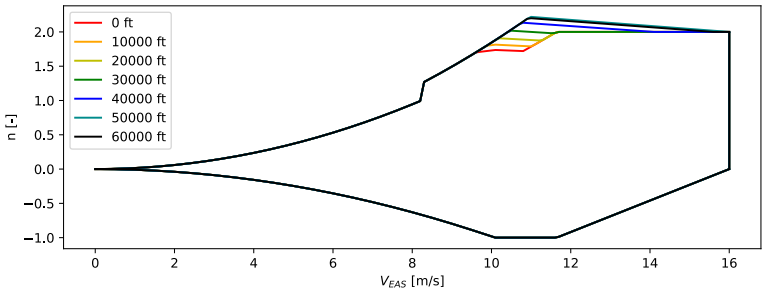

Figure 6.1: The computed flight envelope of the AHAPS at an altitude between 0 ft and its cruising altitude of 60,000 ft. The most critical case is at an altitude of around 50,000 ft, with a maximum limit load of 2.2 and a minimum limit load of −1.0. These are composed of heavily approximated static gust loads, but are sufficient for a conceptual sizing of the structural system.

Static Performance

With the maximum load factors defined, a structural analysis is performed, determining the effects on the airframe. As described in Section 4.4, the wing structure was sized to endure the maximal and minimal loads during all phases in flight, including load factors described in Section 6.1.1. As such, the airframe is capable of sustaining the static loads.

On the other hand, this sizing procedure does not consider deflection of the wings. Wing deflections largely stem from bending and torsional moments, with shear and normal forces producing negligible deflections [25]. These factors are exacerbated by the lightweight wing structure and the large aspect ratio. Therefore, analysing wing deflection is a necessary validation, as excessive wing deflection can degrade aerodynamic and control system performance.

Bending deflections are calculated by taking the wing spar as the only load-bearing structure. Using the `aerosandbox` lifting line computation tool, all aerodynamic forces and moments are calculated [3, 28]. For bending in the x-axis, bending relief is also considered. This is because the flying wing has no fuselage, and therefore, proportionally heavier compared to commercial aircraft, significantly reducing bending loads and deflections. With this, the second derivative of deflection can be calculated using Euler-Bernoulli beam theory [**noauthor_aircraft_2022**]. As such, this can be twice integrated to find the full deflection as a function of wing span. This process is followed for the cruise load factor, as long as the maximum and minimum load factors are determined by Figure 6.1. From the deflection diagrams in Figure 6.2, it can be seen that the load factors linearly correlate to the lateral displacement. However, the same is not true for vertical deflection, due to bending relief, which significantly reduces deflection for the load factor of 1 and amplifies it for the load factor of -1. This is observed by noting the maximum deflection for load factors 1 and -1 of 2.0 m and −6.0 m, respectively. The positive vertical bending produces an induced dihedral, which is beneficial for the lateral stability of the aircraft. Positive lateral deflection induces a more positive sweep, improving lateral stability. Both of these induced changes also result in slight lift decreases; however, this is a negative feedback loop as decreased lift will decrease the wing deflections.

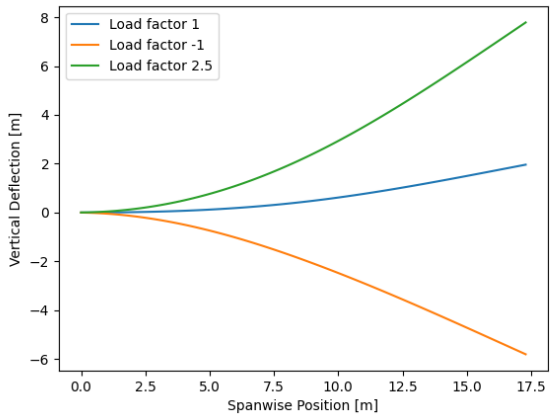

(a) Vertical displacement of the AHAPS wing as a function of span for 1, -1, and 2.5 load factors. The maximum deflection for each load factor is 2.0 m, -6.0 m, and 8.0 m respectively

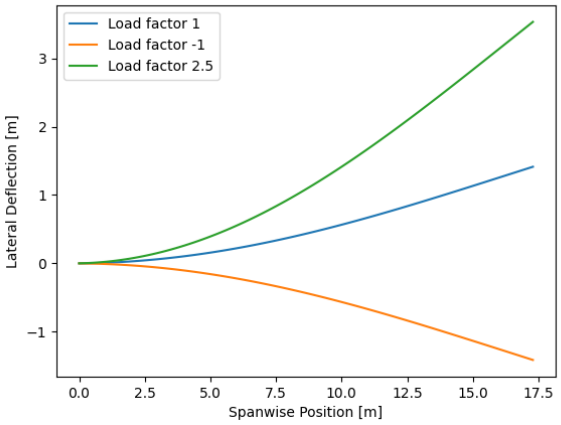

(b) Lateral displacement of the AHAPS wing as a function of span for 1, -1, and 2.5 load factors. The maximum deflection for each load factor is 1.3 m, -1.3 m, and 3.5 m respectively.

Figure 6.2: Vertical and lateral deflection spanwise wing deflection of the AHAPS. The former has significantly larger deflections, due to greater loading. Three deflection curves are shown, corresponding to the load factors of 1, -1, and 2.5, derived from the minimum, cruise, and maximum load factors.

In the design of the airframe, the skin was designed to sustain all torsional loading. Naturally, in actuality the wing spar and other load-bearing structures also sustain these loads. By using the torsion equation for thin-walled structures, it can be seen that the spar does not fail from torsion [25]. This is also the case when the maximum and minimum load factors are applied.

Next, twist deflection from the wing's torsional moment is considered. The torsional moment is from the lifting line computation. Deflection of the wing is now determined by Bredt-Batho theory [**noauthor_aircraft_2022**]. For twist, the stiffness of the airframe skin and spar is combined, using the compatibility equation. With individual loading, the derivative of the shear for both structures is found. By integration, the twist distribution as a function of span is calculated, which can be performed for cruise, maximum, and minimum load factors. These deflections can be seen in Figure 6.3. Similarly to lateral deflection, these curves also scale linearly. The negative deflection twists the wings downward, delaying stall at wingtips, which is beneficial for maintaining controllability [43].

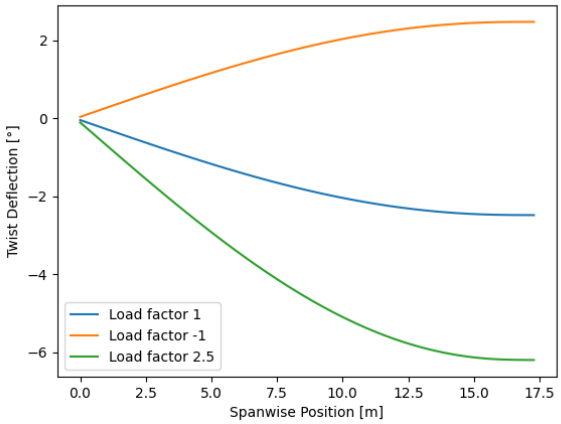

Figure 6.3: Spanwise twist displacement in degrees for the AHAPS wing. Three displacement curves are present corresponding to the load factors of 1, -1, and 2.5. These factors are derived from the minimum, cruise, and maximum load factors. The maximum twist at each load factor is -2.4°, 2.4°, and -6.0°.

Dynamic Performance
A full dynamic structural analysis using finite element analysis is outside of the scope of this project. However, it is addressed in the recommendations, shown in Section 8.1.

6.1.2. Stability and Control
The design of a new aircraft configuration introduces the necessity for evaluation of the aircraft on its stability and control characteristics. This is done for both the longitudinal and lateral directions of the aircraft.

Using the 'AeroBuildup' Python library of the 'AeroSandbox' package, the aircraft was modelled and the control derivatives of the aircraft, shown in Table 6.1, were found using the VLM solver. Then, after determining the required C.G. for equilibrium, the control surfaces needed to reach the control requirements were sized. Afterwards, the aircraft was also evaluated on its stability during the short-period, phugoid, Dutch roll, and spiral eigenmotions. The longitudinal and lateral stability & control performance of the AHAPS are examined respectively, and a summary of the eigenmotion properties is provided at the end of the section.

Table 6.1: Stability and control coefficients used in the EOM Section 4.7 to analyse the dynamic responses of the aircraft.

Derivative	Value	Derivative	Value	Derivative	Value
C_{X_u}	0.00061185	C_{X_α}	1.61570666	C_{X_q}	0.1416841
$C_{X_{\delta_e}}$	0.12631441	C_{Z_u}	0.03286512	C_{Z_α}	-5.531434
C_{Z_q}	-0.78524617	$C_{Z_{\delta_e}}$	-0.91039384	C_m	-0.002174
C_{m_u}	0.02515464	C_{m_α}	-1.16748081	C_{m_q}	-3.01246955
$C_{m_{\delta_e}}$	-0.90660709	C_{Y_β}	-0.05441167	C_{Y_p}	-0.06405861
C_{Y_r}	0.0319185	$C_{Y_{\delta_a}}$	-0.03586255	$C_{Y_{\delta_r}}$	0.28387402
C_{l_β}	-0.03172923	C_{l_p}	-0.95023027	C_{l_r}	0.05990826
$C_{l_{\delta_a}}$	-0.46704213	$C_{l_{\delta_r}}$	0.01159312	C_{n_β}	0.00532951
C_{n_p}	-0.28152238	C_{n_r}	-0.01531195	$C_{n_{\delta_a}}$	-0.08202693
$C_{n_{\delta_r}}$	-0.02029647	K_X^2	0.047617	K_Y^2	1.309867
K_Z^2	0.050699	K_{XZ}	0.0001165	μ_c	21.633389

Longitudinal Performance
Flying wings, by virtue of their lack of empennage, require careful balancing of the C.G., airfoil selection, and wing geometry to maintain longitudinal equilibrium and stability. Statically, the platform is stable with equilibrium at α_{cruise} = 10.3° and C_{m_α} = -1.167 rad^{-1}, when loaded with a C.G = 2.64 m. Dynamically, the aircraft has a stable, highly-damped short-period mode, but a slightly unstable phugoid mode, as shown by the eigenvalues in Figure 6.4 with positive real components.

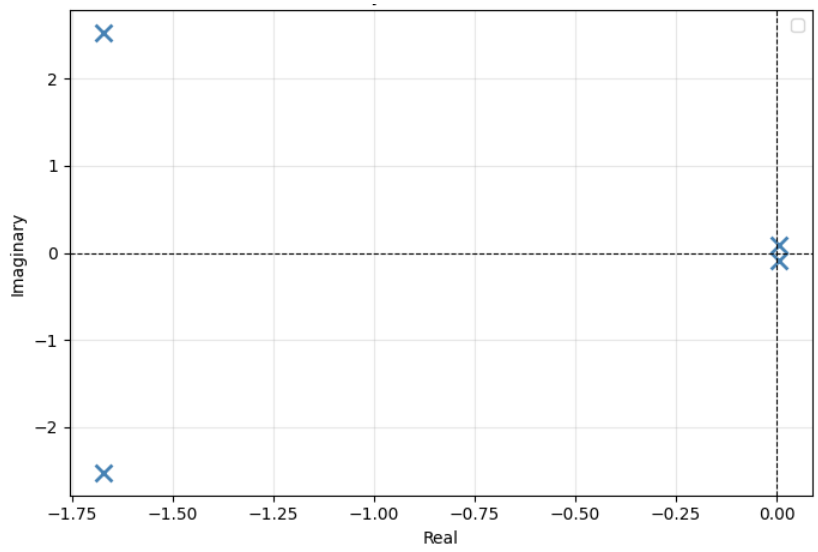

Figure 6.4: AHAPS linearised EOM symmetric poles. The poles responsible for the unstable phugoid response are the two poles with a positive real value.

Whereas an unstable phugoid mode would be problematic on manned aircraft with direct controls, due to an increase in pilot workload, the AHAPS will use a fly-by-wire control system with a velocity controller. As such, the flight computer will oppose any diverging velocity-altitude oscillations by adjusting motor power. This would nullify the main concern, which would be an increase in the expected duty cycle of the control system and the flight computer, and its effect on wear. Additionally, the period and time to double amplitude are both in the order of minutes, which generally reduces the risk of divergence. A time plot of the phugoid mode is shown below in Figure 6.5.

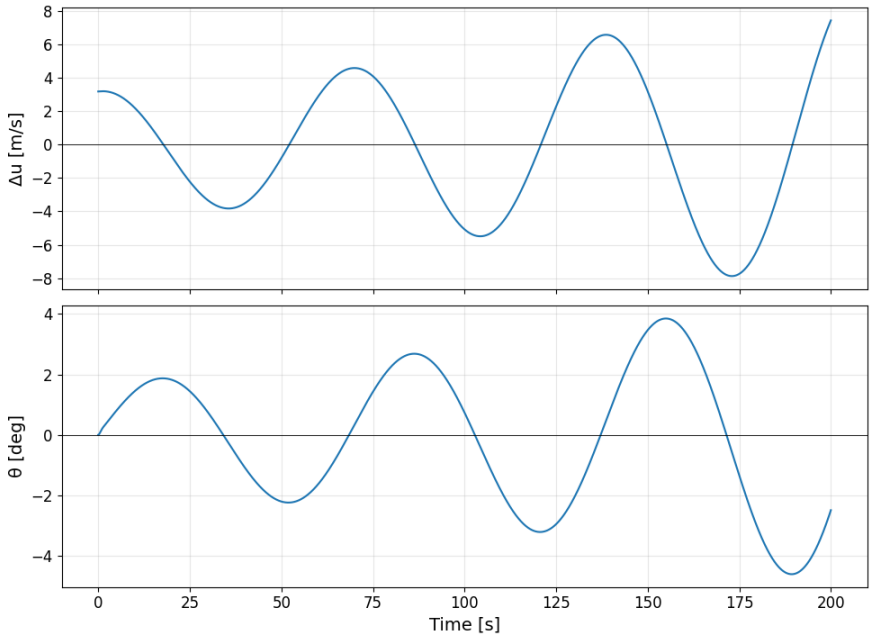

Figure 6.5: AHAPS response to phugoid mode excitation with a $\Delta u_0 = 3.18$ m/s.

Controllability-wise, the AHAPS meets the longitudinal requirement of 3°/s, as shown in Figure 6.6, using inboard elevators between 60% and 70% of the half span. Using inboard elevators reduced the size requirement for the ailerons, and protected the elevators from early stall, as aft-swept wings stall at the tips first. Additionally, an effective wing twist of −5° and placement of the elevator aft of the outboard motor all help to protect against loss of control in the high-angle-of-attack regime and subsequent pitch-up, which is inherent to aft-swept wing configurations.

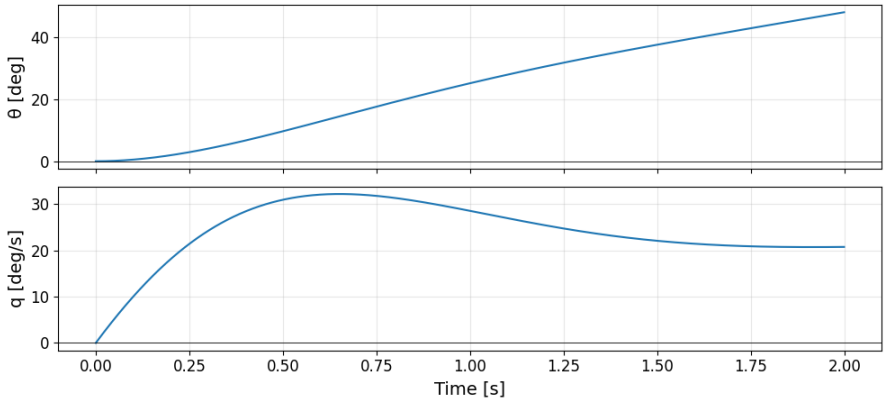

Figure 6.6: AHAPS response to maximum elevator deflection $\Delta e = -20°$.

Lateral Performance

The lateral performance of a flying wing is also of great interest due to the often-lacking fuselage damping, large wing sweep, and potentially significant control coupling. As shown in Figure 6.7, both the Dutch roll and spiral modes are stable, with the Dutch roll being more heavily damped, achieved primarily by the effective dihedral induced by wing deflection under loading, the selected sweep of 15°, and the appropriately sized winglets. No simulation was performed for the aperiodic roll mode, since the roll damping coefficient C_{l_p} is negative and the mode has no significant coupling with the other eigenmodes.

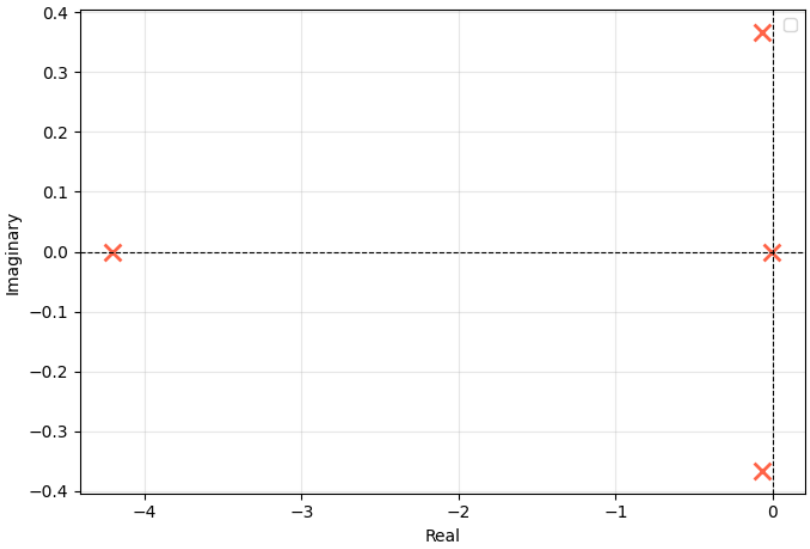

Figure 6.7: AHAPS linearised EOM asymmetric poles.

Roll control is also sufficient, with the aircraft being able to reverse a 45° turn within 11.8 s, as demonstrated by the simulation in Figure 6.8. Lastly, the rudder is sufficiently sized to maintain directional control during the critical OEI condition, requiring a deflection of 24°, and provide a yaw rate of at least 5°/s with the remaining 6° of deflection available. To prevent the sizing of excessively large rudders, which would detrimentally affect wing loading and structural sizing, the opposing motor will be reduced to a maximum of 50% thrust. This would still provide the AHAPS with sufficient performance for recovery.

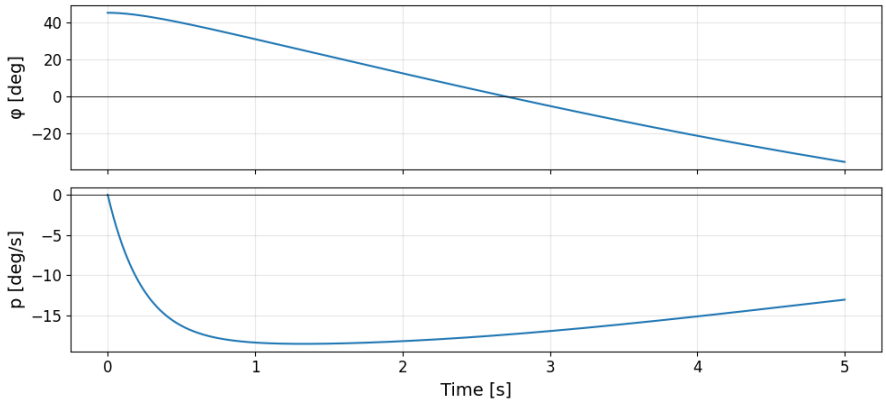

Figure 6.8: AHAPS response to maximum aileron deflection $\Delta a = 20°$.

Eigenmotion Properties

In summary, the AHAPS is sufficiently stable in the short-period, Dutch roll, and spiral modes, with mild instability in the long-period phugoid mode, and the control surfaces can provide sufficient control over all three axes.

The simulation, however, is preliminary, being a VLM solver. Its primary limitation is that viscous effects are not modelled, reducing the fidelity of the simulation at higher angles of attack, particularly with respect to C_X - and in some cases C_Z - terms, which are more heavily dependent on drag. Fortunately, these terms only affect the symmetric equations of motion and have minimal effect, mostly on the phugoid mode.

The eigenmotion properties are given in Table 6.2 below. It includes the eigenvalues, and where applicable, the period, time to half amplitude, and damping constant.

Table 6.2: Overview of eigenmotion properties of the AHAPS.

Mode	**Eigenvalue(s)**	**Period (P) (s)**	**Time to half amplitude ($T_{1/2}$) (s)**	**Damping constant (ζ)**
Phugoid	$0.0053 \pm 0.091\,j$	69.05	–	-0.058
Short period	$-1.67 \pm 2.53\,j$	2.48	0.41	0.55
Dutch roll	$-6.82e^{-02} \pm 0.37\,j$	16.98	10.16	0.181
Aperiodic roll	-4.20	–	0.16	1
Spiral motion	$-3.48e^{-03}$	–	199.18	1

6.1.3. Aerodynamic Performance

The aerodynamic properties of the AHAPS determine its in-flight efficiency values and thus dictate its required propulsive power, which is a driving metric for the power system. Considering that the mass fraction of batteries and solar panels alone comprises around half of the MTOW of the entire aircraft, as can be seen in Table 5.2, it is important to once again quantify its basic aerodynamic coefficients after the sizing process. Furthermore, as has been mentioned in Section 4.4, the coefficients computed throughout the optimiser are the result of a combination of the vortex lattice and quasi-linear lifting line methods, due to the latter outputting unrealistic performance values by itself. As such, due to the non-standard workflow and analysis combination that was followed, these results must be verified. To this end, the final configuration has been analysed using XFLR5.

To start, one can list the cruise conditions, as determined by the inner iterator, utilising `aerosandbox`:

Table 6.3: Aerodynamic coefficients and cruise conditions computed using aerosandbox with vortex lattice (VLM) and lifting line (LLT) methods.

Parameter	**Mixed VLM and LLT**	**LLT Only**
Cruise C_L	0.828	0.828
Cruise C_D	0.020	0.026
Cruise C_L/C_D	42.2	31.8
Cruise α (°)	10.4	10.4
Cruise V_{TAS} (m/s)	32.7	32.7
Drag Polar C_{D_0}	0.010	0.010
Drag Polar k_1	-0.00143	-0.00130
Drag Polar k_2	0.0156	0.0246

As can be inferred from the lift-over-drag and drag polar coefficients (k_1 and k_2), the unpatched lifting line implementation in `aerosandbox` predicts significantly worse performance.

To continue with the verification procedure of the mixed method and quantify the final aerodynamic performance of the AHAPS via XFLR5, the airfoils have first been imported, as can be seen in Figure 6.9. Flapped versions of these foils are also modelled, with the maximum control deflection, for the purposes of aileron reversal analysis.

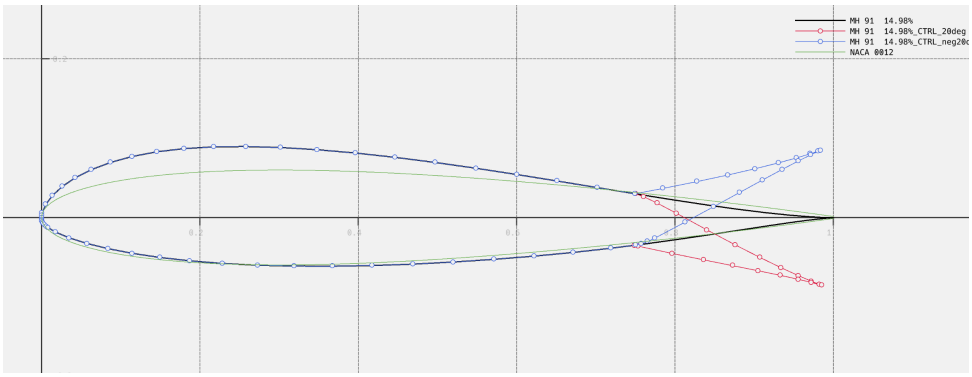

Figure 6.9: XFLR5 definition of the AHAPS airfoils, including maximum control surface deflections

Afterwards, a batch analysis of these airfoils at the expected Reynolds numbers and angles of attack is performed to provide the 3D solver with sufficient interpolation data. Finally, the plane can be defined via wing cross-sections set at various coordinates, with the required twist and dihedral angles. It is worth noting that the winglets can also be included in this definition via short wing sections with large dihedrals (in the order of 70° to 85°).

Given the AHAPS geometry and airfoil data, it is now possible to conduct an aerodynamic analysis of the aircraft. Three sets have thus been computed, corresponding to separate methods: LLT (lifting line theory), VLM1 (horseshoe vortex lattice method, including viscous corrections), and VLM2 (ring vortex lattice method, including viscous corrections). The results can then be plotted as a set of five graphs, presented in Figure 6.10 and Figure 6.11.

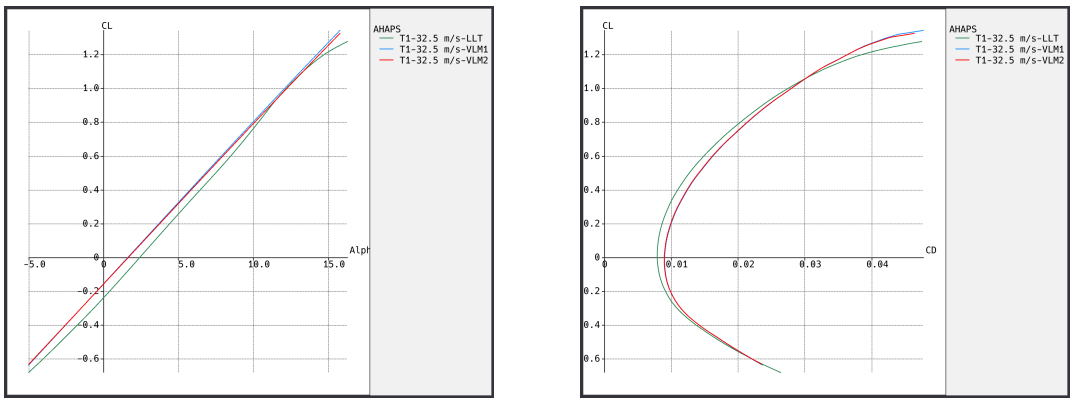

(a) AHAPS lift curve computed in XFLR5.

(b) AHAPS drag polar computed in XFLR5.

Figure 6.10: Lift and drag curves of the AHAPS computed in XFLR5.

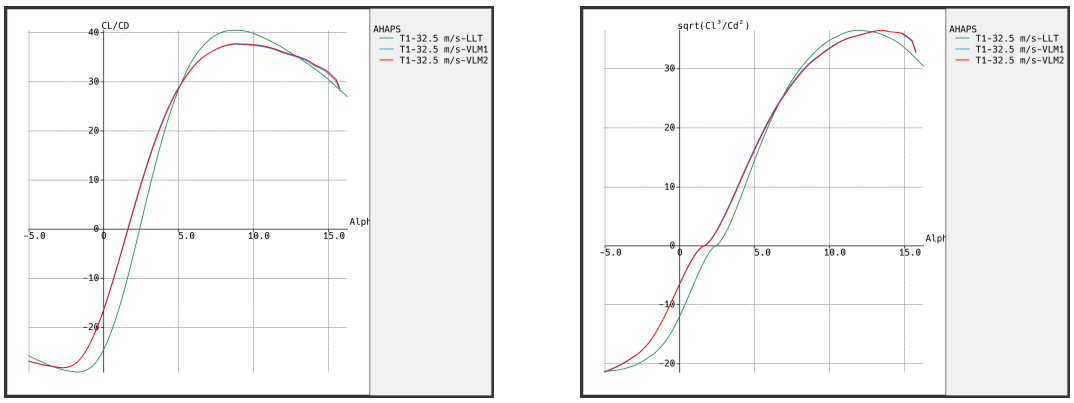

(a) AHAPS lift-over-drag curve computed in XFLR5.

(b) AHAPS endurance curve computed in XFLR5.

Figure 6.11: Lift-over-drag and endurance curves of the AHAPS computed in XFLR5.

These results support the use of the mixed model for sizing purposes, as the lift-over-drag ratio at 10 degrees angle of attack approaches 40 according to LLT, which is significantly above the 32.7 figure predicted by the default `aerosandbox` lifting line, with both VLM versions yielding around 37. Furthermore, the XFLR5 lift curves all indicate a lift coefficient of 0.82 at the cruise AoA of 10.4 degrees. Finally, the endurance graph (C_L^3/C_D^2) appears to indeed grow towards larger angles of attack, justifying the logic of the inner iterations outlined in Section 4.1.3.

It is also worth noting that the zero-lift drag is slightly lower according to the XFLR5 results, with the maximum lift coefficient being higher by around 0.2. However, these analysis methods are not reliable in stall conditions, and conservative margins should thus be considered in design, even if the AHAPS could, theoretically, fly in a slightly more efficient regime at a lower TAS. The effect of these uncertainties may be quantified via the results of the sensitivity analysis in Section 7.1, namely through the added drag parameter.

6.1.4. Deployability

One of the main performance measures is the deployability of the aircraft. The deployability tool outputs at what times the AHAPS can be launched such that it will reach cruising altitude with sufficient battery level to fly for at least 28 consecutive days at cruising level. The results are shown in Figure 6.12.

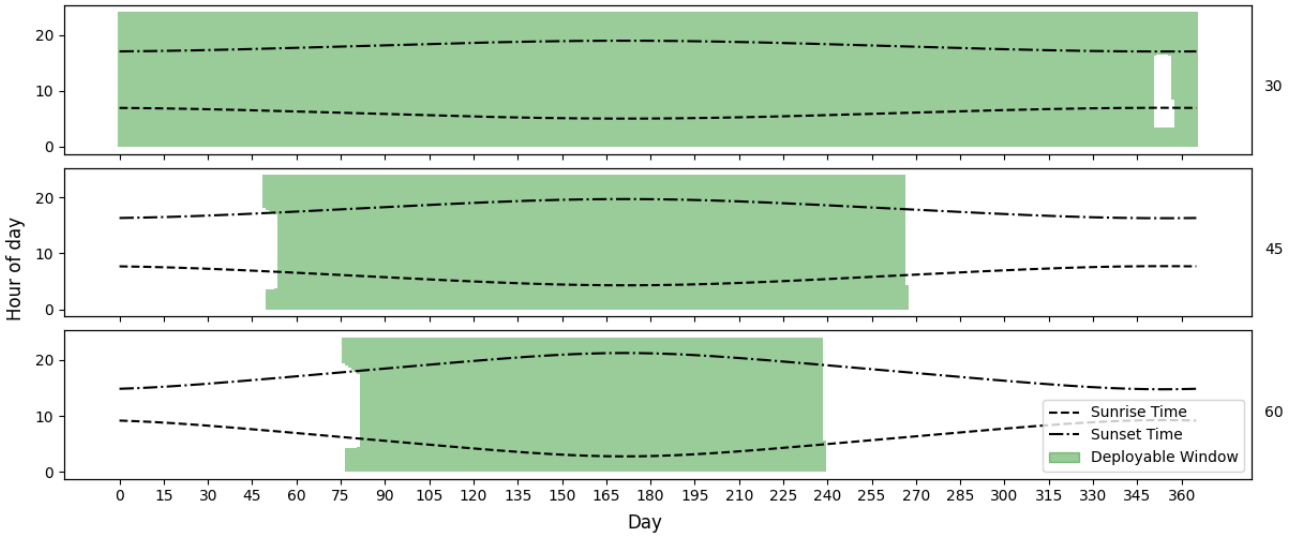

Figure 6.12: The 28-day deployability of the AHAPS concept throughout the year, at latitudes of 30°, 45° and 60° respectively. The green region indicates times within which the AHAPS can be launched and subsequently fly at cruising altitude for at least 28 consecutive days.

For shorter missions utilising a few days, the launch times ensure that at least 2 consecutive days of cruise time are shown in Figure 6.13.

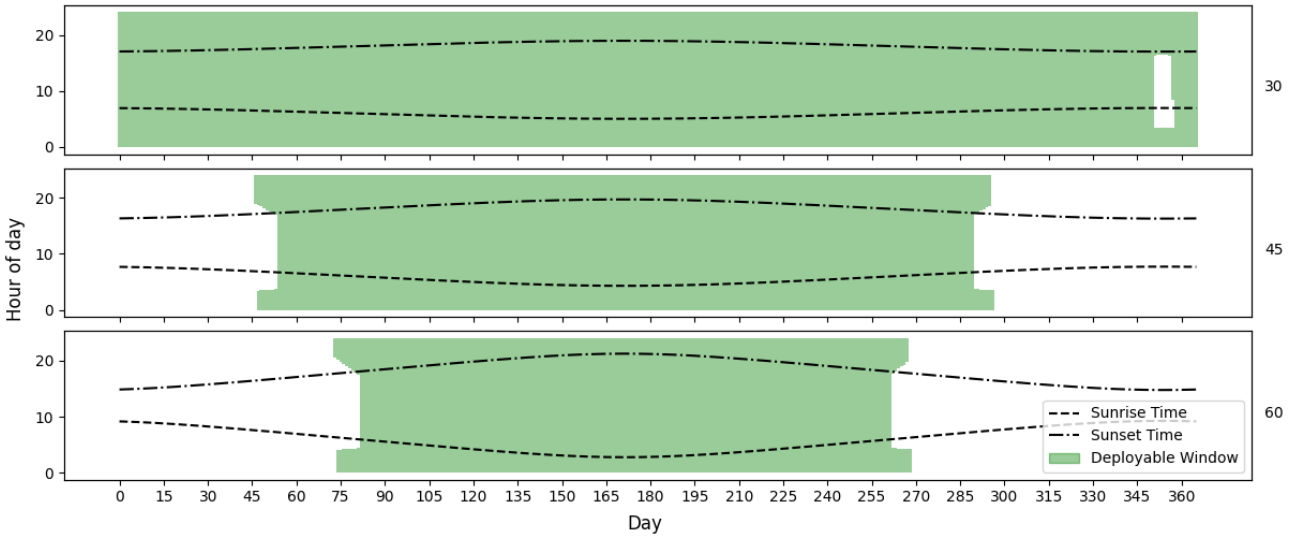

Figure 6.13: The 2-day deployability of the AHAPS concept throughout the year, at latitudes of 30°, 45° and 60° respectively. The green region indicates times within which the AHAPS can be launched and subsequently fly at cruising altitude for at least 2 consecutive days.

6.1.5. Mission Simulation

After take-off, the AHAPS will perform an en route climb to the area of interest, after which it will perform an ascending spiral until it reaches operational altitude. Figure 6.14 shows the climb profile of the AHAPS that has been computed, as described in Section 4.6.2. The total time to climb to the loitering altitude of 60,000 ft is approximately 14 hours. To determine the maximum distance the take-off location can be from the area of interest, the horizontal distance covered during the climb phase is computed. This leads to the starting point for the loitering process of the area of interest, not further than 1078 km.

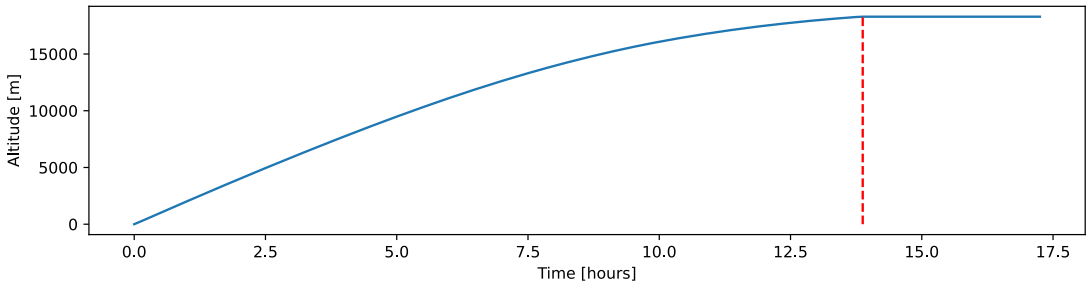

Figure 6.14: The climb profile of the AHAPS mission takes ≈ 14 hours to reach its cruise altitude of 60,000 ft.

To ensure the AHAPS can fulfill the mission according to the operator's preferences, a flight planning system is implemented [71]. This is used to generate an optimal flight path during loitering operations based on the coordinates of the service area, payload resolution requirements, aircraft turn radius, and weather conditions.

Once at operational altitude, it will initiate the first survey leg. Once it approaches the border of the service area, the aircraft will perform a 180° turn with a radius of half of the width between the legs that the flight planning system has determined. As an example, a loitering mission where the 400 x 400 km area of interest is viewed once is outlined. A loitering time of 28 days is taken in accordance with **REQ-STK-1.1**. At a cruise speed of 32.7 m/s, it will take approximately 3.4 hours per leg. This will allow a total of 196 legs with a width between the legs of 2.04 km. This loitering case is shown in more detail in Figure 6.15.

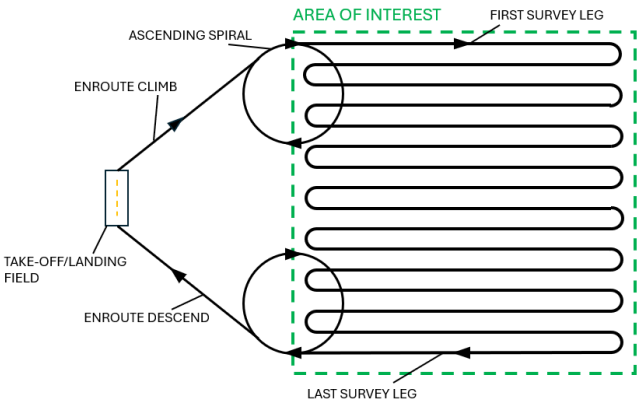

Figure 6.15: An example of a loitering simulation where the AHAPS covers the full 400 x 400 km area of interest once.

Once the area of interest has been fully covered, the aircraft will perform a descending spiral followed by a return to the landing site. The descent takes as long as the climb, which is ≈ 14 hours. After which it can perform its landing.

6.2. Operations and Logistics

Setting out the expected operations profile will identify the metrics that define the logistics efficiency for each concept. The flowchart in Figure 6.16 shows the typical profile before, during, and after a mission.

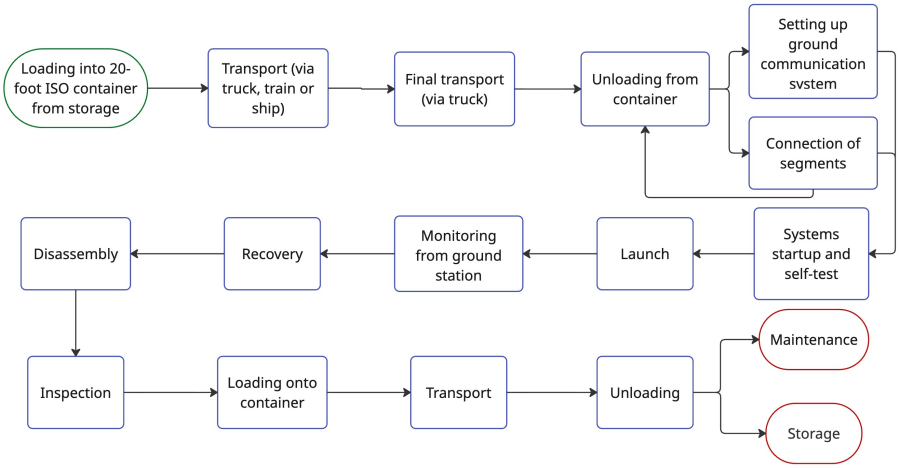

Figure 6.16: Operations & logistics flow diagram for the AHAPS system, enclosing all steps regarding operating the AHAPS in the correct manner.

Since the adaptability and modularity of this HAPS is a significant part of its competitiveness in the current market, a lot of compromises for the design were made to make sure the AHAPS keeps this competitive edge. In this section, a detailed description will be presented about the constraining segments in the operations & logistics flow and how they are met.

6.2.1. Transportation and Container Packing

For the transportation of the AHAPS, a stakeholder requirement has been stated that the AHAPS shall be transportable in a 20 ft ISO container. During the transportation, it is assumed that all the general subsystems which are mounted within the airfoil are transported within the airfoil as well, to optimise packing density. Also, it is assumed that the solar panels stay embedded in the wing surface during transport. There is one exception for the batteries, for which shipping laws state that degraded batteries have to be transported in a separate box with a maximum of 35 kg per box [72].

Based on UAV traffic model planning research, it is assumed that 20% extra volume of cushioning per package is sufficient to transport the AHAPS safely in the container [5]. Below, a list is presented with all packages that fit in the 20 ft ISO container:

- 9 wing sections (1 main root section, 6 middle sections, and 2 tip sections)
- 2 winglets
- 2 propulsion boxes (2 propulsion assemblies per box)
- 4 battery boxes
- 2 pitot tubes
- 8 wheel struts
- 8 wheel tires

Below, a visual representation is shown with all the AHAPS parts, including the required assembly and inspection tools and the ground station setup.

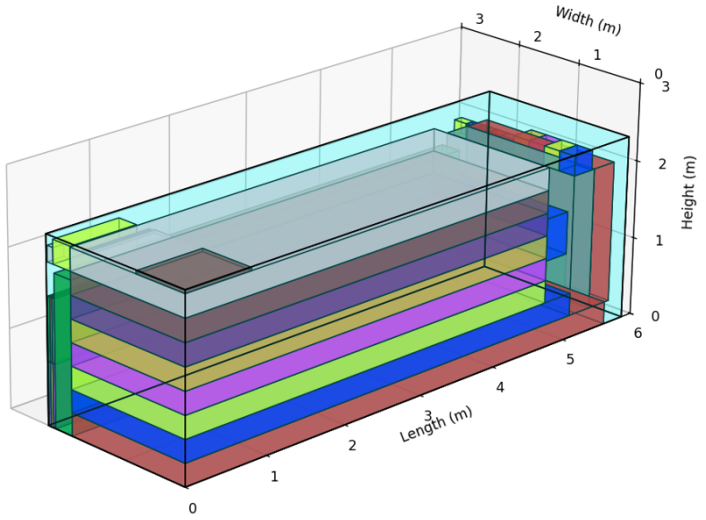

Figure 6.17: Visual representation of the inside of the 20 ft ISO container including all assembly parts and tools.

6.2.2. Ground Station Set-Up

To minimise the storage data required within the AHAPS, a small ground station setup is proposed to receive and store transmitted data from the AHAPS. This station only needs to consist of the following systems:

- Receiving antenna
- Transmitter
- Computer system
- Data storage

It is assumed that the battery cell storage of the truck transporting the 20 ft ISO container has enough energy to power the ground station once every 24 hours for at least 28 days.

6.2.3. Assembly Instructions

During the assembly itself, the most limiting constraint comes from the requirement stating the maximum limit of three in-field assemblers. According to the European labour law, an individual cannot lift anything heavier than 23 kg[1]. This means that no part can weigh any more than 46 kg such that two people can hold up one part and the third can assemble it.

Step-by-Step Procedure

Below, an ordered Step-by-Step guide is presented, feasible for an assembly team of three persons:

- **Step 1** - Put the assembly jack in the field and place the main root section securely on it, as can be seen in Figure 6.18.

[1]https://www.arboportaal.nl/onderwerpen/fysieke-belasting/tillen-en-dragen/wat-zegt-de-wet-over-tillen-en-dragen [cited 20 May 2026]

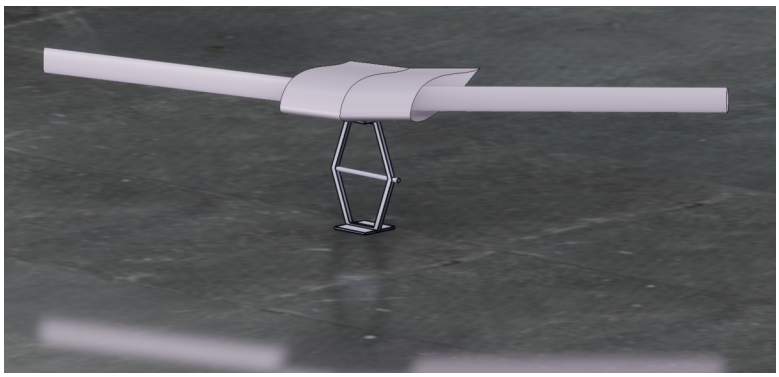

Figure 6.18: Section I of the wing on the assembly jack.

- **Step 2** - Secure all the general subsystems and payload in their dedicated positions within the main root section I.
- **Step 3** - Put the required cabling in the subsystems and guide the cables to the edges of the section I.
- **Step 4** - Lift one side of section II with two people next to the main root section around the spar, whilst the third person connects the two sections.
- **Step 5** - Apply the appropriate take-off gear under the hold-up wing section as the current assembly shown in Figure 6.19.

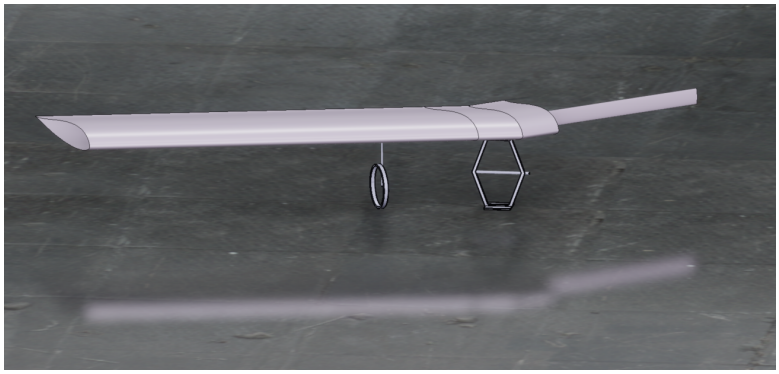

Figure 6.19: Section II of the wing connected to section I.

- **Step 6** - Mount a new spar section in section II, connecting it to the prior spar part by compressing the three clamps, such that half of the spar section sticks out again as shown in Figure 6.20.

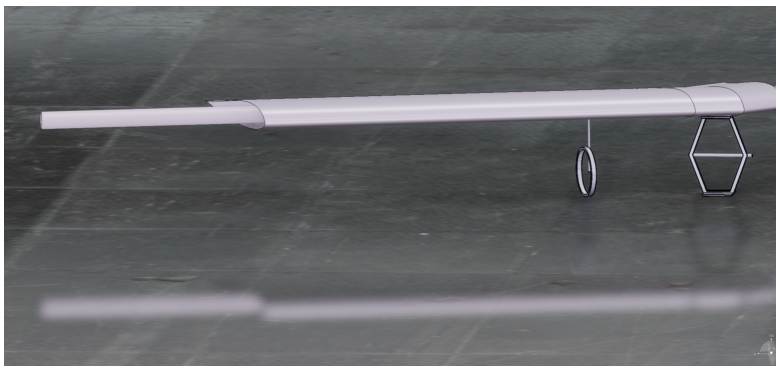

Figure 6.20: Section II of the wing the new spar section in it.

- **Step 7** - Repeat steps 4, 5, and 6 for the second part of section II in the opposite span direction as presented in Figure 6.21.

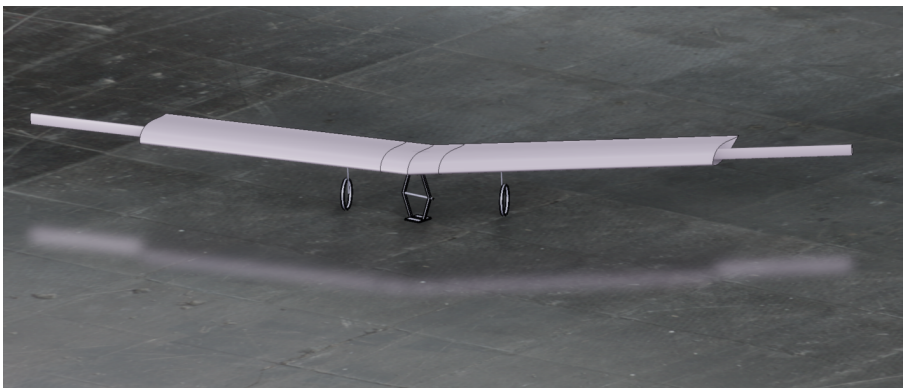

Figure 6.21: Section II repeated in the other span direction.

- **Step 8** - Assemble half of the total battery system and mount the insulating aerogel around the total package, including the heater.
- **Step 9** - Slide the finished battery assembly into wing section III and connect the appropriate cabling.
- **Step 10** - Mount a new spar section in section III, connecting it to the prior spar part by compressing the three clamps, such that half of the spar section sticks out again.
- **Step 11** - Repeat step 8, 9, and 10 for the opposite section III in the span direction.
- **Step 12** - Now, lift section IV with two people next to section III around the spar, whilst the third person connects the two sections.
- **Step 13** - Apply the according take-off gear under the hold-up wing section.
- **Step 14** - Put the required cabling through for the power, control, and propulsion systems.
- **Step 15** - Mount a new spar section in section IV, connecting it to the prior spar part by compressing the three clamps, such that half of the spar section sticks out again.
- **Step 16** - Repeat steps 12 to 15 for the assembled tip section V, including the wing tip, successively on both sides of the span direction. The current assembly should look like Figure 6.22

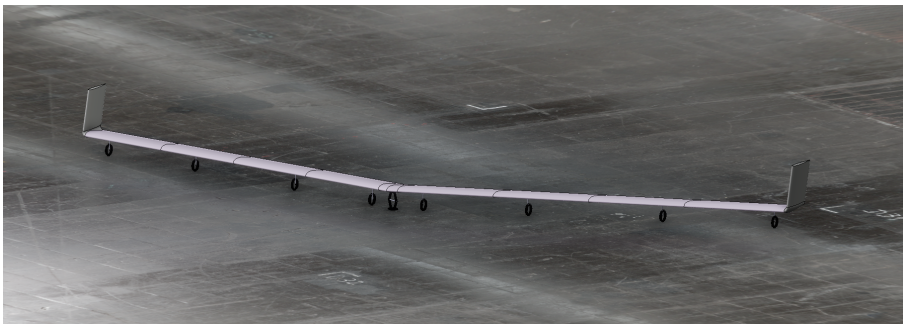

Figure 6.22: All sections connected, including the wingtips.

- **Step 17** Attach all the control systems to the appropriate cabling on both sides in the span direction.
- **Step 18** - Attach the four propulsion assemblies at their assigned positions.
- **Step 19** - Remove the assembly jack underneath the main root section. The current assembly should look like Figure 6.23

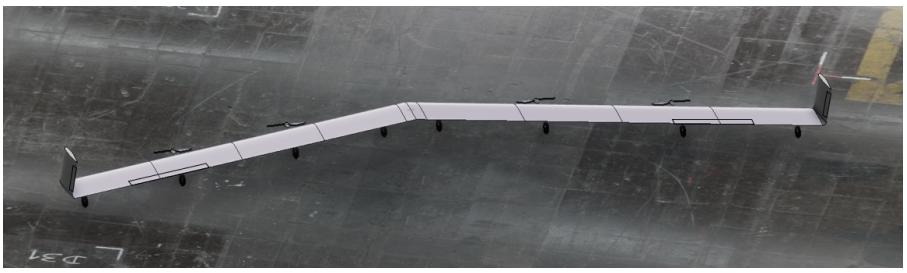

Figure 6.23: Assembly representation with assembly jack removed and added propellers.

- **Step 20** - Mount the synthetic aperture radar antenna and the two pitot tubes to section I and connect to the relevant cabling.
- **Step 21** - Confirm with the computer system that all connections are correct and working.

Assembly Tools List

Below, the tool and inspection parts list required to assemble and maintain the AHAPS in the field is presented. The tools mentioned will be put in the container that contains redundant tools to minimise the likelihood of having to import new things from the main factory.

Table 6.4: Assembly tools and inspection parts list.

Category	Item	Purpose
Assembling tool	Assembly jack (1)	Supports and holds the main root wing section securely in place during assembly.
Assembling tool	Power wrenches (2)	Quickly tighten or loosen structural bolts and fasteners during assembly.
Assembling tool	Torque wrenches (2)	Apply a precise, calibrated torque to bolted connections to meet structural specifications.
Assembling tool	Soldering kits (2)	Make or repair electrical connections between cabling and subsystems.
Inspection part	Spare mylar rolls and patches	Repair tears or damage to the wing's mylar skin covering.
Inspection part	Spare bolts	Replace lost, damaged, or corroded fasteners used throughout assembly.
Inspection tool	Heat guns (2)	Shrink and seal mylar patches onto the wing surface during repairs.
Inspection part	Adhesive products	Bond patches, panels, or components together during repair or assembly.
Inspection part	Spare clamps	Replace the clamps used to join successive spar sections together.
Inspection part	Spare insulation layers	Replace damaged thermal insulation protecting the battery assembly.
Inspection part	Spare battery cells	Replace failed or degraded cells within the battery packs.
Inspection part	Spare cabling	Replace damaged electrical cabling connecting subsystems.

Note that the spare parts are not represented in Figure 6.17, but it can be seen that there is sufficient space left for these spare parts.

6.2.4. Runway Preparations

Based on market analysis requirements, the AHAPS take-off structure and thrust required are designed to be feasible for runways labeled as bad as "Hard Desert Sand", "Hard Grass", and "Small Tarmac Runway, Poor Foundation", which allow a maximum allowable tire pressure of 280 kPa, 310 kPa and 340 kPa respectively [57]. It is expected from the infield assemblers to prepare the runway sufficiently to qualify for these

labels. This implies the removal of any significant debris and making sure the runway is being sufficiently dried to not fall in the categories "Wet, Boggy Grass" or "Soft, Loose Dessert Sand" [57]. By integrating the acceleration from Section 4.6.2, it has been determined that a take-off runway length of at least 54.6 metres after the initial push is required. As for the landing manoeuvre, it is assumed that this distance is sufficient for the skids to bring the AHAPS to a full stop as well.

6.2.5. Communication Flow Diagram

The communication between the different systems that perform the mission follows a certain structure. The ground station sends commands to the AHAPS about the intended path and payload operation. This information is also communicated with Air Traffic Control (ATC) to allow for airspace management. When the path given to the AHAPS is not deemed feasible by ATC, for example when the AHAPS interferes with other aircraft if it follows the instructions, these instructions can be overridden. When this occurs, the ground station is informed so the mission can be adapted if necessary. Additionally, the AHAPS communicates with other aircraft in its proximity in order to avoid dangerous situations or even collisions. The interplay between these systems ensures the AHAPS performs its mission as intended, without compromising the aerial safety. The structure is visualised in Figure 6.24.

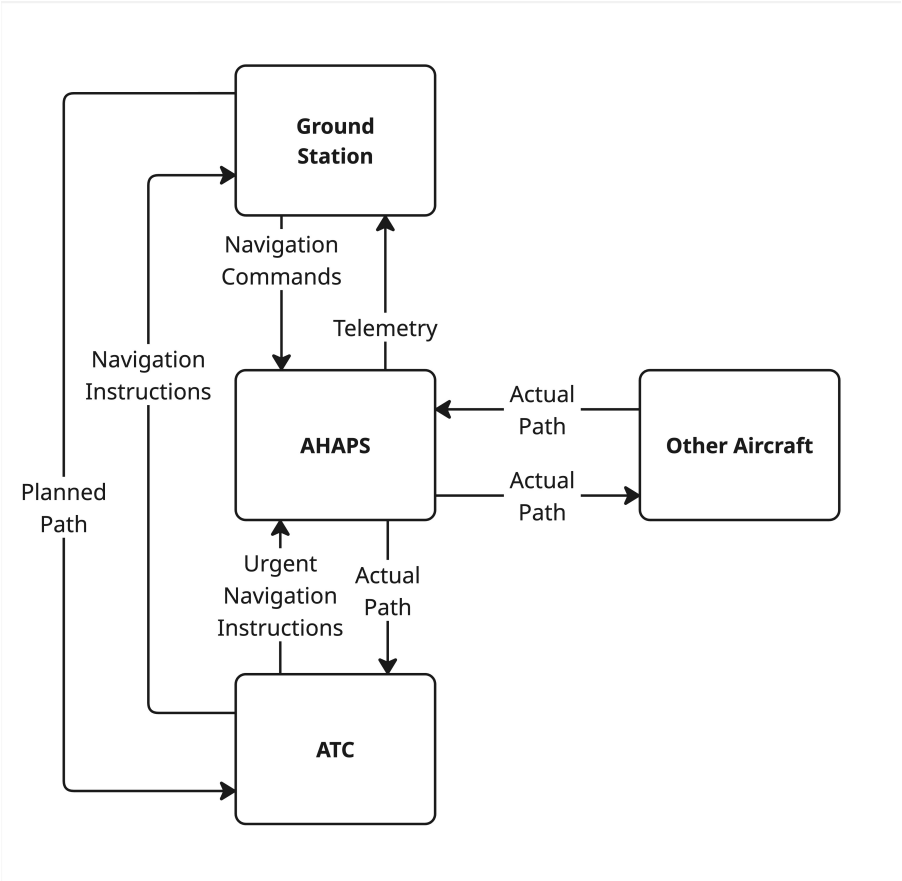

Figure 6.24: Flow diagram of the communication between the main systems performing the mission.

7. Design Robustness

In order to ensure that the design of the AHAPS is suitable for long-term operations, it is important to investigate the robustness of the design. This means that the design is strong enough to survive potential risks and hazards over time. A quantitative sensitivity analysis is done in Section 7.1. Following this, a technical risk assessment is performed in Section 7.2. Building on the technical risk analysis, the reliability, along with availability, maintainability, and safety, are evaluated in Section 7.3. Lastly, the verification and validation of the system, including the compliance matrix, is in Section 7.4.

7.1. Sensitivity Analysis

This section outlines the sensitivity analysis process of the AHAPS design. It quantifies the increments in several monitoring variables based on changes in likely input parameters, including added mass, power, drag, and modified efficiency values or design choices. It starts by describing possible changes to the design in Section 7.1.1 together with the parameter variation procedures. Afterwards, expected impacts are listed in Section 7.1.2. Finally, the actual observed increments are presented and interpreted in Section 7.1.3.

7.1.1. Potential Design Changes

In terms of probable changes to the detailed design concept, one may refer to uncertainties and errors incurred within the sizing process or to literature-sourced parameters that may still be subject to change. Regarding the former, subsequent detailed design of some subsystems may mandate an increase or decrease in their respective masses and required powers. In the case of the latter, it may pertain to values such as the aspect ratio, taper, and electrical component efficiencies. These are based on the availability of off-the-shelf parts.

Such alterations would generally be reflected in modifications to the mass and geometric footprints of the AHAPS, by virtue of larger required batteries, solar arrays, or structural elements. As has been observed during the design process and illustrated in Section 6.2.1, the most immediately restrictive requirement of the design in this regard is that it must be able to be transported entirely within a 20 ft ISO container. Therefore, it is of interest to quantify the sensitivity of the design's MTOW, wing surface area, and wing span to changes in several input parameters.

First, uncertainties and over- or under-estimations have been quantified by a set of parasitic mass, power, and drag parameters. Second, important performance metrics of off-the-shelf components have been considered, namely the battery energy density and the solar panel efficiency, as these have been observed via repeated runs of the iterator in Section 4.1.3 to be of significance when concerning convergence. Finally, several of the aforementioned design choices and considerations have been included in this sensitivity analysis to ensure their validity: aspect ratio, twist angle, and ultimate load factor.

To obtain variations in the aforementioned monitored values, all parameters have been sequentially varied by 2.5% and fed into the main sizing optimiser, as per Section 4.1.3. Said variation has been applied in both the positive and negative directions and taken as a percentage of each parameter's current value. The only exceptions to this rule are the parasitic mass, power, and drag inputs, where the default values of the MTOW, cruise required power, and parasitic drag, respectively, have been considered for the 2.5% increment instead.

7.1.2. Expected Impact

Throughout the sizing process, it has been observed that the AHAPS final parameters are particularly sensitive to additional mass increments, as well as to battery energy density parameters. This is to be expected, since total mass is linked directly to required thrust, and thus power, which mandates both a certain battery mass and a minimum solar panel area. The power system comprises more than half of the AHAPS' total mass. As such, any additional requirements for its performance metrics are expected to lead to particularly noticeable jumps in geometric and mass footprint.

Furthermore, additional electrical power has been observed to cause similar effects, though to a lesser de-

gree, a fact that may be caused by the total power requirement being dominated by the cruise propulsive power instead of other subsystems (as can be seen in Table 5.2, in the order of 85%). Solar panel efficiency, too, is expected to be less significant, as the all-season requirement imposed on the sizing procedure has generally been reflected more through increased battery mass, rather than solar panel area. That is, repeated runs of the optimiser have shown that power generation throughout the shortened days restricts the design space less than energy storage for the longer nights.

Finally, regarding design choices, the impact is foreseen to be dependent on how close to local optimum points the current values are. The aspect ratio, in particular, has been observed to be relatively close to said optimum, as increments by 1.0 in either direction seem to increase both MTOW and span. This would agree with Ma and Elham, as lower aspect ratios are known to decrease aerodynamic efficiency, while higher ones can significantly increase the structural mass of the aircraft [73]. The effect of the load factor may also potentially be lessened, especially in the negative direction. This is due to the fact that the structural optimisation code has strictly imposed geometric bounds, and will thus not attempt to reduce the structural size below manufacturable limits.

7.1.3. Observed Impact

Following the procedure outlined earlier in Section 7.1.1, the aforementioned increments in the monitored parameters have been obtained for every input change and compiled in Table 7.1.

Table 7.1: Sensitivity analysis of the total mass, wing surface area, total span, and total power consumption of the AHAPS design to changes in design variables.

Parameter	−2.5%				+2.5%			
	ΔMTOW (kg)	ΔS [m^2]	Δb (m)	ΔP_r (W)	ΔMTOW (kg)	ΔS [m^2]	Δb (m)	ΔP_r (W)
m_{extra}	−22.23	−3.85	−1.13	−229.23	+22.00	+3.79	+1.08	+225.63
P_{extra}	−10.26	−2.84	−0.83	−166.6	+10.29	+2.86	+0.82	+167.09
C_{D_0}	−4.60	−1.26	−0.36	−74.74	+4.60	+1.26	+0.36	+74.74
A	+2.80	+0.85	−0.20	+50.21	−1.57	−0.61	+0.25	−36.16
n	−1.67	−0.29	−0.08	−17.22	+2.69	+0.46	+0.13	+27.67
$\rho_{E_{bat}}$	+9.45	+1.63	+0.47	+97.14	−8.58	−1.48	−0.43	−88.40
η_{solar}	+1.68	+1.31	+0.38	−15.02	−1.11	−1.22	−0.35	+15.90
δ_{twist}	+0.07	+0.01	+0.00	+0.81	−0.12	−0.03	−0.01	−1.85

The largest impact, as predicted, has been encountered in the event of parasitic mass changes: a maximum of 6.97% increment to the MTOW for every 2.5% mass added with respect to the current MTOW. Values were computed via division, considering the maximum 22.23 kg increment observed in Table 7.1. Similar results include a 6.12% increment to the surface area, 3.19% to the span, and 6.12% to the total required cruise power.

The other input parameters generally result in significantly lower effects on the monitored values and align with the expectations set in Section 7.1.2. Added power is indeed the second most impactful, presenting roughly half to two-thirds of the values characteristic of parasitic mass, depending on the monitored metric.

The aspect ratio sensitivity, too, appears relatively low in comparison and seems to decrease the mass, surface area, and required power for larger values. However, the effect on span is positive and would thus interfere with the 20 ft ISO container requirement. As such, the current value of 20 has been deemed appropriate.

The sensitivities to load factor and twist angle are the lowest, bound by 0.84% to MTOW,0.73% to area, 0.37% to span, and 0.74% to required power. Therefore, the design is not at risk of being deemed unfeasible by changes in these metrics. In particular, the in-flight twist deflection is not mission-threatening.

Finally, the sensitivity to battery energy density is several times higher than solar panel efficiency. As such, it can be concluded that advances in battery technology may benefit the design of the AHAPS more than solar arrays, and should thus be prioritised in terms of off-the-shelf component acquisition.

7.2. Technical Risk Assessment

In this section, the technical risks of the AHAPS will be addressed. Technical risks have to be identified, assessed, and, if necessary, mitigated to increase the probability of success. This section presents this process, starting with a discussion about the contingency management in Section 7.2.1. The design risks are identified and assessed in Section 7.2.2. All risk maps are shown in Section 7.2.3, as well as the mitigation strategies for the risks that require mitigation.

7.2.1. Contingency Management

Contingencies are a quantitative way to keep track of the design maturity. Throughout the design process, the specific design characteristics and specifications become clear and with that the contingency reduces. An overview of the contingency values per subsystem is shown in Table 7.2. The design presented in the current report is a detailed design, but it is not yet finished. Therefore, some contingency still exists for the subsystems airframe, power, propulsion, control, thermal management, and undercarriage. The subsystems' payload, flight condition, computer, and communication are finished. This is due to the fact that these consist primarily of commercial off-the-shelf components, of which the exact characteristics are known.

Table 7.2: Overview of contingency percentages per subsystem and design stage. The current design stage is detailed design.

	Contingency (%)									
Design Maturity	**Payload**	**Flight Condition**	**Computer**	**Communication**	**Airframe**	**Power**	**Propulsion**	**Control**	**Temp. Management**	**Undercarriage**
Conceptual Design	30	30	30	30	30	30	30	30	30	30
Preliminary Design	25	25	20	25	25	25	20	20	20	25
Detailed Design	0	0	0	0	15	20	10	10	10	10
Final Design	0	0	0	0	8	8	8	5	5	5
End of Design	0	0	0	0	0	0	0	0	0	0

7.2.2. Design Risks

During detailed design, even more risks were identified compared to the risks already known during earlier stages of the project. The risks are identified per function the AHAPS has to perform and subsequently linked to the relevant subsystem that is responsible for fulfilling that function. Also an external factor is taken into account. This also regards mission systems such as the ground station. As a result, a clearly structured risk table is shown in Table 7.3.

Table 7.3: Overview of all the identified technical risks.

Subsystem	**Risk ID**	**Risk Description**	**Subsystem**	**Risk ID**	**Risk Description**
Communicate			***Take-off***		
Comms	TR-COM-01	Antenna Failure	Propulsion	TR-TAO-01	One Engine Inoperative
Computer	TR-COM-02	Wiring Failure	Computer	TR-TAO-02	Wiring Failure
Computer	TR-COM-03	Data Saving Failure	Control	TR-TAO-03	Controllability Loss
Computer	TR-COM-04	Data Processing Failure	Power	TR-TAO-04	Power Outage
Power	TR-COM-05	Power Outage	Power	TR-TAO-05	Energy Storage Failure
Power	TR-COM-06	Energy Storage Failure	Flight Condition	TR-TAO-06	Sensor Failure

Continued on next page

Table 7.3 continued from previous page

Subsystem	Risk ID	Risk Description	Subsystem	Risk ID	Risk Description
Computer	TR-COM-07	Computer Failure	Computer	TR-TAO-07	Computer Failure
External	TR-COM-08	Third-Party Interference	External	TR-TAO-08	Third-Party Interference
Thermal Management	TR-COM-09	Temperature Failure	Thermal Management	TR-TAO-09	Temperature Failure
Airframe	TR-COM-10	Structure Fracture	Airframe	TR-TAO-10	Structure Fracture
Airframe	TR-COM-11	Weather Condition Impact	Airframe	TR-TAO-11	Weather Condition Impact
Airframe	TR-COM-12	Minor Environment Impact	Airframe	TR-TAO-12	Minor Environment Impact
Airframe	TR-COM-13	Major Environment Impact	Airframe	TR-TAO-13	Major Environment Impact
External	TR-COM-14	Ground Station Failure	Undercarriage	TR-TAO-14	Landing Gear Failure
Comms	TR-COM-15	No Line of Sight	External	TR-TAO-15	Ground Station Failure
			Undercarriage	TR-TAO-16	Runway Failure
			Undercarriage	TR-TAO-17	Wheel Locks
			Thermal Management	TR-TAO-18	Overcooling
			Thermal Management	TR-TAO-19	Overheating
			Payload	TR-TAO-20	Payload not secured
			Payload	TR-TAO-21	No power connection to payload
			Payload	TR-TAO-22	No data connection to payload
Climb			***Cruise***		
Propulsion	TR-CLB-01	One Engine Inoperative	Propulsion	TR-CRS-01	One Engine Inoperative
Computer	TR-CLB-02	Wiring Failure	Computer	TR-CRS-02	Wiring Failure
Control	TR-CLB-03	Controllability Loss	Control	TR-CRS-03	Controllability Loss
Power	TR-CLB-04	Power Outage	Power	TR-CRS-04	Power Outage
Power	TR-CLB-05	Energy Storage Failure	Power	TR-CRS-05	Energy Storage Failure
Flight Condition	TR-CLB-06	Sensor Failure	Flight Condition	TR-CRS-06	Sensor Failure
Computer	TR-CLB-07	Computer Failure	Computer	TR-CRS-07	Computer Failure
External	TR-CLB-08	Third-Party Interference	External	TR-CRS-08	Third-Party Interference
Thermal Management	TR-CLB-09	Temperature Failure	Thermal Management	TR-CRS-09	Temperature Failure
Airframe	TR-CLB-10	Structure Fracture	Airframe	TR-CRS-10	Structure Fracture
Airframe	TR-CLB-11	Weather Condition Impact	Airframe	TR-CRS-11	Weather Condition Impact
Airframe	TR-CLB-12	Minor Environment Impact	Airframe	TR-CRS-12	Minor Environment Impact
Airframe	TR-CLB-13	Major Environment Impact	Airframe	TR-CRS-13	Major Environment Impact
Undercarriage	TR-CLB-14	Take-off Gear Failure	Undercarriage	TR-CRS-14	Landing Gear Failure
External	TR-CLB-15	Ground Station Failure	External	TR-CRS-15	Ground Station Failure
Undercarriage	TR-CLB-16	Take-off structure does not disconnect	Thermal Management	TR-CRS-16	Overcooling
Thermal Management	TR-CLB-17	Overcooling	Thermal Management	TR-CRS-17	Overheating
Thermal Management	TR-CLB-18	Overheating	Payload	TR-CRS-18	Payload not secured
Payload	TR-CLB-19	Payload not secured	Payload	TR-CRS-19	No power connection to payload
Payload	TR-CLB-20	No power connection to payload	Payload	TR-CRS-20	No data connection to payload
Payload	TR-CLB-21	No data connection to payload			
Descend			***Land***		
Propulsion	TR-DES-01	One Engine Inoperative	Propulsion	TR-LAN-01	One Engine Inoperative
Computer	TR-DES-02	Wiring Failure	Computer	TR-LAN-02	Wiring Failure
Control	TR-DES-03	Controllability Loss	Control	TR-LAN-03	Controllability Loss
Power	TR-DES-04	Power Outage	Power	TR-LAN-04	Power Outage
Power	TR-DES-05	Energy Storage Failure	Power	TR-LAN-05	Energy Storage Failure
Flight Condition	TR-DES-06	Sensor Failure	Flight Condition	TR-LAN-06	Sensor Failure

Continued on next page

Table 7.3 continued from previous page

Subsystem	Risk ID	Risk Description	Subsystem	Risk ID	Risk Description
Computer	TR-DES-07	Computer Failure	Computer	TR-LAN-07	Computer Failure
External	TR-DES-08	Third-Party Interference	External	TR-LAN-08	Third-Party Interference
Thermal Management	TR-DES-09	Temperature Failure	Thermal Management	TR-LAN-09	Temperature Failure
Airframe	TR-DES-10	Structure Fracture	Airframe	TR-LAN-10	Structure Fracture
Airframe	TR-DES-11	Weather Condition Impact	Airframe	TR-LAN-11	Weather Condition Impact
Airframe	TR-DES-12	Minor Environment Impact	Airframe	TR-LAN-12	Minor Environment Impact
Airframe	TR-DES-13	Major Environment Impact	Airframe	TR-LAN-13	Major Environment Impact
Undercarriage	TR-DES-14	Landing Gear Failure	Undercarriage	TR-LAN-14	Landing Gear Failure
External	TR-DES-15	Ground Station Failure	External	TR-LAN-15	Ground Station Failure
Thermal Management	TR-DES-16	Overcooling	Undercarriage	TR-LAN-16	Runway Failure
Thermal Management	TR-DES-17	Overheating	Undercarriage	TR-LAN-17	Skid Locks
Payload	TR-DES-18	Payload not secured	Thermal Management	TR-LAN-18	Overcooling
Payload	TR-DES-19	No power connection to payload	Thermal Management	TR-LAN-19	Overheating
Payload	TR-DES-20	No data connection to payload	Payload	TR-LAN-20	Payload not secured
Undercarriage	TR-DES-21	Skids do not deploy	Payload	TR-LAN-21	No power connection to payload
			Payload	TR-LAN-22	No data connection to payload

7.2.3. Risk Mitigation

The risk score is determined by multiplying the likelihood by the consequence level, following Table 7.4. The risk scores pre-mitigation for all risks are visualised in the left-hand side of Table 7.5, Table 7.6, Table 7.7, Table 7.8, Table 7.9 and Table 7.10. Mitigation is necessary for some risks, namely the ones that have a risk score higher than nine, as scores at or above this threshold represent an unacceptable combination of likelihood and consequence per the team's risk acceptance criteria. In the tables, these are the risks located in the top left area.

Table 7.4: Consequence and likelihood level definitions.

Consequence Level	Description	Failure Consequence	Likelihood Level	Description	Failure Probability
1	Negligible	$C \leq 0.3$	1	Very unlikely	$P \leq 0.01$
2	Marginal	$0.3 < C \leq 0.6$	2	Unlikely	$0.01 < P \leq 0.3$
3	Critical	$0.6 < C \leq 0.8$	3	Moderate	$0.3 < P \leq 0.5$
4	Catastrophic	$C > 0.8$	4	Likely	$0.5 < P \leq 0.7$
			5	Very likely	$P > 0.7$

Table 7.5: Risk maps pre and post mitigation for the communicate function.

Pre Mitigation	Catastrophic	Critical	Marginal	Negligible
Very Likely				
Likely				
Moderate	TR-COM-02	TR-COM-01		
Unlikely	TR-COM-05, TR-COM-06, TR-COM-07, TR-COM-09, TR-COM-14	TR-COM-03, TR-COM-04		TR-COM-12
Very Unlikely	TR-COM-13	TR-COM-11, TR-COM-15	TR-COM-08, TR-COM-10	

Post Mitigation	Catastrophic	Critical	Marginal	Negligible
Very Likely				
Likely				
Moderate			TR-COM-02	
Unlikely	TR-COM-05, TR-COM-06, TR-COM-07, TR-COM-09, TR-COM-14	TR-COM-03, TR-COM-04		TR-COM-12
Very Unlikely	TR-COM-13	TR-COM-01, TR-COM-11, TR-COM-15	TR-COM-08, TR-COM-10	

Table 7.6: Risk maps pre and post mitigation for the take-off function.

Pre Mitigation	Catastrophic	Critical	Marginal	Negligible		*Post Mitigation*	Catastrophic	Critical	Marginal	Negligible
Very Likely				TR-TAO-12		**Very Likely**				TR-TAO-12
Likely						**Likely**				
Moderate						**Moderate**				
Unlikely	TR-TAO-13	TR-TAO-16				**Unlikely**	TR-TAO-13	TR-TAO-16		
Very Unlikely	TR-TAO-04, TR-TAO-05, TR-TAO-07, TR-TAO-10, TR-TAO-11, TR-TAO-14, TR-TAO-17, TR-TAO-20	TR-TAO-01, TR-TAO-02, TR-TAO-03, TR-TAO-08, TR-TAO-09, TR-TAO-18, TR-TAO-19	TR-TAO-06, TR-TAO-15	TR-TAO-21, TR-TAO-22		**Very Unlikely**	TR-TAO-04, TR-TAO-05, TR-TAO-10, TR-TAO-11, TR-TAO-14, TR-TAO-17, TR-TAO-20	TR-TAO-01, TR-TAO-02, TR-TAO-03, TR-TAO-07, TR-TAO-08, TR-TAO-09, TR-TAO-18, TR-TAO-19	TR-TAO-06, TR-TAO-15	TR-TAO-21, TR-TAO-22

Table 7.7: Risk maps pre and post mitigation for the climb function.

Pre Mitigation	Catastrophic	Critical	Marginal	Negligible		*Post Mitigation*	Catastrophic	Critical	Marginal	Negligible
Very Likely						**Very Likely**				
Likely						**Likely**				
Moderate		TR-CLB-11				**Moderate**			TR-CLB-11	
Unlikely	TR-CLB-10, TR-CLB-13	TR-CLB-06	TR-CLB-17			**Unlikely**	TR-CLB-10, TR-CLB-13		TR-CLB-17	
Very Unlikely	TR-CLB-01, TR-CLB-02, TR-CLB-03, TR-CLB-04, TR-CLB-05, TR-CLB-07, TR-CLB-09, TR-CLB-19	TR-CLB-08, TR-CLB-16	TR-CLB-14, TR-CLB-15, TR-CLB-18, TR-CLB-20, TR-CLB-21	TR-CLB-12		**Very Unlikely**	TR-CLB-01, TR-CLB-02, TR-CLB-03, TR-CLB-04, TR-CLB-05, TR-CLB-07, TR-CLB-09, TR-CLB-19	TR-CLB-06, TR-CLB-08, TR-CLB-16	TR-CLB-14, TR-CLB-15, TR-CLB-18, TR-CLB-20, TR-CLB-21	TR-CLB-12

Table 7.8: Risk maps pre and post mitigation for the cruise function.

Pre Mitigation	Catastrophic	Critical	Marginal	Negligible		*Post Mitigation*	Catastrophic	Critical	Marginal	Negligible
Very Likely						**Very Likely**				
Likely		TR-CRS-16				**Likely**				
Moderate	TR-CRS-02, TR-CRS-04, TR-CRS-06	TR-CRS-01				**Moderate**			TR-CRS-02	
Unlikely	TR-CRS-09					**Unlikely**	TR-CRS-09		TR-CRS-01	
Very Unlikely	TR-CRS-03, TR-CRS-10, TR-CRS-12, TR-CRS-18, TR-CRS-19, TR-CRS-20	TR-CRS-07, TR-CRS-15, TR-CRS-17	TR-CRS-05, TR-CRS-08, TR-CRS-14	TR-CRS-11, TR-CRS-13		**Very Unlikely**	TR-CRS-03, TR-CRS-04, TR-CRS-10, TR-CRS-12, TR-CRS-18, TR-CRS-19, TR-CRS-20	TR-CRS-06, TR-CRS-07, TR-CRS-15, TR-CRS-16, TR-CRS-17	TR-CRS-05, TR-CRS-08, TR-CRS-14	TR-CRS-11, TR-CRS-13

Table 7.9: Risk maps pre and post mitigation for the descend function.

Pre Mitigation	Catastrophic	Critical	Marginal	Negligible		*Post Mitigation*	Catastrophic	Critical	Marginal	Negligible
Very Likely						**Very Likely**				
Likely						**Likely**				
Moderate		TR-DES-11		TR-DES-14		**Moderate**			TR-DES-11	TR-DES-14
Unlikely	TR-DES-03, TR-DES-04, TR-DES-13	TR-DES-06	TR-DES-02, TR-DES-16			**Unlikely**	TR-DES-03, TR-DES-04, TR-DES-13	TR-DES-16	TR-DES-02	
Very Unlikely	TR-DES-05, TR-DES-07, TR-DES-15, TR-DES-18	TR-DES-08, TR-DES-09, TR-DES-21	TR-DES-01, TR-DES-17	TR-DES-10, TR-DES-12, TR-DES-19, TR-DES-20		**Very Unlikely**	TR-DES-05, TR-DES-07, TR-DES-15, TR-DES-18	TR-DES-06, TR-DES-08, TR-DES-09, TR-DES-21	TR-DES-01, TR-DES-17	TR-DES-10, TR-DES-12, TR-DES-19, TR-DES-20

Table 7.10: Risk maps pre and post mitigation for the land function.

Pre Mitigation	Catastrophic	Critical	Marginal	Negligible		*Post Mitigation*	Catastrophic	Critical	Marginal	Negligible
Very Likely				TR-LAN-12		**Very Likely**				TR-LAN-12
Likely		TR-LAN-11				**Likely**			TR-LAN-11	
Moderate						**Moderate**				
Unlikely	TR-LAN-03, TR-LAN-13, TR-LAN-14, TR-LAN-16	TR-LAN-10	TR-LAN-02			**Unlikely**	TR-LAN-03, TR-LAN-13, TR-LAN-14, TR-LAN-16	TR-LAN-10	TR-LAN-02	
Very Unlikely	TR-LAN-04, TR-LAN-05, TR-LAN-07, TR-LAN-20	TR-LAN-08, TR-LAN-09	TR-LAN-01, TR-LAN-06, TR-LAN-17	TR-LAN-15, TR-LAN-18, TR-LAN-19, TR-LAN-21, TR-LAN-22		**Very Unlikely**	TR-LAN-04, TR-LAN-05, TR-LAN-07, TR-LAN-20	TR-LAN-08, TR-LAN-09	TR-LAN-01, TR-LAN-06, TR-LAN-17	TR-LAN-15, TR-LAN-18, TR-LAN-19, TR-LAN-21, TR-LAN-22

For the risks that require mitigation, the strategies are summarised in Table 7.11. The responsibility for the mitigation is assigned to the department under which the subsystem falls. It can be seen that, despite the defined threshold of the risk score to require mitigation, two risks appear in the table that have a risk score lower than the threshold, namely TR-CLB-06 and TR-DES-06. This has to do with TR-CRS-06, which requires mitigation due to its risk score. The mitigation involves adding redundant sensors, which has a mitigating effect on the risk during climb and descend as well. These two extra risks do therefore still appear in the table.

Table 7.11: Mitigation strategies and resulting risk-level changes.

ID	Mitigation Strategy	Change (L×C)
TR-COM-01	Increase antenna robustness	(3×3)=9 → (1×3)=3
TR-COM-02	Redundant wiring	(3×4)=12 → (3×2)=6
TR-CLB-06	Redundant sensors	(2×3)=6 → (1×3)=3
TR-CLB-11	Design for higher temperature tolerances	(3×3)=9 → (3×2)=6
TR-CRS-01	Choose/design reliable motors and implement control margin	(3×3)=9 → (2×2)=4
TR-CRS-02	Redundant wiring	(3×4)=12 → (3×2)=6
TR-CRS-04	Implement redundancy	(3×4)=12 → (1×4)=4
TR-CRS-06	Redundant sensors	(3×4)=12 → (1×3)=3
TR-CRS-16	Implement heating system	(4×3)=12 → (1×3)=3
TR-DES-06	Redundant sensors	(2×3)=6 → (1×3)=3
TR-DES-11	Design for higher temperature tolerances	(3×3)=9 → (3×2)=6
TR-LAN-11	Design for higher temperature tolerances	(4×3)=12 → (4×2)=8

The resulting risk maps, after the mitigation has been performed, are shown in the right-hand side of Table 7.5, Table 7.6, Table 7.7, Table 7.8, Table 7.9 and Table 7.10.

7.2.4. Mean Time Between Failure

In order to perform a quantified RAMS analysis in Section 7.3, a mean time between failure (MTBF) needs to be found for each subsystem. This is done based on the likelihood score of each risk linked to the certain subsystem. First the consequence of a specific risk is checked. If the risk is above a consequence level of 2, it is deemed mission ending. This corresponds to a failure, then based on its probability or its likelihood its MTBF is calculated using Equation 7.1 and Equation 7.2.

$$MTBF = \frac{t_{mission}}{-ln(\mathscr{R})} \tag{7.1}$$

$$\mathscr{R} = 1 - \mathscr{L} \tag{7.2}$$

Applying this for both pre-mitigation and post-mitigation results in the table shown in Table 7.12. This takes into account zero maintenance and thus represents continuous use.

Table 7.12: Subsystem MTBF before and after mitigation.

Subsystem	Pre-mitigation MTBF (hrs)	Post-mitigation MTBF (hrs)
Payload	134060	134060
Flight Condition System	1320	134060
Computer	1320	4130
Communication	1320	134060
Airframe	730	4130
Power	1320	4130
Propulsion	1320	134060
Control	4130	4130
Temperature Management	4130	4130
Undercarriage	4130	4130
External	4130	4130

7.3. Reliability, Availability, Maintainability, and Safety Assessment

A RAMS analysis, short for reliability, availability, maintainability, and safety, assesses the potential that the design has when it goes into operation. It tests core aspects of the design in a global way, and determines whether the design is robust enough to survive in the long term. The four aspects of this analysis will be assessed sequentially, starting with the reliability in Section 7.3.1, then the availability in Section 7.3.3, following this with the maintainability in Section 7.3.2 and ending with the safety in Section 7.3.4.

Table 7.13: Assumption made for the reliability analysis.

Assumption ID	Category	Assumption	Justification
ASP-RLB-1	Reliability	It is assumed that the inclusion of regular maintenance checks increase the mean time between failures (MTBF) with 10.	Maintenance increases the MTBF significantly and this will give an accurate estimation for the AHAPS[a].

[a] https://mapex.io/en/news/mtbf-what-it-is-and-how-to-improve-it/ [cited 17 June 2026]

7.3.1. Reliability

The reliability assesses the AHAPS on its potential for failure and the severity of its consequences. It assesses which potential points of failure are present in the design and whether this impacts the rest of the design in its operations. In Figure 7.1, the connections between the importance of different subsystems can be seen. This shows which subsystems have a backup system, such that if one fails, not the whole system fails. Furthermore, the goal of completing the mission and the goal of ensuring safe flight can be distinguished. As can be seen, all subsystems contribute to the mission, while the aircraft can still be recovered without the payload system or the communication system. All blocks in series play a key role in the functioning of the system, while the blocks in parallel do not immediately terminate the system as long as there is still one functional. Note that the order of the blocks inside each frame is not essential for the function of the block diagram.

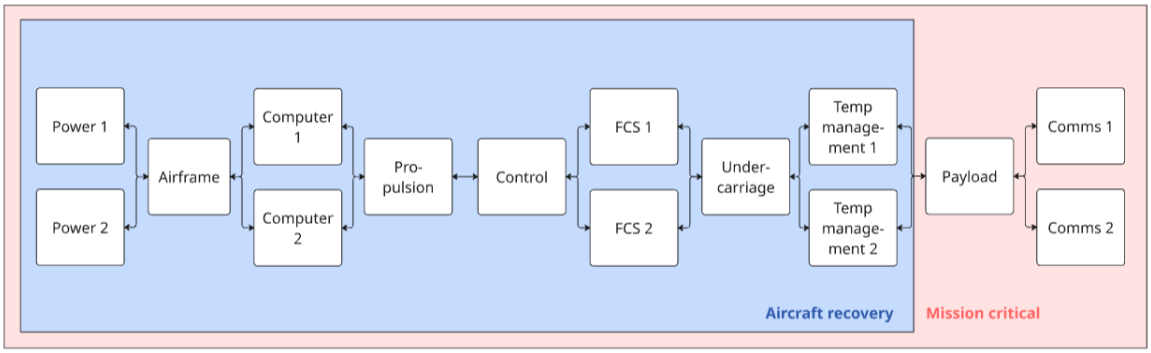

Figure 7.1: Reliability block diagram, showcasing the redundancy implemented throughout the AHAPS design.

Reliability Calculation

In order to quantify the reliability of each subsystem and, with that, the reliability of the entire system, Equation 7.3 and Equation 7.4 are used according to Kapur [74]. In these equations, R is the reliability which is given as an index between 0 and 1, with 1 being the highest. Then, t is the time that the mission takes, with MTBF being the mean time between failures of the system to be examined.

$$R_{series} = \prod_{i=1}^{n} e^{-\frac{t}{MTBF}} \tag{7.3}$$

$$R_{parallel} = 1 - \prod_{i=1}^{n} (1 - e^{-\frac{t}{MTBF}}) \tag{7.4}$$

For each system listed below, a description is given of their potential ways of failure. Next to this, their MTBF is given such that the reliability of the entire system can be calculated.

- **Payload:** The payload system connects the payload to the AHAPS and makes sure the payload can be sustained. Due to vibrations and flight loads, the connection could get damaged, which would endanger or terminate the payload. Or, if the temperature sensor has a defect, the payload temperature could rise dangerously high without a warning, endangering the mission.
- **Flight Condition System:** The flight condition system houses all the sensors necessary for reading flight parameters and position. Failures include, for instance, a frozen pitot tube, disabling it from reading airspeed and altitude. Another failure is that it displays a wrong location or attitude, causing the computer to react which could cause a dangerous situation for the aircraft.
- **Computer:** Every system is connected to the flight computer, which does all the required flight calculations and processing. It includes the navigation system and can be seen as the brain of the aircraft. Failure of this system would have fatal consequences and therefore there is a backup system in the AHAPS.
- **Communication:** The communication system of the AHAPS is responsible for all data exchange between the vehicle and the user. As the AHAPS loiters autonomously, failure would not terminate the aircraft, but it could terminate the mission.
- **Airframe:** The airframe provides the main structure of the aircraft which carries all of the dynamic loads and keeps the different subsystems in place. Although the structure can withstand all flight loads, it has several connections and weak spots which would be the first to fail in an extreme case. The structure also has to withstand extreme wing flexing, which provides an additional loading challenge.
- **Power:** The power system includes all components for the power generation and transportation of the aircraft. It has solar panels, batteries and power cables. Types of failure that could occur are solar cell damage, power cable defects, or battery damage or leaks. Also, temperature could play a large role in the performance. Since this is sensitive equipment used in harsh conditions, it is prone to failure. To mitigate this, the batteries are safely stored when on the ground and should be regularly checked.

- **Propulsion:** The propulsion system consists of four propellers and is essential for a safe operation of the vehicle. As the motor has to withstand large flight loads, a crack or minor damage in the blades or shaft could jeopardise the motor. Additionally, the motors generate heat and, when not sufficiently cooled or being operated in an extreme hot environment, could overheat. Another risk is ice formation on the motor, degrading efficiency or damaging the motors. Since the aircraft can still fly safely with only three motors available, this is recognised as a k out of n system. Therefore, the reliability of this subsystem is calculated according to Equation 7.5. After this is calculated, the reliability of the entire propulsion system will be taken into account for the total system as can be seen in Figure 7.1.

$$R_{prop} = \sum_{i=3}^{4} \binom{4}{i} R_{eng}^{i} (1 - R_{eng})^{4-i} \tag{7.5}$$

- **Control:** The control system of the aircraft includes the actuators, which are being controlled by the flight computer. Failure includes e.g. actuators which break or control surfaces which get jammed.
- **Temperature Management:** The temperature management system of the AHAPS regulates the cooling of the aircraft and ensures that the system does not overheat. Failure means overheating or freezing the batteries and other systems, which can prohibit the survival of the aircraft.
- **Undercarriage:** The undercarriage of the AHAPS is used to safely launch the system. If this structure fails due to the repetitive usage or an unexpected bump, this would, in the worst case, crash the aircraft into the ground, causing major damage to the design.

With all potential failure modes being laid out, the subsystem being clear and the equations defined, the reliability of the system can be found. For this, the values of MTBF should be found, which have been calculated for the current design in Section 7.2. As stated in **ASP-RLB-01**, these values will first be multiplied by 10 to take into account the maintenance which will regularly take place. More detailed information on this maintenance follows in Section 7.3.2. These values can be used in the equations described above, together with the mission duration which is taken to be 28 days, to find the total reliability of the system. As discussed in the technical risk assessment in Section 7.2, there is a difference between the MTBF before mitigation of the risk, and after mitigation. An overview of the reliability before and post-mitigation can be found in Table 7.14.

Table 7.14: Reliability of each subsystem pre- and post-mitigation, both as an MTBF and a fraction.

Subsystem	**MTBF pre-mit. (hrs)**	**Reliability pre-mit.**	**MTBF post-mit. (hrs)**	**Reliability post-mit**
Payload	1340637	0.9995	1340637	0.9995
Flight condition system	13155	0.9975	1340637	1
Computer	13155	0.9975	41349	0.9997
Communications	13155	0.9975	1340637	1
Airframe	7334	0.9124	41349	0.9839
Power	13155	0.9975	41349	0.9997
Propulsion	13155	0.9861	1340637	1
Control	41349	0.9839	41349	0.9839
Thermal management	41349	0.9997	41349	0.9997
Undercarriage	41349	0.9839	41349	0.9839
Total system	**-**	**0.8617**	**-**	**0.9512**

7.3.2. Maintainability

Even though this is a RAMS analysis, the maintainability is discussed before the availability. This is since data from the maintainability part is used in the availability calculations of the AHAPS. As was stated in Section 7.3.1, this subsection reports more detail about the maintenance habits to be performed on the

aircraft. Maintainability covers the maintenance necessities of the aircraft and the regulated scheduling of this maintenance. There are four different standard classes of maintenance which are defined as follows[1]:

- A-Checks: This is light maintenance that is typically done every 500 flight hours. It is meant for minor issues that are typically resolvable in 10 to 24 hours.
- B-Checks: This is maintenance that is done every six to eight months or 800 to 1000 flight hours. The maintenance covers systems that do not need daily attention but should still be checked regularly, and this takes about two to three days.
- C-Checks: These are thorough checks of the aircraft that take about one to two weeks to complete. Every system is covered, and these checks occur once in 20 to 24 months or 4000 to 5000 flight hours.
- D-checks: These checks are the most thorough of the four classes and happen once every six to eight years or around 20000 flight hours. The aircraft is completely stripped and then assembled again, which will take around 30 to 60 days.

Figure 7.2 shows a visualisation of this maintenance schedule over a timespan of seven years. This is done such that the D-check occurs one time in the timespan and that the total periodic downtime can be computed. Using this data, the availability of the AHAPS can be calculated. It is important to note that this maintenance schedule should be adjusted to fit the exact mission durations/wishes of the client. The checks can be rescheduled such that they take place before or after a mission, as with the current mean time between failures, this would not compromise the aircraft.

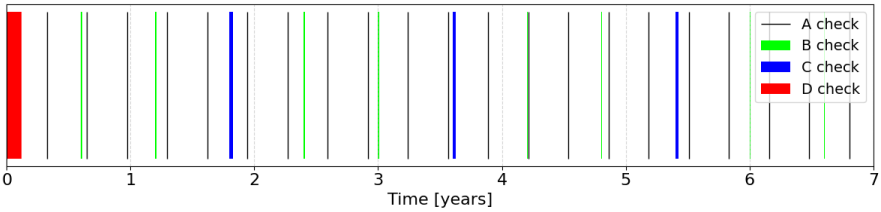

Figure 7.2: Standard aviation maintenance schedule over 7 years consisting of standard defined A-, B-, C-, and D-checks[1].

7.3.3. Availability

The availability of the product defines the fraction and the amount of time the product is operational. Non-operational time is defined mainly by maintenance time, which is compared with the operational time, giving the overall availability of the product. There are three ways of determining availability as shown in an availability prediction by NASA[2]. The last method can be seen in Equation 7.6, which uses the downtime and the total time to calculate availability.

$$A = \frac{Uptime}{Uptime + Downtime} \tag{7.6}$$

The data for this equation can be found in Figure 7.2, where the maintenance schedule for a time of seven years had been plotted. After calculations and taking into account the down time over the total time, it led to an availability of $A = 0.9530$, with a total downtime of 0.329 years. It is important to note that this number only includes scheduled maintenance and that unexpected maintenance, due to failures, should be included for a realistic estimate. Using engineering judgement, it is assumed 20% of the maintenance is unscheduled, since this is still a new and unique design. Taking this value into account leads to a final downtime of 0.411 years per cycle of seven years, leading to a final availability of:

$$A = 0.94$$

[1] https://www.gmx.aero/understanding-a-b-c-and-d-checks/ [cited 15 June 2026]
[2] https://extapps.ksc.nasa.gov/reliability/Documents/Preferred_Practices/at3.pdf [cited 15 June 2026]

7.3.4. Safety

During the preliminary design phase of the AHAPS, safety has been briefly addressed. Being far into the detailed design phase, this safety topic can be further explored. With the addition of new technology in the different subsystems of the AHAPS, this introduces new risks. These risks have been addressed, including their mitigation strategy in Section 7.2. In the new design, much emphasis has been laid on redundancy by incorporating sufficient backup systems, as can be seen in the communication flow chart in Figure 6.24. Furthermore, special cases such as one engine inoperative (OEI) have been accounted for during the design of the control systems, ensuring that even during emergencies, the aircraft stays operational and can safely return to a landing site. Potential fire hazards from batteries have also been accounted for using a solid thermal management system and proper insulation. Additionally, the structure has been designed to withstand all of the flight loads that could be encountered during the flight operations, including a gust load analysis. Safety is a topic of priority throughout the whole design, and this will ensure that the AHAPS will be a suitable design for the long term.

7.4. Verification and Validation

In this final section, system requirements compliance is verified to ensure that the requirements for which the system is designed are met. Additionally, the post-design plan for verification and validation of the AHAPS will be presented, setting a framework for the future further design of the product. In Section 7.4.1, the current design is checked for all subsystem requirements for compliance, after which in Section 7.4.2 the second order V&V plan for the final design has been laid out.

7.4.1. Compliance Matrix

In this section, the compliance matrix regarding all subsystem requirements will be shown. The methodology of requirements compliance checking will be addressed in this section as well. Additionally, the limitations of this will be elaborated on.

Compliance Assessment Method

To test the AHAPS compliance with the set requirements at the beginning of the project, there are three labels to be given to the requirements: *Pass*, *Unknown*, or *Fail*. If it is a proper design, none of the requirements will be given the *Fail* label. Each requirement will get a justification of its compliance in the last column of the compliance matrix table.

Compliance Matrix Table

In this subsection, the subsystem requirements compliance table is shown in Table 7.15.

Table 7.15: AHAPS subsystem requirements compliance matrix.

ID	Requirement Description	Compliance	Justification
REQ-SSY-1.02	The airframe subsytem shall provide heat management capabilities (dissipation, redirection, and generation) to sustain the operating temperatures of the payload, power, and computer systems.	Pass	A heating system is fitted for the power system, whereas heat dissipation will be facilitated through the airframe structure for the payload and computer systems
REQ-SSY-1.04	The airframe system shall nominally generate sufficient lift during cruise to incur a load factor of 1.	Pass	It is a constraint in the sizing code for the airframe
REQ-SSY-1.05	The airframe system shall withstand a maximum lift equivalent to 2.5 times the nominal MTOW during cruise.	Pass	It is a constraint in the airframe sizing code
REQ-SSY-1.06	The airframe system shall prevent a deflection of the wing greater than 5 m during nominal cruise conditions	Pass	Deflection is limited to less than 2 m under the greatest load factor of 2.5
REQ-SSY-1.07	The airframe system shall withstand a maximum drag equivalent to 2.5 times the nominal drag during cruise.	Pass	It is a constraint in the airframe sizing code
REQ-SSY-1.08	The airframe system shall structurally resist load factors of up to 2.5 g	Pass	It is a constraint in the airframe sizing code
REQ-SSY-1.15	The airframe system shall facilitate take-off and landing from a prepared sand-covered runway.	Pass	The take-off system uses mountain bike wheels
REQ-SSY-1.16	The airframe system shall facilitate take-off and land from a prepared gravel runway.	Pass	The take-off system uses mountain bike wheels

Continued on next page

ID	Requirement Description	Compliance	Justification
REQ-SSY-1.17	The airframe system shall facilitate take-off and landing from a prepared grass runway.	Pass	The take-off system uses mountain bike wheels
REQ-SSY-1.18	The airframe system shall ensure appropriate operational radiation shielding for its inner content for a radiation level up to TBD rad/s.	Unknown	Advanced radiation analysis is in recommendations
REQ-SSY-1.20	The airframe system shall support a payload mass budget of at least 20 kg.	Pass	It is a constraint in airframe sizing code
REQ-SSY-1.21	The airframe system shall be capable of managing payload heat dissipation of up to 150 W.	Pass	Shall be dissipated through structure during cruise
REQ-SSY-1.22	The total cost of the airframe system shall not exceed €270,000.	Pass	Cost is €183,000 (including temperature management and undercarriage)
REQ-SSY-1.25	The airframe system shall adhere to all of the general subsystem requirements	Pass	See REQ-SSY-9.X in Table 2.2
REQ-SSY-2.01	The communication system shall contain an ADS-B transmitter.	Pass	It is included in mass and volume calculation
REQ-SSY-2.02	The communication system shall contain an Emergency Locator Transmitter (ELT) beacon.	Pass	It is included in mass and volume calculation
REQ-SSY-2.03	The communication system shall provide a horizontal communication range of at least 400 km between the platform and ground subsystems.	Pass	It is a constraint in the communication sizing
REQ-SSY-2.04	The communication system shall contain a Secondary Surveillance Radar (SSR) transponder.	Pass	It is included in mass and volume calculation
REQ-SSY-2.05	The communication system shall be capable of providing a minimum payload data stream of 1 Mbit/s.	Pass	It is a constraint in the communication sizing
REQ-SSY-2.06	The communication system shall provide a communications link to the payload supporting control.	Pass	Link is detailed in data handling diagram
REQ-SSY-2.07	The communication system shall provide a communications link to the subsystem monitoring telemetry.	Pass	Link is detailed in data handling diagram
REQ-SSY-2.08	The total cost of the communication system shall not exceed €67,500.	Pass	Cost is €13,000
REQ-SSY-2.11	The AHAPS user shall not require to allocate more than 3 individuals for external communications.	Pass	Can be operated by 1 person
REQ-SSY-2.12	The communication system shall adhere to all of the general subsystem requirements	Pass	See REQ-SSY-9.X in Table 2.2
REQ-SSY-3.2	The manufacturing cost of the computer system cost shall not exceed €2,000.	Pass	Cost is €1,000
REQ-SSY-3.5	The computer system shall adhere to all of the general subsystem requirements	Pass	See REQ-SSY-9.X in Table 2.2
REQ-SSY-3.7	The computer system shall be radiation hardened for TBD rad/s	Unknown	Advanced radiation analysis is in recommendations
REQ-SSY-4.01	The computer system shall be able to provide the control commands at a frequency of TBD Hz	Unknown	Advanced analysis of autonomous computer systems and data frequency is in recommendations
REQ-SSY-4.03	The control system shall be able to tolerate a radiation over time of TBD rad/s	Unknown	Advanced radiation analysis is in recommendations
REQ-SSY-4.04	The total cost of the control system shall not exceed €70,000.	Pass	Cost is €54,000
REQ-SSY-4.07	The control system shall adhere to all of the general subsystem requirements	Pass	See REQ-SSY-9.X in Table 2.2
REQ-SSY-4.08	The control system shall be able to loiter the product within an area of 400×400 km^2	Pass	Turn rate analysis in mission simulation
REQ-SSY-4.09	The control system shall provide a yawing effectiveness of at least 5 deg/s at sea level.	Pass	Dynamic simulation
REQ-SSY-4.10	The control system shall provide a pitching effectiveness of at least ±3 deg/s at sea level.	Pass	Dynamic simulation with critical OEI condition
REQ-SSY-4.11	The control system shall be able to reverse a 45 deg turn in less than wingspan/3 sec.	Pass	Dynamic simulation
REQ-SSY-4.15	The control system shall provide sufficient control authority to land the AHAPS in an OEI situation.	Pass	Sufficient rudder authority
REQ-SSY-5.1	The manufacturing cost of the flight condition system cost shall not exceed €63,000.	Pass	It costs €46,000
REQ-SSY-5.4	The flight condition system shall adhere to all of the general subsystem requirements	Pass	See REQ-SSY-9.X in Table 2.2
REQ-SSY-5.6	The flight condition system shall be able to tolerate a radiation over time of TBD rad/s	Unknown	Since flying at a cruising altitude of 60,000 ft, a detailed analysis of the radiation is required, this is shown in the recommendations in Section 8.1.
REQ-SSY-5.7	The flight condition system shall provide its location with error of less than 0.1 NM	Pass	Explained in Section 4.3, the selected GNS has a resolution 2 horizontal metres.

Continued on next page

ID	Requirement Description	Compliance	Justification
REQ-SSY-6.2	The payload system shall be capable of providing a minimum payload data stream of 1 Mbit/s to the communication system.	Pass	The payload is connected via a network cable as explained Section 4.2.
REQ-SSY-6.3	The manufacturing cost of the payload system cost shall not exceed €22,500.	Pass	The payload system costs €5,000.
REQ-SSY-6.6	The payload system shall adhere to all of the general subsystem requirements	Pass	No interference with the general subsystem requirements.
REQ-SSY-6.7	The payload system shall provide a modular payload bay of dimensions equal to at least 0.2 x 0.4 x 0.2 m^3.	Pass	The payload bay is made of a 16 CubeSat size.
REQ-SSY-6.8	The payload system shall provide the structural and interface provisions necessary to mount a synthetic aperture radar (SAR) antenna with a footprint of 1 × 1 m.	Pass	The antenna footprint is shown in Figure 5.3a.
REQ-SSY-7.01	The power system shall have a service life of at least two years, assuming 50% usage (i.e. 180 days operative per year).	Pass	Explained in Section 5.5
REQ-SSY-7.02	The power system shall maintain its temperature between 283 K and 318 K.	Pass	The temperature management system is sized to keep the power system within these bounds.
REQ-SSY-7.03	The power system shall provide 4000 W of power to sustain operations in cruise for a minimum of 28 days.	Pass	The batteries will be able to provide more power.
REQ-SSY-7.04	The power system shall store enough energy to maintain altitude and payload operations continuously, during nighttime at 60,000 ft during the winter solstice, without power generation.	Pass	Verified in Section 6.1.4.
REQ-SSY-7.05	The power system shall provide the payload system with intermittent peak power of up to 250 W within 5-minute windows.	Pass	The batteries and solar panels can provide enough additional power, shown in Section 5.3.3.
REQ-SSY-7.06	The power system shall provide an average payload power of 100 W.	Pass	Sized for, shown in Section 5.3.3.
REQ-SSY-7.08	The manufacturing cost of the power system shall not exceed €270,000.	Pass	Cost of €205,000, shown in Section 4.5.4.
REQ-SSY-7.11	The power system shall adhere to all of the general subsystem requirements	Pass	See REQ-SSY-9.X in Table 2.2
REQ-SSY-7.12	The power system shall provide enough energy to sustain climbing operations without depleting night reserves.	Pass	Verified in Section 6.1.4.
REQ-SSY-7.13	The power system shall generate sufficient power to complete the cruise phase at latitudes between 30°S and 30°N.	Pass	Verified in Section 6.1.4.
REQ-SSY-8.01	The propulsion system shall provide sufficient thrust to maintain a cruise speed of 32.7 m/s	Pass	Sized for in Section 4.6.2
REQ-SSY-8.04	The propulsion system shall generate sufficient thrust for take-off and landing from a prepared sand-covered runway.	Pass	Sized for in Section 4.6.2 and Section 4.9.
REQ-SSY-8.05	The manufacturing cost of the propulsion system shall not exceed €135,000.	Pass	Cost of €108,000, shown in Table 4.30.
REQ-SSY-8.08	The propulsion system shall adhere to all of the general subsystem requirements	Pass	See REQ-SSY-9.X in Table 2.2
REQ-SSY-8.09	The propulsion system shall generate sufficient thrust for take-off and landing from a prepared gravel runway.	Pass	Sized for in Section 4.6.2 and Section 4.9.
REQ-SSY-8.10	The propulsion system shall generate sufficient thrust for take-off and landing from a prepared grass runway.	Pass	Sized for in Section 4.6.2 and Section 4.9.
REQ-SSY-8.11	The propulsion system shall be able to tolerate a radiation over time of TBD rad/s.	Unknown	Advanced radiation analysis is in recommendations.
REQ-SSY-8.12	The propulsion system shall provide enough thrust to achieve a sea level climb angle of 3 deg.	Pass	Verified in Section 6.1.5.
REQ-SSY-9.01	The AHAPS product shall be chemically stable and non-toxic, with no hazardous byproducts upon disposal, as validated by environmental safety testing EPA compliance.	Pass	Explained in Section 5.5.1
REQ-SSY-9.02	The AHAPS product shall utilise a modular architecture that allows for the independent replacement, repair, or upgrade of high-impact components without requiring the disposal of materials.	Pass	Explained in Section 5.5.1.
REQ-SSY-9.03	The AHAPS product shall include a maintenance report to ensure components are inspected, repaired or replaced as needed to achieve 12 mission cycles.	Pass	Explained in Section 7.3.2.
REQ-SSY-9.04	The AHAPS product shall be designed for final field assembly using only standard, handheld tools (e.g., wrenches, screwdrivers, pliers, torque wrenches) commonly available.	Pass	Explained in Section 6.2.3.
REQ-SSY-9.05	All operational resources shall be included in the standard 20 ft ISO shipping container (e.g. tooling, consumables and assembly components etc.).	Pass	Shown in Section 6.2.1.
REQ-SSY-9.06	The AHAPS product shall include a redundant and reusable recovery system.	Pass	The aircraft is fitted with landing skids, shown in Section 4.9.

Continued on next page

ID	Requirement Description	Compliance	Justification
REQ-SSY-9.07	The AHAPS shall be designed to use standard, commercially available fasteners, connectors, and interfaces.	Pass	Bolts used follow a standard size (M6), shown in Table 4.15.
REQ-SSY-9.08	The AHAPS product shall have a health monitoring system that provides data to support operational decision-making.	Pass	Computers on board monitor system health, shown in Section 5.3.4.
REQ-SSY-9.09	The AHAPS products shall be designed to not require any externally supplied consumables (e.g. fuel) for operation.	Pass	Fully independently powered by solar energy, explained in Section 4.5.
REQ-SSY-9.10	The AHAPS components necessary for assembly shall be designed to occupy no more than 95 % of the 20 ft ISO container volume.	Pass	Shown in Section 6.2.1.
REQ-SSY-9.13	The AHAPS product shall include redundant trackable components using GPS to locate and retrieve the product.	Pass	The aircraft is fitted with a GPS, shown in Section 4.3.
REQ-SSY-9.14	The AHAPS product shall be designed with materials and components able to withstand loads to fulfil at least 12 mission cycles before being decommissioned.	Pass	Explained in Section 5.5.2.
REQ-SSY-9.15	The AHAPS product shall maintain all flight-critical functions for at least 12 mission cycles before being overhauled.	Pass	Explained in Section 5.5.2.
REQ-SSY-9.16	The AHAPS concept engineering phase shall be completed within 7 weeks by a design team of 10 persons.	Pass	The design is presented in this report.
REQ-SSY-9.17	The AHAPS product shall be designed to be collapsible or modular in no more than 40 parts to facilitate assembly, disassembly, and secure storage in the 20 ft container.	Pass	The product is stored as 37 parts, outlined in Section 6.2.1.
REQ-SSY-9.18	The AHAPS user shall not be required to allocate more than 3 individuals for transporting the AHAPS product to its designated launch site.	Pass	The AHAPS product fits in a 20 ft ISO container, shown in Section 6.2.1.
REQ-SSY-9.19	The AHAPS user shall not be required to monitor the communication system more than once every 24-hour interval, starting from take-off.	Pass	Computer and control system sized for autonomous flight, shown in Section 4.3 and Section 4.7.
REQ-SSY-9.20	The AHAPS product shall be loaded and unloaded from the 20 ft ISO shipping container by 3 people.	Pass	Explained in Section 6.2.3.
REQ-SSY-9.21	The AHAPS product shall be loaded and unloaded from the 20 ft ISO shipping container without external (not included in the container) machines.	Pass	Explained in Section 6.2.3.
REQ-SSY-9.22	The AHAPS product shall comply with EASA Civil Drones certification requirements, with operations conducted under type 1.	Unknown	EASA Civil Drone certification is conducted on an individual basis

Compliance Assessment Limitations

The compliance assessment, while thorough, remains with some limitations. These limitations are briefly outlined in this section.

The biggest limitation is uncertainties in physical and performance parameters computed during the detailed design phase. While the uncertainties have decreased significantly since the conceptual sizing, there are still a large number of assumptions made in order to obtain the relevant values. For example, aircraft structural loads are only statically determined, as dynamic load analysis is beyond the scope of the current design stage. Therefore, there is a limited accuracy in the loading that the aircraft is sized and tested for [70]. However, generally all parameters are sized with conservative assumptions, meaning that it is still likely that compliance with the requirements will not change with further detailed design.

Another major limitation is the compliance with requirements pertaining to the certification of the aircraft. EASA civil drone certification is conducted on a case-by-case basis, meaning that specific requirements are not known until consultation with EASA. It is therefore possible that some requirements listed have to be changed due to regulatory requirements, which could cause the aircraft to no longer comply with all of the requirements. To mitigate this, most requirements are taken conservatively and with reference to more strict regulatory rules, such as CS-22 regulations [67].

Overall, the compliance matrix gives a useful insight into how well the design meets the stipulated requirements. However, its limitations in accuracy must be taken into account for future design and development progression.

7.4.2. Second Order V&V

The second stage of verification & validation, which will occur when the design reaches completion, will require testing of the subsystems, followed by systems, progressively. In this subsection, the subsystem and

system requirements are detailed respectively, and an initial estimate of the associated costs is quantified.

Subsystem Requirements Verification

The subsystems have unique requirements and repetitive requirements, which lead to the common verification methods. For each of the repetitive requirements, common verification methods are detailed in Table 7.16. These are split into four verification types: Analysis, Test, Inspection, and Demonstration [75].

Table 7.16: Verification methods for multiple corresponding subsystem requirements.

GROUPS	Subsystems	Verification Type	Verification Method	Corresponding Requirements
Unit Cost	ALL	Analysis	Financial Audit	REQ-SSY-1.22–24, REQ-SSY-2.08–2.10, REQ-SSY-3.2–3.4, REQ-SSY-4.04–4.06, REQ-SSY-5.1–5.3, REQ-SSY-6.3–6.5, REQ-SSY-7.08–7.10, REQ-SSY-8.05–8.07
General	ALL	Inspection	Inspect Adherence to Subsystem Requirements	REQ-SSY-1.25, REQ-SSY-2.12, REQ-SSY-3.5, REQ-SSY-4.07, REQ-SSY-5.4, REQ-SSY-6.6, REQ-SSY-7.11, REQ-SSY-8.08
Weight	ALL	Analysis	Weight Computation with CAD Model	REQ-SSY-1.26, REQ-SSY-2.13, REQ-SSY-3.6, REQ-SSY-4.14, REQ-SSY-5.5, REQ-SSY-6.9, REQ-SSY-7.14, REQ-SSY-8.14
Radiation	Airframe, Computer, Propulsion, Flight Condition, Control	Analysis	Simulate Response to the Radiation Dose	REQ-SSY-1.18, REQ-SSY-3.7, REQ-SSY-4.03, REQ-SSY-5.6, REQ-SSY-8.11
Runway	Airframe, Propulsion	Test	Test Effect of Surface Conditions	REQ-SSY-1.15–17, REQ-SSY-8.04, REQ-SSY-8.09–10
Maintain Temperature	Payload, Computer, Power	Test	Test the Subsystem's Temperature whilst Operating	REQ-SSY-3.1, REQ-SSY-6.1, REQ-SSY-7.02

The verification methods for the unique subsystem requirements are detailed below in Table 7.17.

Table 7.17: Other subsystem requirements verification methods.

Corresponding Requirements	Verification Type	Verification Method
REQ-SSY-1.01	Analysis	Descent load analysis using aerodynamic and load modelling
REQ-SSY-1.02	Test	Use a real test to analyse the subsystems on their thermal capabilities
REQ-SSY-1.03	Analysis	Analyse the material performance using data
REQ-SSY-1.04	Analysis	Use flight simulation to analyse lift capabilities at altitude
REQ-SSY-1.05	Analysis	Structural load analysis using cruise conditions
REQ-SSY-1.06	Analysis	Deflection analysis using beam theory
REQ-SSY-1.07	Analysis	Drag estimation at altitude
REQ-SSY-1.08	Analysis	Load analysis using flight envelope
REQ-SSY-1.09	Analysis	Lift analysis in take-off configuration
REQ-SSY-1.10	Analysis	Lift analysis in landing configuration
REQ-SSY-1.11	Analysis	Gust load analysis using aerodynamic and structural models
REQ-SSY-1.12	Analysis	Lift analysis in landing configuration
REQ-SSY-1.13	Analysis	Lift analysis in landing configuration
REQ-SSY-1.14	Analysis	Gust load analysis using aerodynamic and structural models
REQ-SSY-1.19	Analysis	Analyse performance at landing conditions
REQ-SSY-1.20	Analysis	Mass budget calculation
REQ-SSY-1.21	Analysis	Heat dissipation analysis
REQ-SSY-1.27	Analysis	FEM analysis
REQ-SSY-2.01	Inspection	Inspect presence of ADS-B transmitter
REQ-SSY-2.02	Inspection	Inspect presence of ELT beacon
REQ-SSY-2.03	Analysis	Link budget calculation 400 km
REQ-SSY-2.04	Inspection	Inspect presence of SSR transponder
REQ-SSY-2.05	Analysis	Data stream analysis
REQ-SSY-2.06	Analysis	Analysis with communication link model

Table 7.17 continued from previous page

Corresponding Requirements	Verification Type	Verification Method
REQ-SSY-2.07	Analysis	Analysis with communication link model
REQ-SSY-2.11	Demonstration	Demonstrate that operation can be performed with required individuals
REQ-SSY-4.01	Test	Test the command frequency output
REQ-SSY-4.02	Demonstration	Demonstrate landing in maximum gust condition
REQ-SSY-4.08	Analysis	Simulate the subsystem performing required control inputs
REQ-SSY-4.09	Test	Test in a wind tunnel
REQ-SSY-4.10	Test	Test in a wind tunnel
REQ-SSY-4.11	Test	Test in a wind tunnel
REQ-SSY-4.12	Analysis	Simulate whether control response is sufficient
REQ-SSY-4.13	Analysis	Simulate whether control response is sufficient
REQ-SSY-4.15	Analysis	Control simulation using VLM
REQ-SSY-5.7	Demonstration	Demonstrate the system's position error is below requirement
REQ-SSY-6.2	Analysis	Simulate the maximum data stream size
REQ-SSY-6.7	Inspection	Inspect the bay size using the CAD model
REQ-SSY-6.8	Inspection	Inspect that the interface is correct
REQ-SSY-7.01	Analysis	Analyse the power system performance based on 2-year mission profile
REQ-SSY-7.03	Demonstration	Demonstrate that the power system can provide the required power
REQ-SSY-7.04	Analysis	Analyse whether the stored energy is sufficient
REQ-SSY-7.05	Demonstration	Demonstrate that the power system can provide the required power
REQ-SSY-7.06	Demonstration	Demonstrate that the power system can provide the required power
REQ-SSY-7.12	Analysis	Analyse the energy used during climb
REQ-SSY-7.13	Analysis	Analyse the energy generation during cruise
REQ-SSY-8.01	Test - Analysis	Wind tunnel test - Analysis to scale propulsion system to cruise altitude
REQ-SSY-8.02	Test	Wind tunnel to simulate sea level properties
REQ-SSY-8.03	Test	Wind tunnel to simulate sea level properties
REQ-SSY-8.12	Test	Test flight to measure time-to-climb from sea level
REQ-SSY-8.13	Analysis	Performance simulation
REQ-SSY-9.01	Inspection	Material safety data sheets
REQ-SSY-9.02	Demonstration	Replacement procedure without impacting other components
REQ-SSY-9.03	Inspection	Review of the generated Maintenance Manual
REQ-SSY-9.04	Demonstration	Demonstrate assembly
REQ-SSY-9.05	Inspection	Inventory check
REQ-SSY-9.06	Demonstration	Deploy recovery system
REQ-SSY-9.07	Inspection	Review Bill of Material (BoM)
REQ-SSY-9.08	Analysis	Simulate sensor failure
REQ-SSY-9.09	Inspection	Inspect propulsion system for zero-fuel
REQ-SSY-9.10	Analysis	CAD volume analysis
REQ-SSY-9.11	Analysis	CAD volume analysis
REQ-SSY-9.12	Analysis	CAD volume analysis
REQ-SSY-9.13	Test	Power-on testing of GPS system and ground station
REQ-SSY-9.14	Analysis	Life-cycle load simulations
REQ-SSY-9.15	Analysis	Life-cycle load simulations
REQ-SSY-9.16	Inspection	Project-Management audit
REQ-SSY-9.17	Demonstration	Demonstrate assembly
REQ-SSY-9.18	Demonstration	Demonstration of logistic scenario
REQ-SSY-9.19	Demonstration	Demonstrate required monitoring intervals
REQ-SSY-9.20	Demonstration	Physical load/unload exercise
REQ-SSY-9.21	Demonstration	Physical load/unload exercise
REQ-SSY-9.22	Inspection	Certification compliance verification through documentation inspection

System Requirements Verification

Following integration, higher-level system verification can be performed. The verification methods are described in Table 7.18.

Table 7.18: System requirements verification matrix.

Corresponding Requirements	Verification Type	Verification Method
REQ-SYS-1.01, REQ-SYS-1.10, REQ-SYS-1.13, REQ-SYS-1.14, REQ-SYS-1.20	Analysis	Flight endurance simulation

Corresponding Requirements	Verification Type	Verification Method
REQ-SYS-1.02, REQ-SYS-1.03, REQ-SYS-1.22, REQ-SYS-1.23, REQ-SYS-1.24, REQ-SYS-1.26	Analysis	Climb/descent performance analysis
REQ-SYS-1.04, REQ-SYS-1.21, REQ-SYS-1.25	Testing	System/component operational temperature testing
REQ-SYS-1.05, REQ-SYS-1.06, REQ-SYS-1.07, REQ-SYS-1.08, REQ-SYS-1.09	Analysis	Flight load simulation
REQ-SYS-1.11	Testing	Wind tunnel testing
REQ-SYS-1.12	Analysis	Radiation impact assessment
REQ-SYS-1.15, REQ-SYS-1.16	Analysis	Flight path simulation
REQ-SYS-1.17, REQ-SYS-1.18, REQ-SYS-1.19	Demonstration	Control system hardware functionality test
REQ-SYS-1.24, REQ-SYS-1.28	Analysis	Gust analysis
REQ-SYS-1.27	Analysis	Crosswind analysis
REQ-SYS-1.29, REQ-SYS-1.30, REQ-SYS-1.31	Testing	Observe interaction with real surface
REQ-SYS-1.32, REQ-SYS-1.36	Analysis	Link budget calculations
REQ-SYS-1.33, REQ-SYS-1.34, REQ-SYS-1.37, REQ-SYS-1.40, REQ-SYS-1.44	Inspection	CAD inspection
REQ-SYS-1.35	Analysis	Power source degradation modelling
REQ-SYS-1.38	Inspection	Documentation inspection
REQ-SYS-1.39	Analysis	Mass budget calculation
REQ-SYS-1.41, REQ-SYS-1.42	Analysis	Payload power analysis
REQ-SYS-1.43	Analysis	Payload heat analysis
REQ-SYS-1.45	Analysis	Power requirement analysis for SAR
REQ-SYS-1.46, REQ-SYS-1.47	Analysis	Communication capability analysis using models
REQ-SYS-1.48, REQ-SYS-1.49, REQ-SYS-1.50	Demonstration	Operational demonstration
REQ-SYS-1.51, REQ-SYS-1.52	Demonstration	Physical load/unload exercise
REQ-SYS-3.01	Testing	Recovery system deployment test
REQ-SYS-3.10	Inspection	Review bill of materials (BoM)
REQ-SYS-3.11	Analysis	Sensor failure simulation
REQ-SYS-3.12	Inspection	Inspection of propulsion system for zero-fuel condition
REQ-SYS-3.02	Testing	Power-on testing of GPS system and ground station
REQ-SYS-3.03, REQ-SYS-3.04	Analysis	Life-cycle load simulations
REQ-SYS-3.05	Inspection	Project management audit
REQ-SYS-3.06	Inspection	Weighing of all packed components
REQ-SYS-3.07, REQ-SYS-3.09	Demonstration	Assembly demonstration
REQ-SYS-3.08	Inspection	Inventory check
REQ-SYS-4.1	Inspection	Review of generated maintenance manual
REQ-SYS-4.2	Analysis	Component wear analysis
REQ-SYS-4.3	Demonstration	Replacement procedure without impacting other components
REQ-SYS-5.1	Analysis	Disposal/recycling timeline analysis
REQ-SYS-5.2	Inspection	Material safety data sheet inspection
REQ-SYS-6.1	Inspection	Production schedule audit
REQ-SYS-6.2, REQ-SYS-6.3, REQ-SYS-6.4	Inspection	Financial audit

Verification Costs

Since verification is extensive and can require use of specialised facilities or equipment, it is important to estimate cost in advance. Generally, four types of verification methods are used. Analysis and inspection methods usually do not involve significant verification costs as they can be performed with already available resources. Testing and demonstration methods, on the other hand, typically do introduce high costs, since they make use of exclusive resources and facilities. There are a total of six different facilities that should be used in the verification process, which are all property of TU Delft[1]. The cost of each facility is based on the estimated time that it will be required for. Additionally, it is assumed, since they are university property and

[1] https://www.tudelft.nl/en/research/research-facilities [cited 11 May 2026]

that the team is composed of students, a reduction in costs can be arranged. An overview of the six facilities with their estimated costs can be found in Table 7.19.

Table 7.19: Estimated costs of testing facilities for AHAPS verification.

Facility	Estimated Cost (FY26)
Low speed wind tunnel	€25,000[1] (5 days)
Temperature chamber	€22,500[2] (15 days)
Simulation and control lab	€15,000
Power test bench	€20,000
Surface test area	€5,000
Outdoor test field	€5,000

Mission Validation

Mission validation requires ensuring that the requirements set out by the stakeholder are met. As a result of extensive system and subsystem testing, mission validation mostly consists of demonstrating that the integrated product can perform as required. For mission validation, two main campaigns will be used: a pre-flight test inspection and a flight test.

The pre-flight test campaign shall be performed at the assembly facility and will take one week, inspecting the entirety of the AHAPS system, including performing some mission validation. With 10 personnel, the campaign is expected to cost €50,000 with a total estimated cost per hour of €125[3].

The flight test is expected to last two months, allowing small missions with increasing endurance in the first month, culminating in the full 28-day mission profile in the second month. Estimated costs total €100,000, with the potential for it to increase to €200,000 in case the test needs to be re-performed due to an issue at the end of the 28-day profile. This is based on truck rental and accommodation and personnel costs, based on the average Aerospace Engineer salary in the Netherlands and an estimate for contracted flight test specialists of €600 per day, over the course of a month[4][3].

Table 7.20: Mission validation methods.

Corresponding Requirement	Validation Type	Validation Method
REQ-STK-1.1	Test	Flight test with climb to 60,000ft
REQ-STK-1.2	Test	Flight test with endurance of 28 days during winter
REQ-STK-1.3	Test	Flight test with autonomous operation
REQ-STK-1.4	Test	Flight test at northern latitude
REQ-STK-1.5	Demonstration	Deploy from an unpaved but prepared surface
REQ-STK-1.6	Test	Test communication range during flight test cruise
REQ-STK-1.7	Inspection	Check that it is installed
REQ-STK-1.8	Inspection	Check that it is installed
REQ-STK-1.9	Analysis	Analysis based on the service life of established constituent components
REQ-STK-1.10	Test	Check maximum data stream size over 1 [Mbit/s]
REQ-STK-2.1	Demonstration	Show that human monitoring is only required once per day
REQ-STK-2.2	Demonstration	Show the health system influences autonomous decision-making
REQ-STK-2.3	Inspection	Check that it is installed
REQ-STK-2.4	Inspection	Check that all requirements have been verified
REQ-STK-3.1	Analysis	Check that all materials are recyclable or inert

[1] http://erau.edu/research-and-innovation/labs/wind-tunnel-facility [cited 28 May 2026]

[2] https://www.associatedenvironmentalsystems.com/blog/breaking-down-the-cost-of-test-chambers-what-youre-paying-for [cited 28 May 2026]

[3] https://www.glassdoor.nl/Salaries/flight-test-engineer-salary-SRCH_KO0%2C20.htm? [cited 11 May 2026]

[4] https://www.esatrucks.eu/nl/onze-diensten/vrachtwagenverhuur [cited 11 May 2026]

Table 7.20 Continued

Corresponding Requirement	Validation Type	Validation Method
REQ-STK-3.2	Demonstration	Demonstrate that recovery does not leave debris
REQ-STK-3.3	Demonstration	Demonstrate that components can be easily removed or replaced
REQ-STK-4.1	Test	Flight test with a payload of 20 kg
REQ-STK-4.2	Test	Flight test with payload power consumption of 250 W for 5-minute windows
REQ-STK-4.3	Test	Flight test with continuous payload power consumption of 100 W
REQ-STK-4.4	Test	Ground test with 150 W heater in payload bay
REQ-STK-4.5	Inspection	Check that the interface is present and correct
REQ-STK-4.6	Demonstration	Show that payload can communicate to influence control system
REQ-STK-4.7	Demonstration	Show that telemetry can be sent using the communications link
REQ-STK-5.1	Inspection	Check that the concept engineering phase has been completed in 7 weeks by a team of 10
REQ-STK-6.1	Analysis	Analyse the recurring costs per unit and non-recurring costs divided by expected number of units to be built, based on production of test model
REQ-STK-7.1	Demonstration	Demonstrate it can fit and be transported in a 20 ft container
REQ-STK-8.1	Demonstration	Demonstrate that it can be assembled in the field with commonly available, handheld tooling
REQ-STK-8.2	Demonstration	Show that all components required fit into the 20 ft container
REQ-STK-8.3	Demonstration	Demonstrate that it can be operated without any external consumables during flight test

8. Post Design Synthesis Recommendations

This chapter outlines the post-conceptual-design steps associated with the AHAPS project. Due to time, manpower, and scope constraints, several aspects of the mission could not be thoroughly analysed. As such, design recommendations are summarised in Section 8.1. With these aspects in mind, a design and development logic starting after the end of the DSE has been elaborated and presented in Section 8.2. With the necessary additional work performed, a manufacturing and integration plan for the structure and several subsystems is outlined in Section 8.3. Finally, the commercial potential of the AHAPS is assessed in Section 8.4.

8.1. Design Recommendations

Due to **REQ-STK-5.1**, which states that the design team only had seven weeks to complete the concept engineering phase, some design aspects have not been researched at the desired level. This section provides recommendations for the different aspects to design in case more time is allocated for this purpose.

8.1.1. Radiation

During the flight of the AHAPS in the stratosphere for at least 28 consecutive days, significant radiation is endured. Whilst it is now assumed that this radiation will not significantly deteriorate the airframe, theoretical calculation and computer simulation can predict the number of primary defects and of sputtered atoms [76]. Another concern can be raised for the electronic systems within the AHAPS, namely the batteries. Gamma radiation on unprotected batteries triggers cation mixing in the cathode active material, which results in poor polarisation and capacity [77]. It is recommended to examine to which extent this affects the batteries in the AHAPS, which are generally only slightly protected by a thin layer of solar panels, mylar, and aerogel insulation, with some being shielded by a different battery located on top of them. Finally, computer systems might be quite susceptible to single-event upsets. Data from military and experimental flights and laboratory testing indicate that typical non-radiation-hardened 64 K and 256 K static random access memories (SRAMs) can experience a significant soft upset rate at aircraft altitudes due to energetic neutrons created by cosmic ray interactions in the atmosphere [78]. It is recommended to determine the level of error detection and correction circuitry required or to apply a radiation-hardened wing skin or wingbox in the final product.

8.1.2. Dynamic Analysis

The current structural design presented in this report has focused on static load cases. However, the AHAPS, consisting of a high aspect ratio and low structural weight, is recommended to have undergone a thorough dynamic analysis before any detailed design can be finalised or a prototype cleared for flight [17, 79]. The following topics are strongly recommended for investigation in subsequent design phases.

Dynamic Gust Loads

Although mean wind speeds at 60,000 ft are usually lower than in the jet stream, gusts at these altitudes still impose significant load factors [66]. Unlike traditional aircraft, the slow cruising speed of the AHAPS means that it can encounter gust winds proportional to its own airspeed, causing gust loads to have a great effect on the aircraft [17, 79]. It is therefore recommended to perform a dynamic gust analysis by looking at both certifications CS-23 and CS-25 [66, 68]. Additionally, it is advised to use both the mathematical "1-cosine" gust model and a continuous turbulence model (power spectral density approach, e.g., von Kármán spectrum) to predict for specific critical load points [80].

Eigenfrequencies

A natural frequency analysis is recommended to establish the free-motion modes of the AHAPS. The lowest bending and torsional modes with the significant size and flexibility of the AHAPS may occur at frequencies well within the bandwidth of the flight control system [81]. This creates the potential for aeroservoelastic

coupling and structural resonance during flight [82]. Note, since the AHAPS uses batteries rather than a fuel type and since the payload system is designed for ballast if the payload is less than 20 kg, there is no significant C.G. shift. Therefore, eigenfrequency computations for the wing, propellers, and empennage are recommended.

Fatigue and Creep

The AHAPS is designed for mission operations significantly longer than those of conventional aircraft. This leads to fatigue and creep being a structural concern, particularly at high-stress locations such as wing root joints, spar caps, skin panel attachments, and any areas with geometric stress concentrations. For high-cycle fatigue, it is recommended to develop a comprehensive fatigue life assessment using mission-representative load spectra derived from the gust analysis and operational flight envelope. For low-cycle, it is also recommended to look at the multiple launch/recovery loads, ground assembly handling, and thermal cycles. It is important to take the structural deterioration from radiation, Section 8.1.1, into account which worsens structural fatigue resistance [83].

Aeroelasticity

The static aeroelastic deviations have been determined by the design team. However, redistribution of the load due to bending and twist were not considered, which impact the aerodynamic centre and longitudinal stability [84].

For dynamic aeroelasticity, flutter infliction is one of the main concerns due to the natural thin shape of the AHAPS [85]. It is recommended to conduct a flutter analysis across the full flight envelope, including climb, cruise at altitude, and descent, covering all relevant Mach numbers and altitudes. Classical flutter modes to be investigated include classical bending-torsion flutter of the wing, control surface flutter, and panel flutter of skin surfaces. The analysis should account for the geometric non-linearities introduced by large wing deflections under aerodynamic load (pre-deformed flutter analysis), since the static equilibrium shape of a highly flexible HAPS wing may differ significantly from its unloaded geometry, altering both the aerodynamic load distribution and the structural stiffness [85]. Also, gust response amplification and limit cycle oscillations (LCO) affecting the elasticity, which may persist below the classical flutter speed due to structural non-linearities, are recommended to examine.

It is recommended to integrate aeroelastic analysis throughout the detailed design process using coupled aerodynamic-structural models, for example, the lattice method for subsonic unsteady aerodynamics coupled with a beam or shell model. Aeroelastic tailoring, the deliberate use of composite ply orientation to achieve favorable bending with twist coupling, is a particularly promising strategy for HAPS designs and should be explored as a means of passively reducing loads and improving flutter margins without weight penalty.

Thermal Response

For the design of the aircraft structures, it is recommended to analyse the effects of thermal expansion and contraction. This effect is notable as the temperature difference between cruise and sea-level could reach almost 100°C. Since the CFRP and titanium of the sleeve and spar have different thermal expansion coefficients, this can induce further stresses. Additionally, since the CFRP is not an isotropic material, it will not contract equally in all directions [86]. Thus, with an in-depth analysis of the thermal response of the aircraft, the load-carrying internal structure could change.

Finite Element Method (FEM)

All of the analyses outlined above rely on a high-fidelity finite element model as their structural foundation. The FEM developed during detailed design must go substantially beyond the simplified beam or panel models used, capturing the three-dimensional stiffness and mass distribution of the actual construction. It is recommended to develop a full-aircraft FEM, incorporating shell elements for wing skins and ribs, beam or solid elements for spar caps and webs, and point masses for non-structural components. Material property inputs should reflect measured coupon data rather than handbook values, accounting for the specific fibre volume fraction, resin system, and manufacturing process used. Geometric nonlinearity should be ac-

tivated for all analyses involving the fully loaded wing, given the anticipated large deflections. A mesh convergence study is essential to ensure that stress and strain results used for fatigue and strength assessments are not sensitive to element size. Finally, the FEM should be maintained as a living document throughout the design process and updated as the structural architecture evolves, so that it remains the authoritative source for all structural predictions.

8.1.3. Control Surface Optimisation

For the optimisation of the control surfaces, it is recommended to use Computational Fluid Dynamics (CFD) to reduce the safety margins by increasing the accuracy. With computational fluid dynamics with Reynolds averaged Navier-Stokes (CFD-RANS) analysis in the transonic domain, the margin of error rounds to 5% [87].

After this, it is advised to put the control surface through a physical wind tunnel test. With this, an accurate lift over angle of attack plot can be generated to more accurately account for stall behaviour. Also, with a wind tunnel test, the effects of multiple control surface freeplay non-linearities on the aeroelastic behaviour can be explored [88]. Furthermore, the dependency on side-slip angle for the control surfaces can be modelled [88].

8.1.4. Propeller Optimisation

Similar to the control surfaces, the accuracy of the propeller coefficients can be significantly improved with CFD. For the thrust coefficient (C_T), errors range from 0.35% to 3.94%, while torque coefficient (C_Q) errors range from 0.54% to 2.00% [89]. Furthermore, with wind tunnel tests, the drag analysis can be accurately modelled, rather than the currently used conservative assumptions. Finally, the effect of side-slip angle for the thrust output can be explored [90].

8.1.5. Frequency Autonomy

During the design phase, no confirmations have been made for the autonomy of the computer systems used in the AHAPS or the ground station. For all AHAPS subsystems, no calculations have been made on the required frequency of signal information for the system to be autonomous. In addition, the communication system presented in Section 4.3.2 has been sized around a single, fixed, VHF frequency band, chosen conservatively for power-budget purposes. This is a reasonable simplification for the concept design phase, but it does not yet reflect the regulatory reality the AHAPS will face in operation. Because of **REQ-STK-1.4**, the aircraft is intended to be deployable between at least 30°N and 30°S. This means that the aircraft will fly in the airspace of multiple countries, which each have their own frequency airspace rules. The ITU-R has globally harmonised several bands for HAPS use in the fixed service (31–31.3 GHz, 38–39.5 GHz, and the 47/48 GHz bands), and more recently moved towards permitting HAPS to act as IMT base stations in mobile bands below 2.7 GHz [91]. Other issues can be raised with the lack of redundancy for operating within a singular bandwith [92]. It is recommended to solve all these issues listed above before starting the manufacturing phase.

8.2. Project Design and Development Logic

In Section A.4 the flow structure for the entire AHAPS product life from its post-DSE phase is presented. It shows the recommended detailed design steps explained in Section 8.1. It mentions both the manufacturing and market distribution plans, taking into account the approval for the EASA Civil Drones certification requirements, with operations conducted under type #1 (**REQ-STK-2.4**). Finally, the End-Of-Life phase is considered with the possibility to maintain and replace individual parts of the AHAPS. The time flow dedicated to all these steps is presented in Section A.5.

8.3. Manufacturing, Assembly and Integration Plan

In this section, an overview of the manufacturing of the different subsystems and subassemblies is given. Furthermore, an overview is also given on how the subsystems are integrated into each other to produce the final subassemblies ready for transportation.

8.3.1. Sub-Assembly Manufacturing

Most of the structural elements for the airframe and propulsion system will be manufactured in-house to ensure the desired tolerances and finishes. This subsection outlines the process by which these components are manufactured.

Spar

Since all bending and shear loads are assigned exclusively to the spar, it is of vital importance that it is manufactured correctly. For the manufacturing, a traditional lay-up process is used due to the fact that it is widely used in the automotive and aerospace industry, as well as due to the low-volume nature of the product [93].

The first step is to prepare the mandrel, which is an elliptical mandrel matching the cross-section eccentricity factor of 2.4. The mandrel surface is prepared, and the release agent is uniformly applied.

The second step is to start with the laminate layup. First, the primary plies of 0° unidirectional tape are aligned with the spar's longitudinal axis. After that, interleaved off-axis ±45° plies are applied to account for the shear and torsional stiffness [93]. The plies are vacuum-bagged to ensure ply consolidation. Each spar is laid up as a single straight tube without any twist introduced.

The subsequent step is to insert the lay-up into an autoclave to cure [93]. After it is taken out of the autoclave, the lay-up should be allowed to cool slowly back to room temperature. After it has reached room temperature, the mandrel is removed, the inner surfaces are inspected for delamination, and the spar ends are trimmed to ensure squareness and correct length.

Spar Connector System

The spar connector system consists of the titanium sleeve and a Nylon 6 clamp. These components must be machined to tolerance to ensure snug fits over the spar so that relative lateral motion is prevented. Due to this reason and the low-volume nature of the manufacturing, CNC machining is used for these two components[1]. For potential future high-volume production, injection moulding can be used for the Nylon 6 clamps[2].

Wing Skin

The mylar skin is mainly the aerodynamic surface and provides the plane with marginal torsional stiffness to complement the spar. The skin for each wing section is manufactured separately to ensure modularity and interchangeability.

Firstly, flat-pattern geometries are developed for each wing section using the MH91 airfoil profile, wing section length, and the required geometric twist distribution. These geometries are cut using a CNC flatbed cutter to ensure precise tolerances.

Secondly, the film is prepared for bonding. A visual inspection is performed to ensure there are no scratches, creases, tears, pinholes, or other visible defects. Random points on the skin panel are tested for thickness.

Ribs

The ribs ensure that the wing cross-section is maintained and to prevent spar buckling. Since the ribs are made out of CFRP and have to take the twist into account, the manufacturing is a combination of traditional lay-up and CNC machining [93].

The first step is to lay alternative-oriented plies ($0°/90°/\pm 45°$ for quasi-isotropic characteristics) until the required thickness is achieved [93]. These lay-ups are subsequently placed inside an autoclave to cure.

After the lay-ups have been cooled down to room temperature, they are CNC routed to cut the rib profile to the final MH91 shape with the correct local twist angles. The CNC routing also allows for the spar hole to be cut to sufficient tolerance. After the rib is cut, the edges are deburred, inspected for delamination, and sealed to prevent moisture from propagating delamination.

[1] https://www.cncpioneer.com/blog/nylon-cnc-machining [cited 16 June 2026]

[2] https://www.alpine-mold.com/pa6-pa66-pa12-pa1010-a-complete-guide-to-nylon-injection-molding-process.html [cited 16 June 2026]

Propulsion
For the propulsion system, there are four components that need to be manufactured in-house: the connecting rod, the propeller, the hub, and the nacelle. These components are all made out of CFRP, and thus the manufacturing process is very similar to the ones explained for the ribs and spar. The rods, nacelles, propeller hubs, and propellers can all be manufactured similarly to the spars, using a mandrel or mould [93]. Due to the higher complexity of the propeller geometry, these will additionally be CNC routed to ensure correct geometry and finish.

8.3.2. Sub-Assembly and Integration
After the manufacturing of the components, they are integrated into sub-assemblies to ease the process of in-field assembly for the user. These sub-assemblies will eventually be placed into the 20 ft ISO container to be shipped to the customer.

Airframe
The AHAPS aircraft is split into nine different sections as shown in Section 5.1. Each section is considered a complete sub-assembly in the production facility before shipping. This ensures that the sections are modular and minimises the skilled labour required in the field.

Section I is the main root section and includes the payload bay, second spar, and primary avionics. The first step is to locate the primary spar section in the rib jig and verify alignment, which is followed by the installation of the payload bay structure and the second spar fixture. The ribs are slid over the spars and bolted in place, the ADS-B, ELT, SSR, and SAR antenna brackets are installed with M10 bolts, and finally, the mylar skin is bonded to the ribs. All bonding surfaces are prepared with IPA to get rid of any oils or dirt. The structural adhesive is applied to the rib surfaces and spar flanges, and the skin is applied to the bonding surfaces. Tension is applied to ensure a smooth aerodynamic profile. The skin is clamped to the bonding surfaces to hold its position during the adhesive curing process. This process is finalised by inspecting for wrinkles, bubbles, unbonded areas, and the correct twist angle at each station.

Sections II-IV are structurally similar to Section I, except for the fact that these sections also have landing skids and take-off wheels and that Section IV includes the inner elevon and a part of the outer elevon. The spar connectors are installed and bolted using the titanium bolts. For the landing/take-off structure, the attachment points for the skids and the telescoping mechanism for the skids are installed. Furthermore, the inner elevon actuator mounting bracket needs to be installed in Section IV.

Section V, the wing tip section, is once more structurally similar to the other sections. Furthermore, the winglets are installed, and the actuator brackets are installed for both the rudder and the outer elevon. Lastly, the attachment points for the take-off structure and the telescoping mechanism for the skids are also installed inside the wing structure using M10 bolts.

Propulsion
To simplify the in-field assembly process, the propulsion system will be partially assembled before being shipped to the customer. The propeller hub, the propeller blade, the motor, the ESC, and the nacelle will be one sub-assembly delivered to the customer.

The propeller blades are attached to the hub using a high-strength, aerospace-grade adhesive. The motor is attached to the shaft through a keyed shaft coupling, while the ESC is directly mounted to the motor using a set of six M10 bolts. This whole assembly is inserted inside the nacelle and attached to the motor using a set of ten M10 bolts.

Since the solar panels are thin films, they are easily cut up into parts and attached to their corresponding section. This attachment is done through the use of high-strength, aerospace-grade adhesives to ensure proper adhesion during its operational lifecycle.

8.4. Commercial Potential
The commercial potential of the AHAPS can be assessed based on two aspects. These aspects will be investigated in this section. It starts with a sales price determination, which is discussed in Section 8.4.1. Secondly, an estimation of the return on investment (ROI) is made in Section 8.4.2.

8.4.1. Sales Price Determination

The sales price of the AHAPS is not just the summation of the materials and manufacturing costs. The product is just a detailed conceptual design at this moment, meaning that a lot of further development is necessary before the product can be tested, certified, and sold. Additionally, the company that sells the AHAPS has to make a profit. The sales price can be roughly estimated from estimations of the costs of each aspect named above. An overview of the non-recurring costs is shown in Table 8.1.

Table 8.1: Breakdown of the components that make up the non-recurring costs of the AHAPS.

Component	**Non-recurring Cost (FY26)**
Design finalisation	€15,300,000
Verification & Validation	€92,500
Certification	€250,000
Total	€15,642,500

The further design cost is estimated from a weighted average of development costs for space projects presented at NASA in 2021[1]. The weighted average is calculated from two categories, namely "Robotics, telerobotics, and autonomous systems" on the one hand, and "Science instruments, observatories, and sensor systems" on the other hand. These two categories were selected as they most closely matched the AHAPS system. The design finalisation cost comes down to €15,266,431.34. This empirical estimate is then conservatively rounded up to €15,300,000, to account for the inaccuracy of the cost estimate. Next, the verification and the validation procedure of the product is estimated to be €92.500 in total. This includes €25.000 for the use of a low-speed wind tunnel for 5 days and €22,500 for the use of a temperature chamber for 15 days[12]. The remainder of the cost is estimated from engineering judgement for use of a simulation and control lab, a power test bench, a surface test area, and an outdoor test field. Lastly, certification of the AHAPS is to be done by a pre-flight test campaign and a two-month flight test. The pre-flight test campaign lasts one week, and with 10 personnel, the cost of this campaign is estimated to be €50,000[3]. Additionally, the costs for the flight test are conservatively estimated from truck rental and the salaries of flight engineers[43]. They are €200,000, bringing the total certification costs to €250,000.

Based on the business case as described in Section 3.4, it is reasonable to estimate a total amount of 1000 AHAPS being sold. All the non-recurring costs are thus divided by 1000 to obtain the total non-recurring costs per unit of €15,700. The recurring costs, being the costs for materials and manufacturing, are taken to be equal to the maximum allowable cost from **REQ-STK-6.1**, which is €900,000. The total cost of the product is thus €915,700. A profit margin of 20 % is applied to this product cost, which results in the sales price being at least €1,098,840. This is rounded to €1.1M. A total breakdown of the sales price is shown in Table 8.2.

Table 8.2: Breakdown of the sales price of one AHAPS unit.

Component	**Sales-price contribution**
Non-recurring costs	€15,608.93
Materials and manufacturing	€900,000
Profit margin	20%
Total minimum sales price per unit	€1,100,000

The sales price can be compared to that of the Airbus Zephyr 8S, which was sold to the British Ministry of

[1] https://www.researchgate.net/publication/351854164_Advanced_Cost_Estimating_Methodologies_for_Conceptual_Stage_Technology_Develop [cited 15 June 2026]

[2] https://www.associatedenvironmentalsystems.com/blog/breaking-down-the-cost-of-test-chambers-what-youre-paying-for [cited 28 May 2026]

[3] https://www.glassdoor.nl/Salaries/flight-test-engineer-salary-SRCH_KO0%2C20.htm? [cited 11 May 2026]

[4] https://www.esatrucks.eu/nl/onze-diensten/vrachtwagenverhuur [cited 11 May 2026]

Defence for €5.73M per unit as part of an order of 3 units[1]. This price was agreed on in 2020, when Airbus had announced to pursue serial production of the Zephyr 8S, potentially lowering the price[2]. Nonetheless, the sales price of the AHAPS can be considered very competitive, providing the same functionality as the Zephyr 8S, but at a much more affordable price.

8.4.2. Return On Investment

The AHAPS is intended to be used mostly by non-profit organisations, such as governments, universities, and research institutes. It is therefore less useful to quantify a specific return on investment figure. Instead, a case is made as to why the AHAPS is best suited to perform the various missions, providing a qualitative justification for the employment of the AHAPS. The services that are subject to the investigation are surveillance, communications, and research. The systems that are included in the investigation are the AHAPS presented in this report, a standard satellite in LEO, and the Lockheed Martin U-2 aircraft. Some qualitative characteristics of each system are determined, such as coverage, time resolution, and flexibility. To conclude, the costs of each system providing these services are estimated from acquisition costs and operating costs.

Surveillance

When a certain area of interest is monitored for a prolonged period of time, the operator wants the temporal and spatial resolutions to be as high as possible. The satellite in LEO cannot provide the preferred temporal resolution, as it only flies over the area of interest a couple of times per day. In contrast, the AHAPS is able to continuously loiter over the area to provide as much data as the bandwidth of the communication link allows. It does this with only limited intervention by humans, which it requires at most once per day. The U-2 is also able to provide high data rates, but it requires a human flying the aircraft, as well as fuel. Additionally, several aircraft are required as its endurance does not suffice, and the pilot has to rest after a couple of flight hours. Another characteristic that is relevant for the monitoring of an area of interest is data type. Different use cases might require different sensory equipment. Examples are regular cameras, infrared cameras, radars, or microphones. The AHAPS offers high flexibility in this regard, due to its modularity. The sensors can simply be replaced by a different set on demand and it is designed to make this process as simple as possible. It just requires attaching the payload to the structure and plugging in a power cable and a data cable. The satellite in LEO provides none of this flexibility. Once it is launched, its payload is fixed. Additionally, its higher altitude is a disadvantage for its spatial resolution. The U-2, on the other hand, is capable of providing the same flexibility. However, this, again, comes at a way higher cost. Dedicated crew has to be available at all times and the ground base is much more sophisticated than for the AHAPS, which requires just a flat surface to operate.

Communication

Another mission well suited to the AHAPS is communications. Specifically, delivering a data link to rural areas. Since it can remain airborne for weeks at a time, it offers a reliable, continuous communications link to the region. Satellites, by contrast, can only maintain line of sight with the area of interest for a few minutes per orbit. Therefore, achieving continuous coverage would require a large satellite network, substantially driving up costs. The capabilities of the U-2 also fall short here. Its endurance is limited to less than a day. As a result, the communication link is lost at least every day when one aircraft is available. If a fleet of multiple aircraft is deployed, this comes with significantly higher operating costs compared to the AHAPS. Also, it is less effective in rural areas as these often do not have the required infrastructure available to operate the U-2.

Research

The third regular use case of the AHAPS is specifically of interest to universities and research institutions. They want as many data points as they can get. They also usually have limited liquidity at their disposal, inducing the need for an affordable platform. This is where the AHAPS excels. It is significantly more affordable, both in acquisition and in operation costs, than a satellite in LEO and a U-2 aircraft. Universities and

[1] https://www.usni.org/magazines/proceedings/2020/december/bring-flexibility-fonops-haps [cited 16 June 2026]

[2] https://aerospaceglobalnews.com/news/airbus-opens-first-serial-production-facility-for-zephyr-high-altitude-pseudo-satellites/ [cited 16 June 2026]

research institutes can often invest in just one AHAPS, making the adaptability an important asset. It enables deployment for various research projects in various locations. The AHAPS can easily be transported to any area of interest, be equipped with the relevant instruments and take-off. The time between the idea for the research and the data acquisition is a few weeks at most. This can be repeated multiple times per year, providing the capacity for multiple research projects per year by just one AHAPS. In contrast, the satellite in LEO and the U-2 offer none of these capabilities. In case of the satellite, years of planning and design precede the start of actual measurements. For the Lockheed Martin U-2, dedicated infrastructure and airbases are required, as well as complete flight crews.

To conclude, an overview of the qualitative characteristics of the different systems is given in Table 8.3. It is clear that the AHAPS is capable of providing high quality services at the same level as the U-2 and at an even higher level than the satellite, both in temporal and spatial resolution. All these capabilities are accessible at a much lower price, both in acquisition and in operation.

Table 8.3: Comparison of different systems providing the services of surveillance, communication and research.

Characteristic	**AHAPS**	**Satellite in LEO**	**Lockheed Martin U-2**
Adaptability	High	None	High
Temporal resolution	High	Low	High
Spatial resolution	High	Low	High
Ease of use	High	High	Low
Acquisition cost	Low	High	High
Operation cost	Low	Low	High

9. Discussion and Conclusion

The Adaptable High-Altitude Platform System (AHAPS) was designed to fill the gap between Low Earth Orbit (LEO) satellites and currently available high-altitude platform systems. This was done by offering an affordable, highly modular, adaptable, and reliable platform system. The optimal design of a flying wing with batteries, as shown in Figure 9.1, was sized through a preliminary and detailed conceptual design phase.

The flying wing design proved to perform best, especially in the strict transportation constraint of fitting the entire aircraft in a 20 ft ISO container by subdividing the wing planform into nine modular sections. Able to be assembled with a three-person team, the design minimises ground support. For maximum efficiency and structural integrity, the AHAPS is composed of lightweight CFRP for the spar, ribs, and propulsion structures, paired with a lightweight mylar for the skin, keeping the mass low while delivering the necessary strength.

To satisfy the ambitious performance requirement of maintaining a 28 day continuous loiter at 60,000 ft year-round between latitudes 30°N and 30°S, the AHAPS makes use of industry-leading 500 Wh/kg Amprius batteries together with a 30 % efficient solar panel configuration. Four distributed propulsion systems consisting of optimised stratospheric propellers and brushless DC motors produce the thrust required to take off, climb, and loiter as efficiently as possible.

Although this report describes the comprehensive design of the AHAPS, several limitations, mainly driven by the seven week design constraint, must be acknowledged. Firstly, the structural sizing relied on quasi-static gust load approximations. While a conservative approach was taken, a high aspect ratio and lightweight wing are highly sensitive to dynamic aeroelastic effects, which can be taken into account later through flutter and dynamic load analyses. Secondly, the impact of cosmic radiation at 60,000ft on several critical subsystems was omitted. Although the AHAPS features several systems with watchdog mechanisms and physical shielding, it should still be evaluated before prototyping. Lastly, the thermal management of the full system should be analysed in depth. Operating in an environment of −60°C, mainly the power and computer system should be simulated and undergo physical testing.

To summarise, this report outlines the design of the AHAPS, which fulfills all core stakeholder requirements and mission objectives by being a sustainable, modular, and autonomous flying-wing aircraft capable of 28 day continuous stratospheric operations at 60,000 ft with a 20 kg payload. With the competitive unit price of €1.1 million, the AHAPS proves to be a great alternative to existing Low Earth Orbit (LEO) satellites and existing stratospheric platform systems, making it suitable for telecommunications, research, or use in developing nations. While further simulation and validation can be done in areas like radiation, heat management, and aeroelasticity, the AHAPS establishes a robust foundation for a new generation of high-altitude platform systems.

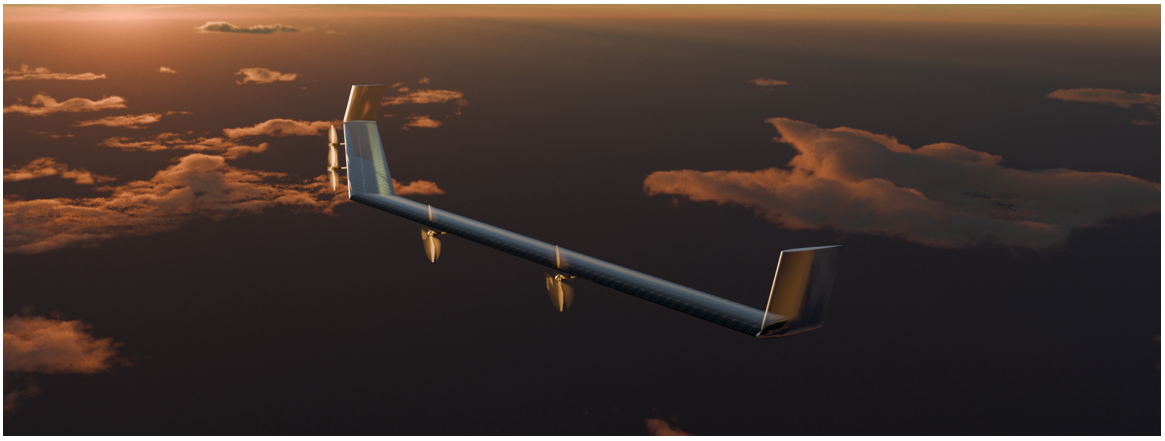

Figure 9.1: Render of the final design of the AHAPS.

Bibliography

[1] Ribeiro, J. S. and Gomes, J. D. O., "Proposed framework for end-of-life aircraft recycling," *Procedia CIRP*, vol. 26, pp. 311–316, 2015, ISSN: 22128271. DOI: 10.1016/j.procir.2014.07.048.

[2] "MC-p-11-15a: Lifecycle emissions report," Zemo Partnership, 2015.

[3] Sharpe, P. D., "AeroSandbox: A differentiable framework for aircraft design optimization," Masters Thesis, Massachusetts Institute of Technology, 2021.

[4] van Paassen, M. M., "AE3-200 project title: AHAPS; adaptable high altitude platform system mission objective," 2026.

[5] Haoran, Z., Wenjie, Y., and Huibin, Z., "UnmannedAerial vehicles rescue system design and traffic model planning," vol. 11, November 2021. DOI: 10.3390/app112110481.

[6] Nickol, C., Guynn, M., Kohout, L., and Ozoroski, T., "High altitude long endurance air vehicle analysis of alternatives and technology requirements development," in *45th AIAA Aerospace Sciences Meeting and Exhibit*, Reno, Nevada: American Institute of Aeronautics and Astronautics, January 8, 2007, ISBN: 9781624100123. DOI: 10.2514/6.2007-1050.

[7] "High altitude platforms market (2024 - 2030)," Grand View Research, GVR-4-68040-164-0, 2023.

[8] "High altitude pseudo satellite haps market," MarketsandMarkets, AS8834, October 2023.

[9] "High-altitude pseudo satellites market size, share, and industry analysis," Fortune Business Insights, FBI115062, April 2026.

[10] Chandwade Ganesh, "High altitude platforms (HAPs) market," Credence Research, 6809, 2023.

[11] "HAPS market report research study on high-altitude pseudo-satellites," Frontex: European Border and Coast Guard Agency, 2023.

[12] Neumann, F., Ossenkopp, A., Chowdhury, K., Hendrick, P., and Sarfo, S., "Sustainable skies: Technical and regulatory considerations for the use of hydrogen as a lifting gas for LTA platforms in the european union," 9 pages, 2023, Artwork Size: 9 pages Medium: PDF. DOI: 10.13009/EUCASS2023-954.

[13] Pawson, S. et al., "The tropical upper troposphere and lower stratosphere in the GEOS-2 GCM," *Advances in Space Research*, vol. 27, no. 8, pp. 1457–1465, January 2001, ISSN: 02731177. DOI: 10.1016/S0273-1177(01)00214-9.

[14] Kasten, F. and Czeplak, G., "Solar and terrestrial radiation dependent on the amount and type of cloud," *Solar Energy*, vol. 24, no. 2, pp. 177–189, 1980, ISSN: 0038092X. DOI: 10.1016/0038-092X(80)90391-6.

[15] Cassir, M., Jones, D., Ringuedé, A., and Lair, V., "Electrochemical devices for energy: Fuel cells and electrolytic cells," in *Handbook of Membrane Reactors*, Elsevier, 2013, pp. 553–606, ISBN: 9780857094155. DOI: 10.1533/9780857097347.3.553.

[16] Basutkar, A., Baruah, K., and Kudari, S. K., "Frequency analysis of aircraft wing using FEM," in *Recent Trends in Mechanical Engineering*, Narasimham, G. S. V. L., Babu, A. V., Reddy, S. S., and Dhanasekaran, R., Eds., Series Title: Lecture Notes in Mechanical Engineering, Singapore: Springer Singapore, 2020, pp. 527–533, ISBN: 978-981-15-1123-3 978-981-15-1124-0. DOI: 10.1007/978-981-15-1124-0_46.

[17] Gonzalo, J., López, D., Domínguez, D., García, A., and Escapa, A., "On the capabilities and limitations of high altitude pseudo-satellites," *Progress in Aerospace Sciences*, vol. 98, pp. 37–56, April 2018, ISSN: 03760421. DOI: 10.1016/j.paerosci.2018.03.006.

[18] Hamada, A., Sultan, A., and Abdelrahman, M., "Design, build and fly a flying wing," *Athens Journal of echnology & Engineering*, vol. 5, no. 3, pp. 223–250, August 31, 2018, ISSN: 22418237. DOI: 10.30958/ajte.5-3-2.

[19] Asaro, S., Atmaca, D., Van Kampen, E.-J., and Vos, R., "Control surface allocation based on offline handling quality simulations for a flying wing aircraft," *CEAS Aeronautical Journal*, October 22, 2025, ISSN: 1869-5582, 1869-5590. DOI: 10.1007/s13272-025-00906-2.

[20] Johanning, A. and Scholz, D., "Propeller efficiency calculation in conceptual aircraft design," Hamburg University of Applied Sciences (HAW), Hamburg, Technical note, August 13, 2012, p. 23.

[21] Roskam, J., *Airplane Design Part VIII: Airplane Cost Estimation: Design, Development, Manufacturing and Operating*, 5th ed. 2018, ISBN: 978-1-884885-55-6.

[22] Merlin, P. W., *Unlimited horizons: design and development of the U-2* (NASA aeronautics book series). Washington, DC: National Aeronautics and Space Administration, 2015, 293 pp., ISBN: 978-1-62683-025-7.

[23] Najafi, Y., "Solar powered aerial communicator," 2011.

[24] Megson, T., *Aircraft Structures for Engineering Students*. Elsevier, 2022, ISBN: 978-0-12-822868-5. DOI: 10.1016/C2019-0-03113-5.

[25] Alderliesten, R., *Introduction to Aerospace Structures and Materials*. Delft: TU Delft OPEN Books, 2018, ISBN: 978-94-6366-075-4. DOI: 10.5074/t.2018.003.

[26] Nusselt, W., "Fundamental law of heat transfer [natural and forced convection]," National Research Council Canada, 1957. DOI: 10.4224/20331615.

[27] Alsahlani, A. A. and Rahulan, T., "Aerofoil design for unmanned high-altitude aft-swept flying wings," *Journal of Aerospace Technology and Management*, vol. 9, no. 3, pp. 335–345, August 3, 2017, ISSN: 2175-9146. DOI: 10.5028/jatm.v9i3.838.

[28] Sharpe, P. D., "Accelerating practical engineering design optimization with computational graph transformations," Ph.D. dissertation, Massachusetts Institute of Technology, 2024.

[29] Güzelbey, İ. H., Eraslan, Y., and Doğru, M. H., "Effects of taper ratio on aircraft wing aerodynamic parameters: A comperative study," *European Mechanical Science*, vol. 3, no. 1, pp. 18–23, March 20, 2019, ISSN: 2587-1110. DOI: 10.26701/ems.487516.

[30] Jang, J.-H. and Ahn, S.-H., "Optimum design of UAV wing skin structure with a high aspect ratio using variable laminate stiffness," *Applied Sciences*, vol. 12, no. 19, p. 9436, September 21, 2022, ISSN: 2076-3417. DOI: 10.3390/app12199436.

[31] Chiozzotto, G., "Conceptual design method for the wing weight estimation of strut-braced wing aircraft," 2015.

[32] Nita, M. and Scholz, D., "Estimating the oswald factor from basic aircraft geometrical parameters," presented at the Deutscher Luft- und Raumfahrtkongress, Deutsche Gesellschaft für Luft- und Raumfahrt - Lilienthal-Oberth e.V., 2012.

[33] Bierig, A., Nikodem, F., and Rothe, D., "General design considerations for solar-electric high-altitude long-endurance aircraft," in *34th Congress of the International Council of the Aeronautical Sciences*, Braunschweig: DLR, September 9, 2024.

[34] Cooper, P., "The absorption of radiation in solar stills," *Solar Energy*, vol. 12, no. 3, pp. 333–346, 1969, ISSN: 0038092X. DOI: 10.1016/0038-092X(69)90047-4.

[35] Law, D. C. et al., "Lightweight, flexible, high-efficiency III-v multijunction cells," in *2006 IEEE 4th World Conference on Photovoltaic Energy Conference*, Waikoloa, HI: IEEE, May 2006, pp. 1879–1882, ISBN: 978-1-4244-0016-4. DOI: 10.1109/WCPEC.2006.279862.

[36] Lohmeyer, W. Q., Aniceto, R. J., Cahoy, K., and Carlton, A., "Solar array degradation on geostationary communications satellites: The quantification of annual degradation and degradation over solar proton events," *International Journal of Space Science and Engineering*, vol. 5, no. 1, p. 61, 2018, ISSN: 2048-8459, 2048-8467. DOI: 10.1504/IJSPACESE.2018.090549.

[37] Herasimenka, S. et al., "Solving long lead times and the high cost of space solar panels with upgraded silicon technology," *Small Satellite Conference*, August 9, 2023. DOI: https://doi.org/10.26077/g9ht-hv69.

[38] Meeus, J., *Astronomical algorithms*, 2nd ed. Richmond, Va: Willmann-Bell, 1998, 477 pp., ISBN: 978-0-943396-61-3.

[39] Hassanzadeh, M., Etezadi-Amoli, M., and Fadali, M., "Practical approach for sub-hourly and hourly prediction of PV power output," in *North American Power Symposium 2010*, Arlington, TX, USA: IEEE, September 2010, pp. 1–5, ISBN: 978-1-4244-8046-3 978-1-4244-8047-0. DOI: 10.1109/NAPS.2010.5618944.

[40] Shreestha, R., "Lithium sulfur battery market - size, share, industry trends, and forecasts (2025-2035)," Consegic Business Intelligence, CBI_3453, March 2026.

[41] Jenish, C. and Jenish, M., "Performance analysis of BLDC motors and its various control strategies," April 28, 2023. DOI: 10.55041/IJSREM18002.

[42] Zhou, K., Gu, M., and Zheng, Y., "Design of high-speed motor system for EV based on 1200 v SiC-MOSFET power module," *Actuators*, vol. 14, no. 5, p. 216, May 2025, ISSN: 2076-0825. DOI: 10.3390/act14050216.

[43] Raymer, D. P., *Aircraft design: a conceptual approach* (AIAA education series), 2nd ed. Washington (D.C.): American institute of aeronautics and astronautics, 1992, ISBN: 978-0-930403-51-5.

[44] Giljarhus, K. E. T., Porcarelli, A., and Apeland, J., "Investigation of rotor efficiency with varying rotor pitch angle for a coaxial drone," *Drones*, vol. 6, no. 4, p. 91, April 2022, ISSN: 2504-446X. DOI: 10.3390/drones6040091.

[45] Liu, X. and He, W., "Performance calculation and design of stratospheric propeller," *IEEE Access*, vol. 5, pp. 14 358–14 368, 2017, ISSN: 2169-3536. DOI: 10.1109/ACCESS.2017.2725303.

[46] García-Gutiérrez, A., Gonzalo, J., Domínguez, D., López, D., and Escapa, A., "Aerodynamic optimization of propellers for high altitude pseudo-satellites," *Aerospace Science and Technology*, vol. 96, p. 105 562, January 1, 2020, ISSN: 1270-9638. DOI: 10.1016/j.ast.2019.105562.

[47] Wei, K., Wu, J., Zhang, J., Peng, G., and Rong, H., "Aerodynamic optimization of a propeller airfoil at low reynolds numbers," *Journal of Physics: Conference Series*, vol. 2369, no. 1, p. 012 006, November 2022, Num Pages: 012006, ISSN: 17426588. DOI: 10.1088/1742-6596/2369/1/012006.

[48] Reuben, U. J., Hiraki, K., and Shohei, M., "NON-LINEAR EFFECTS OF AIRFOIL FORCE DATA ON DESIGN PERFORMANCE OF a LOW-REYNOLDS NUMBER PROPELLER," *International Journal of Research -GRANTHAALAYAH*, vol. 6, no. 8, pp. 196–123, August 31, 2018, ISSN: 2350-0530, 2394-3629. DOI: 10.29121/granthaalayah.v6.i8.2018.1450.

[49] Ma, R., Zhong, B., and Liu, P., "Optimization design study of low-reynolds-number high-lift airfoils for the high-efficiency propeller of low-dynamic vehicles in stratosphere," *Science China Technological Sciences*, vol. 53, no. 10, pp. 2792–2807, October 1, 2010, ISSN: 1862-281X. DOI: 10.1007/s11431-010-4087-0.

[50] Dorfling, J. and Rokhsaz, K., "Constrained and unconstrained propeller blade optimization," *Journal of Aircraft*, vol. 52, no. 4, pp. 1179–1188, July 2015, ISSN: 0021-8669. DOI: 10.2514/1.C032859.

[51] Ciani, L. and Catelani, M., "A fault tolerant architecture to avoid the effects of single event upset (SEU) in avionics applications," *Measurement*, vol. 54, pp. 256–263, August 2014, ISSN: 02632241. DOI: 10.1016/j.measurement.2014.02.018.

[52] Zhang, L., *Primopal PBLR105fh-671118 price*, E-mail, June 9, 2026.

[53] Mulder, J. et al., "AE3202 flight dynamics lecture notes," Technische Universiteit Delft, March 24, 2013, p. 570.

[54] Smith, D. M., Maskara, A., and Boes, U., "Aerogel-based thermal insulation," *Journal of Non-Crystalline Solids*, vol. 225, pp. 254–259, April 1998, ISSN: 00223093. DOI: 10.1016/S0022-3093(98)00125-2.

[55] Megson, T. H. G., "Chapter 8 - columns," in *Aircraft Structures for Engineering Students (Seventh Edition)*, ser. Aerospace Engineering, Butterworth-Heinemann, January 1, 2022, pp. 283–329, ISBN: 978-0-12-822868-5. DOI: 10.1016/B978-0-12-822868-5.00008-5.

[56] Gudmundsson, S., "Aircraft drag analysis," in *General Aviation Aircraft Design*, Elsevier, 2022, pp. 657–752, ISBN: 9780128184653. DOI: 10.1016/B978-0-12-818465-3.00016-1.

[57] Torenbeek, E., *Synthesis of subsonic airplane design: an introduction to the preliminary design of subsonic general aviation and transport aircraft, with emphasis on layout, aerodynamic design, propulsion and performance*, Repr. Dordrecht: Kluwer Academic Publ, 1999, 598 pp., ISBN: 978-90-247-2724-7.

[58] Koelmans, A. A., Redondo-Hasselerharm, P. E., Nor, N. H. M., De Ruijter, V. N., Mintenig, S. M., and Kooi, M., "Risk assessment of microplastic particles," *Nature Reviews Materials*, vol. 7, no. 2, pp. 138–152, January 21, 2022, ISSN: 2058-8437. DOI: 10.1038/s41578-021-00411-y.

[59] Mamat, R., Rashid, M. I. M., Syahir, A., Erdiwansyah, Yusop, A. F., and Tamimi, A., "Carbon fibre for applications in aerospace: A review," *Journal of Alloys and Metallurgical Systems*, vol. 12, p. 100 227, December 2025, ISSN: 29499178. DOI: 10.1016/j.jalmes.2025.100227.

[60] Takeda, O. and Okabe, T. H., "Current status of titanium recycling and related technologies," *JOM*, vol. 71, no. 6, pp. 1981–1990, June 2019, ISSN: 1047-4838, 1543-1851. DOI: 10.1007/s11837-018-3278-1.

[61] Tao, M. et al., "Major challenges and opportunities in silicon solar module recycling," *Progress in Photovoltaics: Research and Applications*, vol. 28, no. 10, pp. 1077–1088, October 2020, ISSN: 1062-7995, 1099-159X. DOI: 10.1002/pip.3316.

[62] Arslan, F., Celik, C., and Arslan, C., "Recycling of waste electrical cables," *Material Science & Engineering International Journal*, vol. 3, no. 4, 2019, ISSN: 25749927. DOI: 10.15406/mseij.2019.03.00099.

[63] Page, H., Griffiths, C. A., and Thomas, A. J., "Economic and environmental analysis of aluminium recycling from retired commercial aircraft," *Sustainability*, vol. 17, no. 19, p. 8556, September 24, 2025, ISSN: 2071-1050. DOI: 10.3390/su17198556.

[64] Liu, X., Su, Q., Zhu, J., and Song, X., "The aging behavior and life prediction of CFRP rods under a hygrothermal environment," *Polymers*, vol. 15, no. 11, p. 2490, May 28, 2023, ISSN: 2073-4360. DOI: 10.3390/polym15112490.

[65] Emmons, R., "An indicated specular degradation rate for aluminized mylar surfaces in near-earth orbit from recent photometric observations of the echo i satellite," NASA, Contractor Report (CR) NASA-CR-80175, June 17, 1964.

[66] "Certification specifications and acceptable means of compliance for large aeroplanes (CS-25)," European Union Aviation Safety Agency, Amendment 28, December 15, 2023.

[67] "Certification specifications, acceptable means of compliance and guidance material for sailplanes and powered sailplanes (CS-22)," European Union Aviation Safety Agency, Amendment 3, September 15, 2021.

[68] "Certification specifications and acceptable means of compliance for normal, utility, aerobatic, an commuter category aeroplanes (CS-23)," European Union Aviation Safety Agency, Amendment 4, July 15, 2015.

[69] Voß, A., Handojo, V., Weiser, C., and Niemann, S., "Preparation of loads and aeroelastic analyses of a high altitude, long endurance, solar electric aircraft," presented at the AEC2020 Aerospace Europe Conference, DLR, February 25, 2020.

[70] Ricciardi, A. P., Patil, M. J., Canfield, R. A., and Lindsley, N., "Evaluation of quasi-static gust loads certification methods for high-altitude long-endurance aircraft," *Journal of Aircraft*, vol. 50, no. 2, pp. 457–468, March 2013, ISSN: 0021-8669, 1533-3868. DOI: 10.2514/1.C031872.

[71] Bouffard, P. M. and Michini, B. J., "Unmanned aerial vehicle area surveying," U.S. Patent 12475802B2.

[72] *Shipping lithium ion batteries and lithium ion batteries in/with equipment: Implementation of dangerous goods transport regulations*, April 2025.

[73] Ma, Y. and Elham, A., "Designing high aspect ratio wings: A review of concepts and approaches," *Progress in Aerospace Sciences*, vol. 145, p. 100 983, February 2024, ISSN: 03760421. DOI: 10.1016/j.paerosci.2024.100983.

[74] Kapur, K. C., *Reliability engineering* (Wiley series in systems engineering and management), in collab. with Pecht, M. Hoboken, N.J: J. Wiley & Sons, 2014, 1 p., ISBN: 978-1-118-14067-3 978-1-118-84179-2.

[75] Guo, J., "Systems engineering for aerospace design (AE3211-i)," 2026.

[76] Eckstein, W., *Computer simulation of ion-solid interactions* (Springer series in materials science 10). Berlin New York Paris [etc.]: Springer, 1991, ISBN: 9783540190578 9780387190570.

[77] Gao, Y. et al., "Radiation effects on lithium metal batteries," *The Innovation*, vol. 4, no. 4, p. 100 468, July 2023, ISSN: 26666758. DOI: 10.1016/j.xinn.2023.100468.

[78] Taber, A. and Normand, E., "Single event upset in avionics," *IEEE Transactions on Nuclear Science*, vol. 40, no. 2, pp. 120–126, April 1993, ISSN: 0018-9499, 1558-1578. DOI: 10.1109/23.212327.

[79] Hasan, Y. J. et al., "Flight mechanical analysis of a solar-powered high-altitude platform," *CEAS Aeronautical Journal*, vol. 14, no. 1, pp. 201–223, January 2023, ISSN: 1869-5582, 1869-5590. DOI: 10.1007/s13272-022-00621-2.

[80] Morfiadakis, E., Glinou, G., and Koulouvari, M., "The suitability of the von karman spectrum for the structure of turbulence in a complex terrain wind farm," *Journal of Wind Engineering and Industrial Aerodynamics*, vol. 62, no. 2, pp. 237–257, September 1996, ISSN: 01676105. DOI: 10.1016/S0167-6105(96)00059-1.

[81] Li, C. and Yang, Y., "A self-powered vibration sensor for real-time vibration monitoring and aeroelastic instability detection in tiltrotor aircraft transition," *AIP Advances*, vol. 15, no. 9, p. 095 314, September 1, 2025, ISSN: 2158-3226. DOI: 10.1063/5.0288836.

[82] Mu, X., Huang, R., Zou, Q., Zhou, X., Liu, H., and Hu, H., "Rigid-elastic-coupled aeroservoelastic modeling and flight test verification of a flexible flying-wing aircraft," *Journal of Sound and Vibration*, vol. 621, p. 119 440, January 2026, ISSN: 0022460X. DOI: 10.1016/j.jsv.2025.119440.

[83] Hirose, T., Tanigawa, H., Ando, M., Kohyama, A., Katoh, Y., and Narui, M., "Radiation effects on low cycle fatigue properties of reduced activation ferritic/martensitic steels," *Journal of Nuclear Materials*, vol. 307-311, pp. 304–307, December 2002, ISSN: 00223115. DOI: 10.1016/S0022-3115(02)01199-6.

[84] Binder, S., Wildschek, A., and De Breuker, R., "The interaction between active aeroelastic control and structural tailoring in aeroservoelastic wing design," *Aerospace Science and Technology*, vol. 110, p. 106 516, March 2021, ISSN: 12709638. DOI: 10.1016/j.ast.2021.106516.

[85] Nikbay, M. and Acar, P., "Flutter based aeroelastic optimization of an aircraft wing with analytical approach," in *53rd AIAA / ASME / ASCE / AHS / ASC Structures, Structural Dynamics and Materials Conference*, Honolulu, Hawaii: American Institute of Aeronautics and Astronautics, April 23, 2012, ISBN: 978-1-60086-937-2. DOI: 10.2514/6.2012-1796.

[86] Srisuriyachot, J. et al., "Quantification of the thermal expansion of carbon fibres in CFRP at low temperatures using x-ray diffraction," *Composites Part B: Engineering*, vol. 305, p. 112 697, October 2025, ISSN: 13598368. DOI: 10.1016/j.compositesb.2025.112697.

[87] Lancelot, P. and De Breuker, R., "Unsteady non-linear control surface modelling for aeroservoelastic applications," *Journal of Aeroelasticity and Structural Dynamics*, no. 1, pp. 23–44, 2020, ISSN: 1974-5117. DOI: 10.3293/asdj.2020.56.

[88] Fonzi, N., Ricci, S., and Livne, E., "Wind tunnel tests of an aeroelastic model with multiple control surface freeplay nonlinearities," *Journal of Fluids and Structures*, vol. 136, p. 104 332, August 2025, ISSN: 08899746. DOI: 10.1016/j.jfluidstructs.2025.104332.

[89] Tan, Q., Ding, Y., Liu, J., and Sui, C., "CFD-based hull-engine-propeller matching study after retrofitting propeller boss-cap-fin (PBCF)," *Ocean Engineering*, vol. 285, p. 115 364, October 2023, ISSN: 00298018. DOI: 10.1016/j.oceaneng.2023.115364.

[90] J. Červinka*, R. Kulhánek, Z. Pátek, V. Kumar, "SIMULATION OF PROPELLER EFFECT IN WIND TUNNEL," presented at the 30th Congress of the international council of aeronautical sciences, Praha, Czech Republic: *VZLÚ - Aerospace Research and Test Establishment, September 25, 2016.

[91] Kurt, G. et al., *A vision and framework for the high altitude platform station (HAPS) networks of the future*, March 18, 2021. DOI: 10.48550/arXiv.2007.15088. arXiv: 2007.15088.

[92] Hu, L., Yan, X., and Yuan, Y., "Development and challenges of autonomous electric vertical take-off and landing aircraft," *Heliyon*, vol. 11, no. 1, e41055, January 2025, ISSN: 24058440. DOI: 10.1016/j.heliyon.2024.e41055.

[93] El-Hofy, M. H., "Milling/routing of carbon fibre reinforced plastic (CFRP) composites," d_ph, University of Birmingham, December 2014, 288 pp.

Functional Breakdown Structure

- **Product Initiation**
  - **F.0.A** Design
    - **F.0.A.1** Follow WFD
  - **F.0.B** Manufacture
    - **F.0.B.1** Initiate Work Environment
    - **F.0.B.2** Acquire Raw materials
    - **F.0.B.3** Process Raw Materials to Parts
    - **F.0.B.4** Acquire Off-the-shelve Parts/Components
    - **F.0.B.5** Assemble Parts/Components
    - **F.0.B.6** Assemble Subsubsystems
    - **F.0.B.7** Assemble Subsystems
    - **F.0.B.8** Assemble System
    - **F.0.B.9** Put in ISO20 Container
  - **F.0.C.** Document
    - **F.0.C.1** Write Assembly Plan
    - **F.0.C.2** Write Item List
    - **F.0.C.3** Write Inspection Checklist
    - **F.0.C.4** Write User Manual
    - **F.0.C.5** Write Maintenance Plan
    - **F.0.C.6** Write End-of-Life Plan
- **Product Introduction**
  - **F.1** Transport
    - **F.1.1** Load into ISO20 Container
    - **F.1.2** Move to Region of Interest (Overseas)
    - **F.1.3** Get Towed by Truck
    - **F.1.4** Drive to Location of Deployment
  - **F.2** Assemble
    - **F.2.1** Unload from ISO20 Container
    - **F.2.2** Assemble According to User Manual
    - **F.2.3** Clean up Assembly
    - **F.2.4** Set Up Monitoring System
- **Product Life**
  - **F.3** Communicate
    - **F.3.1** Establish External Communication Link
      - **F.3.1.1** Point Antenna
      - **F.3.1.2** Generate Power Following Link Budget
      - **F.3.1.3** Process Incoming Signal
    - **F.3.2** Maintain External Communcation Link
      - **F.3.2.1** Send Data to Communication System
      - **F.3.2.2** Point Antenna for Sending
      - **F.3.2.3** Generate Signal Power Following Link Budget
      - **F.3.2.4** Point Antenna for Receiving
      - **F.3.2.5** Send Data to Computer System
      - **F.3.2.6** Process External Data
    - **F.3.3** Extract Internal Data
      - **F.3.3.1** Gather Payload Sensor Data
      - **F.3.3.2** Send Payload Sensor Data to Computer System
      - **F.3.3.3** Gather Flight Condition Sensor Data
      - **F.3.3.4** Send Flight Condition Sensor Data to Computer System
    - **F.3.4** Process Data
      - **F.3.4.1** Apply Controllers
      - **F.3.4.2** Save Data
    - **F.3.5** Execute Control
      - **F.3.5.1** Perform Payload Command
      - **F.3.5.2** Perform Control Command
      - **F.3.5.3** Perform Propulsion Command
      - **F.3.5.4** Perform Power Command
  - **F.4** Take-off
    - **F.4.1** Prepare Runway
    - **F.4.2** Prepare for Take-off
    - **F.3.3** Initiate Take-off Configuration
      - **F.4.3.1** Configure Airframe System for Take-off
      - **F.4.3.2** Configure Power System for Take-off
      - **F.4.3.3** Configure Payload for Take-off
      - **F.4.3.4** Configure Control System for Take-off
      - **F.4.3.5** Configure Propulsion System for Take-off
    - **F.4.4** Execute Take-off
      - **F.4.4.1** Generate Sufficient Lift for Take-off
      - **F.4.4.2** Execute Control System Take-off Command
      - **F.4.4.3** Generate Sufficient Thrust for Take-off
    - **F.4.5** Switch to Flight Configuration
      - **F.4.5.1** Change Airframe System Config. for Flight
      - **F.4.5.2** Change Power System Config. for Flight
      - **F.4.5.3** Change Payload Config. for Flight
      - **F.4.5.4** Change Control System Config. for Flight
      - **F.4.5.5** Change Propulsion System Config. for Flight
  - **F.5** Climb
    - **F.5.1** Achieve Climb Rate
      - **F.5.1.1** Change Power System Config. for Climb
      - **F.5.1.2** Change Control System Config. for Climb
      - **F.5.1.3** Change Propulsion System Config. for Climb
    - **F.5.2** Maintain ROC According to Operations Manual
      - **F.5.2.1** Set Power System Config. According to Operation Manual
      - **F.5.2.2** Set Control System Config. According to Operation Manual
      - **F.5.2.3** Set Propulsion System Config. According to Operation Manual
    - **F.5.3** Set Rate of Climb to 0
      - **F.5.3.1** Set Power System Command for ROC = 0
      - **F.5.3.2** Set Control System Command for ROC = 0
      - **F.5.3.3** Set Propulsion System Command for ROC = 0
  - **F.6** Cruise
    - **F.6.1** Maintain Cruise
      - **F.6.1.1** Generate Sufficient Lift
      - **F.6.1.2** Generate Sufficient Power
      - **F.6.1.3** Provide Sufficient Thrust
      - **F.6.1.4** Provide Control
      - **F.6.1.5** Provide Stability
    - **F.6.2** Execute Payload Mission
      - **F.6.2.1** Go to Area of Interest
        - **F.6.2.1.1** Obtain Area of Interest
        - **F.6.2.1.2** Initiate Flight Path According to User Manual
        - **F.6.2.1.3** Change Flight Level
        - **F.6.2.1.4** Change Speed
        - **F.6.2.1.5** Change Heading
        - **F.6.2.1.6** Maintain Flight Path According to User Manual
        - **F.6.2.1.7** Maintain Flight Level
        - **F.6.2.1.8** Maintain Speed
        - **F.6.2.1.9** Maintain Heading
        - **F.6.2.1.10** Loiter at Area of Interest
      - **F.6.2.2** Dissipate Payload Heat
      - **F.6.2.3** Provide Power to Payload
      - **F.6.2.4** Provide Internal Communication
    - **F.6.3** Return to Landing Location
  - **F.7** Descend
    - **F.7.1** Achieve Rate of Descend
      - **F.7.1.1** Change Power System Config. for Descend
      - **F.7.1.2** Change Control System Config. for Descend
      - **F.7.1.3** Change Propulsion System Config. for Descend
    - **F.7.2** Maintain ROD According to Operations Manual
      - **F.7.2.1** Set Power System Config. According to Operation Manual
      - **F.7.2.2** Set Control System Config. According to Operation Manual
      - **F.7.2.3** Set Propulsion System Config. According to Operation Manual
    - **F.7.3** Prepare for Approach
  - **F.8** Land
    - **F.8.1** Maintain Stable Approach
    - **F.8.2** Switch to Landing Configuration
      - **F.8.2.1** Configure Airframe System for Landing
      - **F.8.2.2** Configure Power System for Landing
      - **F.8.2.3** Configure Payload for Landing
      - **F.8.2.4** Configure Control System for Landing
      - **F.8.2.5** Configure Propulsion System for Landing
    - **F.8.3** Execute Landing
      - **F.8.3.1** Generate Sufficient Lift for Landing
      - **F.8.3.2** Execute Control System Landing Command
      - **F.8.3.3** Generate Sufficient Thrust Lift for Landing
    - **F.8.4** Disengage Systems
      - **F.8.4.1** Disengage Computer System
      - **F.8.4.2** Disengage Power System
      - **F.8.4.3** Disengage Payload System
      - **F.8.4.4** Disengage Propulsion System
      - **F.8.4.5** Disengage Communication System
      - **F.8.4.6** Disengage Flight Condition System
  - **F.9** Disassemble
    - **F.9.1** Disassemble According to User Manual
    - **F.9.2** Clean Up Disassembly
    - **F.9.3** Load into ISO20 Container
    - **F.9.4** Transport to Maint. Location According to **F.1**
  - **F.10** Maintain
    - **F.10.1** Check Item List
    - **F.10.2** Perform Maintenance According to Maint. Plan
  - **F.11** Decommission
    - **F.11.1** Transport to EOL Location According to **F.1**
    - **F.11.2** Decomission According to EOL Plan

LEGEND:

OR

AND

F.# XXX	**REF F.#**
F.#.# XXX - Subsys X	**REF F.#.#**
F.#.#.# XXX - Subsys X	**REF F.#.#.#**
F.#.#.#.# XXX - Subsys X	**REF F.#.#.#.#**

LEGEND:

- Propulsion System
- Control System
- Power System
- Computer System
- Communication System
- Payload System
- Airframe
- Flight Condition System

Functional Flow Diagram

Product Initiation

Product Introduction

Product Life

REF Product Initiation → F.0.A Design → F.0.B Manufacture → F.0.C. Document → REF Product Introduction

REF F.0.A → F.0.A.1 Follow WFD → REF F.0.B

REF F.0.B → F.0.B.1 Initiate Work Environment → AND (F.0.B.2 Acquire Raw materials → F.0.B.3 Process Raw Materials to Parts; F.0.B.4 Acquire Off-the-shelve Parts/Components) → F.0.B.5 Assemble Parts/Components → F.0.B.6 Assemble Subsubsystems → F.0.B.7 Assemble Subsystems → F.0.B.8 Assemble System → F.0.B.9 Put in ISO20 Container → REF F.0.C

REF F.0.C → F.0.C.1 Write Assembly Plan → F.0.C.2 Write Item List → F.0.C.3 Write Inspection Checklist → F.0.C.4 Write User Manual → F.0.C.5 Write Maintenance Plan → F.0.C.6 Write End-of-Life Plan → REF Product Introduction

REF Product Life → F.1 Transport → F.2 Assemble → AND (F.3 Communicate; F.4 Take-off) → F.5 Climb → F.6 Cruise → F.7 Descend → F.8 Land → F.9 Disassemble → OR (F.10 Maintain; F.11 Decommission)

REF F.1 → F.1.1 Load into ISO20 Container → F.1.2 Move to Region of Interest (Overseas) → F.1.3 Get Towed by Truck → F.1.4 Drive to Location of Deployment → REF F.2

REF F.2 → F.2.1 Unload from ISO20 Container → F.2.2 Assemble According to User Manual → F.2.3 Clean up Assembly → F.2.4 Set Up Monitoring System → AND (REF F.3; REF F.4)

REF F.3 → AND (F.3.1 Establish External Communication Link → F.3.2 Maintain External Communcation Link; F.3.3 Extract Internal Data → F.3.4 Process Data → OR (F.3.5 Execute Control; F.3.6 Payload Control) → REF F.9)

REF F.4 → F.4.1 Prepare Runway → F.4.2 Prepare for Take-off → F.4.3 Initiate Take-off Configuration → F.4.4 Execute Take-off → F.4.5 Switch to Flight Configuration → REF F.5

REF F.5 → F.5.1 Achieve Climb Rate → F.5.2 Maintain ROC According to Operations Manual → F.5.3 Set Rate of Climb to 0 → REF F.6

REF F.6 → AND (F.6.1 Maintain Cruise; OR (F.6.2 Execute Payload Mission; F.6.3 Return to Landing Location)) → REF F.7

REF F.7 → F.7.1 Achieve Rate of Descent → F.7.2 Maintain ROD According to Operations Manual → F.7.3 Prepare for Approach → REF F.8

REF F.8 → F.8.1 Maintain Stable Approach → F.8.2 Switch to Landing Configuration → F.8.3 Execute Landing → F.8.4 Disengage Systems → REF F.9

REF F.9 → F.9.1 Disassemble According to User Manual → F.9.2 Clean Up Disassembly → F.9.3 Load into ISO20 Container → F.9.4 Transport to Maint. Location According to F.1 → OR (REF F.10; REF F.11)

REF F.10 → F.10.1 Check Item List → F.10.2 Perform Maintenance According to Maint. Plan

REF F.11 → F.11.1 Transport to EOL Location According to F.1 → F.11.2 Decomission According to EOL Plan

LEGEND:

F.# XXX — REF F.#

AND / OR

F.#.# XXX — REF F.#.#

F.#.#.# XXX — REF F.#.#.#

F.#.#.#.# XXX — REF F.#.#.#.#

Mission Systems:
- Design Team
- Manufacturing Team
- Maintenance Team
- Decommissioning Team
- User
- Product
- Combination User-Product

Functional Flow Diagram

Product Functions

F.3 Communicate → AND (F.4 Take-off; F.5 Climb; F.6 Cruise; F.7 Descend; F.8 Land; REF F.9)

REF F.3 → AND (F.3.1 Establish External; F.3.2 Maintain External; F.3.3 Extract Internal Data; F.3.4 Process Data → OR (F.3.5 Execute Control; F.3.6 Payload Control) → REF F.9)

REF F.3.1 → F.3.1.1 Point Antenna → F.3.1.2 Generate Power Following Link Budget → F.3.1.3 Process Incoming Signal → REF F.3.2

REF F.3.2 → OR (F.3.2.1 Send Data to Communication → F.3.2.2 Point Antenna for Sending → F.3.2.3 Generate Signal Power; F.3.2.4 Point Antenna for Receiving → F.3.2.5 Send Data to Computer System → F.3.2.6 Process External Data) → REF F.9

REF F.3.3 → OR (F.3.3.1 Gather Payload Sensor Data → F.3.3.2 Send Payload Sensor Data to Computer System; F.3.3.3 Gather Flight Condition Sensor Data → F.3.3.4 Send Flight Condition Sensor Data to Computer System) → REF F.3.4

REF F.3.4 → OR (F.3.4.1 Apply Controllers; F.3.4.2 Save Data) → REF F.3.5

REF F.3.5 → OR (F.3.5.1 Perform Payload Command; F.3.5.2 Perform Control Command; F.3.5.3 Perform Propulsion Command; F.3.5.4 Perform Power Command) → REF F.3.6

REF F.4 → F.4.1 Prepare Runway → F.4.2 Prepare for Take-off → F.4.3 Initiate Take-off Configuration → F.4.4 Execute Take-off → F.4.5 Switch to Flight Configuration → REF F.5

REF F.4.3 → AND (F.4.3.1 Configure Airframe System for Take-off; F.4.3.2 Configure Power System for Take-off; F.4.3.3 Configure Payload for Take-off; F.4.3.4 Configure Control System for Take-off; F.4.3.5 Configure Propulsion System for Take-off) → REF F.4.4

REF F.4.4 → AND (F.4.4.1 Generate Sufficient Lift for Take-off; F.4.4.2 Execute Control System Take-off Command; F.4.4.3 Generate Sufficient Thrust for Take-off) → REF F.4.5

REF F.4.5 → AND (F.4.5.1 Change Airframe System Config. for Flight; F.4.5.2 Change Power System Config. for Flight; F.4.5.3 Change Payload Config. for Flight; F.4.5.4 Change Control System Config. for Flight; F.4.5.5 Change Propulsion System Config. for Flight) → REF F.5

REF F.5 → F.5.1 Achieve Climb Rate → F.5.2 Maintain ROC According to Operations Manual → F.5.3 Set Rate of Climb to 0 → REF F.6

REF F.5.1 → AND (F.5.1.1 Change Power System Config. for Climb; F.5.1.2 Change Control System Config. for Climb; F.5.1.3 Change Propulsion System Config. for Climb) → REF F.5.2

REF F.5.2 → AND (F.5.2.1 Set Power System Config. According to Operation Manual; F.5.2.2 Set Control System Config. According to Operation Manual; F.5.2.3 Set Propulsion System Config. According to Operation Manual) → REF F.5.3

REF F.5.3 → AND (F.5.3.1 Set Power System Command for ROC = 0; F.5.3.2 Set Control System Command for ROC = 0; F.5.3.3 Set Propulsion System Command for ROC = 0) → REF F.6

REF F.6 → AND (F.6.1 Maintain Cruise; OR (F.6.2 Execute Payload Mission; F.6.3 Return to Landing Location)) → REF F.7

REF F.6.1 → AND (F.6.1.1 Generate Sufficient Lift; F.6.1.2 Generate Sufficient Power; F.6.1.3 Provide Sufficient Thrust; F.6.1.4 Provide Control; F.6.1.5 Provide Stability) → REF F.7

REF F.6.2 → F.6.2.1 Go to Area of Interest → AND (F.6.2.2 Dissipate Payload Heat; F.6.2.3 Provide Power to Payload; F.6.2.4 Provide Internal) → REF F.6.2.1

REF F.6.2.1 → F.6.2.1.1 Obtain Area of Interest → F.6.2.1.2 Initiate Flight Path According to User Manual → OR (F.6.2.1.3 Change Flight Level; F.6.2.1.4 Change Speed; F.6.2.1.5 Change Heading) → F.6.2.1.6 Maintain Flight Path According to User Manual → OR (F.6.2.1.7 Maintain Flight Level; F.6.2.1.8 Maintain Speed; F.6.2.1.9 Maintain Heading) → F.6.2.1.10 Loiter at Area of Interest → REF F.6.2.2.4

Transit: F.6.3 Return to Landing Location

REF F.7 → F.7.1 Achieve Rate of Descent → F.7.2 Maintain ROD According to Operations Manual → F.7.3 Prepare for Approach → REF F.8

REF F.7.1 → AND (F.7.1.1 Change Power System Config. for Descent; F.7.1.2 Change Control System Config. for Descent; F.7.1.3 Change Propulsion System Config. for Descent) → REF F.7.2

REF F.7.2 → AND (F.7.2.1 Set Power System Config. According to Operation Manual; F.7.2.2 Set Control System Config. According to Operation Manual; F.7.2.3 Set Propulsion System Config. According to Operation Manual) → REF F.7.3

REF F.8 → F.8.1 Maintain Stable Approach → F.8.2 Switch to Landing Configuration → F.8.3 Execute Landing → F.8.4 Disengage Systems → REF F.9

REF F.8.2 → AND (F.8.2.1 Configure Airframe System for Landing; F.8.2.2 Configure Power System for Landing; F.8.2.3 Configure Payload for Landing; F.8.2.4 Configure Control System for Landing; F.8.2.5 Configure Propulsion System for Landing) → REF F.8.3

REF F.8.3 → AND (F.8.3.1 Generate Sufficient Lift for Landing; F.8.3.2 Execute Control System Landing Command; F.8.3.3 Generate Sufficient Thrust Lift for Landing) → REF F.8.4

REF F.8.4 → AND (F.8.4.1 Disengage Computer System; F.8.4.2 Disengage Power System; F.8.4.3 Disengage Payload System; F.8.4.4 Disengage Propulsion System; F.8.4.5 Disengage Communication; F.8.4.6 Disengage Flight Condition) → REF F.9

LEGEND:
- Propulsion System
- Control System
- Power System
- Computer System
- Communication System
- Payload System
- Airframe
- Flight Condition System

F.# XXX — REF F.#

F.#.# XXX — REF F.#.#

F.#.#.# XXX — REF F.#.#.#

F.#.#.#.# XXX — REF F.#.#.#.#

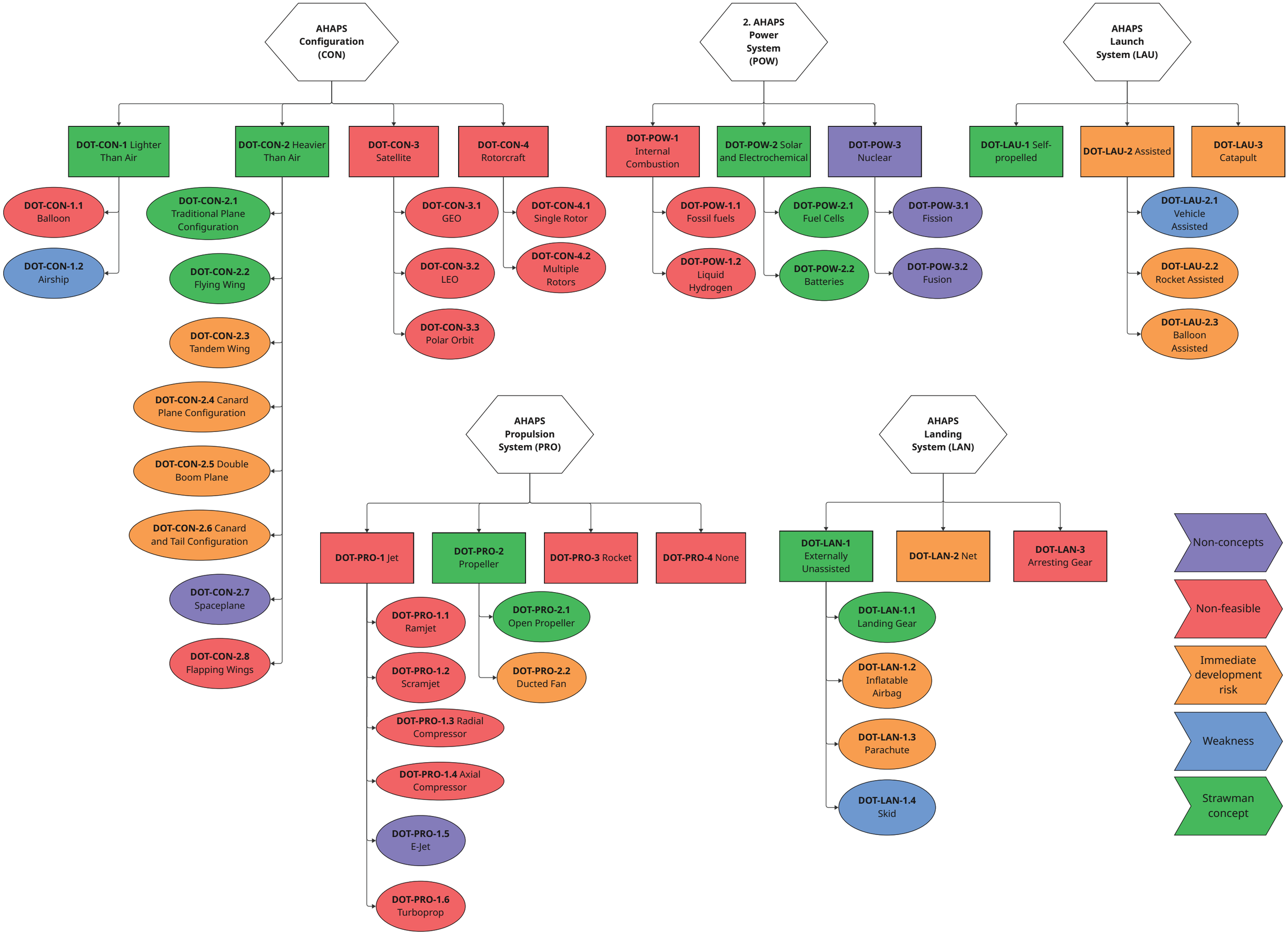
AHAPS Configuration (CON)
DOT-CON-1 Lighter Than Air
DOT-CON-2 Heavier Than Air
DOT-CON-3 Satellite
DOT-CON-4 Rotorcraft
DOT-CON-1.1 Balloon
DOT-CON-1.2 Airship
DOT-CON-2.1 Traditional Plane Configuration
DOT-CON-2.2 Flying Wing
DOT-CON-2.3 Tandem Wing
DOT-CON-2.4 Canard Plane Configuration
DOT-CON-2.5 Double Boom Plane
DOT-CON-2.6 Canard and Tail Configuration
DOT-CON-2.7 Spaceplane
DOT-CON-2.8 Flapping Wings
DOT-CON-3.1 GEO
DOT-CON-3.2 LEO
DOT-CON-3.3 Polar Orbit
DOT-CON-4.1 Single Rotor
DOT-CON-4.2 Multiple Rotors
2. AHAPS Power System (POW)
DOT-POW-1 Internal Combustion
DOT-POW-2 Solar and Electrochemical
DOT-POW-3 Nuclear
DOT-POW-1.1 Fossil fuels
DOT-POW-1.2 Liquid Hydrogen
DOT-POW-2.1 Fuel Cells
DOT-POW-2.2 Batteries
DOT-POW-3.1 Fission
DOT-POW-3.2 Fusion
AHAPS Launch System (LAU)
DOT-LAU-1 Self-propelled
DOT-LAU-2 Assisted
DOT-LAU-3 Catapult
DOT-LAU-2.1 Vehicle Assisted
DOT-LAU-2.2 Rocket Assisted
DOT-LAU-2.3 Balloon Assisted
AHAPS Propulsion System (PRO)
DOT-PRO-1 Jet
DOT-PRO-2 Propeller
DOT-PRO-3 Rocket
DOT-PRO-4 None
DOT-PRO-1.1 Ramjet
DOT-PRO-1.2 Scramjet
DOT-PRO-1.3 Radial Compressor
DOT-PRO-1.4 Axial Compressor
DOT-PRO-1.5 E-Jet
DOT-PRO-1.6 Turboprop
DOT-PRO-2.1 Open Propeller
DOT-PRO-2.2 Ducted Fan
AHAPS Landing System (LAN)
DOT-LAN-1 Externally Unassisted
DOT-LAN-2 Net
DOT-LAN-3 Arresting Gear
DOT-LAN-1.1 Landing Gear
DOT-LAN-1.2 Inflatable Airbag
DOT-LAN-1.3 Parachute
DOT-LAN-1.4 Skid
Non-concepts
Non-feasible
Immediate development risk
Weakness
Strawman concept

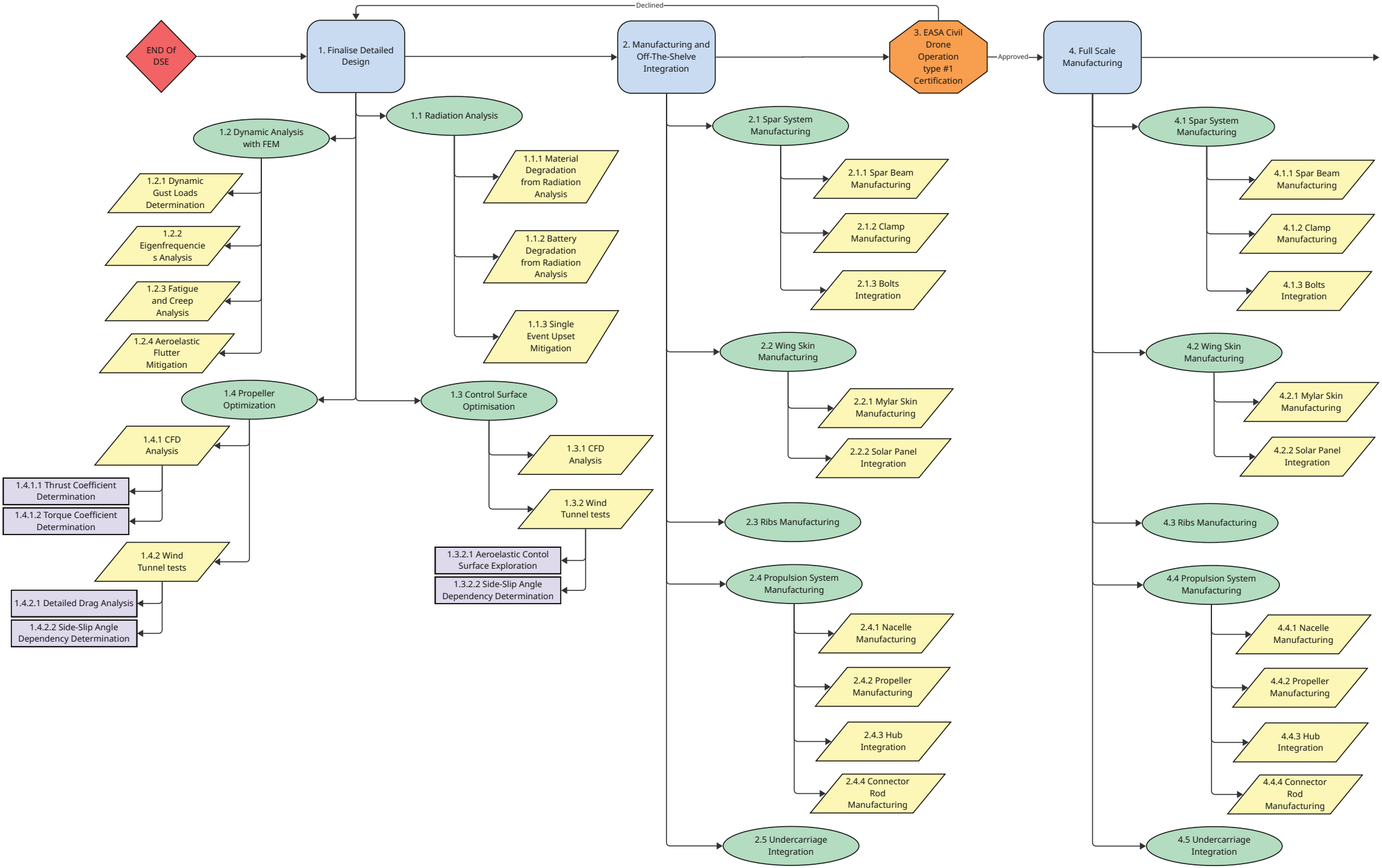
END Of DSE
1. Finalise Detailed Design
Declined
2. Manufacturing and Off-The-Shelve Integration
3. EASA Civil Drone Operation type #1 Certification
Approved
4. Full Scale Manufacturing
1.1 Radiation Analysis
1.1.1 Material Degradation from Radiation Analysis
1.1.2 Battery Degradation from Radiation Analysis
1.1.3 Single Event Upset Mitigation
1.2 Dynamic Analysis with FEM
1.2.1 Dynamic Gust Loads Determination
1.2.2 Eigenfrequencies Analysis
1.2.3 Fatigue and Creep Analysis
1.2.4 Aeroelastic Flutter Mitigation
1.3 Control Surface Optimisation
1.3.1 CFD Analysis
1.3.2 Wind Tunnel tests
1.3.2.1 Aeroelastic Contol Surface Exploration
1.3.2.2 Side-Slip Angle Dependency Determination
1.4 Propeller Optimization
1.4.1 CFD Analysis
1.4.1.1 Thrust Coefficient Determination
1.4.1.2 Torque Coefficient Determination
1.4.2 Wind Tunnel tests
1.4.2.1 Detailed Drag Analysis
1.4.2.2 Side-Slip Angle Dependency Determination
2.1 Spar System Manufacturing
2.1.1 Spar Beam Manufacturing
2.1.2 Clamp Manufacturing
2.1.3 Bolts Integration
2.2 Wing Skin Manufacturing
2.2.1 Mylar Skin Manufacturing
2.2.2 Solar Panel Integration
2.3 Ribs Manufacturing
2.4 Propulsion System Manufacturing
2.4.1 Nacelle Manufacturing
2.4.2 Propeller Manufacturing
2.4.3 Hub Integration
2.4.4 Connector Rod Manufacturing
2.5 Undercarriage Integration
4.1 Spar System Manufacturing
4.1.1 Spar Beam Manufacturing
4.1.2 Clamp Manufacturing
4.1.3 Bolts Integration
4.2 Wing Skin Manufacturing
4.2.1 Mylar Skin Manufacturing
4.2.2 Solar Panel Integration
4.3 Ribs Manufacturing
4.4 Propulsion System Manufacturing
4.4.1 Nacelle Manufacturing
4.4.2 Propeller Manufacturing
4.4.3 Hub Integration
4.4.4 Connector Rod Manufacturing
4.5 Undercarriage Integration

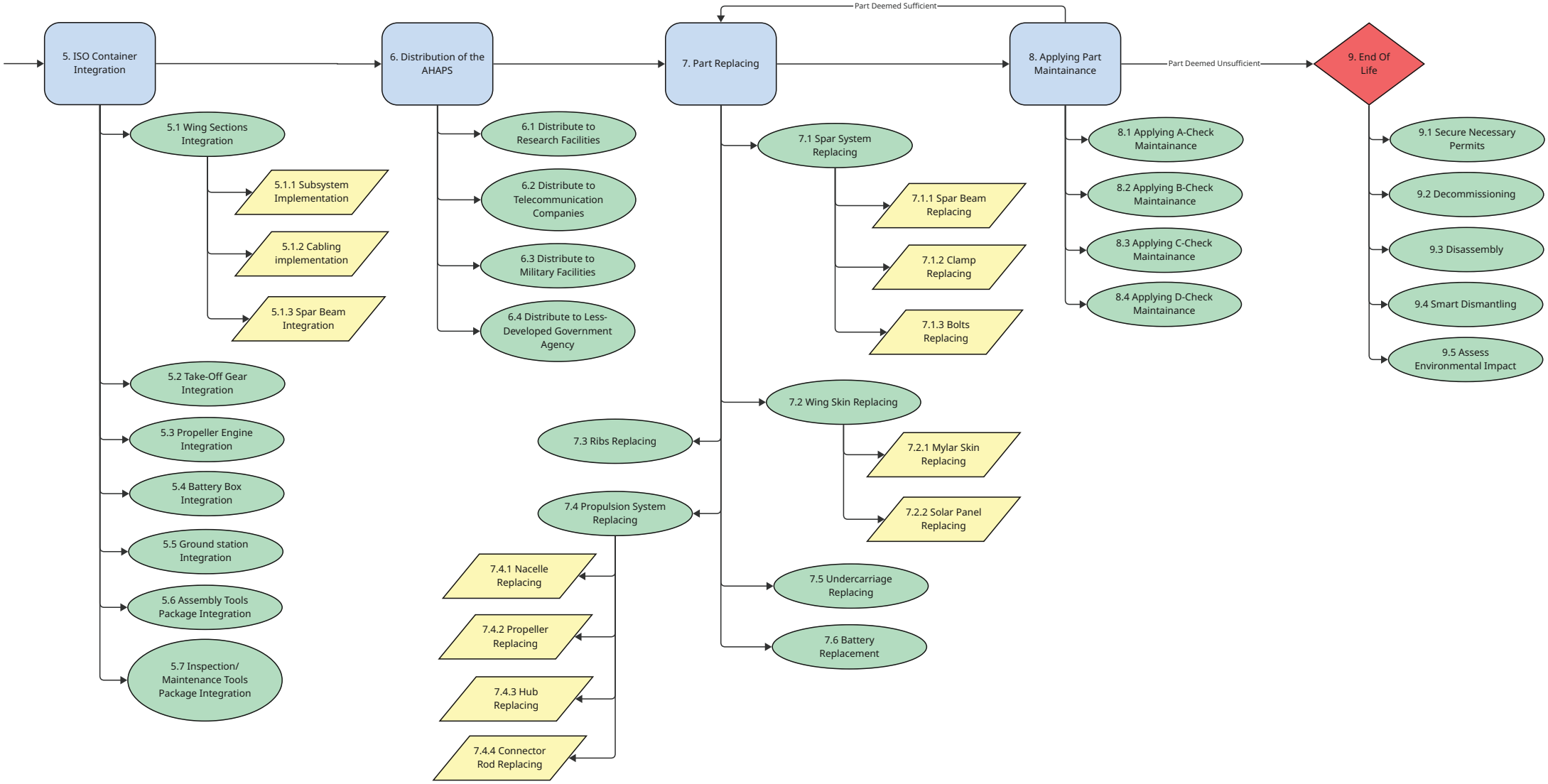
5. ISO Container Integration
6. Distribution of the AHAPS
7. Part Replacing
8. Applying Part Maintainance
9. End Of Life
Part Deemed Sufficient
Part Deemed Unsufficient
5.1 Wing Sections Integration
5.1.1 Subsystem Implementation
5.1.2 Cabling implementation
5.1.3 Spar Beam Integration
5.2 Take-Off Gear Integration
5.3 Propeller Engine Integration
5.4 Battery Box Integration
5.5 Ground station Integration
5.6 Assembly Tools Package Integration
5.7 Inspection/ Maintenance Tools Package Integration
6.1 Distribute to Research Facilities
6.2 Distribute to Telecommunication Companies
6.3 Distribute to Military Facilities
6.4 Distribute to Less-Developed Government Agency
7.1 Spar System Replacing
7.1.1 Spar Beam Replacing
7.1.2 Clamp Replacing
7.1.3 Bolts Replacing
7.2 Wing Skin Replacing
7.2.1 Mylar Skin Replacing
7.2.2 Solar Panel Replacing
7.3 Ribs Replacing
7.4 Propulsion System Replacing
7.4.1 Nacelle Replacing
7.4.2 Propeller Replacing
7.4.3 Hub Replacing
7.4.4 Connector Rod Replacing
7.5 Undercarriage Replacing
7.6 Battery Replacement
8.1 Applying A-Check Maintainance
8.2 Applying B-Check Maintainance
8.3 Applying C-Check Maintainance
8.4 Applying D-Check Maintainance
9.1 Secure Necessary Permits
9.2 Decommissioning
9.3 Disassembly
9.4 Smart Dismantling
9.5 Assess Environmental Impact

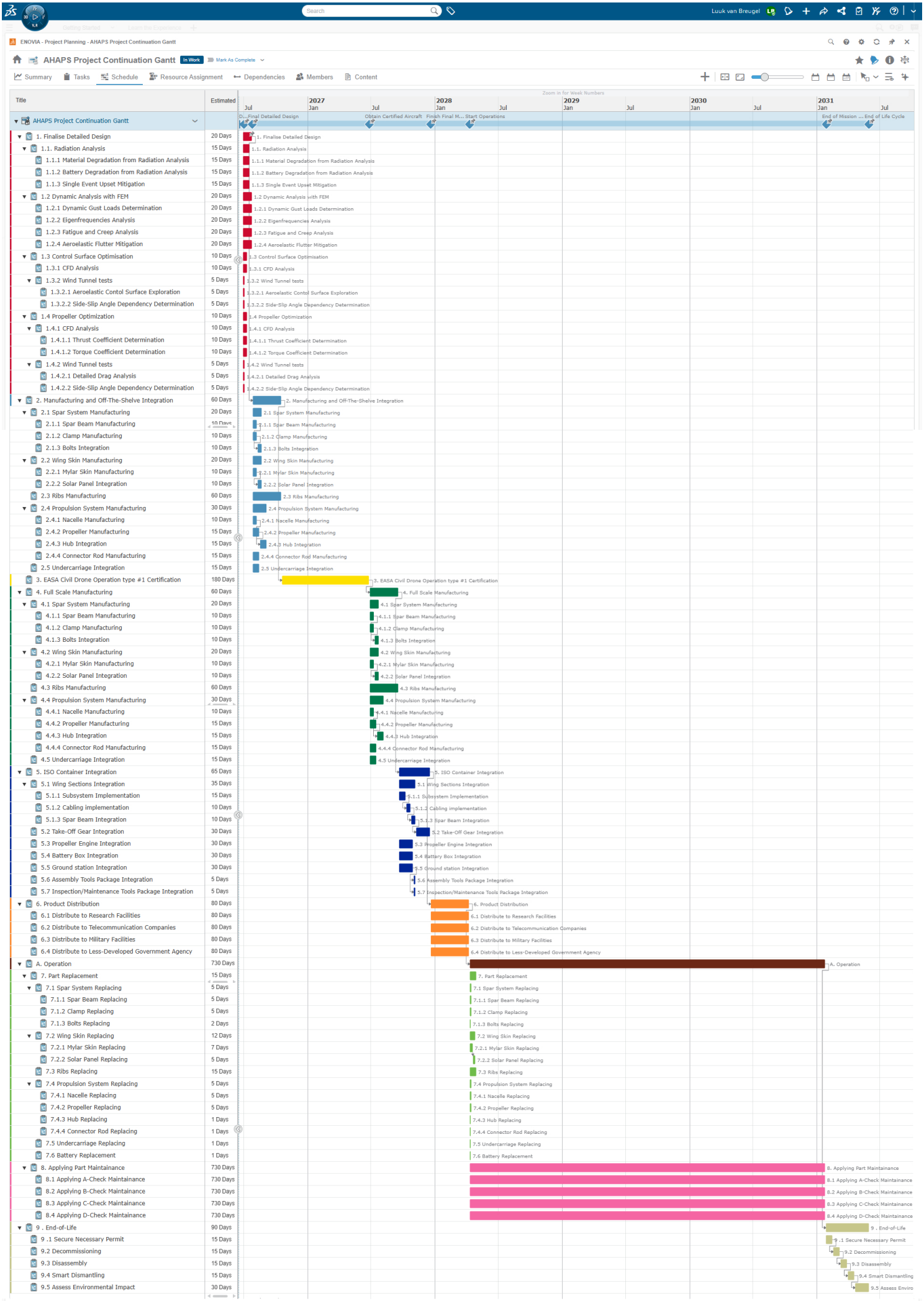
Search
Luuk van Breugel
ENOVIA - Project Planning - AHAPS Project Continuation Gantt
AHAPS Project Continuation Gantt
In Work
Mark As Complete
Summary
Tasks
Schedule
Resource Assignment
Dependencies
Members
Content
Zoom in for Weak Numbers
Title
Estimated
2027
2028
2029
2030
2031
Jan
Jul
Final Detailed Design
Obtain Certified Aircraft
Finish Final M...
Start Operations
End of Mission ...
End of Life Cycle
AHAPS Project Continuation Gantt
1. Finalise Detailed Design 20 Days
1.1. Radiation Analysis 15 Days
1.1.1 Material Degradation from Radiation Analysis 15 Days
1.1.2 Battery Degradation from Radiation Analysis 15 Days
1.1.3 Single Event Upset Mitigation 15 Days
1.2 Dynamic Analysis with FEM 20 Days
1.2.1 Dynamic Gust Loads Determination 20 Days
1.2.2 Eigenfrequencies Analysis 20 Days
1.2.3 Fatigue and Creep Analysis 20 Days
1.2.4 Aeroelastic Flutter Mitigation 20 Days
1.3 Control Surface Optimisation 10 Days
1.3.1 CFD Analysis 10 Days
1.3.2 Wind Tunnel tests 5 Days
1.3.2.1 Aeroelastic Contol Surface Exploration 5 Days
1.3.2.2 Side-Slip Angle Dependency Determination 5 Days
1.4 Propeller Optimization 10 Days
1.4.1 CFD Analysis 10 Days
1.4.1.1 Thrust Coefficient Determination 10 Days
1.4.1.2 Torque Coefficient Determination 10 Days
1.4.2 Wind Tunnel tests 5 Days
1.4.2.1 Detailed Drag Analysis 5 Days
1.4.2.2 Side-Slip Angle Dependency Determination 5 Days
2. Manufacturing and Off-The-Shelve Integration 60 Days
2.1 Spar System Manufacturing 20 Days
2.1.1 Spar Beam Manufacturing 10 Days
2.1.2 Clamp Manufacturing 10 Days
2.1.3 Bolts Integration 10 Days
2.2 Wing Skin Manufacturing 20 Days
2.2.1 Mylar Skin Manufacturing 10 Days
2.2.2 Solar Panel Integration 10 Days
2.3 Ribs Manufacturing 60 Days
2.4 Propulsion System Manufacturing 30 Days
2.4.1 Nacelle Manufacturing 10 Days
2.4.2 Propeller Manufacturing 15 Days
2.4.3 Hub Integration 15 Days
2.4.4 Connector Rod Manufacturing 15 Days
2.5 Undercarriage Integration 15 Days
3. EASA Civil Drone Operation type #1 Certification 180 Days
4. Full Scale Manufacturing 60 Days
4.1 Spar System Manufacturing 20 Days
4.1.1 Spar Beam Manufacturing 10 Days
4.1.2 Clamp Manufacturing 10 Days
4.1.3 Bolts Integration 10 Days
4.2 Wing Skin Manufacturing 20 Days
4.2.1 Mylar Skin Manufacturing 10 Days
4.2.2 Solar Panel Integration 10 Days
4.3 Ribs Manufacturing 60 Days
4.4 Propulsion System Manufacturing 30 Days
4.4.1 Nacelle Manufacturing 10 Days
4.4.2 Propeller Manufacturing 15 Days
4.4.3 Hub Integration 15 Days
4.4.4 Connector Rod Manufacturing 15 Days
4.5 Undercarriage Integration 15 Days
5. ISO Container Integration 65 Days
5.1 Wing Sections Integration 35 Days
5.1.1 Subsystem Implementation 15 Days
5.1.2 Cabling implementation 10 Days
5.1.3 Spar Beam Integration 10 Days
5.2 Take-Off Gear Integration 30 Days
5.3 Propeller Engine Integration 30 Days
5.4 Battery Box Integration 30 Days
5.5 Ground station Integration 30 Days
5.6 Assembly Tools Package Integration 5 Days
5.7 Inspection/Maintenance Tools Package Integration 5 Days
6. Product Distribution 80 Days
6.1 Distribute to Research Facilities 80 Days
6.2 Distribute to Telecommunication Companies 80 Days
6.3 Distribute to Military Facilities 80 Days
6.4 Distribute to Less-Developed Government Agency 80 Days
A. Operation 730 Days
7. Part Replacement 15 Days
7.1 Spar System Replacing 5 Days
7.1.1 Spar Beam Replacing 5 Days
7.1.2 Clamp Replacing 5 Days
7.1.3 Bolts Replacing 2 Days
7.2 Wing Skin Replacing 12 Days
7.2.1 Mylar Skin Replacing 7 Days
7.2.2 Solar Panel Replacing 5 Days
7.3 Ribs Replacing 15 Days
7.4 Propulsion System Replacing 5 Days
7.4.1 Nacelle Replacing 5 Days
7.4.2 Propeller Replacing 5 Days
7.4.3 Hub Replacing 1 Days
7.4.4 Connector Rod Replacing 1 Days
7.5 Undercarriage Replacing 1 Days
7.6 Battery Replacement 1 Days
8. Applying Part Maintainance 730 Days
8.1 Applying A-Check Maintainance 730 Days
8.2 Applying B-Check Maintainance 730 Days
8.3 Applying C-Check Maintainance 730 Days
8.4 Applying D-Check Maintainance 730 Days
9 . End-of-Life 90 Days
9 .1 Secure Necessary Permit 15 Days
9.2 Decommissioning 15 Days
9.3 Disassembly 15 Days
9.4 Smart Dismantling 15 Days
9.5 Assess Environmental Impact 30 Days

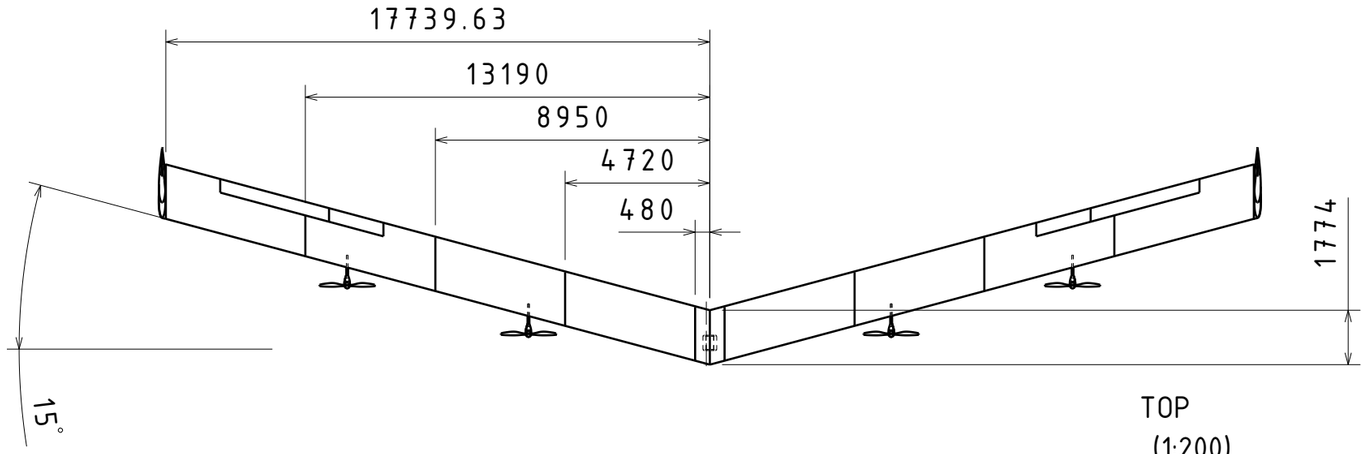

TOP
(1:200)

ISOMETRIC
(1:200)

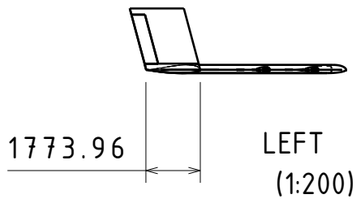

LEFT
(1:200)

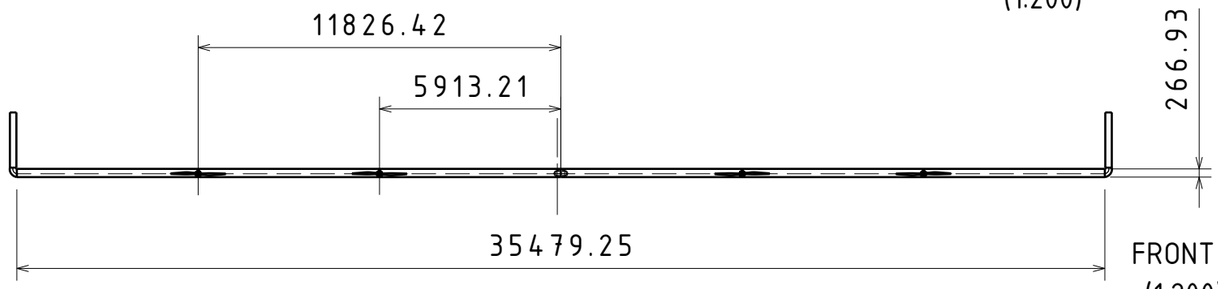

FRONT
(1:200)

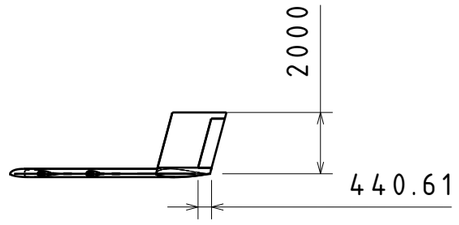

RIGHT
(1:200)

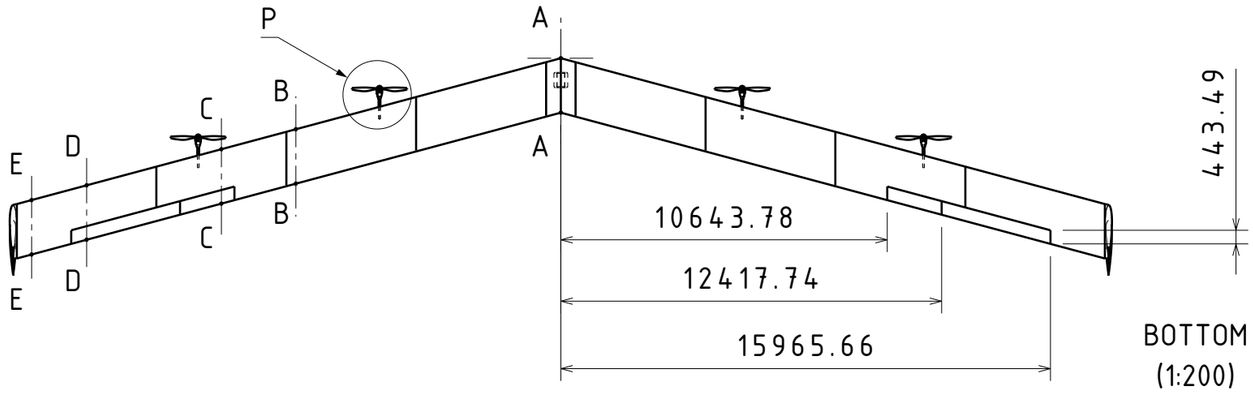

BOTTOM
(1:200)

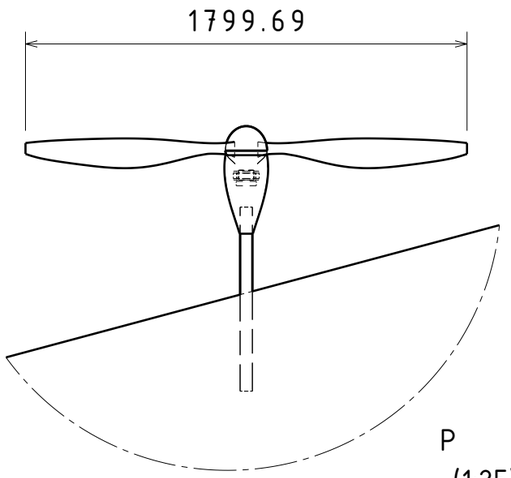

P
(1:25)

DESIGNED BY: Luuk van Breugel DATE: 23-6-2026	ADAPTABLE HIGH-ALTITUDE PLATFORM SYSTEM		
CHECKED BY: Bas van Strien DATE: 23-6-2026			
SIZE A3	DSE GROUP 17 - 2026 Q4		
SCALE 1:200	WEIGHT (kg) XXX	DRAWING NUMBER AHAPS.1	SHEET 1/1

I	–
H	–
G	–
F	–
E	–
D	–
C	–
B	–
A	–